University of Salerno

Department of Mathematics

Ph.D. in Mathematics, Physics and Applications

Adapted numerical methods for evolutionary problems

Leila Moradi

Advisor

Prof. Dajana Conte

Ph.D. Director

Prof. Patrizia Longobardi

Cycle XXXV, SSD MAT/08

Abstract

This study presents new numerical methods for solving differential/integral equations of interest in applications. This thesis consists of four parts. Part I presents numerical methods for solving ordinary differential equations exhibiting oscillatory solutions. This part proposes an adapted numerical integration based on exploiting a-priori known information about the behavior of the exact solution, employing some well-known numerical methods in combination with the technique of exponential fitting. The proposed method is shown to be highly effective in reducing error and improving the accuracy of the numerical solutions.

Parts II and III of this thesis present the numerical methods to solve Volterra integral and fractional integral/differential equations. To accomplish this, we provide effective numerical methods based on spectral methods and new orthogonal functions. The proposed methods are based on using special functions such as Chebyshev polynomials, Chelyshkov functions, and other orthogonal functions. The effectiveness of the proposed methods is examined by providing numerical experiments, which demonstrate the high accuracy and efficiency of the proposed methods. Additionally, the results of the proposed methods are compared with the existing methods, and it is shown that the proposed methods provide more accurate and efficient solutions for the problems considered in this thesis.

Keywords: Exponential fitting, Spectral methods, Ordinary differential equations, Volterra integral equations, Fractional integral/differential equations.

Preface

In recent years, there has been a significant increase in interest in mathematical modeling concerning science, engineering, business, and management. Various problems from physics, chemistry, pharmacology, medicine, and economics can be modeled using a set of functional equations, such as ordinary differential equations (ODEs), Volterra integral equations (VIEs), and fractional differential equations (FDEs). These problems include the growth of biological populations, the spread of diseases, brain dynamics, heat conduction, fluid dynamics, scattering theory, seismology, biomechanics, game theory, control, queuing theory, and many others.

This thesis consists of four parts (twelve chapters):

In Chapter 1, we concentrate our attention on introducing three categories of problems, and we aim to offer some of the most current models of functional equations.

In Chapter 2, we remind the reader of some of the fundamental concepts which are helpful for the thesis and we introduce the two main techniques utilized in the thesis: the exponential fitting and spectral methods.

Part I of this thesis will present numerical methods for the solution of ODEs exhibiting oscillatory solutions. Classical numerical integrators could require a small step size to follow the oscillations, especially when the frequency increases. To develop efficient and accurate numerical methods, we propose an adapted numerical integration based on exploiting a-priori known information about the behavior of the exact solution, employing an exponential fitting strategy. We combine this feature by use of peer methods, which represent a highly structured subclass of General Linear Methods, and are identified with several distinct stages, such as Runge-Kutta methods. This part consists of Chapter 3, Chapter 4, and Chapter 5. Chapter 3 concerns the construction of a general class of Exponentially Fitted (EF) two-step implicit peer methods for the numerical integration of ODEs with oscillatory solution. In Chapter 4 Implicit-Explicit (IMEX) EF peer methods are proposed for the numerical solution of an advection-diffusion problem exhibiting oscillatory solution. In Chapter 5, we investigate how the frequencies can be tuned to obtain the maximal benefit from the exponentially fitted peer methods.

Parts II and III of this thesis deal withon numerical methods to solve VIEs and fractional integral/differential equations. In these parts, we provide effective numerical methods based on new orthogonal functions. Our main approach in this research is to use spectral methods, new orthogonal functions, and operational matrices as significant tools. These numerical methods approximate the unknown function by means of an appropriate polynomial basis and use operational matrices. In this case, the problem becomes a system of algebraic equations, which is much easier to solve than the original problem. It should be noted that integral or derivative operational matrices, in addition to maintaining accuracy in solving the problem, make calculations much simpler.

Part II consists of Chapter 6, Chapter 7 and Chapter 8. The discussion of numerical techniques for resolving VIEs and systems subject to VIEs is the focus of Part II of this work. Chapter 6 will present a new numerical method by using discrete orthogonal Hahn polynomials for solving Volterra-type integral functional equations with variable bounds and mixed delay. In Chapter 7, we will suggest a novel formulation for the numerical solution of optimal control problems related to nonlinear Volterra fractional integral equations systems. Control theory and optimization is a branch of mathematical optimization that deals with finding a control for a dynamical system over time such that an objective function is optimized. For this system, a spectral approach is implemented based on the new polynomials known as Chelyshkov polynomials. Chapter 8 deals with collocation methods for nonlinear VIEs with oscillatory kernel. This work examines nonlinear second kind VIEs and discretizes the oscillatory integrals in the collocation equation using a Filon-type approach.

Part III consists of Chapter 9, Chapter 10, and Chapter 11. The goal of Part III is to present numerical methods for fractional integral/ differential equations. Chapter 9 proposes a numerical technique based on a hybrid of block-pulse functions and Chelyshkov polynomials to solve fractional delay differential equations. Chapter 10 presents a comparative study of numerical solutions to fractional variational problems. Chapter 11 examines and compares the construction of protein-protein interaction (PPI) networks of $CD4^+$ and $CD8^+$ T cells and investigates why studying these cells is critical after HIV infection. This study also examines a mathematical model of fractional HIV infection of $CD4^+$ T cells and proposes a new numerical procedure for this model that focuses on a recent kind of orthogonal polynomials called discrete Chebyshev polynomials.

Part IV shows the conclusions of this thesis and future work.

The contribution of the thesis can be found in the following publications:

1. Conte D., Mohammadi F., Moradi L., Paternoster B., Exponentially fitted two-step peer methods for oscillatory problems, Computational and Applied Mathematics, 2020. https://doi:10.1007/s40314-020-01202-x

2. Conte, D., Moradi L., Paternoster, B., Exponentially fitted IMEX peer methods for an advection-diffusion problem, submitted.

3. Conte, D., Moradi L., Paternoster, B., Frequency evaluation for adapted peer methods, Computational and Applied Mathematics (2023) 42-78 https://doi.org/10.1007/s40314-023-02223-y

4. Conte D., Moradi L., Paternoster B. Numerical solution of delay Volterra functional integral equations with variable bounds. Accepted in Numerical applied mathematics.

5. Moradi L., Conte D., Farsimadan E., Palmieri F., Paternoster B., Optimal control of system governed by nonlinear Volterra integral and fractional derivative equations, Computational and Applied Mathematics, 40, 157 (2021). https://doi.org/10.1007/s40314-021-01541-3

6. Conte D., Moradi L., Paternoster B., Podahisky H. Collocation methods for nonlinear Volterra integral equations with oscillatory kernel, Ready to submit.

7. Conte, D., Farsimadan, E., Moradi L., Palmieri, F., Paternoster, B. (2022). A Galerkin Approach for Fractional Delay Differential Equations Using Hybrid Chelyshkov Basis Functions, Lecture Notes in Computer Science, vol 13375. Springer, Cham. https://doi.org/10.1007/978-3-031-10522-7_10

8. Mohammadi, F., Moradi L., Conte, D., (2021). Discrete Chebyshev Polynomials for Solving Fractional Variational Problems. Statistics, Optimization & Information Computing, 9(3), 502-515. https://doi.org/10.19139/soic-2310-5070-991

9. Farsimadan E., Moradi L., Conte D., Paternoster B., Palmieri F. (2021) Comparison Between Protein-Protein Interaction Networks CD4$^+$T and CD8$^+$T and a Numerical Approach for Fractional HIV Infection of CD4$^+$T Cells, Lecture Notes in Computer Science, vol 12949. Springer, Cham.https://doi.org/10.1007/978-3-030-86653-2_6

Family means nobody gets left behind or forgotten.

Dedicated to my family.
For their endless love, support, and encouragement.

Acknowledgements

I would like to express my deep gratitude to all the individuals who have supported me in my academic journey. I am grateful for the guidance and encouragement my supervisor and other mentors provided, who have played a crucial role in shaping my research and helping me reach this point.

Firstly, I am incredibly grateful to my supervisor, Prof. Dajana Conte, for her invaluable advice, continuous support, and patience during my Ph.D. study. Her immense knowledge and great experience have encouraged me throughout my academic research and daily life.

Besides my advisor, I wish to express my sincere thanks to my advisor, Prof. Beatrice Paternoster, for her treasured support that was influential in my study. She gave me this chance to be in her group on July 2018. I appreciate her for believing in me, helping me, and encouraging and supporting my research.

I sincerely thank Dr. Helmut Podhaisky for having a strong belief in my research, especially during the time I have spent in the Department of Mathematics of Martin Luther University Halle-Wittenberg.

I sincerely thank Prof. Francesco Palmieri, with whom I had the opportunity to collaborate in his scientific research group.

I sincerely thank Prof. Patrizia Longobardi for her guidance and cooperation at each step of my journey.

I would also like to extend my sincere thanks to the reviewers who have generously given their time and expertise to evaluate my work. I am genuinely grateful for the opportunity to incorporate your feedback into my thesis.

I also appreciate the support of my colleagues and friends, "the members of Laboratory number 62", who have been there for me both in good times and in challenging moments.

Their camaraderie and encouragement have been invaluable.

I would like to acknowledge the love and support of my beloved family, especially my husband. Their unwavering encouragement and belief in me have been the driving force behind my success. I am truly thankful for all the support and encouragement I have received during my academic journey, and I would not have been able to achieve this without the help of these individuals.

With heartfelt appreciation,
Leila Moradi

Contents

List of Figures

List of Tables

Chapter 1

Introduction

In recent years, there has been a noticeable rise in interest in mathematical modeling related to science, engineering, business, and management. These models are typically expressed through functional equations, which offer the best and most natural technique to describe evolution in time and space and the presence of memory. Various issues from physics, chemistry, pharmacology, medicine, and economics can be modeled using functional equations, such as ODEs, VIEs, and FDEs. These problems include the growth of biological populations, the spread of diseases, the dynamics of the brain, heat conduction, fluid dynamics, scattering theory, seismology, biomechanics, game theory, control, queuing theory, and many others.

ODEs-based models, for example, can be found in the context of the evolution of biological populations [219, 305, 332], mathematical models in physiology and medicine [30], oncogenesis [165, 288] and spread of infections and diseases [168], economic sciences [108], analysis of signals [231]. Some particular uses of VIEs are models of population dynamics, and the spread of epidemics [141, 142], wave difficulties [115], fluid dynamics [146], contact problems [1], electromagnetic signals [215]. Due to the effective memory performance of fractional derivatives, FDEs have been frequently employed to represent a variety of physical processes, such as seepage flow in porous media and fluid dynamic traffic models. For example, applications of FDEs can be found in mathematical models in physiology [3], viscoelastic [89, 184], bioengineering [193], thermodynamics [262].

The literature has extensively explored theoretical studies on systems of ODEs, VIEs, and FDEs. Most of the time, an analytical method can not be used to get the solution to a functional equation. For this reason, developing numerical techniques to address these issues becomes more important.

1.1 Problems and motivations

Construction, theoretical analysis, and implementation of new efficient, accurate numerical integration methods for the approximate solution of functional equations are the goals of this work. We concentrate our attention on the following categories of problems:

1) *Problem 1:* Systems of first order ordinary differential equations

$$y'(t) = f(t, y(t)), \quad y(t_0) = y_0 \in \mathcal{R}^d, \quad t \in [t_0, T], \tag{1.1.1}$$

where $f : \mathcal{R} \times \mathcal{R}^d \to \mathcal{R}^d$ is sufficiently smooth to ensure that the solution exists and it is uniqe.

The numerical solution of problem (1.1.1) has been extensively explored in the literature [43, 140, 180, 275, 276]. However, the most recent monographs [44, 109, 134, 135, 136, 166] show a continued strong interest in this field. These equations frequently have typical issues (e.g. stiffness [136], metastability [136], periodicity [158], high oscillations [109, 134], and discontinuities [2]) that must efficiently be overcome by using suitable numerical integrators. The focus of Part I of this dissertation is the creation, study, and use of new, effective numerical methods for the integration of the problem 1.1.1) with an oscillatory solution. The derived approaches are compared with those classically considered in the literature to demonstrate the advantages we have achieved. Through the application of these approaches in environments with fixed and variable stepsizes, generated by utilizing the unique structure of the derived numerical methods, the experimental analysis of the developed equations also supports the theoretical analysis.

2) *Problem 2:* Volterra integral equations

$$y(t) = f(t) + \int_0^t K(t, s, y(s))ds, \quad t \in I = [0, T] \ (T < \infty) \tag{1.1.2}$$

where $y(t)$ is the unknown function and $f(t)$ is a given continuous function on I. The function $K = K(t, s, y)$ is assumed to be defined and continuous on $D \times \mathbb{R}$ with $D := \{(t, s) : 0 \leqslant s \leqslant t \leqslant T\}$.

The numerical treatment of VIEs (1.1.2) has garnered much interest in recent decades. Only in 1986 the first monograph on this topic appeared in the literature [40]. As a result, numerous open problems could still be investigated in this area. VIEs are important for simulating phenomena in various relevant domains, such as engineering, mechanics, physics, chemistry, biology, economics, potential theory, and electrostatics, to name a few ([24, 32, 222]). The focus of Part II of the thesis is the discussion of numerical techniques for resolving VIEs and systems subject to VIEs. Several numerical results for various test problems are given to verify the accuracy of the derived numerical methods.

3) Fractional differential equations involve fractional derivatives of the form $(\frac{d^\alpha}{dt^\alpha})$, which are defined for $\alpha > 0$, where α is not necessarily an integer.

   – *Problem 3:* FDE of Riemann–Liouville type:

$$\begin{cases} D^\alpha y(t) = f(t, y(t)), \\ D^{\alpha-k} y(0) = b_k, \qquad k = 0, ..., n-1, \\ I^{n-\alpha} y(0) = b_n, \end{cases} \tag{1.1.3}$$

   – FDE of Caputo type

$$\begin{cases} {}_0^C D_t^\alpha y(t) = f(t, y(t)), \\ {}_0^C D_t^{\alpha-k} y(0) = b_k, \qquad k = 0, ..., n-1, \end{cases} \tag{1.1.4}$$

where f is an analytical function, $b_k, k = 0, 1, ..., n-1$, are real constants, y is the solution to be determined, and $I^{n-\alpha}$ is the fractional integral and $D^\alpha, (n-1 < \alpha \leqslant n)$ is the fractional derivative in the Riemann–Liouville or Caputo sense [227].

Recently, the numerical approach to problems modeled by Riemann-Liouville and Caputo FDEs (1.1.3)-(1.1.4) has been investigated. Fractional calculus is a fascinating topic that has piqued the curiosity of many researchers. G.W. Leibniz (1695, 1697) and Leonhard Euler (1730) pioneered the development of fractional calculus, which has continued to the present day [225]. Although the Riemann-Liouville fractional derivative is of great importance, it may not be suitable to model some real-world phenomena the Caputo fractional derivative is used. Fractional differential equations can describe better certain real-world phenomena. Understandably, systems are frequently imperfect and subject to perturbations such as friction, human intervention, and external forces. Therefore the integer-order derivatives may not be adequate to understand the trajectories of the state variables. By considering fractional derivatives, we have an infinite choice of derivative orders and determine that the fractional differential equation that better describes the dynamics of the model.

In recent decades, scientists have become interested in the applications of fractional calculus in domains such as physics, engineering, and others [21, 107, 132, 137, 138, 182, 194, 202, 223, 245, 254]. Nowadays, journal proceedings and special issues refer to fractional calculus applications in numerous scientific domains, such as special functions, control theory, chemical physics, stochastic processes, anomalous diffusion, and rheology, see [224]. Fractional derivatives and integrals have been practical tools for characterizing memory and hereditary properties in various materials and processes. For instance, fractional differential equations are employed to explain a range of natural phenomena in physics, chemistry, fluid mechanics, and mathematics [243]. Part III discusses numerical approaches to fractional derivatives and fractional integrals problems. The efficiency of the suggested methods in this part is evaluated using numerical experiments.

1.2 Some recent models

This section aims to offer some of the most current models of functional equations (1.1.1), (1.1.2) and (1.1.3)-(1.1.4) that are of importance in the applied sciences.

We first consider some models involving systems of first-order ODEs (1.1.1) of interest in Biology, Medicine, and Cluster Analysis.

1. *Cell cycles.* Cell cycles, basic events in the life of any organism, are composed of succeeding coordinated and oscillatory phases that enable the cell to grow and proliferate appropriately. This has been extensively researched concerning tumor diseases. In [8] (see also the references therein contained), the description of such biological processes has been provided by a set of kinetic equations that define the biochemical reactions together with dynamic equations, structured as systems of first-order ODEs (1.1.1) of the type

$$\frac{dX_i}{dt} = F_i(X_1, X_2, ..., X_n; p_1, p_2, ..., p_m), i = 1, 2, ..., n,$$

where $X_i, i = 1, 2, ..., n$, is a state variable, generally describing the the concentration of a certain species in the studied organism, each function F_i describes the rate of change of the corresponding X_i and $p_j, j = 1, 2, ..., m$ are parameters appearing in each F_i.

2. *A model in epileptic seizures.* It is hypothesized that a specific anomaly in the brain, typically in the hippocampal region of the temporal lobe, is the source of complex partial epileptic seizures. In [181], to model a hippocampus subnetwork thought to be crucial in the production of focused or complicated partial seizures, a system of ODEs (1.1.1) is introduced. The parameters in this model correspond to inhibitory interneurons and archetypal pyramidal cells' membrane potentials in the CA3 area of the hippocampus, where the attention is most likely to be. The model presented in [181] is the following:

$$\begin{cases} \dfrac{dV_i}{dt} = -g_{Ca} m_\infty (V_i - 1) - g_K W_i (V_i - V_i^K) - g_L (V_i V_i^L) + I - \alpha_{inh} Z_i, \\ \dfrac{dZ_i}{dt} = b(cI + \alpha_{exc} V_i), \\ \dfrac{dW_i}{dt} = \dfrac{\phi(w_\infty - W_i)}{\tau_w}, \ i = 1, 2, ..., \end{cases}$$

where V_i and Z_i are the membrane potentials of the pyramidal and inhibitory cells, respectively, while W_i is a relaxation factor, essentially the fraction of open potassium channels in the population of pyramidal cells. The parameters g_{Ca}, g_K , and g_L are the total conductances for the populations of Ca, K , and leakage channels, respectively. V_i^K is the Nernst potential for

potassium in node i; this parameter is used in coupling subnetwork populations into a lattice. V_i^L is a leak potential, τ_w is a voltage dependent time constant for W_i, I is the applied current, while ϕ and b are temperature scaling factors. The parameter c differentially modifies the current input to the inhibitory interneuron. The functions w_∞ and m_∞ are non-dimensional expressions that describe voltage-gated Ca^{2+} channels in the cell membrane, each of which is open or closed at any given moment. The parameters α_{exc} and α_{inh} model the populations of excitatory and inhibitory synaptic connections between pyramidal cells and their interneurons in the population of cells corresponding to the subnetwork model.

3. *A metastable problem: the Becker-Doring equation.* The Becker-Doring [136] model (see also monograph [64]) describes the dynamics of a large system of identical particles that can condense and form clusters. The k-particle clusters per unit volume denote by y_k and assume that the clusters can only gain or lose single particles. The following system arises from ODEs (1.1.1):

$$\begin{cases} \dfrac{dy_1}{dt} = -J_1 - \sum\limits_{k=1}^{N-1} J_k, \\ \dfrac{dy_k}{dt} = J_{k-1} - J_k, k = 2, 3, ..., N-1, \\ \dfrac{dy_N}{dt} = -J_{N-1}, \end{cases}$$

where $J_k = y_1\, y_k - b_{k+1}\, y_{k+1}$ and $b_{k+1} = exp(k^{\frac{2}{3}} - (k-1)^{\frac{2}{3}})$. This problem is intriguing, especially for large values of N, because it exhibits the metastability phenomenon, which causes prolonged changes in the solution over long time intervals (see [64, 136]).

We now provide various models for biology, immunology, and population dynamics based on second-kind Volterra Integral Equations (1.1.2).

1. *Vaccine-induced immune responses on HIV infection.* Anti-HIV-1 vaccinations are a universally acknowledged necessity. The goal of achieving such a vaccine is still elusive. However, several prospective vaccine formulations are currently undergoing clinical trials. This is due to the intricacy of the viral system as well as the trial length and cost requirements. In [129], the authors developed a mathematical model for simulating the development of HIV-1 infection within the body. This model assesses the impact of potential anti-HIV-1 vaccinations with various features. A preventive or therapeutic vaccine's ability to prevent the spread of infection can be predicted based on the model's ability to forecast the immunogenicity features it must have to

be effective. The model developed in [129] assumes the form

$$\begin{cases} P(t) = \int_0^t F(t-x)e^{-\delta(tx)}k_i\, k_s\, V(x)S(x)dx, \\ V(t) = V_0e^{-ct} + \int_0^t e^{-c(tx)}\, pP(x)dx, \\ S(t) = S_0e^{-\delta t} + \int_0^t e^{-\delta(tx)}\left[\delta k_s\, V(x)\, S(x)\right]dx, \end{cases}$$

When three cell populations exist in a unit volume of plasma at the time, t is indicated by the unknown functions $P(t)$, $V(t)$ and $S(t)$: $P(t)$ represents the population of infected cells that produce the virus, $V(t)$ for the population of the virus, and $S(t)$ for the number of susceptible cells.

2. *Age-structured populations: the Lotka-McKendrick model.* Mathematical demographers and population biologists have extensively researched the theory of population dynamics. Age effects are one of the most crucial components to incorporate in realistic models of population dynamics. Sharpe-Lutka and McKendrick introduced the first continuum models, including age effects in 1911 and 1926, respectively. The Lotka-McKendrick model for an age-structured population (compare [159]) assumes the form

$$B(t) = F(t) + \int_0^t \beta(x)B(t-x) - \pi(x)dx,$$

where $B(t)$ denotes the birth density at time t and $u(x,t)$ indicates the age-specific density at time t, i.e., $u(x,t)dx$ is the total number of people aged between x and $x+dx$ at time t, $\beta(x)$ represents the likelihood of surviving from birth to age x, $\pi(x)$ represents the rate of fertility for an individual of age x per unit time, and the forcing function $F(t)$ adopts the form

$$F(t) = \int_0^w \beta(x+t)\, u(x,0)\frac{\pi(x+t)}{\pi(x)}dx,$$

where w is the maximal possible age.

We finally present some models involving systems of FDEs (1.1.3)-(1.1.4), of interest in Human society, Biology, and Dynamics.

1. *World Population Growth.* The World Population Growth [284] has been described in several attempts. The basic model is the Malthusian law of population growth, which is used to anticipate populations under ideal circumstances. Let $N(t)$ be the number of individuals in a population at the

time t , B , and M the birth and mortality rates, respectively, so that the net growth rate is given by

$$N'(t) = (B - M)N(t) = PN(t), \tag{1.2.5}$$

where $P := B - M$ is the production rate. Here, B and M are constant, and thus P is also constant. The solution of this differential equation is the function

$$N(t) = N_0 e^{Pt}, \qquad t \geqslant 0, \tag{1.2.6}$$

where N_0 is the population at $t = 0$. Because of the solution (1.2.6), this model is also known as the exponential growth model.

Considered now that the World Population Growth model is ruled by the fractional differential equation [6]

$$ {}_0^C D_t^\alpha N(t) = PN(t), \qquad t \geqslant 0, \qquad \alpha \in (0, 1). \tag{1.2.7}$$

Observe that, taking the limit $\alpha \longrightarrow 1^{-1}$, Eq (1.2.7) converts into Eq. (1.2.5), but if we consider $\alpha \in (1, 2)$ and take the limit $\alpha \longrightarrow 1^{+1}$, $N'(t) - N'(0) = PN(t)$ is obtained. The solution of this fractional differential equation is the function

$$N(t) = N_0 E_\alpha(Pt^\alpha),$$

where E is the Mittag–Leffler function

$$E_\alpha(t) = \sum_{k=0}^{\infty} \frac{t^k}{\Gamma(\alpha\, k + 1)}, \qquad t \in \mathbb{R}.$$

2. *Blood Alcohol Level.* A simple model for calculating alcohol level that is described by a set of two differential equations [190]. Let A and B represent the alcohol concentration in the stomach and the blood, respectively. The following Cauchy system describes the problem:

$$\begin{cases} A'(t) = -k_1 A(t) \\ B'(t) = k_1 A(t) - k_2 B(t), \\ A(0) = A_0, \\ B(0) = 0, \end{cases}$$

where A_0 is the initial alcohol ingested by the subject and k_1, k_2 some real constants. The two functions give the solution to this system

$$A(t) = A_0 e^{-k_1 t}$$

and

$$B(t) = A_0 \frac{k_1}{k_2 - k_1}(e^{-k_1 t} - e^{-k_2 t}).$$

Suppose the system of fractional differential equations represents the problem. In that case, a curve obtains better in line with the experimental results [6]. Consider the system of fractional differential equations with $\alpha, \beta \in (0, 1)$ as the following form:

$$\begin{cases} {}_0^C D_t^\alpha A(t) = -k_1 A(t) \\ {}_0^C D_t^\beta B(t) = k_1 A(t) - k_2 B(t), \\ A(0) = A_0, \\ B(0) = 0, \end{cases}$$

The solution concerning A is

$$A(t) = A_0 e^{-k_1 t}$$

To determine B, it can be found as the solution of the fractional differential linear equation

$${}_0^C D_t^\beta B(t) = -k_2 B(t) + k_1 A_0 E_\alpha(-k_1 t^\alpha).$$

3. *Video Tape problem.* For the videotape problem, the tape counter must read $n(t)$ at a time $t > 0$. For modeling the problem, consider c denote the thickness and v the velocity of the tape and are constant in time. Also, R(t) represents the wheel's radius filled by the tape, and A(t) measures the angle at time t. The number of turns is proportional to the angle $n(t) = kA(t)$ for a positive constant k. In [117], an ordinary differential equation is obtained to describe the behavior of the model:

$$A'(t) = \frac{v}{R(0)\sqrt{bt + 1}},$$

where

$$b = \frac{cv}{\pi R^2(0)}$$

Using the initial condition $A(0) = 0$, the solution is obtained:

$$A(t) = \frac{2v}{bR(0)}(\sqrt{bt + 1} - 1).$$

In conclusion, the tape counter readings are given by the expression

$$n(t) = a(\sqrt{bt + 1} - 1),$$

where

$$a = \frac{2kv}{bR(0)}.$$

If the video tape problem is represented by a fractional differential equation of order $\alpha \in (0,1)$, it is the form [6]:

$$\begin{cases} {}_0^C D_t^\alpha A(t) = \dfrac{v}{R(0)\sqrt{bt+1}}, \\ A(0) = 0, \end{cases}$$

where

$$b = \frac{cv}{\pi R^2(0)}.$$

Applying the fractional integral operator ${}_0I_t^\alpha$ to both sides of the fractional differential equation that reads as

$${}_0I_t^\alpha \, {}_0^C D_t^\alpha A(t) = A(t) - A(0),$$

if $\alpha \in (0,1)$, the solution is obtained by

$$n(t) = \frac{p}{\Gamma(\alpha) \int\limits_0^t \dfrac{(t-s)^{\alpha-1}}{\sqrt{bs+1}}}$$

where

$$p = \frac{kv}{R(0)}, \qquad b = \frac{cv}{\pi R^2(0)}.$$

Chapter 2

Theoretical frameworks: preliminaries and methods

This chapter serves as a crucial foundation for the rest of the thesis. The first section of the chapter serves as an introduction and provides preliminary materials. These materials will aid in understanding the application of fractional differential equations in later chapters. The second section of the chapter is dedicated to presenting the two methods that will be used throughout the rest of the thesis. These methods are introduced in two separate subsections: exponentially fitted and spectral methods. Exponentially fitted methods are used in part I, while spectral methods are used in parts II and III.

2.1 Preliminaries

Solving many problems in the fields of mathematics, physics, and engineering is done by solving functional equations as follows:

$$Lu = f, \tag{2.1.1}$$

where $L : X \longrightarrow Y$ is an operator between function spaces X and Y, u is an unknown function and f is a known function. Obtaining the exact solution for these equations is not easy in many cases. Approximate methods to solve these equations can be obtained by writing the solution of such equations as a linear combination of orthogonal functions. Then, the problem is converted into a system of linear or non-linear equations using the properties of orthogonal functions. The approximate solution to the problem is obtained by solving this system of equations. Therefore, we will study the concepts of orthogonality and approximation of functions in the following.

2.1.1 Orthogonal functions

It has always been desirable to solve big problems by dividing them into smaller parts, and one of the methods is to use orthogonal functions. The purpose of using orthogonal

functions is to simplify the problem into smaller components. Therefore, these small components should have a simple shape that can solve the problem. To define the orthogonal basis functions, firstly, we introduce the concepts of inner multiplication and orthogonality of two vectors that can be extended for several functions.
Orthogonal functions are divided into three main categories. The first category includes constant piecewise basis functions, such as Walsh and block functions. Pulse, Harr functions, etc., the second category consists of orthogonal polynomials, such as Legendre, Chebyshev, Hermit, Lager, etc. The third category is sine and cosine functions in the Fourier series [9, 22, 69, 68, 88, 106, 111, 125, 126, 131, 139, 171, 185, 196, 210, 218, 250, 258, 222, 307, 308].

Definition 2.1.1. *[70] Suppose $\phi_1(t)$ and $\phi_2(t)$ are two continuous real functions in $[a, b]$. The inner product of these two functions is defined as follows:*

$$\langle \phi_1, \phi_2 \rangle_w = \int_a^b \phi_1(t)\phi_2(t)w(t)dt. \tag{2.1.2}$$

Let $\{t_i, w_i\}_{i=0}^N$ be set of points and weights, and $\phi_1(t)$ and $\phi_2(t)$ are two continuous real functions. The discrete inner product is defined as

$$\langle \phi_1, \phi_2 \rangle_{N,w} = \sum_{i=0}^{N} \phi_1(t_i)\phi_2(t_i)w(t_i), \tag{2.1.3}$$

where $w(t)$ is positive and is named as the weight function.

Definition 2.1.2. *[70] Suppose $\phi_1(t)$ and $\phi_2(t)$ are two continuous real functions in $[a, b]$. These two functions are orthogonal if*

$$\langle \phi_1, \phi_2 \rangle_w = 0.$$

Definition 2.1.3. *[70] Consider $\Phi = \{\phi_k(t),\ \ k = 1, 2, ...\}$ a set of continuous functions in $[a, b]$. Φ is called orthogonal if the two-by-two inner product of this set with respect to the weight function $w(t) > 0$ is as follows:*

$$\int_a^b \phi_i(t)\phi_j(t)w(t)dt = 0, \qquad i \neq j. \tag{2.1.4}$$

A sequence of orthogonal polynomials is a sequence $\{p_n\}_{n=0}^{\infty}$ of polynomials with $deg(p_n) = n$ such that

$$\langle p_i, p_j \rangle_w = 0, \qquad i \neq j.$$

The subject of orthogonal polynomials is a classical one whose origins can be traced to Legendre's work on planetary motion [70]. This topic with many applications in physics, statics, probability, and other branches of mathematics in the first decades of the 20th century, developed surprisingly. Recently, orthogonal basis and especially

orthogonal polynomials are among the most helpful approximation tools, especially in numerical integration methods. By using them, the accuracy of these methods can be increased. However, the use of orthogonal polynomials in computer science, approximation theory, and numerical analysis is not very old. Its history goes back to recent years. Now, we introduce orthogonal polynomials and some of their essential features. Then we examine the application of these polynomials in approximation theory.

Theorem 1. *Consider* $\Phi = \{\phi_k(t), \quad k = 1, 2, ...\}$ *a set of orthogonal continuous functions on* $[a, b]$. *Any continuous function* $\psi(t)$ *can be expanded as:*

$$\psi(t) = \sum_{k=0}^{\infty} c_k \phi_k(t),$$

where the coefficients c_k *are calculated as follows:*

$$c_k = \frac{\langle \psi(t), \phi_k(t) \rangle_w}{\langle \phi_k(t), \phi_k(t) \rangle_w}. \tag{2.1.5}$$

Proof. The proof is available in Theorem 2.2, page 9 [70]. □

2.1.2 Fractional calculus

Fractional differential calculus is one of the branches of mathematical analysis that deals with the integration and derivation of any real positive order. In recent decades, research related to fractional differential calculus has attracted much attention. Fractional derivatives are used in many fields, such as electrical networks, control theory, dynamic systems, statistics and probability, electro-corrosion chemistry, physical chemistry, ophthalmology and optometry, signal processing, fluid flows, and others. Various definitions have been provided for the integral and derivative of fractional order, among which the Riemann-Liouville fractional definition is one of the most basic definitions in mathematics. Since using Riemann-Liouville fractional operator for differential equations of fractional order will lead to the production of initial conditions with fractional order derivatives at the initial point, this operator is less used. Caputo fractional derivative operator is used more in practical problems. Using this definition in FDEs leads to the production of initial conditions with integer order derivatives at the initial point.

Rieman-Liouville Fractional Integral

Definition 2.1.4. *Riemann-Liouville integral operator of order* $\alpha \geqslant 0$ *is defined as follows*

$$\left(I^{\alpha} f\right)(t) = \begin{cases} f(t), & \alpha = 0, \\ \dfrac{1}{\Gamma(\alpha)} \displaystyle\int_0^t \frac{f(s)ds}{(t-s)^{1-\alpha}}, & \alpha > 0. \end{cases}$$

Theorem 2. *[225, 243, 261] Suppose $\alpha, \beta > 0$ and $f \in C([a,b])$. In this case, the following relations hold for the Riemann-Liouville fractional integral operator.*

$$I^{\alpha} I^{\beta} f(t) = I^{\alpha+\beta} f(t),$$

$$I^{\alpha} I^{\beta} f(t) = I^{\beta} I^{\alpha} f(t),$$

$$I^{\alpha} t^{\beta} = \frac{\Gamma(\beta+1)}{\Gamma(\beta+1+\alpha)} t^{\beta+\alpha}$$

Definition 2.1.5. *Consider $m-1 < \alpha \leqslant m$, $m \in \mathbb{N}$ and $f \in C^m[a,b]$. The Riemann-Liouville fractional derivative operator of order α is introduced as follows:*

$$D_a^{\alpha} f(t) = \frac{d^m}{dt^m} I_a^{m-\alpha} f(t) = \frac{1}{\Gamma(m-\alpha)} \frac{d^m}{dt^m} \int_a^t (t-s)^{m-\alpha-1} f^m(s) ds,$$

Theorem 3. *[225, 243, 261] Consider $0 < m \leqslant \alpha < m+1$ and $\beta > -1$, then the following relations are established for the Riemann-Liouville fractional derivative operator*

$$D_a^{\alpha} (t-a)^{\beta} = \frac{\Gamma(1+\beta)}{\Gamma(1+\beta-\alpha)} (t-a)^{\beta-\alpha},$$

$$I_a^{\alpha} (t-a)^{\beta} = \frac{\Gamma(1+\beta)}{\Gamma(1+\beta+\alpha)} (t-a)^{\beta+\alpha},$$

Theorem 4. *[225, 243, 261] Suppose $m-1 < \alpha \leqslant m$ and c is constant, in this case*

$$D_a^{\alpha} c = \frac{c}{\Gamma(1-\alpha)} (x-a)^{-\alpha},$$

$$D_a^{\alpha} c = \frac{c}{\Gamma(1+\alpha)} (x-a)^{\alpha}.$$

Theorem 5. *[225, 243, 261] Consider $m-1 < \alpha \leqslant m$ and $f \in C[a,b]$*

$$D_a^{\alpha} I_a^{\alpha} f(t) = f(t),$$

$$I_a^{\alpha} D_a^{\alpha} f(t) = f(t) + \sum_{k=0}^{m} \frac{(t-a)^{\alpha-k-1}}{\Gamma(\alpha-k)} \frac{d^{m-k}}{dt^{m-k}} [D_a^{m-\alpha-1} f(t)]_{t=a},$$

Caputo fractional derivative

Definition 2.1.6. *Consider $m-1 < \alpha < m$ and $f \in C_{\alpha}^m$. Caputo's fractional derivative operator is expressed as follows*

$${}_0^C D_t^{\alpha} f(t) = \begin{cases} \dfrac{1}{\Gamma(m-\alpha)} \displaystyle\int_0^t \frac{f^{(m)}(s)}{(t-s)^{\alpha-m+1}} ds, \ t > 0, & 0 \leqslant m-1 < \alpha < m, \\ \dfrac{d^m f(t)}{dt^m}, & \alpha = m \in \mathbb{N}. \end{cases}$$

We can briefly define the Caputo derivative as follows:

$$ {}_0^C D_t^\alpha f(t) = \begin{cases} I_a^{m-\alpha} f^{(m)}(t), & m-1 < \alpha < m, \\ \dfrac{d^m}{dt^m} f(t), & \alpha = m. \end{cases} \tag{2.1.6} $$

Theorem 6. *[225, 243, 261] If I_a^α and D_a^α Riemann-Liouville integral and derivative operators and ${}_0^C D_t^\alpha$ be the Caputo derivative operator, then*

$$ \begin{gathered} {}_0^C D_t^\alpha I_a^\alpha f(t) = f(t), \\ I_a^\alpha {}_0^C D_t^\alpha f(t) = f(t) - \sum_{k=0}^{m-1} f^{(k)}(a^+) \tfrac{t^k}{k!}, \quad t > 0 \end{gathered} \tag{2.1.7} $$

.

Theorem 7. *[225, 243, 261] Suppose $0 \leqslant m \leqslant \alpha < m+1$, D_a^α and ${}_0^C D_t^\alpha$ be the Riemann-Liouville and Caputo fractional derivative operators, in this case:*

$$ D_a^\alpha f(t) = {}_0^C D_t^\alpha f(t) + \sum_{k=0}^{m} \frac{(t-a)^{k-\alpha}}{\Gamma(k-\alpha+1)} f^{(k)}\left(a^+\right). \tag{2.1.8} $$

Therefore, the Riemann-Liouville and Caputo derivative operators of the function f are not equal except under the assumption that if m is the first derivative of the function f in $t = a$ be zero.

2.1.3 Optimal control theory

Optimal control theory is a branch of mathematical and engineering sciences that studies the behavior of dynamic systems. When one or more system outputs are supposed to follow a certain reference in the time interval, a control variable changes the system inputs to make suitable changes in the system output. The system behavior is closer to the desired behavior. The goal of optimal control theory is to minimize or maximize the value of a certain quantity in the system that controls the system's behavior. In other words, the optimal control problem controls a parameter during a mathematical model to produce an optimal output using some optimization methods. Every controllable dynamic system has several state characteristics and control parameters. The state parameters are expressed at any moment, and the control parameters provide the possibility of controlling the system to reach the desired conditions.
To express the governing equations of dynamic processes in an optimal control problem, a set of dynamic equations is presented, which can be used to obtain the state of the system for the control input values at any moment. These equations are known as state equations:

$$ x(t) = f(x(t), u(t), t), $$

where the control variable $u(t)$ controls the system at each moment. The optimal control problem is defined in a time interval, the moment of the start t_0 that is generally known,

and the final time t_f that can be specified.
Various constraints are defined based on device limitations, environmental limitations, or the desired conditions of designers. These conditions are generally divided into two categories: point and directional conditions. Point conditions are applied to the problem at specific and individual times. The initial Ψ_0 and final Ψ_f conditions of the problem are defined at the beginning and end moments of the path and are point conditions.

$$\textit{initial conditions} : \Psi_0(x(t_0), t_0)$$

$$\textit{final conditions} : \Psi_f(x(t_f), t_f)$$

Path conditions are applied during a time of the problem, which can be the whole or a part of the time of the problem.

$$\mathcal{L}(x(t), u(t), t) \geqslant 0$$

The range of changes in state and control variables can be defined, limited, and bounded. These demarcations of state variables are defined based on physical limitations or designers' intent, and the demarcation of control variables is defined based on the limitations of control components.

$$x_l \leqslant x(t) \leqslant x_u \qquad u_l \leqslant u(t) \leqslant u_u$$

The goal of optimal control problems is to achieve an optimal event. This optimal event is the form of a scalar objective $\mathcal{J}$, which is generally formulated as follows and must be minimized:

$$\mathcal{J} = \phi[x(t_0), t_0, x(t_f), t_f] + \int_{t_0}^{t_f} \mathcal{L}[t, x(t), u(t)],$$

where the expression ϕ is a function of the state variables at the final moment of the problem, and $\mathcal{L}$ is the integral function of the state and control variables during the time interval.

Numerical methods for solving optimal control problems

Solving optimal control systems has certain complexities. In classical control theory, input, output, and error variables are important. The unique characteristic of classical control theory is that it is based on the input-output relationship of systems. The major drawback of this theory is that it can only be used for time-independent linear systems with one input and one output. Therefore, from the point of view of this theory, time-dependent systems, nonlinear systems, and multi-input-multi-output systems cannot be investigated and analyzed. In addition, classical methods are often not applicable for optimal control systems with nonlinear time-dependent behavior. Therefore, providing suitable and efficient numerical methods for solving real optimal control systems is particularly important. Numerical methods for solving optimal control problems are

divided into two categories: indirect methods and direct methods.

Indirect methods: the solution is obtained by means of Hamiltonian boundary value problem, which can be solved using a numerical method. One of the primary advantages of indirect methods is the high confidence factor of the obtained numerical solution, which is due to satisfying the conditions of a Hamiltonian boundary value problem. These methods have many disadvantages. First, the necessary conditions of a Hamiltonian boundary value problem should be obtained analytically, which is not easily possible in most cases. Second, indirect methods have a small radius of convergence, which means that a very accurate initial guess is required for the unknown boundary conditions. Finally, in many cases, indirect methods require an accurate initial guess for the equations of state, which are not intuitive in practice.

Direct methods: the main idea is discretizing the optimal control problem and turning it into a nonlinear programming problem. For the obtained numerical solution, existing advanced algorithms are used. The advantage of direct methods in comparison with indirect methods is that there is no need to find initial conditions. In addition, these methods have a much larger radius of convergence, and there is no need for an accurate initial guess for the unknown boundary conditions and the state equations. However, the obtained numerical solution may not be the optimal solution, which is the disadvantage of these methods. One of the characteristics of direct methods is the use of orthogonal functions to approximate the solution.

2.2 Methods

This section of this chapter delves into the specific methods and techniques that will be used throughout the rest of the thesis. By the end of this section, readers should have a solid understanding of the key concepts and principles of Exponential fitting and spectral methods.

2.2.1 Exponential fitted methods

Exponential fitting is a procedure for an efficient numerical approach to functions consisting of weighted sums of exponential, trigonometric, or hyperbolic functions with slowly varying weight functions. Operations on such functions as numerical differentiation, quadrature, interpolation, or solving ordinary differential equations whose solution is of this type are of genuine interest nowadays in many phenomena such as oscillations, vibrations, rotations, or wave propagation. This type of functions also describes the behavior of quantum particles.

The Exponential fitting process was originally suggested a few decades ago to reform the classical algorithms to be particularly effective in resolving differential equa-

tions [76, 78, 97, 98, 99, 158, 161, 164, 237, 280, 281, 303]. Exponentially Fitted (EF) algorithms for numerical integration problems with oscillating or periodic solutions permit the development of efficient and accurate numerical methods. When the frequency increases, classic numerical integrators need very small stepsizes to obtain accurate solutions. In contrast, EF numerical methods can achieve the same accuracy with a significantly larger step size.

This section presents the main mathematical elements of the exponential fitting procedure. It will be seen that this procedure is rather general. The basic idea behind EF methods is to derive numerical methods better suited for oscillatory problems. These EF methods are always based on non-fitted counterparts. To make a clear distinction between, e.g., an EF Trapezoidal rule and the Trapezoidal rule, we will refer to the latter as the classical Trapezoidal rule. Part I of this thesis considers the numerical solution of ordinary differential equations. We refer the reader to the extensive overview in [158] for the other applications.

A classical method performs best when the solution is a polynomial or can aptly be represented as one locally. A k-step Adams-Bashforth method can find a polynomial solution of degree k without errors. In exponential fitting terminology, it is said that the method has a fitting space

$$\mathcal{F} = \left\{1, t, t^2, \ldots, t^K\right\}.$$

Suppose the solution of the problem at hand is a linear combination of these monomials. The method can solve the problem up to machine accuracy in that case. The solution is said to fall within the fitting space of the method. To obtain an exponentially fitted variant of a method, a few of the highest-order monomials are replaced by exponentials. The most general fitting space is of the form

$$\left\{1, t, t^2, \ldots, t^K, e^{\mu_0 t},\ e^{\mu_1 t}, e^{\mu_2 t}, \ldots, e^{\mu_P t}\right\}.$$

Any solution that is a linear combination of these functions can be found up to machine accuracy by a method with said fitting space. Such a method has coefficients that depend on the parameters $\mu_0, ..., \mu_P$ multiplied by the step-size h. If all the parameter values tend to zero, then the classical counterpart appears. The coefficients sometimes become numerically unstable for small values of $\mu_i h$. One should then resort to MacLaurin expansions instead.

Usually, however, the parameters are chosen symmetrically across the origin

$$\left\{1, t, t^2, \ldots, t^K, e^{\pm\mu_0 t},\ e^{\pm\mu_1 t}, e^{\pm\mu_2 t}, \ldots, e^{\pm\mu_P t}\right\},$$

because the fitting space can then be written as

$$\left\{1, t, t^2, \ldots, t^K,\ cosh(\mu_0 t),\ sinh(\mu_0 t), \ldots, cosh(\mu_P t),\ sinh(\mu_P t), \right\},$$

In principle, the parameters $\mu_0, ..., \mu_P$ can all be given different values. It can, however, be interesting to specify a relation between the different parameters. The approach that we will consider in most of this work is $\mu_0 = \mu_1 = ... = \mu_P$, a choice that leads to a fitting space of the form

$$\left\{1, t, t^2, \ldots, t^K, e^{\pm\mu t}, t\, e^{\pm\mu t}, t^2 e^{\pm\mu t}, \ldots, t^P e^{\pm\mu t}\right\}. \tag{2.2.9}$$

This is the approach taken by Ixaru et al., [160], Vanden Berge et al., [104, 158, 300, 298, 299] and Simos et al., [277, 278, 279]. A different strategy is to consider

$$\left\{1, t, t^2, \ldots, t^K,\, e^{\pm\mu t}, e^{\pm 2\mu t}, \ldots,\, e^{\pm P\mu t}\right\},$$

a choice made by Calvo et al., cf. i.a. [47, 48, 49] and Paternoster [236]. Regardless of the form of the fitting space, it is usually imposed that the parameter value(s) are either real or imaginary. In Part I, we will consider general exponential fitting, i.e., fitting spaces of the form (2.2.9).

Six-step procedure

In [154, 158], the authors provide a six-step procedure (the six-step flow chart) that one can follow to construct exponentially fitted methods with a fitting space of the form (2.2.9). Since we will follow this procedure in part I, we here review it. To make the procedure easily understable we describe it on a specific problem. We consider the approximation of the first derivative of $y(t)$ at t_1 of the three-point formula.
Central difference formula: This is

$$y'(t_1) \approx \frac{1}{h}[a_0\, y(t_0) \,+\, a_1\, y(t_1) \,+\, a_2\, y(t_2)], \qquad t_i = t_1 + \,(i-1)\, h, \tag{2.2.10}$$

and we want to determine the values of the three coefficients a_0, a_1 and a_2.

Step 1
We write down the linear difference operator $\mathcal{L}[h, \mathbf{w}]$ related to the scheme under consideration. Vector $\mathbf{w}$ is defined as the list of coefficients we need to find expressions.

The corresponding linear difference operator $\mathcal{L}[h, \mathbf{w}]$ for (2.2.10) is then given by

$$\mathcal{L}[h, \mathbf{w}] := y'(t) - \frac{1}{h}[a_0\, y(t-h) \,+\, a_1\, y(t) \,+\, a_2\, y(t+h)]$$

where $\mathbf{w} = [a_0, a_1, a_2]$.

Using the linear difference operator (2.2.1), we construct the classic moments

$$\mathcal{L}_m(h, \mathbf{w}) = \mathcal{L}[h, \mathbf{w}]t^m|_{t=0},$$

therefore

$$\mathcal{L}_0(h,\mathbf{w}) = -h(a_0+a_1+a_2), \quad \mathcal{L}_1(h,\mathbf{w}) = 1+a_0-a_2,$$
$$\mathcal{L}_{2k}(h,\mathbf{w}) = -h^{2k-1}(a_0+a_2), \quad \mathcal{L}_{2k+1}(h,\mathbf{w}) = h^{2k}(a_0-a_2), \quad k=1,2,...$$

and the dimensionless classic moments

$$\mathcal{L}^*_m(h,\mathbf{w}) = \frac{\mathcal{L}_m(h,\mathbf{w})}{h^m}$$

and therefore

$$\mathcal{L}^*_{2k}(h,\mathbf{w}) = -(a_0+\delta_{0k}a_1+a_2), \quad \mathcal{L}^*_{2k+1}(h,\mathbf{w}) = (\delta_{0k}+a_0-a_2), \;\; k=0,1,2,...$$

Step 2
We determine the maximum value of M such that the algebraic system

$$\mathcal{L}^*_m(h,\mathbf{w}) = 0, \qquad m=0,1,\ldots,M-1, \tag{2.2.11}$$

is compatible. This is equivalent to annihilating the difference operator (2.2.1) on polynomials with a degree less or equal to $M-1$.

For the scheme considered in (2.2.10) the value of M is $M=3$. The solution of the system (2.2.11) is the set of the classical coefficients $a_2 = -a_0 = \frac{1}{2}, a_1 = 0$.

Step 3
Annihilating the difference operator (2.2.1) on the functions $t^m e^{\mu t}$ is equivalent to annihilating in $\pm z$ the so-called dimensionless μ-moments of order m

$$E^*_m(z,\mathbf{w}) = \frac{1}{h^m}\mathcal{L}[h,w]t^m e^{\mu t}|_{t=0}, \tag{2.2.12}$$

where $z=\mu h$.

For the scheme considered in (2.2.10) dimensionless μ-moments of order m are

$$E^*_m(z,\mathbf{w}) \;=\; z - a_0 exp(-z) - a_1 - a_2 exp(z),$$

We next observe that the system

$$E_m^*(\pm z, \mathbf{w}) = 0, \quad m = 0, 1, \ldots, P,$$

is equivalent to the system

$$G^{\pm(m)}(Z, \mathbf{w}) = 0, \quad m = 0, 1, \ldots, P,$$

where $Z = z^2$, $G^{\pm}(Z, \mathbf{w})$ are the $G-$functions

$$G^+(Z, \mathbf{w}) = \frac{E_0^*(z, w) + E_0^*(-z, w)}{2},\ G^-(Z, \mathbf{w}) = \frac{E_0^*(z, w) - E_0^*(-z, w)}{2z}, \tag{2.2.13}$$

and the superscript (m) denotes the m-th derivatives. Therefore

for the scheme considered in (2.2.10)

$$G^+(Z, \mathbf{w}) = -a_1 - \tfrac{1}{2}[exp(z) + exp(-z)](a_0 + a_2) = -a_1 - (a_0 + a_2)\eta_{-1}(Z),$$

$$G^-(Z, \mathbf{w}) = 1 + \tfrac{1}{2z}[exp(z) - exp(-z)](a_0 - a_2) = 1 + (a_0 - a_2)\eta_0(Z),$$

where $\eta_{-1}(Z)$ and $\eta_0(Z)$ are the η-functions defined in [158] as follows:

- if Z is real

$$\eta_{-1}(Z) = \frac{e^{\sqrt{Z}} + e^{-\sqrt{Z}}}{2} = \begin{cases} \cos\sqrt{|Z|} & \text{if } Z < 0 \\ \cosh\sqrt{Z} & \text{if } Z \geqslant 0 \end{cases} \tag{2.2.14a}$$

$$\eta_0(Z) = \begin{cases} \dfrac{e^{\sqrt{Z}} - e^{-\sqrt{Z}}}{2\sqrt{Z}} & \text{if } Z \neq 0 \\ 1 & \text{if } Z = 0 \end{cases} = \begin{cases} \dfrac{\sin(\sqrt{|Z|})}{\sqrt{|Z|}} & \text{if } Z < 0 \\ 1 & \text{if } Z = 0 \\ \dfrac{\sinh(\sqrt{Z})}{\sqrt{Z}} & \text{if } Z > 0 \end{cases} \tag{2.2.14b}$$

(2.2.14c)

- if Z is purely imaginary

$$\eta_{-1}(Z) = \cos\left(\mathrm{i}\sqrt{Z}\right) \tag{2.2.15a}$$

$$\eta_0(Z) = \begin{cases} \dfrac{\sin\left(\mathrm{i}\sqrt{Z}\right)}{\mathrm{i}\sqrt{Z}} & \text{if } Z \neq 0 \\ 1 & \text{if } Z = 0 \end{cases} \tag{2.2.15b}$$

In both cases, $\eta_\sigma(Z)$, for $\sigma > 0$, satisfy the relation:

$$\eta_\sigma(Z) = \begin{cases} \dfrac{\eta_{\sigma-2}(Z) - (2\sigma-1)\eta_{\sigma-1}(Z)}{Z} & \text{if } Z \neq 0 \\ \dfrac{2^\sigma \sigma!}{(2\sigma+1)!} & \text{if } Z = 0 \end{cases}. \tag{2.2.16}$$

We recall that their derivatives verify the condition

$$\eta'_\sigma(Z) = \frac{1}{2}\eta_{\sigma+1}(Z), \quad \sigma = -1, 0, 1, \ldots \tag{2.2.17}$$

For more details on these functions see [72, 74, 75, 158] or the Appendix of [154]. The differentiation relations (2.2.17) permit to compute the derivatives of $G^{\pm}(Z, \mathbf{w})$.

For the scheme considered in (2.2.10), we find that

$$G^{+P}(Z, \mathbf{w}) = -2^{-P}(a_0 + a_2)\eta_{P-1}(Z), \qquad G^{-P}(Z, \mathbf{w}) = 2^{-P}(a_0 - a_2)\eta_P(Z).$$

Step 4
We choose a reference set of M functions:

$$\left\{1, t, t^2, \ldots, t^K, e^{\pm\mu t}, t\,e^{\pm\mu t}, t^2 e^{\pm\mu t}, \ldots, t^P e^{\pm\mu t}\right\},$$

with taking into account that $M = 3$ and the self-consistency condition

$$K + 2P = M - 3. \tag{2.2.18}$$

Two pairs P, K are consistent with $M = 3$, that is $P = -1, K = 2$ (the classical option), and $P = K = 0$.
Step 5
We obtain the coefficients of the exponentially fitted peer method by solving the system:

$$\mathcal{L}^*_m(h, \mathbf{w}) = 0, \quad m = 0, \ldots, K, \tag{2.2.19a}$$
$$G^{\pm(m)}(Z, \mathbf{w}) = 0, \quad m = 0, \ldots, P. \tag{2.2.19b}$$

Therefore, for the latter option, the algebraic system for the coefficients is

$$\mathcal{L}_0^*(h, \mathbf{w}) = G^{\pm}(Z, \mathbf{w}) = 0, \quad K = P = 0,$$

with the solution

$$a_2(Z) = -a_0(Z) = \frac{1}{2\eta_0(Z)}, \;\; a_1(Z) = 0.$$

This differs from the classical set of coefficients by a factor $\dfrac{1}{\eta_0(Z)}$ which is $\mu\, h\, sin(\mu\, h)$ if $\mu = i\omega$. Note also that $\dfrac{1}{\eta_0(0)} = 1$ i.e. the classical coefficients are re-obtained for $Z = 0$.

Step 6
We compute the leading term of the local truncation error as follows:

$$lte_{ef} = (-1)^{P+1} h^{M+l} \frac{\mathcal{L}_{K+1}^*(h, \mathbf{w})}{(K+1)!\, Z^{P+1}}\; D^{K+1}(D^2 - \mu^2)^{P+1} y(t), \tag{2.2.20}$$

where we denote by D the derivative with respect to time.

As we choose $K = 0$ and $P = 0$, for this set of coefficients, we have

$$\mathcal{L}_1^*(h, \mathbf{w}) = 1 - 2\, a_2\,(Z) = \frac{(\eta_0(Z) - 1)}{\eta_0(Z)}$$

. In this case, the aforementioned leading term assumes the following expression:

$$lte_{ef} = -h^2 \frac{(\eta_0(Z) - 1)}{Z\eta_0(Z)} D\,(D^2 - \mu^2)\, y(t). \tag{2.2.21}$$

In the limit for μ, $Z \longrightarrow 0$ this becomes

$$lte_{ef} = \frac{-h^2}{6}\, y^{(3)}(t). \tag{2.2.22}$$

To see this, the l'Hospital rule can be used for the factor in the middle. We have

$$(\eta_0(Z) - 1)' = \frac{\eta_1(Z)}{2}$$

and

$$(Z\eta_0(Z))' = \eta_0(Z) + \frac{Z\eta_1(Z)}{2},$$

and since $\eta_1(0) = \frac{1}{3}$, the factor in discussion becomes $\frac{1}{6}$.

2.2.2 Spectral methods

This section constitutes a short introduction to spectral methods. Spectral methods are considered a class of solution techniques using sets of known functions to solve differential equations [67, 68, 124, 128, 46, 170, 207, 322, 326]. These techniques are typically considered high-order and can produce high-resolution solutions. Unlike finite-difference and finite-element approaches, spectral methods express the solution of a differential equation by an expansion in terms of global basis functions instead of local. These methods accurately resolve phenomena on the scale of the mesh spacing when used properly. Additionally, mesh refinement improves the order of truncation error decay compared to finite-difference and finite-element approaches. It is conceivable to construct a spectral method for problems with smooth solutions whose truncation error approaches zero faster than any finite power of the mesh spacing (exponential convergence).

Spectral methods are a wide class of discretization schemes known as Weighted Residual Methods (WRM) [149, 65, 226]. The key elements of the WRM are the trial functions (also called the expansion or approximating functions) and the test functions (also known as weight functions). The trial functions are the basis functions for a truncated series expansion of the solution. The test functions are used to ensure that the truncated series expansion satisfies the differential equation as closely as possible. This is achieved by minimizing the residual, i.e., the error in the differential equation produced by using the truncated expansion instead of the exact solution concerning a suitable norm. An equivalent requirement is that the residual satisfies a suitable orthogonality condition for each test function. Mainly three types of spectral methods can be identified: collocation, tau, and Galerkin. The choice of the type of method depends essentially on the application. Collocation methods are suited to nonlinear problems or having complicated coefficients. In contrast, Galerkin methods have the advantage of a more convenient analysis and optimal error estimates. The tau method is applicable in the case of complicated (even nonlinear) boundary conditions, where the Galerkin approach would be impossible and the collocation extremely tedious [121].

The first unifying mathematical assessment of the theory of spectral methods was introduced by Gottlieb and Orszag (1977) [128]. Since then, the methods have been extended to cover various problems, such as variable-coefficient and nonlinear equations. Stability and convergence analyses for spectral methods have been based on several approaches. The interpretation of spectral methods as MWR methods (or, in mathematical terms, as variational methods) has proven very successful in the theoretical investigation. It has opened the route for using functional analysis techniques to handle complex problems and obtain the sharpest results.

The idea behind the spectral methods

The spectral methods (approximations) approximate functions (solutions of differential equations, partial differential equations, etc.) employing truncated series of orthogonal functions (polynomials), say $\phi_k, k \in \mathbb{N}$. The well-known Fourier series (for periodic problems) and the series made up of Chebyshev, or Legendre polynomials (for non-periodic problems) are examples of such a series of orthogonal functions.
Roughly speaking, the basic idea behind the spectral methods is to approximate any function employing truncated series of basis functions. In general, a certain function $u(t)$ will be approximated by the finite sum

$$u_N(t) = \sum_{k=0}^{N} c_k \phi_k(t), \quad N \in \mathbb{N}, \tag{2.2.23}$$

where the real (or complex) coefficients c_k are unknown and $\phi_k(t)$ are known and called the basis (trial) functions. A spectral method is characterized by a specific way to determine the coefficients c_k. Depending on the choice of trial functions, one can generate various classes of numerical techniques, such as finite difference and spectral methods. Spectral methods are important due to their high accuracy and fast convergence. In the following, we will introduce spectral methods and consider the $\phi_k(t)$ to be global polynomials. Different types of spectral methods can be introduced according to the selection of basic functions. These methods are divided into three main types: Galerkin, Tau, and Collocation. In this chapter, WRM is described first, and then we introduce the Galerkin, Tau, and Collocation methods.

WRM

The WRM is one of the efficient methods to obtain the approximate solution of functional equations, and are based on the idea of weighted residuals. To express this method, consider the following system

$$\begin{aligned} &Lu = s, \quad in\ \Omega \subseteq \mathbb{R}^n, \\ &Bu = 0, \quad for\ \ on \in \partial\Omega, \end{aligned} \tag{2.2.24}$$

where L is, a linear differential operator and B is a differential operator for boundary conditions. s is a known function and u is the unknown function. A numerical solution of the system (2.2.24) is a function $\bar{u} = \sum_{k=0}^{N} c_k \phi_k(t)$, which satisfies boundary condition of system (2.2.24) and makes the residual

$$R := L\bar{u} - s$$

small. To quantify what this "small" means, the weighted residual method relies on family of $N+1$ tests functions $(\psi_0, ..., \psi_N)$ to define the smallness of the residual R: we ask that the scalar product of R with those functions is exactly zero:

$$\langle \psi_k, R \rangle = 0, \quad k = 0, ..., N.$$

Of course, as N increases, the obtained solution is closer and closer to the real one. Depending on the choice of spectral basis and test functions, one can generate various spectral solvers. In the following, the three most commonly used spectral schemes are presented and applied to a simple case.

A test problem

Consider the equation:

$$\frac{d^2u}{dt^2} - 4\frac{du}{dt} + 4u = e^t - \frac{4e}{1+e^2}, \quad t \in [-1, 1] \tag{2.2.25}$$

with boundary condition

$$u(1) = 0, \quad u(-1) = 0.$$

Under these conditions, the solution is unique and analytical:

$$u(t) = e^t - \frac{sinh(1)}{sinh(2)}e^{2t} + \frac{e}{1+e^2}.$$

The linear operator L is $\frac{d^2}{dt^2} - 4\frac{d}{dt} + 4\mathbb{I}$, ($\mathbb{I}$ is identity matrix). Let us find a numerical solution of (2.2.25) using the five first Chebyshev polynomials

$$\begin{aligned} T_0(t) &= 1, \\ T_1(t) &= t, \\ T_2(t) &= 2t^2 - 1, \\ T_3(t) &= 4t^3 - 3t, \\ T_4(t) &= 8t^4 - 8t^2 + 1. \end{aligned} \tag{2.2.26}$$

with orthogonality condition as follows:

$$\int_{-1}^{1} T_i(t)T_j(t)\frac{1}{\sqrt{1-t^2}}dx = \frac{\pi}{2}(1 + \delta_{0j})\delta_{ij},$$

where $\frac{1}{\sqrt{1-t^2}}$ is the weight function for Chebyshev polynomials.
The unknown function $u(t)$ can approximated by the finite sum

$$\bar{u}(t) = \sum_{k=0}^{4} c_k T_k(t).$$

while $N = 4$.
To expand the source $s(t)$ onto Chebyshev polynomials, we have:

$$s(t) = \sum_{k=0}^{4} \hat{s}_k T_k(t).$$

where from (2.1.5) $\hat{s}_k$ are

$$\hat{s}_k = \frac{\langle s, T_k \rangle_w}{\langle T_k, T_k \rangle_w} = \frac{2}{\pi(1+\delta_{0k})} \int_{-1}^{1} s(t) T_k(t) \frac{dt}{\sqrt{1-t^2}}, \quad k = 0, ..., 4.$$

Therefore

$$\hat{s}_0 = -0.03004, \hat{s}_1 = 1.130, \hat{s}_2 = 0.2715, \hat{s}_3 = 0.04488, \hat{s}_4 = 0.005474$$

Let us recall that if $\bar{u}(t) = \sum\limits_{k=0}^{4} c_k T_k(t)$, then $L\bar{u} = \sum\limits_{k=0}^{4} \sum\limits_{l=0}^{4} c_k A_{kl} T_l(t)$.

$$L = \frac{d^2}{dt^2} - 4\frac{d}{dt} + 4\mathbb{I}.$$

The matrices of derivative operators concerning the Chebyshev basis T_0, T_1, T_2, T_3, T_4 are

$$\frac{d^2}{dt^2} = \begin{bmatrix} 0 & 0 & 4 & 0 & 32 \\ 0 & 0 & 0 & 24 & 0 \\ 0 & 0 & 0 & 0 & 48 \\ 0 & 0 & 0 & 0 & 0 \\ 0 & 0 & 0 & 0 & 0 \end{bmatrix}, \quad \frac{d}{dt} = \begin{bmatrix} 0 & 1 & 0 & 3 & 0 \\ 0 & 0 & 4 & 0 & 8 \\ 0 & 0 & 0 & 6 & 0 \\ 0 & 0 & 0 & 0 & 8 \\ 0 & 0 & 0 & 0 & 0 \end{bmatrix}$$

Therefore the matrix of the differential operator L is

$$A_{kl} = \begin{bmatrix} 4 & -4 & 4 & 12 & 32 \\ 0 & 4 & -16 & 24 & -32 \\ 0 & 0 & 4 & -24 & 48 \\ 0 & 0 & 0 & 4 & -32 \\ 0 & 0 & 0 & 0 & 4 \end{bmatrix}$$

Galerkin method

The Galerkin approach is perhaps the most esthetically pleasing of the methods of weighted residuals since the trial functions, and the test functions are the same. The physical problem can be discretized in terms of a variational principle. Finite-element methods customarily use this approach. Moreover, the first serious application of spectral methods to PDE's-that of Silberman (1954) for meteorological modeling-was a Galerkin method [150]. Recently, [200, 214, 213, 323] applied this method to the problems and developed it as a general method for solving differential equations.

Consider the differential equation (2.2.24). In the Galerkin method, the test functions are equal to basis functions ($\phi_n = \psi_n$). Each ϕ_k satisfy the boundary condition $B\phi = 0$ on $\partial\Omega$. So the smallness condition for the residual reads, for all $n \in \{0, ..., N\}$,

$$\langle\, \phi_n, R \,\rangle = 0 \Longleftrightarrow \langle\, \phi_n, L\bar{u} - s \,\rangle = 0 \Longleftrightarrow$$

$$\langle\, \phi_n, L\sum_{k=0}^{N} c_k\phi_k - s \,\rangle = 0 \Longleftrightarrow \langle\, \phi_n, L\sum_{k=0}^{N} c_k\phi_k \,\rangle - \langle\, \phi_n, s \,\rangle = 0$$

$$\sum_{k=0}^{N} c_k \langle\, \phi_n, L\phi_k \,\rangle - \langle\, \phi_n, s \,\rangle = 0 \Longleftrightarrow \sum_{k=0}^{N} c_k L_{nk} = \langle \phi_n, s \,\rangle \tag{2.2.27}$$

where L_{nk} denotes the matrix $L_{nk} = \langle\, \phi_n, L\phi_k \,\rangle$.
Solving for the linear system (2.2.27) leads to the $(N+1)$ coefficients c_k of $\bar{u}$. By placing the coefficients of c_k in relation (2.2.23), the approximate value of u is obtained.

The basic idea of the Galerkin method is to expand the solution, not in terms of usual orthogonal polynomials, but of some linear combinations of polynomials that fulfill the boundary conditions. It is usually better if the Galerkin basis can be easily written in terms of the original basis.

For the considered equation (2.2.25), we have the following Galerkin basis:

$$\begin{aligned} &\phi_0(t) = T_2(t) - T_0(t) = 2t^2 - 2, \\ &\phi_1(t) := T_3(t) - T_1(t) = 4t^3 - 4t, \\ &\phi_2(t) := T_4(t) - T_0(t) = 8t^4 - 8t^2, \end{aligned} \tag{2.2.28}$$

- Each of the ϕ_i, $i = 0, 1, 2$ satisfies the boundary conditions: $\phi_i(1) = \phi_i(-1) = 0$. Note that the ϕ_i are not orthogonal.

Let us first expand the Galerkin basis $\phi_i(t)$ onto the Chebyshev polynomials:

$$\phi_i(t) = \sum_{k=0}^{4} \hat{\phi}_{ki} T_k(t), \quad \forall i \leqslant N-2,$$

where

$$\hat{\phi}_{ki} = \begin{bmatrix} -1 & 0 & -1 \\ 0 & -1 & 0 \\ 1 & 0 & 0 \\ 0 & 1 & 0 \\ 0 & 0 & 1 \end{bmatrix}$$

Chebyshev coefficients and Galerkin coefficients:

$$\bar{u}(t) = \sum_{k=0}^{4} c_k T_k(t) = \sum_{i=0}^{2} \hat{c}_i^{\phi} \phi_i(t)$$

The matrix $\hat{\phi}_{ki}$ relates the two sets of coefficients via the matrix product $C = \Phi \times \hat{C}^{\phi}$. For the Galerkin method, the test functions are equal to the trial functions so that the condition of small residual writes:

$$\langle \phi_i, L\bar{u} - s \rangle = 0 \Longleftrightarrow \sum_{j=0}^{2} \langle \phi_i, L\phi_j \rangle \hat{c}_j^{\phi} = \langle \phi_i, s \rangle$$

with

$$\langle \phi_i, L\phi_j \rangle = \sum_{k=0}^{4}\sum_{l=0}^{4} \langle \hat{\phi}_{ki} T_k, L\hat{\phi}_{lj} T_l \rangle = \sum_{k=0}^{4}\sum_{l=0}^{4} \hat{\phi}_{ki}\hat{\phi}_{lj} \langle T_k, LT_l \rangle$$

$$\sum_{k=0}^{4}\sum_{l=0}^{4} \hat{\phi}_{ki}\hat{\phi}_{lj} \langle T_k, \sum_{m=0}^{4} A_{ml} T_m \rangle = \sum_{k=0}^{4}\sum_{l=0}^{4} \hat{\phi}_{ki}\hat{\phi}_{lj} \sum_{m=0}^{4} A_{ml} \langle T_k, T_m \rangle$$

$$\sum_{k=0}^{4}\sum_{l=0}^{4} \hat{\phi}_{ki}\hat{\phi}_{lj} \frac{\pi}{2}(1+\delta_{0k}) A_{kl} = \frac{\pi}{2} \sum_{k=0}^{4}\sum_{l=0}^{4} (1+\delta_{0k}) \hat{\phi}_{ki} A_{kl} \hat{\phi}_{lj}$$

In the above expression appears the transpose matrix

$$Q_{ik} = [(1+\delta_{0k})\hat{\phi}_{ki}]^T = \begin{bmatrix} -2 & 0 & 1 & 0 & 0 \\ 0 & -1 & 0 & -1 & 0 \\ -2 & 0 & 0 & 0 & 1 \end{bmatrix}$$

The small residual condition amounts then to solve the following linear system in $\hat{C}^\phi = (\hat{c}_0^\phi, \hat{c}_1^\phi, \hat{c}_2^\phi)$:

$$Q \times A \times \Phi \times \hat{C}^\phi = Q \times \hat{s}$$

i.e.

$$\begin{bmatrix} 4 & -8 & -8 \\ 16 & -16 & 0 \\ 0 & 16 & -52 \end{bmatrix} \begin{bmatrix} \hat{c}_0^\phi \\ \hat{c}_1^\phi \\ \hat{c}_2^\phi \end{bmatrix} = \begin{bmatrix} 0521 \\ -1.70 \\ 0.103 \end{bmatrix}$$

The coefficients of the solution with 4 significant digits, are $\hat{c}_0^\phi = -0.1596, \hat{c}_1^\phi = -0.09176, \hat{c}_2^\phi = -0.02949$. Therefore, the Chebyshev coefficients are obtained by taking the matrix product by $c_0 = 0.1891, c_1 = 0.09176, c_2 = -0.1596, c_3 = -0.09176, c_4 = -0.02949$

Tau method

The tau approach is a modification of the Galerkin method that applies to problems with non-periodic boundary conditions. It may be viewed as a special case of the Petrov-Galerkin method. It has proven useful for constant coefficient problems or subproblems, e.g., for semi-implicit time-stepping algorithms. Tau method for fractional differential equations has been employed in the works [211, 326].

In this method, the test functions ψ_k are chosen to be the same as the spectral functions of decomposition, but the ϕ_k do not satisfy the boundary conditions i. e. $B\phi_n \neq 0$ on $\partial\Omega$. Therefore, these conditions are enforced by an additional set of equations. Let (g_p) be an orthonormal basis of $M+1 < N+1$ functions on the boundary $\partial\Omega$ and let us expand $B\phi_n$ for $a \in \partial\Omega$ upon it:

$$B\phi_k(a) = \sum_{p=0}^{M} b_{pk} g_p(a)$$

The boundary condition then becomes

$$Bu(a) = 0 \iff \sum_{k=0}^{N} \sum_{p=0}^{M} c_k b_{pk} g_p(a) = 0$$

hence the $M+1$ conditions:

$$\sum_{k=0}^{N} c_k b_{pn} = 0, \;\; 0 \leqslant p \leqslant M$$

The system of linear equations for the $N+1$ coefficients c_k is then taken to be the $N-M$ first raws of the Galerkin system (2.2.27) plus the $M+1$ equations above:

$$\begin{aligned} &\sum_{k=0}^{N} c_k L_{nk} = \langle \phi_n, s \rangle, \quad 0 \leqslant n \leqslant N-M-1 \\ &\sum_{k=0}^{N} c_k b_{pk} = 0, \;\; 0 \leqslant p \leqslant M \end{aligned} \tag{2.2.29}$$

Solving for the linear system (2.2.29) leads to the $(N+1)$ coefficients c_k of $\bar{u}$.

For the considered equation (2.2.25), by using Tau method, trial functions are equal to test functions and Chebyshev polynomials T_0, T_1, T_2, T_3, T_4. Since $T_k(-1) = (-1)^k$ and $T_k(1) = 1$, the boundary condition operator has the matrix

$$\big(b_{pk}\big)_{p=\{1,2\},k=\{1,..,4\}} = \begin{bmatrix} 1 & -1 & 1 & -1 & 1 \\ 1 & 1 & 1 & 1 & 1 \end{bmatrix}.$$

The Tau system is obtained by replacing the last two rows of the matrix L by $\big(b_{pk}\big)$:

$$\begin{bmatrix} 4 & -4 & 4 & 12 & 32 \\ 0 & 4 & -16 & 24 & -32 \\ 0 & 0 & 4 & -24 & 48 \\ 1 & -1 & 1 & -1 & 1 \\ 1 & 1 & 1 & 1 & 1 \end{bmatrix} \begin{bmatrix} c_0 \\ c_1 \\ c_2 \\ c_3 \\ c_4 \end{bmatrix} = \begin{bmatrix} \hat{s}_0 \\ \hat{s}_1 \\ \hat{s}_2 \\ 0 \\ 0 \end{bmatrix}.$$

The coefficients of the solution with 4 significant digits, are $c_0 = 0.1456, c_1 = 0.07885, c_2 = -0.1220, c_3 = -0.07885, c_4 = -0.02360$

Collocation method

The collocation approach is the simplest within MWR methods. It was introduced and applied by Slater (1934) and Kantorovic (1934) in specific applications. Frazer, Jones, and Skan (1937) developed it as a general method for solving ODEs. They used a variety of trial functions and an arbitrary distribution of collocation points. For the first time, Lanczos (1938) established that a proper choice of trial functions and distribution of collocation points are crucial to the accuracy of the solution. Perhaps he should be credited with laying down the foundation of the orthogonal collocation method. Several investigators have discussed this method and its application [105, 66, 210, 307, 308].
In this method, the test functions are represented by delta functions at special points, called collocation points, i.e., $\psi_k = \delta(x - x_k)$. In other words, the residual converges to zero at a collocation set of points.The smallness condition for the residual reads, for all $n \in \{0, .., N\}$,

$$\langle \psi_n, R \rangle = 0 \Longleftrightarrow \langle \delta(x - x_n), R \rangle = 0 \Longleftrightarrow$$

$$R(x_n) = 0 \Longleftrightarrow L\bar{u}(x_n) = s(x_n) \Longleftrightarrow \sum_{k=0}^{N} L\phi_k(x_n)c_k = s(x_n) \tag{2.2.30}$$

The boundary condition is imposed as in the Tau method. One then drops $M+1$ raws in the linear system (2.2.30) and solve the system:

$$\begin{array}{l} \sum\limits_{k=0}^{N} L\phi_k(x_n)c_k = s(x_n), \quad 0 \leqslant n \leqslant N-M-1 \\ \sum\limits_{k=0}^{N} c_k b_{pk} = 0, \;\; 0 \leqslant p \leqslant M \end{array} \tag{2.2.31}$$

Solving for the linear system (2.2.31) leads to the $(N+1)$ coefficients c_k of $\bar{u}$.

For the considered equation (2.2.25), by using Collocation method, trial functions are equal to Chebyshev polynomials T_0, T_1, T_2, T_3, T_4 and test functions are $\delta(t-t_k)$. The Collocation system is

$$\sum_{k=0}^{4} LT_k(t_n)c_k = s(x_n) \Longleftrightarrow \sum_{k=0}^{4}\sum_{l=0}^{4} A_{lk}T_l(t_n)c_k = s(t_n).$$

From a matrix point of view: $T \times A \times C = s$, where

$$T_l(t_n) = \big(T_{nl}\big) = \begin{bmatrix} 1 & -1 & 1 & -1 & 1 \\ 1 & \frac{-1}{\sqrt{2}} & 0 & \frac{1}{\sqrt{2}} & -1 \\ 1 & 0 & -1 & 0 & -1 \\ 1 & \frac{1}{\sqrt{2}} & 0 & \frac{-1}{\sqrt{2}} & -1 \\ 1 & 1 & 1 & 1 & 1 \end{bmatrix}.$$

To take into account the boundary conditions, replace the first row of the matrix $T \times A$ by b_{0k} and the last row by b_{1k}, and end up with the system

$$\begin{bmatrix} 1 & -1 & 1 & -1 & 1 \\ 4 & -6.82 & 15.3 & -26.1 & 28 \\ 4 & -4 & 0 & 12 & -12 \\ 4 & -1.17 & -7.31 & 2.14 & 28 \\ 1 & 1 & 1 & 1 & 1 \end{bmatrix} \begin{bmatrix} c_0 \\ c_1 \\ c_2 \\ c_3 \\ c_4 \end{bmatrix} = \begin{bmatrix} 0 \\ s(t_1) = -0.80 \\ s(t_2) = -0.30 \\ s(t_3) = 0.73 \\ 0 \end{bmatrix}.$$

The coefficients of the solution with 4 significant digits, are $c_0 = 0.1875, c_1 = 0.08867, c_2 = -0.1565, c_3 = -0.8867, c_4 = -0.03104$.

Part I

Numerical solution of ordinary differential equations

Chapter 3

Exponentially fitted two-step peer methods for oscillatory problems

This chapter introduces implicit EF peer methods for the numerical solution of ODEs that exhibit oscillatory solutions. The methods are derived by following a six-step procedure presented in the previous chapter, and [158]. The strategy is to adapt existing methods to be exact on trigonometric or hyperbolic functions. The last step of the procedure is to compute the leading term of the local truncation error. This could lead to an estimate of the parameter characterizing the basis functions, as shown in Chapter 5. The chapter includes numerical experiments that have shown the effectiveness of the approach.

Therefore, we are interested in the numerical solution of initial value problems for ODEs exhibiting oscillatory solutions. Classical numerical integrators could require a very small step size to follow the oscillations, especially when the frequency increases. To develop efficient and accurate numerical methods, we propose an adapted numerical integration based on exploiting a-priori known information about the behavior of the exact solution, utilizing exponential fitting strategy [158]. We combine this feature with the usage of peer methods, which represent a highly structured subclass of General Linear Methods [166] and are identified with several distinct stages, such as Runge-Kutta methods.

Peer methods have been introduced in the linearly-implicit form in [266]. Explicit peer methods have been derived in [179, 265, 270, 313], while implicit peer methods are described in [26, 242, 268, 269, 271, 286]. The attribute “peer" means that all s stages have the same good accuracy properties. A linearly-implicit implementation using only one Newton-step is possible for implicit methods since accurate predictors are easily available [266]. Moreover, as the internal stages are external variables, the stage order is equal to the order. Therefore implicit peer methods are quite efficient for stiff problems since they do not show order reduction like one-step methods but still allow easy stepsize control due to the two-step structure [267, 271, 286]. Furthermore, they

have good stability properties in comparison with other multistep methods. In other words, peer methods combine the benefits of the Runge-Kutta and multistep approach, thus obtaining good stability properties without reducing orders for very stiff systems [269]. Moreover, for suitable choice of the parameters, these methods have an inherent parallelism across the method [266, 271]. This feature may be very useful in discretizing PDEs when the number of spatial points increases (see [120] for applications of peer methods to large-scale problems).

We combine peer methods with exponential fitting strategy [158] to obtain more convenient formulae for solving oscillatory problems. Classical peer methods are developed to be exact (within round-off error) on polynomials up to a certain degree. We propose EF peer methods, which are constructed to be exact on functions other than polynomials. The basis functions are normally supposed to belong to a finite-dimensional space $\mathcal{F}_q = \{\phi_0(t), \phi_1(t), \ldots, \phi_q(t)\}$ called fitting space and are selected according to the a-priori known information concerning the behavior of the exact solution. As a result, the coefficients of the corresponding methods are no longer constant as in the classic case but depend on parameters characterizing the exact solution (i.e., the frequency of oscillation), whose values may be unknown. Hence, the exponential fitting technique requires choosing a suitable fitting space and estimation or the computation of the aforementioned parameters.

By following [158], the exponential fitting strategy has led to EF methods for a wide range of problems such as interpolation, numerical differentiation, and quadrature [72, 76, 78, 79, 154, 156, 176, 177, 297], numerical solution of integral equations [55, 56, 57, 58], PDEs [96, 97, 100, 99] and ODEs [50, 94, 98, 280, 281, 300, 301]. In particular, 2-step hybrid exponentially fitted methods are proposed for integrating second-order differential equations in [90, 93]. In contrast, various estimates for the parameter characterizing the coefficients of the methods are presented in [91, 92, 96]. Adapted Runge-Kutta methods are introduced in [91, 95, 99, 101, 155, 158, 233, 236, 280, 281]. In [233], it has been shown that for any fitting space $\mathcal{F}_q$ of smooth linearly independent real functions, there exists a q-stage Runge-Kutta method fitted to $\mathcal{F}_q$. However, the stage order of a Runge-Kutta method influences the highest dimension that can be achieved by the fitting space, especially in the case of explicit Runge-Kutta methods. For instance, in [300], an explicit four-stage RK method has been constructed on a fitting space having the maximum dimension equal to 3. By contrast, linear multistep methods do not impose such a strong dimensional limit, as shown in [119]. Indeed, a k-step method can be fitted on a $k+1$-dimensional fitting space. EF peer methods, which can combine the advantages of Runge-Kutta and multistep methods, have been derived in [73, 77], where explicit EF peer methods having order equal to the number of stages have been developed. Other families of adapted peer methods have been constructed in [51, 212].

In this chapter, we develop a general class of EF implicit peer method having order

equal to the number of stages and lower triangular coefficients matrix by employing the six-step procedure described in [158].

This chapter focuses on developing and implementing EF implicit peer methods for the numerical solution of ODEs with oscillatory or periodic solutions. We aim to comprehensively understand these methods, their construction, and their performance. Section 3.1 gives a brief overview of classical implicit peer methods to provide a foundation for developing EF peer methods. Section 3.2 outlines the construction of implicit EF peer methods adapted to a general fitting space, which is a crucial step in developing these methods. In Section 3.3, several examples of EF peer methods with 2 and 3 stages are presented to demonstrate these methods' versatility and ability to solve different types of problems. The experimental results of these methods are presented in Section 3.4, providing valuable insights into the performance of these methods and their accuracy and efficiency. Finally, Section 3.5 summarizes the results of the chapter and concludes by highlighting the importance of implicit EF peer methods.

3.1 Classical implicit peer methods

Consider initial value problems for ODEs of the form

$$y'(t) = f(t, y(t)), \quad y(t_0) = y_0 \in \mathcal{R}^d, \quad t \in [t_0, T], \tag{3.1.1}$$

where $f : \mathcal{R} \times \mathcal{R}^d \to \mathcal{R}^d$ is smooth enough to guarantee the solution's existence and uniqueness. We suppose that for any stepsize $h > 0$ there exists a starting procedure to approximate the solution in the internal grid points $t_{0i} = t_0 + c_i\, h,\ i = 1, \ldots, s$. We consider s-stage two-step peer methods with fixed stepsize h, that have the following expression:

$$\begin{aligned} Y_{ni} &= \sum_{j=1}^{s} b_{ij}\ Y_{n-1,j} + h \sum_{j=1}^{s} a_{ij}\ f(t_{n-1,j}, Y_{n-1,j}) + h \sum_{j=1}^{i} r_{ij}\ f(t_{nj}, Y_{nj}), \\ & i = 1, \ldots, s \end{aligned} \tag{3.1.2}$$

where

$$Y_{ni} \approx y(t_{ni}), \quad t_{ni} = t_n + c_i\, h, \quad i = 1, \ldots, s.$$

No extra ordinary numerical solution with different properties is computed: in peer methods it is assumed that $c_s = 1$, so Y_{ns} is the approximation of the solution at grid point t_{n+1}. The other nodes are chosen such that $c_i < 1$ for $i = 1, \ldots, s-1$.

3.1.1 Order conditions:

For simplicity of notation, from now on, we assume that problem (3.1.1) is scalar, and we employ the following notation:

$$\begin{aligned} Y_n &= [Y_{ni}]_{i=1}^{s}\,, F(Y_n) = [f(t_{ni}, Y_{ni})]_{i=1}^{s}\,, \\ A &= [a_{ij}]_{i,j=1}^{s}\,, B = [b_{ij}]_{i,j=1}^{s}\,, R = [r_{ij}]_{i,j=1}^{s}\,, \end{aligned}$$

where A and B are full matrices and R is a lower triangular matrix. A compact representation of the method (3.1.2) is as follows:

$$Y_n = B\,Y_{n-1} + h\,A\,F(Y_{n-1}) + h\,R\,F(Y_n). \tag{3.1.3}$$

The matrices of coefficients A, B, and R are constructed to achieve high order (uniformly for all components Y_{ni}) and good stability properties. We consider singly implicit methods, i.e. the matrix R is lower triangular with $r_{\rm ii} = \gamma \geqslant 0$ (when $\gamma = 0$ we have an explicit method). We recall that the method (3.1.2) has the order of consistency p if $\Delta_{ni} = \mathcal{O}(h^p)$ for $i = 1, \ldots, s$, where Δ_{ni} is the residual obtained by inserting the exact solution in the numerical scheme (3.1.2). Schmitt and Weiner in [266] have related this property to the simplifying condition

$$\begin{aligned} \mathrm{AB}(q) = c_i^m - \sum_{j=1}^{s} b_{ij}\,(c_j-1)^m - m\sum_{j=1}^{s} a_{ij}\,(c_j-1)^{m-1} - m\sum_{j=1}^{i} r_{ij}\,c_j^{m-1} = 0, \\ m = 0, \ldots, q-1,\ i = 1, \ldots, s \end{aligned} \tag{3.1.4}$$

as follows:

Theorem 8. *If* AB$(p+1)$ *is verified, the implicit* s*-stage peer method* (3.1.2) *has order of consistency* p*.*

Corollary 3.1.1. *The peer method* (3.1.2) *has order* $p \geqslant s$ *if*

$$B\,\mathbf{1} = \mathbf{1}, \tag{3.1.5a}$$

$$AV_1D \;\; = CV_0 - B\,(C - \mathbb{I})V_1 - RV_0D, \tag{3.1.5b}$$

where $\mathbf{1} = [1, 1, \ldots, 1]^T$*,* $C = diag(c_1, \ldots, c_s)$*,* $D = diag(1, \ldots, s)$ *and*

$$V_0 = \begin{bmatrix} 1 & c_1 & \ldots & c_1^{s-1} \\ \vdots & \vdots & \vdots & \vdots \\ 1 & c_s & \ldots & c_s^{s-1} \end{bmatrix}, \quad V_1 = \begin{bmatrix} 1 & (c_1-1) & \ldots & (c_1-1)^{s-1} \\ \vdots & \vdots & \vdots & \vdots \\ 1 & (c_s-1) & \ldots & (c_s-1)^{s-1} \end{bmatrix}.$$

3.2 EF implicit peer methods

In order to construct EF-implicit peer methods we first of all consider the fitting space as follows:

$$\mathcal{F} = \left\{1, t, t^2, \ldots, t^K, e^{\pm\mu t}, t\,e^{\pm\mu t}, t^2e^{\pm\mu t}, \ldots, t^Pe^{\pm\mu t}\right\}, \tag{3.2.6}$$

where μ is a parameter characterizing the exact solution and it is real or imaginary, if the exact solution belongs to the space spanned by hyperbolic functions or trigonometric functions, respectively. Additionally, assume that $K = -1$ if there are no classical components and $P = -1$, if there are not exponential fitting ones.

We then define the linear operator as the residual obtained by inserting the exact solution in the method (3.1.2) as follows:

$$\begin{aligned}\mathcal{L}_i[h,\mathbf{w}]\, y(t) = y(t+c_i\,h) - \sum_{j=1}^{s} b_{ij}\; y(t+(c_j-1)\,h) \\ - h\sum_{j=1}^{s} a_{ij}\; y'(t+(c_j-1)\,h) - h\sum_{j=1}^{i} r_{ij}\; y'(t+c_j\,h),\; i=1,\ldots,s,\end{aligned} \tag{3.2.7}$$

where $\mathbf{w}$ contains the coefficients of the method. The method (3.1.2) is adapted to the fitting space $\mathcal{F}$ if the difference operator (3.2.7) annihilates on these basis functions. This procedure leads to a system having the coefficients of the method as unknowns, because of the dependence of the difference operator on such coefficients. These basic concepts have given raise to the six-step algorithm presented in [158] which we use below for the construction of desidered adapted peer method (3.1.2).

Step 1

Here, by using the linear difference operator (3.2.7) associated to the implicit peer method (3.1.2), we construct the dimensionless classic moments

$$\mathcal{L}^*_{i\,m}(h,\mathbf{w}) = \frac{1}{h^m}\mathcal{L}_i[h,\mathbf{w}]t^m|_{t=0}, \quad i=1,\ldots,s, \tag{3.2.8}$$

which have the form:

$$\begin{aligned}\mathcal{L}^*_{i\,m}(h,\mathbf{w}) = c_i^m - \sum_{j=1}^{s} b_{ij}\;(c_j-1)^m - m\sum_{j=1}^{s} a_{ij}\;(c_j-1)^{m-1} - m\sum_{j=1}^{i} r_{ij}\;c_j^{m-1}, \\ \text{for}\;\; i=1,\ldots,s, \quad m=0,1,\ldots,M-1.\end{aligned} \tag{3.2.9}$$

Step 2

We now look for the maximum value M that ensures the compatibility of the system

$$\mathcal{L}^*_{i\,m}(h,\mathbf{w}) = 0, \quad i=1,\ldots,s, \quad m=0,1,\ldots,M-1, \tag{3.2.10}$$

which is equivalent to annihilating the difference operator (3.2.7) on polynomials with a degree less or equal to $M-1$. This system corresponds to the simplifying condition (3.1.4) with $q=M$

$$\begin{aligned}\mathrm{AB}(M) = c_i^m - \sum_{j=1}^{s} b_{ij}\;(c_j-1)^m - m\sum_{j=1}^{s} a_{ij}\;(c_j-1)^{m-1} \\ - m\sum_{j=1}^{i} r_{ij}\;c_j^{m-1} = 0, i=1,\ldots,s, \quad m=0,\ldots,M-1.\end{aligned} \tag{3.2.11}$$

Therefore, we may construct an s-order peer method if $M=s+1$, due to the Theorem 15 and Corollary 3.1.1.

Step 3

Annihilating the difference operator (3.2.7) on the functions $t^m e^{\pm\mu t}$ is equivalent to annihilating in $\pm z$ the so-called dimensionless μ-moments of order m

$$E^*_{i\,m}(z,\mathbf{w}) = \frac{1}{h^m}\mathcal{L}_i[h,\mathbf{w}]t^m e^{\mu t}|_{t=0}, \quad i=1,\dots,s, \tag{3.2.12}$$

where $z=\mu h$. We next exploit that the system

$$E^*_{i\,m}(\pm z,\mathbf{w}) = 0, \quad m=0,1,\dots,P, \quad i=1,\dots,s,$$

is equivalent to the system

$$G_i^{\pm(m)}(Z,\mathbf{w}) = 0, \quad m=0,1,\dots,P, \quad i=1,\dots,s,$$

where $Z=z^2$ and $G_i^{\pm(m)}(Z,\mathbf{w})$ are the $G-$functions at each stage i

$$G_i^+(Z,\mathbf{w}) = \frac{E^*_{i0}(z,w)+E^*_{i0}(-z,w)}{2},\ G_i^-(Z,\mathbf{w}) = \frac{E^*_{i0}(z,w)-E^*_{i0}(-z,w)}{2z}, \tag{3.2.13}$$

for $m=0$ and the related derivatives for $m>0$. In the following theorem, we find an explicit expression for the μ-moments of order $m=0$ on $\mathcal{L}$.

Theorem 9. *The μ-moments of order $m=0$ assume the following form:*

$$\begin{aligned} E^*_{i0}(z,\mathbf{w}) = e^{zc_i} - \sum_{j=1}^{s} b_{ij}\ e^{z\,(c_j-1)} - z\sum_{j=1}^{s} a_{ij}\ e^{z\,(c_j-1)} \\ - z\sum_{j=1}^{i} r_{ij}\ e^{z\,c_j}, \quad i=1,\dots,s. \end{aligned} \tag{3.2.14}$$

Proof. Applying (3.2.12) with $m=0$ and $i=1,\dots,s$, we obtain

$$\begin{aligned} E^*_{i0}(z,\mathbf{w}) = \mathcal{L}_i[h,\mathbf{w}]e^{\mu t}|_{t=0} = e^{\mu\,(t+c_i h)} - \sum_{j=1}^{s} b_{ij}\ e^{\mu\,(t+(c_j-1)\,h)} \\ - h\sum_{j=1}^{s} a_{ij}\ \mu\, e^{\mu\,(t+(c_j-1)\,h)} - h\sum_{j=1}^{i} r_{ij}\ \mu\, e^{\mu\,(t+c_j h)}\Big|_{t=0}, \end{aligned}$$

which leads to the thesis by replacing $z=\mu h$ and $t=0$. □

For a simpler construction of G-functions, we employ the η-functions defined in [158] and recalled in the Section 2.2.1 of Chapter 2. In the following theorem, we express the G-functions and their derivatives in terms of the η-functions.

Theorem 10. *The G-functions and their derivatives assume the following expressions for $i = 1, \ldots, s$:*

$$\begin{aligned} G_i^+(Z, \mathbf{w}) = \eta_{-1}\left(c_i^2 Z\right) - \sum_{j=1}^{s} b_{ij}\, \eta_{-1}\left((c_j-1)^2 Z\right) \\ - Z \sum_{j=1}^{s} a_{ij}\,(c_j-1)\,\eta_0\left((c_j-1)^2 Z\right) - Z \sum_{j=1}^{i} r_{ij}\, c_j\, \eta_0\left(c_j^2 Z\right) \end{aligned} \tag{3.2.15}$$

$$\begin{aligned} G_i^-(Z, \mathbf{w}) = c_i\, \eta_0\left(c_i^2 Z\right) - \sum_{j=1}^{s} b_{ij}\,(c_j-1)\,\eta_0\left((c_j-1)^2 Z\right) \\ - \sum_{j=1}^{s} a_{ij}\, \eta_{-1}\left((c_j-1)^2 Z\right) - \sum_{j=1}^{i} r_{ij}\, \eta_{-1}\left(c_j^2 Z\right), \end{aligned} \tag{3.2.16}$$

$$\begin{aligned} G_i^{+(m)}(Z, \mathbf{w}) = \frac{c_i^{2m}}{2^m}\eta_{m-1}\left(c_i^2 Z\right) - \sum_{j=1}^{s} b_{ij}\, \frac{(c_j-1)^{2m}}{2^m}\eta_{m-1}\left((c_j-1)^2 Z\right) \\ - \sum_{j=1}^{s} a_{ij}\, \left[\frac{m\,(c_j-1)^{2m-1}}{2^{m-1}}\eta_{m-1}\left((c_j-1)^2 Z\right)\right. \\ \left. + \frac{(c_j-1)^{2m+1}}{2^m}\, Z\, \eta_m\left((c_j-1)^2 Z\right)\right] \\ - \sum_{j=1}^{i} r_{ij}\, \left[\frac{m\, c_j^{2m-1}}{2^{m-1}}\eta_{m-1}\left(c_j^2 Z\right) + \frac{c_j^{2m+1}}{2^m} Z \eta_m\left(c_j^2 Z\right)\right], \\ m = 1, \ldots, P, \end{aligned} \tag{3.2.17}$$

$$\begin{aligned} G_i^{-(m)}(Z, \mathbf{w}) = \frac{c_i^{2m+1}}{2^m}\eta_m\left(c_i^2 Z\right) - \sum_{j=1}^{s} b_{ij}\, \frac{(c_j-1)^{2m+1}}{2^m}\eta_m\left((c_j-1)^2 Z\right) \\ - \sum_{j=1}^{s} a_{ij}\, \frac{(c_j-1)^{2m}}{2^m}\eta_{m-1}\left((c_j-1)^2 Z\right) \\ - \sum_{j=1}^{i} r_{ij}\, \frac{c_j^{2m}}{2^m}\eta_{m-1}\left(c_j^2 Z\right),\ m = 1, \ldots, P. \end{aligned} \tag{3.2.18}$$

Proof. From the defintion (3.2.13) of the G-functions and the expression of the μ-moments E_{i0}^* obtained in Theorem (9), we have

$$\begin{aligned} G_i^+(Z, \mathbf{w}) = \frac{1}{2}\left(e^{z\,c_i} + e^{-z\,c_i}\right) - \frac{1}{2}\sum_{j=1}^{s} b_{ij}\, \left(e^{z\,(c_j-1)} + e^{-z\,(c_j-1)}\right) \\ - \frac{z}{2}\sum_{j=1}^{s} a_{ij}\, \left(e^{z\,(c_j-1)} - e^{-z\,(c_j-1)}\right) - \frac{z}{2}\sum_{j=1}^{i} r_{ij}\, \left(e^{z\,c_j} - e^{-z\,c_j}\right), \end{aligned} \tag{3.2.19}$$

which leads to Eq. (3.2.15) by evaluating functions η_{-1} and η_0 in $c_i^2 Z$ and $(c_j-1)^2 Z$, where $Z = z^2$.
Eq. (3.2.16) can be proved in a similar way.
We next derive function G_i^+ (3.2.15) taking into account the relation (2.2.17) among the derivatives of $\eta-$functions, obtaining

$$\begin{aligned} G_i^{+(1)}(Z,w) = & \frac{c_i^2}{2}\eta_0\left(c_i^2 Z\right) - \sum_{j=1}^{s} b_{ij}\,\frac{(c_j-1)^2}{2}\eta_0\left((c_j-1)^2 Z\right) \\ & - \sum_{j=1}^{s} a_{ij}\,\left[(c_j-1)\,\eta_0\left((c_j-1)^2 Z\right) + \frac{(c_j-1)^3}{2} Z\,\eta_1\left((c_j-1)^2 Z\right)\right] \\ & - \sum_{j=1}^{i} r_{ij}\,\left[c_j\,\eta_0\left(c_j^2 Z\right) + \frac{c_j^3}{2} Z\,\eta_1\left(c_j^2 Z\right)\right], \end{aligned} \tag{3.2.20}$$

so Eq. (3.2.17) is proved for $m = 1$. We get Eq. (3.2.17) for $m > 1$ by induction.
On the other hand, the first derivative of G_i^- (3.2.16) is

$$\begin{aligned} G_i^{-(1)}(Z,w) = & \frac{c_i^3}{2}\,\eta_1\left(c_i^2 Z\right) - \sum_{j=1}^{s} b_{ij}\,\frac{(c_j-1)^3}{2}\,\eta_1\left((c_j-1)^2 Z\right) \\ & - \sum_{j=1}^{s} a_{ij}\,\frac{(c_j-1)^2}{2}\eta_0\left((c_j-1)^2 Z\right) - \sum_{j=1}^{i} r_{ij}\,\frac{c_j^2}{2}\,\eta_0\left(c_j^2 Z\right), \end{aligned} \tag{3.2.21}$$

which leads to Eq. (3.2.18) for $m > 1$ by induction. □

Step 4

We construct the possible expressions for the fitting space (3.2.6) taking into account that $M = s + 1$ and the self-consistency condition

$$K + 2P = M - 3 \tag{3.2.22}$$

has to be verified. We observe that the number of stages s and the dimension M of the system (3.2.10) are of different parities, so the the number $K + 1 = s - 1 - 2P$ of classic functions in the fitting space is odd or even, if s is even or odd, respectively.
For simplicity, we choose

- $K = 0$ if s is even, so the fitting space is

$$\mathcal{F} = \left\{1, e^{\pm\mu t}, t\,e^{\pm\mu t}, t^2\,e^{\pm\mu t}, \ldots, t^P\,e^{\pm\mu t}\right\}; \tag{3.2.23}$$

- $K = -1$ if s is odd, so the fitting space is

$$\mathcal{F} = \left\{e^{\pm\mu t}, t\,e^{\pm\mu t}, t^2\,e^{\pm\mu t}, \ldots, t^P\,e^{\pm\mu t}\right\}. \tag{3.2.24}$$

Step5

We obtain the coefficients of the EF peer method by solving the system:

$$\mathcal{L}^*_{i\,m}(h,\mathbf{w}) = 0, \quad i = 1,\dots,s, \quad m = 0,\dots,K, \tag{3.2.25a}$$

$$G_i^{\pm(m)}(Z,\mathbf{w}) = 0, \quad i = 1,\dots,s, \quad m = 0,\dots,P. \tag{3.2.25b}$$

Remark 1. *For the afore-mentioned fitting spaces* (3.2.23)-(3.2.24)*, the system* (3.2.25a)-(3.2.25b) *becomes:*

- *if s is even*

$$\mathcal{L}^*_{i0}(h,\mathbf{w}) = 0, \quad i = 1,\dots,s \tag{3.2.26a}$$

$$G_i^{\pm(m)}(Z,\mathbf{w}) = 0, \quad i = 1,\dots,s, \quad m = 0,\dots,P, \tag{3.2.26b}$$

where $P = \dfrac{s}{2} - 1, K = 0$ due to the self-consistency condition (3.2.22)*.*

- *if s is odd*

$$G_i^{\pm(m)}(Z,\mathbf{w}) = 0, \quad i = 1,\dots,s, \quad m = 0,\dots,P, \tag{3.2.27}$$

where $P = \dfrac{s-1}{2}, K = -1$ due to the self-consistency condition (3.2.22)*.*

We recast such systems in order to drive the coefficients of exponentially fitted peer methods.

Theorem 11. *Assume s is even. The peer method* (3.1.2) *has order $p = s$ and is adapted to the fitting space*

$$\mathcal{F} = \left\{1, e^{\pm\mu t}, t\,e^{\pm\mu t}, t^2 e^{\pm\mu t}, \dots, t^{\frac{s}{2}-1} e^{\pm\mu t}\right\},$$

if the coefficient matrices A and B satisfy

$$B\,\mathbf{1} = \mathbf{1}, \tag{3.2.28a}$$

$$AD_3 \;= D_1 - B\,D_2 - RD_4, \tag{3.2.28b}$$

where $\mathbf{1} = [1,1,\dots,1]^T$, and

$$D_1 = \begin{bmatrix} \dots & \dfrac{1}{2^i}\,c_1^{2i}\,\eta_{i-1}\left(c_1^2\,Z\right) & \dfrac{1}{2^i}c_1^{2i+1}\,\eta_i\left(c_1^2\,Z\right) & \dots \\ & \vdots & \vdots & \\ \dots & \dfrac{1}{2^i}\,c_s^{2i}\,\eta_{i-1}\left(c_s^2\,Z\right) & \dfrac{1}{2^i}c_s^{2i+1}\,\eta_i\left(c_s^2\,Z\right) & \dots \end{bmatrix},$$

$$D_2 = \begin{bmatrix} \dots & \dfrac{1}{2^i}\,\hat{c}_1^{2i}\,\eta_{i-1}\left(\hat{c}_1^2\,Z\right) & \dfrac{1}{2^i}\hat{c}_1^{2i+1}\,\eta_i\left(\hat{c}_1^2\,Z\right) & \dots \\ & \vdots & \vdots & \\ \dots & \dfrac{1}{2^i}\,\hat{c}_s^{2i}\,\eta_{i-1}\left(\hat{c}_s^2\,Z\right) & \dfrac{1}{2^i}\hat{c}_s^{2i+1}\,\eta_i\left(\hat{c}_s^2\,Z\right) & \dots \end{bmatrix}, \tag{3.2.29}$$

$$D_3 = \begin{bmatrix} \cdots & \frac{i}{2^{i-1}}\,\hat{c}_1^{2i-1}\,\eta_{i-1}\left(\hat{c}_1^2\,Z\right) + \frac{1}{2^i}\,\hat{c}_1^{2i+1}\,Z\eta_i\left(\hat{c}_1^2\,Z\right) & \frac{1}{2^i}\hat{c}_1^{2i}\,\eta_{i-1}\left(\hat{c}_1^2\,Z\right) & \cdots \\ & \vdots & & \\ \cdots & \frac{i}{2^{i-1}}\,\hat{c}_s^{2i-1}\,\eta_{i-1}\left(\hat{c}_s^2\,Z\right) + \frac{1}{2^i}\,\hat{c}_s^{2i+1}\,Z\eta_i\left(\hat{c}_s^2\,Z\right) & \frac{1}{2^i}\hat{c}_s^{2i}\,\eta_{i-1}\left(\hat{c}_s^2\,Z\right) & \cdots \end{bmatrix},$$

$$D_4 = \begin{bmatrix} \cdots & \frac{i}{2^{i-1}}\,c_1^{2i-1}\,\eta_{i-1}\left(c_1^2\,Z\right) + \frac{1}{2^i}\,c_1^{2i+1}\,Z\eta_i\left(c_1^2\,Z\right) & \frac{1}{2^i}c_1^{2i}\,\eta_{i-1}\left(c_1^2\,Z\right) & \cdots \\ & \vdots & & \\ \cdots & \frac{i}{2^{i-1}}\,c_s^{2i-1}\,\eta_{i-1}\left(c_s^2\,Z\right) + \frac{1}{2^i}\,c_s^{2i+1}\,Z\eta_i\left(c_s^2\,Z\right) & \frac{1}{2^i}c_s^{2i}\,\eta_{i-1}\left(c_s^2\,Z\right) & \cdots \end{bmatrix}.$$

with $i = 0, 1, ..., P$ *and* $P = \frac{s}{2} - 1$. *Moreover* $\hat{c}_j = 1 - c_j, \quad j = 0, 1, ..., s.$

Proof. Annihilating the dimensionless classic moments of order $m = 0$ in (3.2.26a) is equivalent to solving the system

$$\mathcal{L}^*_{i0}(h, \mathbf{w}) = 1 - \sum_{j=1}^{s} b_{ij} \; = 0, \quad i = 1, \ldots, s,$$

which can be recasted in a matrix form as follows

$$\mathbf{1} - B\,\mathbf{1} = \mathbf{0}, \qquad \mathbf{0} = (0, 0, \ldots, 0)^T.$$

Therefore, (3.2.28a) holds.
System (3.2.26b) for G_i^+ assumes the following expression:

$$\begin{aligned} G_i^+(Z, w) &= \eta_{-1}\left(c_i^2 Z\right) - \sum_{j=1}^{s} b_{ij}\;\eta_{-1}\left((c_j - 1)^2 Z\right) \\ &- Z\sum_{j=1}^{s} a_{ij}\;(c_j - 1)\,\eta_0\left((c_j - 1)^2 Z\right) - Z\sum_{j=1}^{i} r_{ij}\;c_j\,\eta_0\left(c_j^2 Z\right) = 0, \quad i = 1, \ldots, s, \end{aligned} \tag{3.2.30}$$

which can be written in a compact form

$$\theta_{-1,\,c} - B\,\theta_{-1,\,c-\mathbf{1}} - Z\,A\,(\,\hat{C}\,\theta_{0,\,c-\mathbf{1}}\,) - Z\,R\,(C\,\theta_{0,\,c}) = \mathbf{0}, \tag{3.2.31}$$

where $C = \mathrm{diag}(c_1, \ldots, c_s)$, $\hat{C} = diag(c_1 - 1, \ldots, c_s - 1)$ and the vector $\theta_{\sigma,v}$ associated to a vector v of dimension s, is defined as follows

$$\theta_{\sigma,v} = \left[\eta_\sigma\,(v_1^2\,Z), \ldots, \eta_\sigma\,(v_s^2\,Z)\right]. \tag{3.2.32}$$

On the other hand, system (3.2.26b) for G_i^- can be recasted in

$$C\,\theta_{0,\,c} - B\,(\,\hat{C}\,\theta_{0,\,c-\mathbf{1}}\,) - A\,\theta_{-1,\,c-\mathbf{1}} - R\,\theta_{-1,\,c} = \mathbf{0}. \tag{3.2.33}$$

In a similar way, systems (3.2.26b) for $G_i^{+(m)}$ and $G_i^{-(m)}$ with $m = 1, \ldots, P$ are respectively equivalent to

$$\begin{aligned} &\frac{1}{2^m} C^{2m}\,\theta_{m-1,\,c} - B\,\left(\frac{1}{2^m}\hat{C}^{2m}\,\theta_{m-1,\,c-\mathbf{1}}\right) - A\,\left(\frac{m}{2^{m-1}}\hat{C}^{2m-1}\,\theta_{m-1,\,c-\mathbf{1}}\right. \\ &\left. + \frac{Z}{2^m}\hat{C}^{2m+1}\theta_{m,c-1} - R\left(\frac{m}{2^{m-1}}C^{2m-1}\,\theta_{m-1,\,c} + \frac{Z}{2^m}C^{2m+1}Z\theta_{m,\,c}\right) = \mathbf{0}, \right. \end{aligned} \tag{3.2.34a}$$

$$\frac{1}{2^m}\left(C^{2m+1}\theta_{m,c} - B\left(\hat{C}^{2m+1}\theta_{m,c-\mathbf{1}}\right) - A\left(\hat{C}^{2m}\theta_{m-1,c-\mathbf{1}}\right) - R\,C^{2m}\theta_{m-1,c}\right) = \mathbf{0}. \tag{3.2.34b}$$

We next construct the matrix D_1 such that its first and second columns correspond to the first vectors of the systems (3.2.31) and (3.2.33), respectively. Then the other columns are the first vectors of the system (3.2.34a) and (3.2.34b), alternatively.
We construct the remaining matrices D_k, $k = 2, 3, 4$ in (3.2.28b) by considering them as columns the vectors multiplying B, A and R, respectively, in equations (3.2.31)–(3.2.34b). Then, system (3.2.31)–(3.2.34b) is equivalent to equation (3.2.28b). □

In similar way, in case of odd number of stages we have the following theorem:

Theorem 12. *Assume s is odd. The peer method* (3.1.2) *has order $p = s$ and is adapted to the fitting space*

$$\mathcal{F} = \left\{e^{\pm\mu t}, t\,e^{\pm\mu t}, t^2 e^{\pm\mu t}, \ldots, t^{\frac{s-1}{2}} e^{\pm\mu t}\right\},$$

if the coefficient matrices A and B satisfy

$$B\,\theta_{-1,\,c-\mathbf{1}} = \theta_{-1,\,c} - Z\,A\,(\,\hat{C}\,\theta_{0,\,c-\mathbf{1}}\,) - Z\,R\,(C\,\theta_{0,\,c}), \tag{3.2.35a}$$

$$AF_3 \;\; = F_1 - B\,F_2 - RF_4, \tag{3.2.35b}$$

where $\theta_{\sigma,v}$ are defined in (3.2.32) *and F_k for $k = 1, 2, 3, 4$ are obtained by deleting the first column to the matrices D_k defined in Theorem 11 (when s odd, $P = \frac{s-1}{2}$ and D_k have dimensions $s \times (s+1)$) .*

Step 6

We compute the leading term of the local truncation error at each stage, as follows:

$$(lte_{ef})_i = (-1)^{P+1} h^{s+1} \frac{\mathcal{L}^*_{i,K+1}(h, \mathbf{w})}{(K+1)!\,Z^{P+1}}\; D^{K+1}(D^2 - \mu^2)^{P+1} y(t), \quad i = 1, \ldots, s, \tag{3.2.36}$$

where we denote D the derivative with respect to time.
As before, we choose $K = 0$ and $K = -1$ for s even or odd, respectively. In these cases, the afore-mentioned leading term assumes the following expressions:

- if s is even

$$(lte_{ef})_i = \frac{(-1)^{\frac{s}{2}}\, h^{s+1}}{Z^{\frac{s}{2}}} \left(c_i - \sum_{j=1}^{s} b_{ij}\,(c_j - 1) - \sum_{j=1}^{s} a_{ij}\; - \sum_{j=1}^{i} r_{ij} \right) D(D^2 - \mu^2)^{\frac{s}{2}} y(t), \tag{3.2.37}$$

- if s is odd

$$(lte_{ef})_i = \frac{(-1)^{\frac{s+1}{2}}\, h^{s+1}}{Z^{\frac{s+1}{2}}} \left(1 - \sum_{j=1}^{s} b_{ij} \right) (D^2 - \mu^2)^{\frac{s+1}{2}} y(t). \tag{3.2.38}$$

3.3 Derivation of EF implicit peer method

In order to derive EF implicit peer method which can efficiently integrate stiff problems, we will determine the coefficients $A = A(Z), B = B(Z)$ and $R = R(Z)$ by satisfying the order conditions of Theorems 11 and 12, and we will verify that, when $Z \to 0$, they tend to classical implicit peer methods derived by Soleimani et al. in [286]. The following theorems describe the derivation of such coefficients.

Lemma 3.3.1. *Let $u \in \mathbb{R}^s$ and $H = (\mathbf{0} \mid u) \in \mathbb{R}^{s\times s}$ with $\mathbf{0} \in \mathbb{R}^{s\times s-1}$ having all null entries. Then*

$$H\theta_{-1,\,c-\mathbf{1}} = u,$$

and

$$HF_2 = 0,$$

where the vector $\theta_{-1,\,c-\mathbf{1}}$ is defined in (3.2.32) *and F_2 is defined in Theorem 11.*

Proof. From (3.2.32), by exploiting:

$$h_{ij} = \begin{cases} 0 & j < s, \\ u_i & j = s, \end{cases}$$

and $c_s = 1$, $\eta_{-1}(0) = 1$, we get

$$(H\theta_{-1,c-1})_i = \sum_{j=1}^{s} h_{ij}\eta_{-1}((c_j - 1)^2 Z) = h_{is}\eta_{-1}((c_s - 1)^2 Z) = u_i. \tag{3.3.39}$$

Moreover as the last row of matrix F_2 is zero (compare (3.2.29) and remind that F_2 is obtained from D_2 by deleting the first column) we have

$$(HF_2)_{ij} = \sum_{k=1}^{s} h_{ik}(F_2)_{kj} = h_{is}(F_2)_{sj} = 0,$$

which completes the proof. □

Let $\bar{B}$ be a constant matrix satisfying the order condition (3.1.5a) associated to classical peer methods.

Theorem 13. *Assume s is even and the matrix D_3 defined in Theorem 11 is invertible. Then the EF peer method having coefficients*

$$B = \bar{B} \tag{3.3.40a}$$
$$A = (D_1 - \bar{B}\, D_2 - RD_4)D_3^{-1}, \tag{3.3.40b}$$

has order $p = s$ and is adapted to fitting space

$$\mathcal{F} = \left\{1, e^{\pm\mu t}, t\, e^{\pm\mu t}, t^2\, e^{\pm\mu t}, \ldots, t^{\frac{s}{2}-1}\, e^{\pm\mu t}\right\}. \tag{3.3.41}$$

Proof. It is immediate to verify the order conditions (3.2.28a)-(3.2.28b). □

Theorem 14. *Assume s is odd and the matrix F_3 defined in Theorem 12 is invertible. Consider the EF peer method having coefficients*

$$B = \bar{B} + H_1 - ZA\, H_2 - ZR\, H_3, \tag{3.3.42a}$$
$$A = [F_1 - \bar{B}F_2 - RF_4]F_3^{-1}, \tag{3.3.42b}$$

where

$$H_1 = (\mathbf{0}\,|\,\theta_{-1,\,c} - \bar{B}\theta_{-1,\,c-\mathbf{1}}), \quad H_2 = (\mathbf{0}\,|\,\hat{C}\,\theta_{0,\,c-\mathbf{1}}), \quad H_3 = (\mathbf{0}\,|\,C\,\theta_{0,\,c}) \in \mathbb{R}^{s\,\times\, s},$$

and F_i are defined in Theorem 12.
The above EF peer method has order $p = s$ and is adapted to the fitting space

$$\mathcal{F} = \left\{e^{\pm\mu t}, t\, e^{\pm\mu t}, t^2\, e^{\pm\mu t}, \ldots, t^{\frac{s-1}{2}}\, e^{\pm\mu t}\right\}. \tag{3.3.43}$$

Proof. In order to verify order condition (3.2.35a) we compute, by exploiting Lemma 3.3.1,

$$B\theta_{-1,c-1} = (\bar{B} + H_1 - ZAH_2 - ZRH_3)\theta_{-1,c-1} = \theta_{-1,c} - ZA\hat{C}\theta_{0,c-1} - ZRC\theta_{0,c},$$

which corresponds to order condition (3.2.35a).
By substituting the matrix B (3.3.42a) into condition (3.2.35b), we find that it is equivalent to

$$A = [F_1 - (\bar{B} + H_1)F_2 - R(F_4 - ZH_3F_2)](F_3 - ZH_2F_2)^{-1}. \tag{3.3.44}$$

Then, from Lemma 3.3.1 we have $H_1F_2 = H_3F_2 = H_2F_2 = 0$ and the proof is completed. □

3.3.1 Examples of methods with $s = 2$

By refering to Section 3.2, in this case $K = 0$ and $P = 0$. We fix $c_1 = 0$, $c_2 = 1$,

$$\bar{B} = \begin{bmatrix} 0 & 1 \\ 0 & 1 \end{bmatrix} \tag{3.3.45}$$

satisfying (3.1.5a), R having lower triangular structure with $r_{11} = r_{22} = \gamma$ and derive the matrices A and B according to Theorem 13.
Then we get that the EF peer method with coefficients

$$c = \begin{bmatrix} 0 \\ 1 \end{bmatrix}, \quad B = \begin{bmatrix} 0 & 1 \\ 0 & 1 \end{bmatrix}, R = \begin{bmatrix} \gamma & 0 \\ r_{21} & \gamma \end{bmatrix}, \tag{3.3.46a}$$

$$A = \begin{bmatrix} 0 & -\gamma \\ \frac{1-\eta_{-1}(Z)}{Z\eta_0(Z)} + \gamma & \frac{\eta_{-1}(Z)}{Z\eta_0(Z)}(\eta_0(Z) - 1 - r_{21} - \gamma(Z\eta_0(Z) - \eta_{-1}(Z))) + \eta_0(Z) - 1 - r_{21} \end{bmatrix} \tag{3.3.46b}$$

has order $p = 2$ and is adapted to the fitting space

$$\left\{1, e^{\pm\mu t}\right\}.$$

As a matter of fact B satisfies (3.3.40a) of Theorem 13 and from $c_1 = 0$, $c_2 = 1$, we have $\hat{c}_1 = -1$, $\hat{c}_2 = 0$ and

$$D_1 = \begin{bmatrix} 1 & 0 \\ \eta_{-1}(Z) & \eta_0(Z) \end{bmatrix}, \quad D_2 = \begin{bmatrix} \eta_{-1}(Z) & -\eta_0(Z) \\ 1 & 0 \end{bmatrix},$$

$$D_3 = \begin{bmatrix} -Z\eta_0(Z) & \eta_{-1}(Z) \\ 0 & 1 \end{bmatrix}, \quad D_4 = \begin{bmatrix} 0 & 1 \\ Z\eta_0(Z) & \eta_{-1}(Z) \end{bmatrix}.$$

If D_3 is invertible, we can compute the matrix A. Now, we compute determinant of D_3 in both trigonometric and hyperbolic cases.

Trigonometric case: $Z = -\omega^2 h^2$

$$Det\ (D_3) = -Z\eta_0(Z) = -\omega h sin(\omega h).$$

Therefore the matrix D_3 is invertible, when $h \neq \frac{k\pi}{\omega}$, $k \in \mathbf{N}$.

Hyperbolic case: $Z = \mu^2 h^2,\ \mu \in \mathbf{R}$

$$Det\ (D_3) = \mu h sinh(\mu h).$$

Therefore the matrix D_3 is invertible $\forall h > 0$.

Then from (3.3.40b) of Theorem 13 the expression of A follows.

The corresponding classic peer method is obtained in the limit as $Z \to 0$ and has coefficients:

$$c = \begin{bmatrix} 0 \\ 1 \end{bmatrix}, \quad B = \begin{bmatrix} 0 & 1 \\ 0 & 1 \end{bmatrix}, \quad R = \begin{bmatrix} \gamma & 0 \\ r_{21} & \gamma \end{bmatrix}, \tag{3.3.47a}$$

$$A = \begin{bmatrix} 0 & -\gamma \\ \gamma & -r_{21} \end{bmatrix}. \tag{3.3.47b}$$

3.3.2 Examples of methods with $s = 3$

Due to Section 3.2, in this case, $K = -1$ and $P = 1$. We set c, $\bar{B}$ and R from paper [286] in order to have an A-stable method in the limit when $Z \to 0$ and derive matrices B and A from Theorem 14.
Then, for example, the EF peer method with coefficients

$$\mathrm{c} = \begin{pmatrix} 8.170765826910428900\mathrm{e}-01 \\ 6.112848743494372300\mathrm{e}-01 \\ 1.000000000000000000\mathrm{e}+00 \end{pmatrix}, \tag{3.3.48}$$

$$R = \begin{pmatrix} +3.32082968680\mathrm{e}-01 & 0 & 0 \\ -4.64383283259\mathrm{e}-02 & 3.32082968680\mathrm{e}-01 & 0 \\ -6.03010600818\mathrm{e}-01 & 1.08071195621\mathrm{e}+00 & 3.32082968680\mathrm{e}-01 \end{pmatrix}, \tag{3.3.49}$$

$$B = [\mathbf{0} \,|\, \mathbf{0} \,|\, v_1 - \bar{B}v_0 - ZAv_2 - ZRv_3], \quad A = [F_1 - \bar{B}F_2 - RF_4]F_3^{-1}, \tag{3.3.50}$$

where $\mathbf{0} = [0, 0, 0]^T$,

$$\bar{B} = \begin{pmatrix} 4.49089617867\mathrm{e}-01, & -6.61026939991\mathrm{e}-01 & 1.21193732212\mathrm{e}+00 \\ 3.05103275940\mathrm{e}-01 & -4.49089617867\mathrm{e}-01 & 1.14398634192\mathrm{e}+00 \\ 0 & 0 & 1 \end{pmatrix}, \tag{3.3.51}$$

$$v_0 = \begin{bmatrix} \eta_{-1}(\hat{c}_1^2 Z) \\ \eta_{-1}(\hat{c}_2^2 Z) \\ 1 \end{bmatrix}, v_1 = \begin{bmatrix} \eta_{-1}(c_1^2 Z) \\ \eta_{-1}(c_2^2 Z) \\ \eta_{-1}(Z) \end{bmatrix},$$

$$v_2 = \begin{bmatrix} \hat{c}_1 \eta_0(\hat{c}_1^2(Z)) \\ \hat{c}_2 \eta_0(\hat{c}_2^2(Z)) \\ 0 \end{bmatrix}, v_3 = \begin{bmatrix} c_1 \eta_0(c_1^2(Z)) \\ c_2 \eta_0(c_2^2(Z)) \\ \eta_0(Z) \end{bmatrix},$$

$$F_1 = \begin{bmatrix} c_1\eta_0(c_1^2(Z)) & \frac{1}{2}c_1^2\eta_0(c_1^2(Z)) & \frac{1}{2}c_1^3\eta_0(c_1^2(Z)) \\ c_2\eta_0(c_2^2(Z)) & \frac{1}{2}c_2^2\eta_0(c_2^2(Z)) & \frac{1}{2}c_2^3\eta_0(c_2^2(Z)) \\ \eta_0(Z) & \frac{1}{2}\eta_0(Z) & \frac{1}{2}\eta_1(Z) \end{bmatrix},$$

$$F_2 = \begin{bmatrix} \hat{c}_1\eta_0(\hat{c}_1^2(Z)) & \frac{1}{2}\hat{c}_1^2\eta_0(\hat{c}_1^2(Z)) & \frac{1}{2}\hat{c}_1^3\eta_0(\hat{c}_1^2(Z)) \\ \hat{c}_2\eta_0(\hat{c}_2^2(Z)) & \frac{1}{2}\hat{c}_2^2\eta_0(\hat{c}_2^2(Z)) & \frac{1}{2}\hat{c}_2^3\eta_0(\hat{c}_2^2(Z)) \\ 0 & 0 & 0 \end{bmatrix},$$

$$F_3 = \begin{bmatrix} \eta_{-1}(\hat{c}_1^2(Z)) & \hat{c}_1^2\eta_0(\hat{c}_1^2(Z)) + \frac{\hat{c}_1^3 Z}{2}\eta_1(\hat{c}_1^2(Z)) & \frac{1}{2}\hat{c}_1^2\eta_0(\hat{c}_1^2(Z)) \\ \eta_{-1}(\hat{c}_2^2(Z)) & \hat{c}_2^2\eta_0(\hat{c}_2^2(Z)) + \frac{\hat{c}_2^3 Z}{2}\eta_1(\hat{c}_2^2(Z)) & \frac{1}{2}\hat{c}_2^2\eta_0(\hat{c}_2^2(Z)) \\ 1 & 0 & 0 \end{bmatrix},$$

$$F_4 = \begin{bmatrix} 1 & 0 & 0 \\ \eta_{-1}(c_2^2(Z)) & c_2^2\eta_0(c_2^2(Z)) + \frac{c_2^3 Z}{2}\eta_1(c_2^2(Z)) & \frac{1}{2}c_2^2\eta_0(c_2^2(Z)) \\ \eta_{-1}(c_3^2(Z)) & c_3^2\eta_0(c_3^2(Z)) + \frac{c_3^3 Z}{2}\eta_1(c_3^2(Z)) & \frac{1}{2}c_3^2\eta_0(c_3^2(Z)) \end{bmatrix},$$

has order $p = 3$ and is adapted to the fitting space

$$\left\{e^{\pm\mu t}, te^{\pm\mu t}\right\}.$$

We note that the expression of B follows from

$$H_1 = [\mathbf{0}\,|\,\mathbf{0}\,|\,v_1 - \bar{B}v_0], \quad H_2 = [\mathbf{0}\,|\,\mathbf{0}\,|\,v_2], \quad H_3 = [\mathbf{0}\,|\,\mathbf{0}\,|\,v_3],$$

and condition (3.3.42a).

If F_3 is invertible, we can compute the matrix A. Now, we compute determinant of F_3 in both trigonometric and hyperbolic cases.

$$F_3 = \begin{bmatrix} \eta_{-1}(Z) & -\eta_0(Z) - \frac{Z}{2}\eta_1(Z) & \frac{1}{2}\eta_0(Z) \\ \eta_{-1}(\frac{Z}{4}) & -\frac{1}{2}\eta_0(\frac{Z}{4}) - \frac{Z}{16}\eta_1(\frac{Z}{4}) & \frac{1}{8}\eta_0(\frac{Z}{4}) \\ 1 & 0 & 0 \end{bmatrix},$$

$$Det\ (F_3) = \frac{1}{32}\left(4\eta_0(\frac{Z}{4})\eta_0(Z) - 2Z\eta_0(\frac{Z}{4})\eta_1(Z) + Z\eta_1(\frac{Z}{4})\eta_0(Z)\right).$$

Trigonometric case: $Z = -\omega^2 h^2$

Therefore the matrix F_3 is invertible, when

$$2\omega h\ sin(\frac{\omega h}{2}) + cos(\frac{\omega h}{2}) - cos(\frac{3\omega h}{2}) \neq 0,$$

this means that $h \neq \frac{2\pi}{\omega}$.

Hyperbolic case: $Z = \mu^2 h^2$

Therefore the matrix F_3 is invertible, when

$$2\mu h\ sinh(\frac{\mu h}{2}) + cosh(\frac{\mu h}{2}) - cosh(\frac{3\mu h}{2}) \neq 0,$$

this means that the matrix F_3 is invertible $\forall h > 0$.

The corresponding classic peer method is obtained in the limit as $Z \to 0$ and has coefficients:

$$\mathrm{A} = \begin{pmatrix} 2.9548\text{e -}01 & -4.0890\text{e -}01 & 4.2361\text{e -}01 \\ 1.4466\text{e -}01 & -1.9826\text{e -}01 & 2.6048\text{e -}01 \\ 1.1464\text{e -}15 & -2.5388\text{e -}16 & 1.9022\text{e -}01 \end{pmatrix}, \quad B = \bar{B}, \tag{3.3.52}$$

and c, R given by (3.3.48) and (3.3.49), respectively.

3.4 Numerical experiments

In this section, we present some numerical results obtained first of all by comparing the derived implicit EF peer methods with their classic counterparts. We moreover show the improvement concerning explicit EF peer method of [73] on stiff problems. Finally, we compare EF Runge-Kutta methods derived in [301] and EF linear multistep methods presented in [157].

The tables will report the error computed as the infinite norm of the difference between the numerical solution and the exact solution at the end point. Moreover, we will adopt the following notation to indicate the used numerical method:

- CL = classic,
- EF = exponentially fitted,
- EX P2 = explicit peer method of order 2 from [73],
- EX P3 = explicit peer method of order 3 from [73],
- IM P2 = implicit peer method of order 2 from Section 3.3.1 with $r_{21} = 0$ and $\gamma = -1$,
- IM P3 = implicit peer method of order 3 from Section 3.3.2,
- RK3 = Runge-Kutta method of order 3 from [301],
- LMM3 = linear multistep method of order 3 from [157].

Example 1. *Let us consider the Prothero-Robinson problem [134]*

$$\begin{aligned} &y'(t) = \lambda\,(\,y(t) - \sin(\omega\,t + t)\,) + (\omega + 1)\,\cos(\omega\,t + t), \quad t \in \left[0, \frac{\pi}{2}\right], \\ &y(0) = 0, \end{aligned} \tag{3.4.53}$$

whose exact solution is

$$y(t) = \sin(\omega\, t + t) = \sin(\omega\, t)\, \cos(t) + \cos(\omega\, t)\, \sin(t).$$

The oscillating behavior of the exact solution leads us to utilize the EF methods with the parameter $\mu = \mathrm{i}\,\omega$, $Z = -\omega^2 h^2$.
We consider two cases:

- $\lambda = -1$ *(non stiff case)*
- $\lambda = -10^{-6}$ *(stiff case)*

First of all, we consider $\lambda = -1$. *The results reported in Table 3.1 show that EF implicit peer methods produce smaller errors than their classic counterparts. The improvement is much more visible as the frequency* ω *increases. We report in Table 3.2 the corresponding results obtained by explicit EF peer methods of [73]. We note that for* $s = 2$, *the methods have the same behavior in accuracy, while for* $s = 3$ *implicit method is more accurate. We report in Table 3.3 the estimated order of EF peer method, computed as:*

$$p(h) \approx \log_2 \left(\frac{E(h)}{E(h/2)} \right), \tag{3.4.54}$$

where $E(h)$ *and* $E(h/2)$ *are the errors with a stepsize* h *and* $h/2$, *respectively. We notice that for* $s = 2$ *the implicit EF peer method shows effective order* 2, *as in the explicit case [73]. As regards* $s = 3$, *we notice superconvergent behavior with order* $p = s + 1 = 4$. *This can be motivated because the classic coefficients* (3.3.52) *taken from [286] were derived by imposing superconvergence.*

		N		
Methods	ω	160	320	640
CL IM P2	50	$1.53e-01$	$3.78e-02$	$9.33e-03$
EF IM P2	50	$5.68e-03$	$1.45e-03$	$3.62e-04$
CL IM P3	50	$4.16e-05$	$2.44e-06$	$1.45e-07$
EF IM P3	50	$7.65e-08$	$3.41e-09$	$2.02e-10$
CL IM P2	100	$4.39e-01$	$1.31e-01$	$3.45e-02$
EF IM P2	100	$8.25e-03$	$2.53e-03$	$6.77e-04$
CL IM P3	100	$4.98e-04$	$3.31e-05$	$2.16e-06$
EF IM P3	100	$2.33e-07$	$1.10e-08$	$4.77e-09$

Table 3.1: Errors of the implicit peer methods on problem (3.4.53) with $\lambda = -1$, N grid points and different values for the frequency ω, Example 1.

		N		
Methods	ω	160	320	640
CL EX P2	50	$1.05e-01$	$2.65e-02$	$6.60e-03$
EF EX P2	50	$4.10e-03$	$1.00e-03$	$2.57e-04$
CL EX P3	50	$1.10e-02$	$9.42e-04$	$8.98e-05$
EF EX P3	50	$1.07e-05$	$1.26e-06$	$1.33e-7$
CL EX P2	100	$3.02e-01$	$9.33e-02$	$2.47e-02$
EF EX P2	100	$5.30e-03$	$1.80e-03$	$4.86e-04$
CL EX P3	100	$6.92e-02$	$2.40e-03$	$1.22e-04$
EF EX P3	100	$3.08e-05$	$2.30e-06$	$1.58e-08$

Table 3.2: Errors of the explicit peer methods on problem (3.4.53) with $\lambda = -1$, N grid points and different values for the frequency ω, Example 1.

N	**EF IM P2**	**EF IM P3**
160	1.73	4.40
320	1.97	4.48
640	2.00	4.07

Table 3.3: Estimated order of the implicit EF peer methods on problem (3.4.53) with $\lambda = -1$, $\omega = 50$, Example 1.

We now consider the case in which the oscillatory frequency ω is not known exactly. Therefore by denoting with δ the relative error on the frequency, we employ the EF peer methods whose coefficients are computed in correspondence of a perturbed frequency $\tilde{\omega} = (1 + \delta)\omega$. We report in Tables 3.4 and 3.5 the results obtained with implicit and explicit EF peer methods, respectively. The results shows that an accurate computation of the frequency is a crucial point. However it is not a dramatic situation as the error of EF peer methods keeps smaller than that of the corresponding classic counterparts and, for increasing δ, it approaches the error of classic methods.

	N		
Methods	160	320	640
CL IM P3	$4.16e-5$	$2.43e-6$	$1.45e-7$
EF IM P3 $\delta = 0.3$	$2.17e-05$	$1.09e-06$	$6.09e-08$
EF IM P3 $\delta = 0.1$	$1.37e-6$	$7.33e-8$	$4.34e-9$
EF IM P3 $\delta = 0$	$7.64e-8$	$3.41e-9$	$2.01e-10$

Table 3.4: Errors of implicit peer method of order 3 on problem (3.4.53) with $\lambda = -1$ and perturbed frequency $\tilde{\omega} = (1+\delta)\omega$, $\omega = 50$, Example 1.

	N		
Methods	160	320	640
CL EX P3	$1.09e-02$	$9.42e-04$	$8.98e-05$
EF EX P3 $\delta = 0.3$	$2.13e-03$	$2.68e-04$	$3.30e-05$
EF EX P3 $\delta = 0.1$	$1.70e-04$	$2.11e-05$	$2.32e-06$
EF EX P3 $\delta = 0$	$1.07e-05$	$1.26e-06$	$1.33e-07$

Table 3.5: Errors of explicit peer method of order 3 [73] on problem (3.4.53) with $\lambda = -1$ and perturbed frequency $\tilde{\omega} = (1+\delta)\omega$, $\omega = 50$, Example 1.

We now consider $\lambda = -10^6$. As in the non stiff case, Table 3.6 shows as the EF peer method produces smaller errors with respect to classic one. We do not report results for explicit methods because for $\lambda = -10^6$ they are unstable. Table 3.7 shows the estimated order. In Table 3.8 we report the results obtained in correspondence of "wrong" frequency $\tilde{\omega} = (1+\delta)\omega$, showing a similar behavior as in the nonstiff case.

	N		
Methods	160	320	640
CL IM P2	$2.17e-6$	$2.16e-7$	$2.55e-8$
EF IM P2	$6.01e-8$	$7.74e-9$	$9.73e-10$
CL IM P3	$1.79e-7$	$2.51e-8$	$3.22e-9$
EF IM P3	$2.42e-10$	$3.48e-11$	$4.88e-12$

Table 3.6: Errors of the implicit peer methods on problem (3.4.53) with $\lambda = -10^6$, N grid points and $\omega = 50$, Example 1.

N	EF IM P2	EF IM P3
320	2.95	2.79
640	2.99	2.83
1280	3.00	3.13

Table 3.7: Estimated order of implicit EF peer methods on problem (3.4.53) with $\lambda = -10^6$, $\omega = 50$, Example 1.

	N		
Methods	160	320	640
CL IM P3	$1.79e-07$	$2.52e-08$	$3.22e-09$
EF IM P3 $\delta = 0.3$	$8.91e-06$	$8.48e-09$	$1.19e-09$
EF IM P3 $\delta = 0.1$	$4.06e-09$	$6.02e-10$	$8.26e-11$
EF IM P3 $\delta = 0$	$2.42e-10$	$3.48e-11$	$4.88e-12$

Table 3.8: Errors of implicit peer method of order 3 on problem (3.4.53) with $\lambda = -10^6$ and perturbed frequency $\tilde{\omega} = (1+\delta)\omega$, $\omega = 50$, Example 1.

Example 2. *Let us consider the system of two equations known as Lambert equations [180]:*

$$\begin{aligned} y_1^{'} &= -2y_1 + y_2 + 2\sin(\omega t), \qquad t \in [0, 10]\,, \\ y_2^{'} &= -(\beta+2)y_1 + (\beta+1)(y_2 + \sin(\omega t) - \cos(\omega t)), \end{aligned} \tag{3.4.55}$$

with the initial conditions $y_1(0) = 2$ *and* $y_2(0) = 3$.
The exact solutions of this system are $y_1(t) = 2\exp(-t)+\sin(\omega t)$ *and* $y_2(t) = 2\exp(-t)+\cos(\omega t)$ *and are* β*-independent.*

We consider the two cases:

- $\beta = -3$ *(non stiff case)*
- $\beta = -1000$ *(stiff case)*

Lambert's system has been employed in [157, 180, 301]. In [301], Vanden Berghe et. al used EF Runge–Kutta methods for Lambert's system. In [157], Ixaru et. al proposed EF linear multistep algorithms for this system.
According to the exact solution, we consider EF methods with $\mu = \mathrm{i}\omega$, $Z = -\omega^2 h^2$. *We report in Table 3.9 and 3.10 the errors obtained in correspondence of* $\omega = 1$ *with* $\beta = -3$ *and* $\beta = -1000$, *respectively. In both cases, we observe that EF peer methods produce smaller errors with respect to classic ones.*

Methods	$h = 0.1$	$h = 0.05$	$h = 0.025$
CL IM P2	$3.62e-03$	$8.97e-04$	$2.24e-04$
EF IM P2	$1.04e-05$	$2.66e-06$	$6.65e-07$
CL IM P3	$2.43e-07$	$1.57e-08$	$9.97e-10$
EF IM P3	$1.24e-09$	$6.95e-11$	$9.62e-12$

Table 3.9: Errors of the implicit peer methods on problem (3.4.55) with $\omega = 1, \beta = -3$ and stepsize h, Example 2.

Methods	$h = 0.1$	$h = 0.05$	$h = 0.025$
CL IM P2	$3.62e-03$	$8.97e-04$	$2.24e-04$
EF IM P2	$1.04e-05$	$2.66e-06$	$6.65e-07$
CL IM P3	$2.43e-07$	$1.57e-08$	$9.97e-10$
EF IM P3	$1.24e-09$	$6.95e-11$	$9.62e-12$

Table 3.10: Errors of the implicit peer methods on problem (3.4.55) with $\omega = 1, \beta = -1000$ and stepsize h, Example 2.

In addition, for $\beta = -1000$, Tables 3.11 and 3.12 provide a comparison between the our obtained results and those reported in Refs.[156, 301]. From these Tables we realize that errors of implicit EF peer methods are smaller with respect to Runge-Kutta and linear multistep methods of the same order.

Methods	$h = 0.1$	$h = 0.05$	$h = 0.025$
CL RK3	$1.92e-04$	$1.68e-04$	$1.19e-05$
EF RK3	$6.03e-06$	$6.66e-07$	$8.00e-08$

Table 3.11: Errors of Runge–Kutta methods [301] on problem (3.4.55) with $\omega = 1, \beta = -1000$ and stepsize h, Example 2.

Methods	$h = 0.1$	$h = 0.05$	$h = 0.025$
CL LMS3	$2.25e-03$	$5.70e-04$	$1.43e-04$
EF LMS3	$2.41e-04$	$2.36e-05$	$2.52e-06$

Table 3.12: Errors of the linear multistep methods [157] on problem (3.4.55) with $\omega = 1, \beta = -1000$ and stepsize h, Example 2.

3.5 Conclusion

In this chapter, implicit EF peer methods have been introduced for the numerical solution of ordinary differential equations exhibiting an oscillatory solution. A general class of implicit EF peer methods was derived by following the six-step procedure presented in [158]. The adopted strategy is based on adapting already existing methods in order to be exact (within round-off error) on trigonometric or hyperbolic functions. In the sixth step procedure, we have computed the expression of the leading term of the local truncation error, which may lead to an estimate of the parameter characterizing the basis functions, as shown in Chapter 5. Numerical experiments have confirmed the effectiveness of the approach.

Chapter 4

Exponentially fitted IMEX peer methods for an advection-diffusion problem

Advection-diffusion equations are used to model a wide range of engineering and industrial applications [282], as well as many problems in physics, chemistry, and other areas of science. For example, they are used to model the dispersion of solutes in the liquid flowing through a tube [13], the dispersion of detectors in a porous media [114], the dispersion of groundwater soluble salts [130], the heat transfer in a discharge film [152], the transfer of water in the soil [234], the dispersion of pollutants in shallow lakes [260] and long-term transfer of pollutants into the atmosphere [331].

IMEX methods are widely used strategies for problems characterized by the sum of two terms: a stiff term and a non-stiff one. IMEX methods aim to treat the stiff part by implicit methods so that the stepsize is not constrained by stability requirements and the non-stiff part by explicit methods due to their low cost per step. The literature is rich in contributions in the field of IMEX numerical methods, see [15, 33, 122, 123] for IMEX Runge-Kutta methods, [14, 103, 116, 147, 255] for IMEX linear multistep methods [35, 45, 166, 329] for IMEX general linear methods, [330] for IMEX two-step Runge-Kutta methods and [306] for IMEX Galerkin methods.

In the paper [287], IMEX peer methods based on implicit peer methods for the stiff part [286] and explicit peer methods for the non-stiff part [314] were derived. For more knowledge on the properties of implicit and explicit peer methods, refer to [25, 26, 120, 242, 269, 271] and [314, 315], respectively.

When the solution of advection-diffusion problems has a high oscillatory behavior both in space and in time, classical methods can require a very small stepsize to accurately follow the oscillating behavior of the exact solution because they are based on general-purpose formulas constructed to be exact on polynomials up to a certain

degree (within round off error). As we concentrate on systems with an exact oscillating solution, fitting formulae developed to be accurate on other functions than polynomials can be used more conveniently and the basic functions usually belong to a finite dimensional fitting space, as shown in Chapters 2, 3.

The fitting space is chosen based on the apriori known exact solution information and, as a direct result of that choice, the basic functions typically rely on solution related parameters (e.g., oscillation frequency for oscillatory problems) . As a consequence, selecting an appropriate fitting space and correctly estimating the unknown parameters are the critical challenges associated with appropriate EF methods [92, 91, 102].

This chapter aims to derive EF IMEX peer methods for the numerical solution of ODEs that exhibit oscillatory solutions. This is achieved by combining the EF implicit peer methods introduced in [80] and explicit peer methods [73]. The derived methods will then be applied to the numerical solution of advection-diffusion problems [59, 189, 203, 316] after a spatial semi-discretization using EF finite differences. The chapter will also present the stability properties of the proposed methods and present numerical experiments to demonstrate their effectiveness.

Section 4.1 of the chapter discusses the concept of s-stage partitioned peer methods and the order conditions associated with them. These methods are based on splitting the ODE into two parts, the stiff and the non-stiff parts, and handling them separately. The implicit EF peer method is used for the stiff part, while the explicit EF peer method is used for the non-stiff part. This results in a more efficient and accurate numerical solution for ODEs with oscillatory solutions. In Section 4.3, the chapter focuses on applying these methods to advection-diffusion problems. Advection-diffusion problems are a class of problems that arise in various fields of science and engineering, including fluid dynamics and heat transfer. The chapter discusses the use of IMEX EF peer methods in space and time for the numerical solution of advection-diffusion problems after a spatial semi-discretization using EF finite differences. In Section 4.4, the stability properties of the proposed methods are analyzed and discussed in detail. This is an essential aspect of numerical methods, as stability ensures that the numerical solution remains consistent and accurate over time. Finally, in Section 4.5, the results of numerical experiments are presented and discussed, demonstrating the proposed methods' effectiveness and efficiency. The chapter concludes in Section 4.6 with a summary of the results and conclusions.

4.1 EF IMEX peer methods for ODEs

In many engineering and science problems, the right side is naturally split into two parts, one non-stiff and one stiff. For such systems IMEX methods involves implicit methods for the stiff part and explicit methods for the non-stiff part [15, 14, 306].

It is possible to write such systems in the following form:

$$y'(t) = f(t, y(t)) + g(t, y(t)), \qquad y(t_0) = y_0 \in \mathcal{R}^d, \qquad t \in [t_0, T], \tag{4.1.1}$$

where $f, g : \mathcal{R} \times \mathcal{R}^d \to \mathcal{R}^d$ are sufficiently smooth to ensure the solution exists and is unique. In addition, $f(t, y(t))$ depicts the stiff diffusion term and $g(t, y(t))$ specifies the non-stiff advection term.

4.1.1 Partitioned peer methods

System (4.1.1) can be transformed into a partitioned system of the form [287]:

$$z^{'} = \begin{pmatrix} u^{'} \\ v^{'} \end{pmatrix} = \begin{pmatrix} \tilde{f}(t, u, v) \\ \tilde{g}(t, u, v) \end{pmatrix}, \tag{4.1.2}$$

by setting $y = u + v,\ u' = \tilde{f}(t, u, v) = f(t, u + v),\ v' = \tilde{g}(t, u, v) = g(t, u + v)$ and $z = \begin{pmatrix} u \\ v \end{pmatrix}$.
Here $u^{'} = f$ is the stiff part and will be treated by implicit peer methods and $v^{'} = g$ shows the non-stiff part and will be treated by explicit peer methods.

We assume that for each stepsize $h > 0$ there exists a starting procedure for approximating the solution at the grid points the internal $t_{0,i} = t_0 + c_i\, h,\ i = 1, \ldots, s$. The following expression is used for a s-stage two step partitioned peer method with fixed step-size h:

$$\begin{aligned} &U_{ni} = \textstyle\sum_{j=1}^{s} b_{ij}\ U_{n-1,j} + h \sum_{j=1}^{s} a_{ij}\ \tilde{f}(t_{n-1,j}, U_{n-1,j}, V_{n-1,j}) \\ &+h \textstyle\sum_{j=1}^{i} r_{ij}\ \tilde{f}(t_{nj}, U_{nj}, V_{nj}), \\ &V_{ni} = \textstyle\sum_{j=1}^{s} \hat{b}_{ij}\ V_{n-1,j} + h \sum_{j=1}^{s} \hat{a}_{ij}\ \tilde{g}(t_{n-1,j}, U_{n-1,j}, V_{n-1,j}) \\ &+h \textstyle\sum_{j=1}^{i-1} \hat{r}_{ij}\ \tilde{g}(t_{nj}, U_{nj}, V_{nj}), \end{aligned} \tag{4.1.3}$$

where

$$U_{ni} \approx u(t_{ni}), \qquad V_{ni} \approx v(t_{ni}), \qquad t_{ni} = t_n + c_i\, h, \qquad i = 1, \ldots, s.$$

No extraordinary numerical solution is determined with distinct features: for peer methods $c_s = 1$ and select the other nodes such that $c_i < 1$ for $i = 1, \ldots, s - 1$.

We define the vectors and matrices

$$U_n = [U_{ni}]_{i=1}^{s}\,,\ F(U_n,V_n) = \left[\tilde{f}(t_{ni},U_{ni},V_{ni})\right]_{i=1}^{s}\,,\ A = [a_{ij}]_{i,j=1}^{s}\,,$$

$$B = [b_{ij}]_{i,j=1}^{s}\,,\ R = [r_{ij}]_{i,j=1}^{s}\,,$$

$$V_n = [V_{ni}]_{i=1}^{s}\,,\ G(U_n,V_n) = [\tilde{g}(t_{ni},U_{ni},V_{ni})]_{i=1}^{s}\,,\ \hat{A} = [\hat{a}_{ij}]_{i,j=1}^{s}\,,$$
$$\hat{B} = \left[\hat{b}_{ij}\right]_{i,j=1}^{s}\,,\ \hat{R} = [\hat{r}_{ij}]_{i,j=1}^{s}\,,$$

where $A, \hat{A}, B$ and $\hat{B}$ are full matrices, R is a lower triangular matrix and $\hat{R}$ is a strictly lower triangular matrix. Method (4.1.3) can be then written in the compact form

$$\begin{aligned} U_n &= (B\otimes \mathbb{I}_d)\,U_{n-1} + h\,(A\otimes \mathbb{I}_d)\,F(U_{n-1},V_{n-1}) + h\,(R\otimes \mathbb{I}_d)\,F(U_n,V_n),\\ V_n &= (\hat{B}\otimes \mathbb{I}_d)\,V_{n-1} + h\,(\hat{A}\otimes \mathbb{I}_d)\,G(U_{n-1},V_{n-1}) + h\,(\hat{R}\otimes \mathbb{I}_d)\,G(U_n,V_n), \end{aligned} \tag{4.1.4}$$

where $\mathbb{I}_d$ is the identity matrix of dimension d. The coefficient matrices A, B, R, $\hat{A}$, $\hat{B}$ and $\hat{R}$ are determined to achieve high order (uniform for all components U_n and V_n) together with good stability properties.

We recall that the method (4.1.4) has consistency order p if $\Delta_n = \begin{pmatrix} \mathcal{O}(h^{p+1}) \\ \mathcal{O}(h^{p+1}) \end{pmatrix}$, where Δ_n denotes the residuals of the stiff and of the non-stiff part which are obtained by inserting the exact solutions in the numerical method (4.1.4). The following Theorem summarizes the order conditions.

Theorem 15. *[287] If the coeffiicients of the partitioned peer method* (4.1.4) *satisfy the conditions*

$$\mathrm{AB_i}(m) = \hat{\mathrm{AB}}_\mathrm{i}(m) = 0, \quad m = 0,\dots,p,\ i = 1,\dots,s$$

with

$$\mathrm{AB_i}(m) = c_i^m - \sum_{j=1}^{s} b_{ij}\,(c_j-1)^m - m\sum_{j=1}^{s} a_{ij}\,(c_j-1)^{m-1} - m\sum_{j=1}^{i} r_{ij}\,c_j^{m-1}, \tag{4.1.5}$$

$$\hat{\mathrm{AB}}_\mathrm{i}(m) = c_i^m - \sum_{j=1}^{s} \hat{b}_{ij}\,(c_j-1)^m - m\sum_{j=1}^{s} \hat{a}_{ij}\,(c_j-1)^{m-1} - m\sum_{j=1}^{i-1} \hat{r}_{ij}\,c_j^{m-1}, \tag{4.1.6}$$

then the s-stage partitioned peer method (4.1.4) *has order of consistency p.*

Corollary 4.1.1. *The partitioned peer method* (4.1.4) *has order $p \geqslant s$ if*

$$B\,\mathbf{1} = \hat{B}\,\mathbf{1} = \mathbf{1}, \tag{4.1.7a}$$
$$AV_1D = CV_0 - B\,(C-\mathbb{I}_s)V_1 - RV_0D, \tag{4.1.7b}$$
$$\hat{A}V_1D = CV_0 - \hat{B}\,(C-\mathbb{I}_s)V_1 - \hat{R}V_0D, \tag{4.1.7c}$$

where $\mathbf{1} = [1, 1, ..., 1]^T$, $C = diag(c_1, \ldots, c_s)$, $D = diag(1, \ldots, s)$ *and*

$$V_0 = \begin{bmatrix} 1 & c_1 & \ldots & c_1^{s-1} \\ \vdots & \vdots & \vdots & \vdots \\ 1 & c_s & \ldots & c_s^{s-1} \end{bmatrix}, \quad V_1 = \begin{bmatrix} 1 & (c_1-1) & \ldots & (c_1-1)^{s-1} \\ \vdots & \vdots & \vdots & \vdots \\ 1 & (c_s-1) & \ldots & (c_s-1)^{s-1} \end{bmatrix}. \tag{4.1.8}$$

4.1.2 EF IMEX peer methods

In order to construct EF IMEX peer methods let us to introduce the linear difference operators

$$\begin{aligned} &\mathcal{L}_i[h, \mathbf{w}]\, u(t) \\ &= u(t + c_i\, h) - \textstyle\sum_{j=1}^{s} b_{ij}\, u(t + (c_j - 1)\, h) - h \sum_{j=1}^{s} a_{ij}\, u^{'}(t + (c_j - 1)\, h) \\ &-h \textstyle\sum_{j=1}^{i} r_{ij}\, u^{'}(t + c_j\, h), \quad i = 1, \ldots, s, \end{aligned} \tag{4.1.9}$$

$$\begin{aligned} &\mathcal{L}_i[h, \hat{\mathbf{w}}]\, v(t) \\ &= v(t + c_i\, h) - \textstyle\sum_{j=1}^{s} \hat{b}_{ij}\, v(t + (c_j - 1)\, h) - h \sum_{j=1}^{s} \hat{a}_{ij}\, v^{'}(t + (c_j - 1)\, h) \\ &-h \textstyle\sum_{j=1}^{i-1} \hat{r}_{ij}\, v^{'}(t + c_j\, h), \quad i = 1, \ldots, s, \end{aligned} \tag{4.1.10}$$

where the vectors $\mathbf{w}$ and $\hat{\mathbf{w}}$ contain all the coefficients of the method (4.1.4) and the u and v functions belong to the fitting space as follows:

$$\mathcal{F} = \{1, t, t^2, \ldots, t^K, e^{\pm\mu t}, t\, e^{\pm\mu t}, t^2 e^{\pm\mu t}, \ldots, t^P e^{\pm\mu t}\}, \tag{4.1.11}$$

with $\mu = i\omega$, where $\omega \in \mathbb{R}$ is problem's oscillating frequency. The constants K and P are related by $K + 1 = s - 1 - 2P$, and we will consider the choices for classical (CL) and EF peer methods summarized in Table 4.1.

By using the linear difference operators (4.1.9)-(4.1.10), the six-step algorithm pre-

Table 4.1: Choices for K and P in the fitting space (4.1.11)

Method	K	P
CL peer	s	-1
EF peer, with s even	0	$\frac{s}{2} - 1$
EF peer, with s odd	-1	$\frac{s-1}{2}$

sented in [158] and by following the idea introduced in [73, 80] for the construction of EF peer method, order conditions for the coefficient matrices $A, \hat{A}, B, \hat{B}, R$ and $\hat{R}$ of partitioned EF peer methods of the form (4.1.4) are derived, as summarized in the following theorem.

This theorem makes use of the η-functions introduced in [72, 158] and recalled in the Section 2.2.1 of Chapter 2. Moreover, for a vector v of dimension s, we define

$$\theta_{\sigma,v} = \left[\eta_\sigma\left(v_1^2\, Z\right), \ldots, \eta_\sigma\left(v_s^2\, Z\right)\right]. \tag{4.1.12}$$

Theorem 16. *For any fixed matrices $\bar{B}$, $\hat{\bar{B}}$, lower triangular R and strictly lower triangular $\hat{R} \in \mathbb{R}^{s\times s}$ such that $\bar{B}\,\mathbf{1} = \hat{\bar{B}}\,\mathbf{1} = \mathbf{1}$, the peer method (4.1.4) has order $p = s$ and is adapted to the fitting space (4.1.11) with K and P given in Table 4.1, if the coefficient matrices $A, \hat{A}$ and $B, \hat{B}$ are calculated as*

$$A = (E_1 - \bar{B}E_2 - RE_4)E_3^{-1}, \tag{4.1.13a}$$
$$B = \bar{B} + \mathcal{H}_1 - ZA\mathcal{H}_2 - ZR\mathcal{H}_3, \tag{4.1.13b}$$

$$\hat{A} = (E_1 - \hat{\bar{B}}E_2 - \hat{R}E_4)E_3^{-1}, \tag{4.1.14a}$$
$$\hat{B} = \hat{\bar{B}} + \hat{\mathcal{H}}_1 - Z\hat{A}\mathcal{H}_2 - Z\hat{R}\mathcal{H}_3, \tag{4.1.14b}$$

where $Z = \mu^2 h^2$ the matrices E_i, $i = 1, 2, 3, 4$ are listed in Table 4.2 and the matrices $\mathcal{H}_j$, $j = 1, 2, 3$ and $\hat{\mathcal{H}}_1$ are listed in Table 4.3. In Tables 4.2-4.3, the matrices V_0, V_1, C and D are defined in Corollary 4.1.1, the vector $\theta_{\sigma,v}$ is defined in (4.1.12), matrices D_k, $k = 1, 2, 3, 4$ are reported in Table 4.4 and the matrices F_k, $k = 1, 2, 3, 4$ are obtaind by deleting the first column from the corresponding matrix D_k.

Table 4.2: Matrices E_i in order conditions (4.1.13a)-(4.1.14b).

Method	E_1	E_2	E_3	E_4
CL peer	CV_0	$(C - \mathbb{I}_s)V_1$	V_1D	V_0D
EF peer, with s even	D_1	D_2	D_3	D_4
EF peer, with s odd	F_1	F_2	F_3	F_4

Now, in order to derive EF IMEX peer methods, we determine the coefficients $A = A(Z)$, $B = B(Z)$, $R = R(Z)$, $\hat{A} = \hat{A}(Z)$, $\hat{B} = \hat{B}(Z)$ and $\hat{R} = \hat{R}(Z)$ by satisfying the order conditions of the Theorem 16. In the following, by using the idea of Soleimani et. al in [287], we describe the derivation of EF IMEX peer method.
Consider the system of ODEs (4.1.1). Using the framework presented in [15, 14, 306], system (4.1.1) can be converted into a system partitioned by components as follows:

$$\begin{aligned} &y = u + v, \\ &u' = \tilde{f}(u, v) = f(u + v), \\ &v' = \tilde{g}(u, v) = g(u + v). \end{aligned} \tag{4.1.15}$$

Table 4.3: Matrices $\mathcal{H}_j$ in order conditions (4.1.13a)-(4.1.14b).

Method	$\mathcal{H}_1$	$\hat{\mathcal{H}}_1$	$\mathcal{H}_2$	$\mathcal{H}_3$
CL peer	0	0	0	0
EF peer, s even	0	0	0	0
EF peer, s odd	$(\mathbf{0}\,\vert\,\theta_{-1,\,c}-\bar{B}\theta_{-1,\,c-\mathbf{1}})$	$(\mathbf{0}\,\vert\,\theta_{-1,\,c}-\hat{\bar{B}}\theta_{-1,\,c-\mathbf{1}})$	$(\mathbf{0}\,\vert\,(C-\mathbb{I}_s)\,\theta_{0,\,c-\mathbf{1}})$	$(\mathbf{0}\,\vert\,C\,\theta_{0,\,c})$

Table 4.4: Elements of the matrices $D_k = D_k(c, Z)$, $k = 1, 2, 3, 4$, for $i = 1, , s$ and $j = 1, \ldots, s$ if s is even while $j = 1, \ldots, s+1$ if s is odd.

Matrix	j odd, $k_j = \frac{j-1}{2}$	j even, $k_j = \frac{j-2}{2}$
$(D_1)_{i,j}$	$\frac{1}{2^{k_j}}\, c_i^{2k_j}\, \eta_{k_j-1}\,(c_i^2\, Z)$	$\frac{1}{2^{k_j}} c_i^{2k_j+1}\, \eta_{k_j}\,(c_i^2\, Z)$
$(D_2)_{i,j}$	$\frac{1}{2^{k_j}}\, \hat{c}_i^{2k_j}\, \eta_{k_j-1}\,(\hat{c}_i^2\, Z)$	$\frac{1}{2^{k_j}} \hat{c}_i^{2k_j+1}\, \eta_{k_j}\,(\hat{c}_i^2\, Z)$
$(D_3)_{i,j}$	$\frac{k_j}{2^{k_j-1}}\, \hat{c}_i^{2k_j-1}\, \eta_{k_j-1}\,(\hat{c}_i^2\, Z) + \frac{1}{2^{k_j}}\, \hat{c}_i^{2k_j+1}\, Z\eta_{k_j}\,(\hat{c}_i^2\, Z)$	$\frac{1}{2^{k_j}} \hat{c}_i^{2k_j}\, \eta_{k_j-1}\,(\hat{c}_i^2\, Z)$
$(D_4)_{i,j}$	$\frac{k_j}{2^{k_j-1}}\, c_i^{2k_j-1}\, \eta_{k_j-1}\,(c_i^2\, Z) + \frac{1}{2^{k_j}}\, c_i^{2k_j+1}\, Z\eta_{k_j}\,(c_i^2\, Z)$	$\frac{1}{2^{k_j}} c_i^{2k_j}\, \eta_{k_j-1}\,(c_i^2\, Z)$

In order to define an EF IMEX peer methods, we refer to Theorem 16 and choose an even number s of stages. Then, by fixing $\bar{B} = \hat{\bar{B}}$, according to Table 4.3, we have $B(Z) = \hat{B}(Z) = \bar{B}$ and the method (4.1.4) assumes the form:

$$\begin{aligned} U_n &= (\bar{B} \otimes \mathbb{I}_d)\, U_{n-1} + h\,(A(Z) \otimes \mathbb{I}_d)\, F(U_{n-1} + V_{n-1}) + h\,(R(Z) \otimes \mathbb{I}_d)\, F(U_n + V_n), \\ V_n &= (\bar{B} \otimes \mathbb{I}_d)\, V_{n-1} + h\,(\hat{A}(Z) \otimes \mathbb{I}_d)\, G(U_{n-1} + V_{n-1}) + h\,(\hat{R}(Z) \otimes \mathbb{I}_d)\, G(U_n + V_n). \end{aligned} \tag{4.1.16}$$

Adding the equations (4.1.16), by (4.1.15), it follows:

$$\begin{aligned} Y_n &= (\bar{B} \otimes \mathbb{I}_d)\, Y_{n-1} + h\,(A(Z) \otimes \mathbb{I}_d)\, F(Y_{n-1}) + h\,(R(Z) \otimes \mathbb{I}_d)\, F(Y_n) \\ &+ h\,(\hat{A}(Z) \otimes \mathbb{I}_d)\, G(Y_{n-1}) + h\,(\hat{R}(Z) \otimes \mathbb{I}_d)\, G(Y_n). \end{aligned} \tag{4.1.17}$$

Method (4.1.17) is called EF IMEX peer method. We observe that $\bar{B}$, $A(Z)$ and $R(Z)$ are cofficients of an implicit EF peer method of order s while $\bar{B}$, $\hat{A}(Z)$ and $\hat{R}(Z)$ are cofficients of an explicit EF peer method of order s. The order conditions follow directly from Theorem 16. Moreover, when $Z \longrightarrow 0$, (4.1.17) tends to CL IMEX peer methods [287].

4.2 An Advection-Diffusion model

Dynamic interactions between aquifers and the sea in coastal regions can be modeled by the Boussinesq equation, which can be written in the following form [203, 316]

$$\frac{\partial \phi}{\partial t} = \frac{K}{S}(\phi \frac{\partial^2 \phi}{\partial x^2} + (\frac{\partial \phi}{\partial x})^2 - \vartheta \frac{\partial \phi}{\partial x}),$$

where S is the drainable porosity, K is the hydraulic conductivity and ϑ is impermeable base slope. If $\phi = \phi(X,t)$ shows a slight deviation from the depth of weight, by setting $\gamma = \frac{T}{S}$, $\nu = K\frac{\vartheta}{S}$, where $T = K\phi$ is referred to as transmissivity in groundwater hydrology, the model can be written as:

$$\frac{\partial \phi}{\partial t} = (\gamma \frac{\partial^2 \phi}{\partial x^2} - \nu \frac{\partial \phi}{\partial x}),$$

where $(x,t) \in [0,+\infty) \times [0,+\infty)$ and equipping it with the following initial and boundary conditions

$$\phi(x,0) = \phi_0(x), \quad \phi(0,t) = \phi(X(t),t) = f(t),$$

where $X(t) = cot(\gamma) f(t)$ is the moving boundary depending on time of the parametric formulation [292].
Therefore we consider the linear advection-diffusion problem

$$\begin{array}{ll} \phi_t(x,t) = \gamma \phi_{xx}(x,t) - \nu \phi_x(x,t), & (x,t) \in (0,X) \times (0,T) \\ \phi(x,0) = \phi_0(x), & x \in [0,X], \\ \phi(0,t) = \phi(X,t) = f(t), & t \in [0,T]. \end{array} \tag{4.2.18}$$

with an arbitrary periodic boundary condition

$$f(t) = \exp(i\omega t). \tag{4.2.19}$$

Logan and Zlotnik have shown in [189], that the problem described by (4.2.18)-(4.2.19) exhibits a solution of the form

$$\phi(x,t) = \exp(\alpha x + i(\beta x + \omega t)) = \exp((\alpha + i\beta)x) \cdot \exp(i\omega t) \tag{4.2.20}$$

where i is the imaginary unit and

$$\alpha = \frac{\nu}{2\gamma} - \mu, \quad \beta = -\rho, \tag{4.2.21}$$

with

$$\mu = \frac{1}{2\gamma}\sqrt{2\gamma\sqrt{\omega^2 + \frac{\nu^4}{16\gamma^2}} + \frac{\nu^2}{2\gamma}}, \qquad \rho = \frac{1}{2\gamma}\sqrt{2\gamma\sqrt{\omega^2 + \frac{\nu^4}{16\gamma^2}} - \frac{\nu^2}{2\gamma}}.$$

4.3 EF IMEX peer methods for Boussinesq equation

In this section we construct EF IMEX peer methods for problem (4.2.18)-(4.2.19), whose solution, by (4.2.20), oscillates both in space and in time. Following the method of lines [151, 263, 264], we spatially discretize the domain D in

$$D_{\Delta x} = \{(x_n, t) : x_n = n\Delta x,\ n = 0, ..., N-1, \Delta x = \frac{X}{N-1}\},$$

where Δx is the spatial integration step. The resulting semi-discrete system (4.2.18) assumes the form

$$\begin{array}{ll} \phi_0^{'}(t) = f^{'}(t), & \\ \phi_n^{'}(t) = \gamma\theta_{2,n} - \nu\theta_{1,n}, & 1 \leqslant n \leqslant N-2, \\ \phi_{N-1}^{'}(t) = f^{'}(t), & \\ \phi_n(0) = \phi_0(x_n), & 0 \leqslant n \leqslant N-1. \end{array} \tag{4.3.22}$$

where $\phi_n(t) \simeq \phi(x_n, t)$, while $\theta_{1,n}$ and $\theta_{2,n}$ are finite differences approximating the first and second spatial derivatives in (4.2.18), respectively:

$$\theta_{1,n} = \frac{b_0\phi(x_{n-1}, t) + b_1\phi(x_n, t)}{\Delta x}, \quad \theta_{2,n} = \frac{a_0\phi(x_{n-1}, t) + a_1\phi(x_n, t) + a_2\phi(x_{n+1}, t)}{\Delta x^2}, \tag{4.3.23}$$

The coefficients a_0, a_1, a_2, b_0 and b_1 will be derived by the EF proccedure [100, 99] by considering the following fitting spaces $\mathcal{G}$ and $\mathcal{F}$ for the first and second spatial derivatives, respectively.

$$\begin{array}{l} \mathcal{G} = \{1,\ exp(\zeta x)\}, \\ \mathcal{F} = \{1,\ exp(\zeta x), xexp(\zeta x)\}, \end{array} \tag{4.3.24}$$

where $\zeta = \alpha + i\beta \in \mathbb{C}$, $z = \zeta\Delta x$.

The choice of fitting spaces (4.3.24) is motivated by (4.2.20).

4.3.1 Discretization of the diffusion terms

Using the fitting space $\mathcal{F}$ for the second order spatial derivative, we provide the approximation $\theta_{2,n}$ and evaluate a_0, a_1 and a_2. In summary, we have:

$$\phi_{xx}(x_n, t) \simeq \theta_{2,n} = \frac{a_0\phi(x_{n-1}, t) + a_1\phi(x_n, t) + a_2\phi(x_{n+1}, t)}{\Delta x^2}. \tag{4.3.25}$$

For computation of coefficients a_0, a_1 and a_2, we consider the following linear difference operator

$$\mathcal{L}[\Delta x]\,\phi(x, t) = \phi_{xx}(x, t) - \frac{a_0\phi(x - \Delta x, t) + a_1\phi(x, t) + a_2\phi(x + \Delta x, t)}{\Delta x^2}. \tag{4.3.26}$$

Enforcing the exactness of (4.3.25) on functions of the fitting space $\mathcal{F}$ in (4.3.24) is equivalent to annihilating the linear difference operator (4.3.26) on such functions. According to [158], it is enough to annihilate them for $x = 0$:

$$\begin{aligned} &\mathcal{L}[\Delta x]\, 1_{|x=0} = a_0 + a_1 + a_2 = 0, \\ &\mathcal{L}[\Delta x]\, \exp(\zeta x)_{|x=0} = z^2 - a_0 \exp(-z) - a_1 - a_2 \exp(z) = 0, \\ &\mathcal{L}[\Delta x]\, x \exp(\zeta x)_{|x=0} = 2z + a_0 \exp(-z) - a_2 \exp(z) = 0. \end{aligned} \tag{4.3.27}$$

Then, the coefficients are

$$\begin{aligned} a_0 = -\frac{zexp(z)(2 - 2exp(z) + zexp(z))}{(exp(z) - 1)^2},\ a_1 = \frac{z(2 - 2exp(2z) + z + zexp(2z))}{(exp(z) - 1)^2}, \\ a_2 = -\frac{z(2 - 2exp(z) + z)}{(exp(z) - 1)^2}. \end{aligned} \tag{4.3.28}$$

These coefficients are functions of z, where $z = \zeta \Delta x = (\alpha + i\beta)\Delta x$.

Generally, $z \neq 0$ since Δx and ζ are non-zero. Moreover, as z tends to 0, the coefficients tend to the classic finite difference values:

$$a_0 = a_2 = 1,\ a_1 = -2. \tag{4.3.29}$$

Also EF finite differences preserve the accuracy of classical finite differences, which is equal to 2.

4.3.2 Discretization of the advection terms

Now we discretize the advection term by using the fitting space $\mathcal{G}$ for the first order spatial derivative, we approximate $\theta_{1,n}$ and compute the b_0 and b_1. In this case, we have:

$$\phi_x(x_n, t) \simeq \theta_{1,n} = \frac{b_0 \phi(x_{n-1}, t) + b_1 \phi(x_n, t)}{\Delta x}, \tag{4.3.30}$$

We use the following linear difference operator for computation of coefficients b_0 and b_1,

$$\mathcal{M}[\Delta x]\, \phi(x, t) = \phi_x(x, t) - \frac{b_0 \phi(x - \Delta x, t) + b_1 \phi(x, t)}{\Delta x}. \tag{4.3.31}$$

By imposing the exactness of (4.3.30) on functions of the fitting space $\mathcal{G}$ (4.3.24), i.e. by annihilating the linear difference operator (4.3.31) on such functions, we obtain

$$\begin{aligned} &\mathcal{M}[\Delta x]\, 1_{|x=0} = b_0 + b_1 = 0, \\ &\mathcal{M}[\Delta x]\, \exp(\zeta x)_{|x=0} = z - b_0 \exp(-z) - b_1 = 0. \end{aligned} \tag{4.3.32}$$

Then, the coefficients are

$$b_0 = \frac{z}{(exp(-z)-1)},\ b_1 = -\frac{z}{(exp(-z)-1)}. \tag{4.3.33}$$

These coefficients are functions of z, where $z = \zeta\Delta x = (\alpha + i\beta)\Delta x$.

Also in this case, the obtaining coefficients, when z tends to 0, follow the classic finite difference values

$$b_0 = -1,\ \ b_1 = 1. \tag{4.3.34}$$

Also EF finite differences preserve the accuracy of classical finite differences, which is equal to 1.

4.3.3 The EF IMEX peer methods

Now, we concentrate on time integration of the spatially semidiscretized system (4.3.22), which assumes the compact form

$$\boldsymbol{\phi}'(t) = \mathcal{A}(z)\boldsymbol{\phi}(t) + \mathcal{B}(z)\boldsymbol{\phi}(t) + g(z,t), \tag{4.3.35}$$

where

- $x_n = n\Delta x$, $n = 0, \ldots, N-1$, $x_0 = 0$, $x_{N-1} = X$,
- $z = (\alpha + i\beta)\Delta x$,
- $\boldsymbol{\phi}(t) = [\phi(x_n, t)]_{n=1}^{d}$, $d = N-2$,
- $\mathcal{A}(z) = \frac{\gamma}{\Delta x^2}\mathtt{diag}(a_0, a_1, a_2), \mathcal{B}(z) = -\frac{\nu}{\Delta x}\mathtt{diag}(b_0, b_1, 0)$, tridiagonal matrices of dimension d,
- $g(z,t) = \left(\frac{\gamma a_0}{\Delta x^2} - \frac{\nu b_0}{\Delta x}\right) f(t)\mathbf{e_1} + \frac{\gamma a_2}{\Delta x^2} f(t)\mathbf{e_d}$, with $\mathbf{e_1} = (1, 0, ..., 0)^T \in \mathbb{R}^d$ and $\mathbf{e_d} = (0, ..., 0, 1)^T \in \mathbb{R}^d$.

The vector field of the system of ODEs (4.3.35) derives from processes of the advection and diffusion. The first summand is diffusion term that is typically stiff and depends on matrix $\mathcal{A}(z)$, and implicit methods have to be used. The part depending on matrix $\mathcal{B}(z)$, advection term, is non-stiff and can be treated by explicit methods [14, 148]. Indeed, IMEX methods, which implicitly integrate only the stiff constituents and explicitly integrate the others, can achieve benefits in stability and efficiency [14, 33, 34, 148].

We consider the fully discretized domain

$$D_{\Delta x,\Delta t} = \{(x_n, t_j) : x_n = n\Delta x,\ t_j = j\Delta t,\ n = 0, ..., N-1,\ j = 0, ..., M-1\}$$

being $\Delta x = \frac{X}{N-1}$, $\Delta t = \frac{T}{M-1}$. As the exact solution of the problem (4.2.18)-(4.2.19) has the form (4.2.20), we consider the time discretization by the adapted s-stage EF

IMEX peer method (4.1.17) with $h = \Delta t$ and $Z = \mu^2(\Delta t)^2 = -\omega^2(\Delta t)^2$. Therefore, by applying to (4.3.35) the adapted s-stage EF IMEX peer method (4.1.17), we have:

$$\begin{aligned}\Phi_{j+1} &= (\bar{B} \otimes \mathbb{I}_d)\, \Phi_j + \Delta t\, (A(Z) \otimes \mathbb{I}_d)\, F(\Phi_j) + \Delta t\, (R(Z) \otimes \mathbb{I}_d)\, F(\Phi_{j+1}) \\ &+\Delta t\, (\hat{A}(Z) \otimes \mathbb{I}_d)\, G(\Phi_j) + \Delta t\, (\hat{R}(Z) \otimes \mathbb{I}_d)\, G(\Phi_{j+1})\end{aligned} \tag{4.3.36}$$

where

$$\begin{aligned}F(\Phi_j) &= (\mathbb{I}_s \otimes \mathcal{A}(z))\, \Phi_j, \\ G(\Phi_j) &= (\mathbb{I}_s \otimes \mathcal{B}(z))\, \Phi_j + g(z, t_j + c\Delta t),\end{aligned} \tag{4.3.37}$$

where $c = (c_1, ..., c_s)^T$ and

$$\Phi_j \simeq \begin{pmatrix} \phi(x_1,\ t_j + c\Delta t) \\ \vdots \quad \vdots \qquad \vdots \quad \vdots \\ \phi(x_{N-2}, t_j + c\Delta t) \end{pmatrix} \in\ R^{sd},\ \ d = N - 2,$$

with

$$\phi(x_n,\ t_j + c\Delta t) = [\ \phi(x_n,\ t_j + c_1\Delta t), ...,\ \phi(x_n,\ t_j + c_s\Delta t)]^T \in\ R^s,\ n = 1, ..., N - 2.$$

Remark 2. *Observe that fully implicit peer methods derived in [80], applied to system* (4.3.35) *assume the form* (4.3.36) *with* $\hat{A}(Z) = A(Z)$ *and* $\hat{R}(Z) = R(Z)$.

4.4 Stability analysis

We now analyze the stability properties of the proposed numerical method. According to the framework of [285], our goal is to verify stability by controlling the propagation of the error caused by an incoming perturbation. The solution of (4.3.36) Φ_j, $j = 0, ..., M - 1$ is then perturbed, as follows:

$$\tilde{\Phi}_j = \Phi_j + \delta^j,$$

and we analyze the behavior of the error

$$E_j = \Phi_j - \tilde{\Phi}_j. \tag{4.4.38}$$

We have the following stability theorem.

Theorem 17. *For the EF IMEX peer methods* (4.3.36) *applied to the semidiscrete problem* (4.1.17)*, we obtain the following stability inequality*

$$\|E_{j+1}\|_\infty \leqslant\ \|\mathcal{M}\|_\infty \|E_j\|_\infty ,$$

where

$$\mathcal{M} = \Omega^{-1}\,\Lambda, \tag{4.4.39}$$

being

$$\Omega = (\mathbb{I}_{d.s} - \Delta t\,(R(Z)\otimes\mathbb{I}_d)\,(\mathbb{I}_s\otimes\mathcal{A}(z)) - \Delta t\,(\hat{R}(Z)\otimes\mathbb{I}_d)\,(\mathbb{I}_s\otimes\mathcal{B}(z))), \tag{4.4.40}$$

and

$$\Lambda = (\bar{B}\otimes\mathbb{I}_d + \Delta t\,(A(Z)\otimes\mathbb{I}_d)\,(\mathbb{I}_s\otimes\mathcal{A}(z)) + \Delta t\,(\hat{A}(Z)\otimes\mathbb{I}_d)\,(\mathbb{I}_s\otimes\mathcal{B}(z))). \tag{4.4.41}$$

Proof. By the discretization error in a fixed time grid point (4.4.38) and applying the IMEX EF peer method (4.3.36), we have:

$$\begin{aligned} E_{j+1} &= (\bar{B}\otimes\mathbb{I}_d)\,E_j + \Delta t\,(A(Z)\otimes\mathbb{I}_d)\,(F(\Phi_j) - F(\tilde{\Phi}_j)) + \Delta t\,(R(Z)\otimes\mathbb{I}_d)\,(F(\Phi_{j+1}) \\ &-F(\tilde{\Phi}_{j+1})) + \Delta t(\hat{A}(Z)\otimes\mathbb{I}_d)(G(\Phi_j) - G(\tilde{\Phi}_j)) + \Delta t(\hat{R}(Z)\otimes\mathbb{I}_d)(G(\Phi_{j+1}) - G(\tilde{\Phi}_{j+1})) \end{aligned} \tag{4.4.42}$$

Applying (4.3.37) and taking into (4.4.42), we have:

$$E_{j+1} = \Omega^{-1}\,\Lambda\,E_j.$$

where Ω and Λ are given by (4.4.40) and (4.4.41), respectively. The tesis immediately follows. □

According to Theorem 17, stability is ensured if $\|\mathcal{M}\|_\infty < 1$, where $\mathcal{M}$ given by the (4.4.39).

Since infinity norm of

$$\|\mathcal{B}(z)\|_\infty = \frac{(|b_0| + |b_1|)|\nu|}{\Delta x}$$

and

$$\|\mathcal{A}(z)\|_\infty = \frac{(|a_0| + |a_1| + |a_2|)|\gamma|}{\Delta x^2},$$

then,

$$\|\mathcal{M}\|_\infty \leqslant \|\Omega^{-1}\|_\infty \Big(\left\|\bar{B}\right\|_\infty + \Delta t\,\|A(Z)\|_\infty\,(\frac{3(|z(2-2exp(2z)+z+zexp(z))|)|\gamma|}{\Delta x^2|(exp(z)-1)^2|})$$

$$+\Delta t\left\|\hat{A}(Z)\right\|_\infty\,(\frac{2(|z|)|\nu|}{\Delta x|(exp(-z)-1)|})\Big).$$

By setting: $\varepsilon_1 = \|A(Z)\|_\infty$, $\hat{\varepsilon_1} = \left\|\hat{A}(Z)\right\|_\infty$, $\varphi(z) = \dfrac{(|z(2-2exp(2z)+z+zexp(z))|)}{|(exp(z)-1)^2|}$ and $\hat{\varphi}(z) = \dfrac{(|z|)}{|(exp(-z)-1)|}$, the stability condition $\|\mathcal{M}\|_\infty < 1$ reduces to:

$$\|\Omega^{-1}\|_\infty \left(\|\bar{B}\|_\infty + 6\frac{\Delta t}{\Delta x^2}|\gamma|\varepsilon_1\varphi(z) + 2\frac{\Delta t}{\Delta x}|\nu|\hat{\varepsilon_1}\hat{\varphi}(z)\right) < 1.$$

For the classical case, when z tend to zero, $\lim\limits_{z\to 0}\ \varphi(z) = 2$, $\lim\limits_{z\to 0}\ \hat{\varphi}(z) = 1$, then for stability condition it is enough to ensure that:

$$\|\Omega^{-1}\|_\infty \left(\|\bar{B}\|_\infty + 12\frac{\Delta t}{\Delta x^2}|\gamma|\varepsilon_1 + 2\frac{\Delta t}{\Delta x}|\nu|\hat{\varepsilon_1}\right) < 1.$$

4.5 Numerical experiments

In this section we present the numerical results obtained by applying the IMEX EF peer method developed in the previous section to Boussinesq equation (4.2.18)-(4.2.19). We report in the tables the error calculated as the infinite norm of the difference at the end point between the numerical solution and the exact solution. Moreover, in the figures, we represent the profile of real part of numerical solutions computed by different solvers and compare them based on stability behavior.

Example 3. *We consider the Boussinesq equation* (4.2.18) *with* $X = 10$ *and* $T = 10$ *with the periodic boundary conditionf*$(t) = \exp(i\omega t)$ *and* $h_0(x) = e^{\alpha x + i\beta x}$ *where* α *and* β *given by* (4.2.21).

Consider $s = 2$. By according to Section 8.1.2, in this case $K = 0$ and $P = 0$. We fix $c_1 = 0$, $c_2 = 1$, the corresponding EF IMEX peer method is

$$\begin{aligned}
&\bar{B} = \begin{bmatrix} 0 & 1 \\ 0 & 1 \end{bmatrix},\ R(Z) = \begin{bmatrix} 1 & 0 \\ 0 & 1 \end{bmatrix},\ \hat{R}(Z) = \begin{bmatrix} 0 & 0 \\ 0 & 0 \end{bmatrix},\\
&\hat{A}(Z) = \begin{bmatrix} 0 & 0 \\ \frac{1-\eta_{-1}(Z)}{Z\eta_0(Z)} & -\eta_{-1}(Z)\frac{1-\eta_{-1}(Z)}{Z\eta_0(Z)} + \eta_0(Z) \end{bmatrix},\\
&A(Z) = \begin{bmatrix} 0 & -1 \\ \frac{1-\eta_{-1}(Z)}{Z\eta_0(Z)} + 1 & \frac{\eta_{-1}(Z)}{Z\eta_0(Z)}(\eta_0(Z) - 1 - (Z\eta_0(Z) - \eta_{-1}(Z))) + \eta_0(Z) - 1 \end{bmatrix},
\end{aligned} \tag{4.5.43}$$

by refering to Theorem 16.

The corresponding classical IMEX peer method is obtained in the limit when $Z \to 0$ and has coefficients:

$$\begin{aligned}
&c = \begin{bmatrix} 0 \\ 1 \end{bmatrix},\quad \bar{B} = \begin{bmatrix} 0 & 1 \\ 0 & 1 \end{bmatrix},\quad R = \begin{bmatrix} 1 & 0 \\ 0 & 1 \end{bmatrix},\quad \hat{R} = \begin{bmatrix} 0 & 0 \\ 0 & 0 \end{bmatrix},\\
&A = \begin{bmatrix} 0 & -1 \\ 1 & 0 \end{bmatrix},\quad \hat{A} = \begin{bmatrix} 0 & 0 \\ \frac{1}{2} & \frac{3}{2} \end{bmatrix},
\end{aligned} \tag{4.5.44}$$

The EF IMEX peer method introduced in Section 4.3 for the numerical solution of (4.2.18) in based on two levels of adaptation: in space by means of EF finite differences, and in time by means of EF peer methods. We will use the following notations to indicate the usage of classical or adapted numerical methods:

- **CL FD:** Spatial semidiscretization based on classical finite difference (4.3.35) with coefficients (4.3.29) and (4.3.34),
- **EF FD:** Spatial semidiscretization based on EF finite difference (4.3.35) with coefficients (4.3.28) and (4.3.33),
- **CL IMEX P2:** Classical IMEX peer time integration of order 2 with coefficients (4.5.44),
- **EF IMEX P2:** EF IMEX peer time integration of order 2 with coefficients (4.5.43),
- **CL IM P2:** Classical implicit peer time integration of order 2 with coefficients $\bar{B}$, A, R (4.5.44) and $\hat{A} = A$, $\hat{R} = R$ according to Remark 2,
- **EF IM P2:** EF implicit peer time integration of order 2 with coefficients $\bar{B}$, $A(Z)$, $R(Z)$ (4.5.43) and $\hat{A(Z)} = A(Z)$, $\hat{R(Z)} = R(Z)$ according to Remark 2.

The obtained results confirm the effectiveness of the proposed EF IMEX method. In Tables 4.5 and 4.7 we compare fully implicit peer methods [80] and IMEX peer methods for system (4.3.35). We observe that EF explicit peer methods reported in [73, 77] are unstable because of the presence of stiff part. From Tables 4.5 and 4.7 we observe that implicit and IMEX peer methods have the same behavior in accuracy but the IMEX methods have smaller computational cost. Also the results listed in Tables 4.5 and 4.7 show that the EF peer methods produce smaller errors with respect to their classic counterparts and the best results are obtained by adapting the method both in space and time.

Tables 4.6 and 4.8 show the behavior of the methods when the parameters ω, α and β characterizing the exact solution are not known exactly. By denoting with δ the relative error in the parameters, we apply EF FD combined with EF IM and EF IMEX peer methods whose coefficients are calculated in correspondence of $z = (\alpha(1+\delta) + i\beta(1+\delta))\Delta x$, $Z = -\omega^2(1+\delta)^2(\Delta t)^2$. Observe that the error of EF peer methods keeps smaller than the corresponding classic counterparts and when δ increases it approachs the result of classic methods.

Figure 4.1 represents the profile of real part of numerical solution computed by both classical methods in space and time, while in Figure 4.2 we employed EF methods both in space and time. We observe that an unstable behavior of CL FD+CL IMEX P2

solver is clearly visible, while EF FD+EF IMEX P2 solver is able to correctly reproduce the profile of the solution.

Table 4.5: Errors with parameter values $\gamma = 5, \nu = 2, \omega = 2, \Delta x = \Delta t = 0.1$, Example 3.

Space/Time	CL IM P2	CL IMEX P2	EF IM P2	EF IMEX P2
CL FD	$6.05e-03$	$2.59e-02$	$5.04e-03$	$5.04e-03$
EF FD	$9.84e-03$	$2.71e-02$	$6.67e-14$	$6.57e-14$

Table 4.6: Errors with parameter values $\gamma = 5, \nu = 2, \omega = 2, \Delta x = \Delta t = 0.1$ when the coefficients of EF FD and EF P2 are computed in correspondence of $z = (\alpha(1+\delta) + i\beta(1+\delta))\Delta x$, $Z = -\omega^2(1+\delta)^2(\Delta t)^2$, Example 3.

	EF	EF $\delta = 10^{-7}$	EF $\delta = 10^{-1}$	CL
FD + IM P2	$6.67e-14$	$2.40e-09$	$2.30e-03$	$6.05e-03$
FD + IMEX P2	$6.57e-14$	$5.39e-09$	$7.76e-03$	$2.59e-02$

Table 4.7: Errors with parameter values $\gamma = 5, \nu = 2, \omega = 20, \Delta x = \Delta t = 0.1$, Example 3.

Space/Time	CL IM P2	CL IMEX P2	EF IM P2	EF IMEX P2
CL FD	$1.03e-01$	$1.53e+00$	$3.85e-03$	$3.85e-03$
EF FD	$3.98e-01$	$1.53e+00$	$5.36e-15$	$4.00e-15$

Table 4.8: Errors with parameter values $\gamma = 5, \nu = 2, \omega = 20, \Delta x = \Delta t = 0.1$ when the coefficients of EF FD and EF P2 are computed in correspondence of $z = (\alpha(1+\delta) + i\beta(1+\delta))\Delta x$, $Z = -\omega^2(1+\delta)^2(\Delta t)^2$, Example 3.

	EF	EF $\delta = 10^{-7}$	EF $\delta = 10^{-1}$	CL
FD + IM P2	$5.36e-15$	$4.31e-08$	$3.37e-02$	$4.03e-01$
FD + IMEX P2	$4.00e-15$	$2.57e-07$	$2.12e-01$	$1.53e+00$

Figure 4.1: Profile of real part of numerical solution computed by CL FD+CL IMEX P2 solver for $\gamma = 5, \nu = 20, \omega = 20, \Delta x = \Delta t = 0.1$, Example 3.

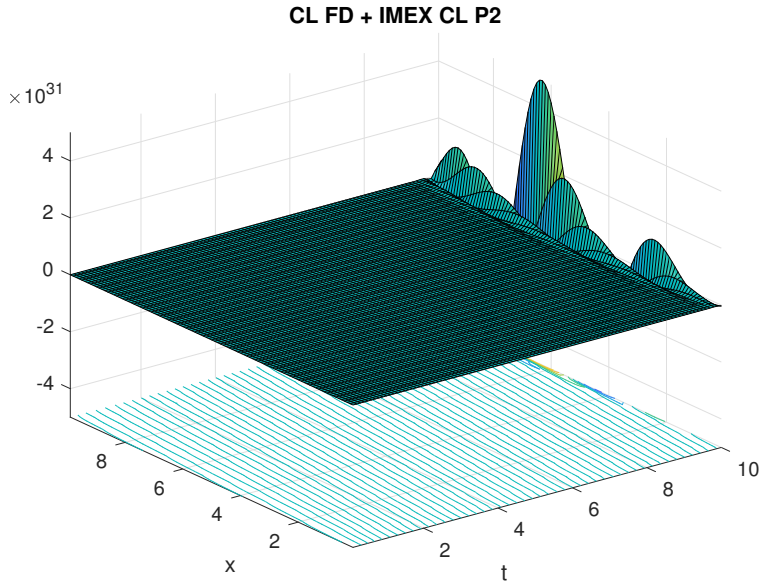

Figure 4.2: Profile of real part of numerical solution computed by EF FD+EF IMEX P2 solver for $\gamma = 5, \nu = 20, \omega = 20, \Delta x = \Delta t = 0.1$, Example 3.

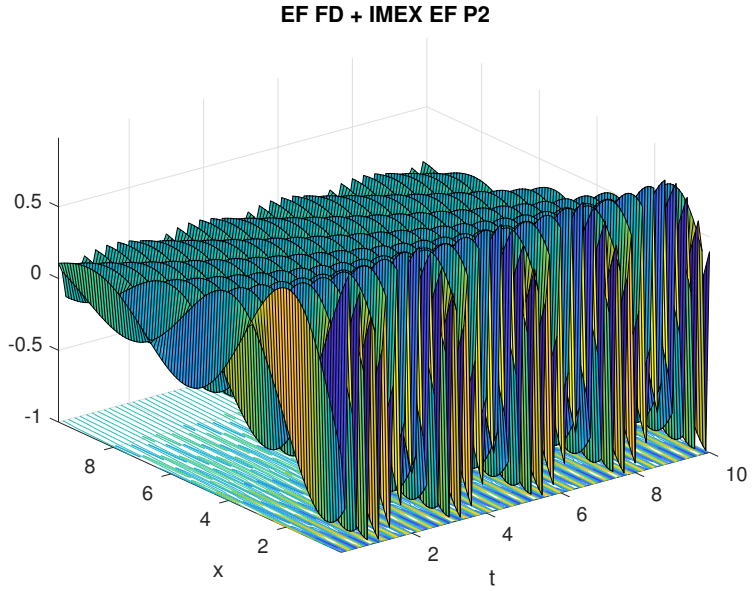

4.6 Conclusion

In this chapter, we have developed a novel IMEX method for numerical solution of advection-diffusion problems with oscillatory solutions. Infact we have proposed an adapted numerical method both in space and in time. The spatial semidiscretization of the problem is based on finite differences, adapted to both to the diffusion and advection terms while the time discretization employed EF implicit-explicit peer methods. Numerical experiments shown the convenience of the new method with respect to classical, fully implicit and IMEX methods.

Chapter 5

Frequency evaluation for adapted peer methods

As observed in Chapters 3 and 4, EF technique has been widely studied in the past few decades to improve the efficiency and accuracy of numerical solutions for problems with oscillating or periodic solutions [76, 78, 97, 98, 99, 158, 161, 164, 280, 281, 303, 237]. EF algorithms were designed to overcome the limitations of classical algorithms, which require very small step sizes for accuracy when the oscillation frequency is high. With the EF technique, the same level of accuracy can be achieved with larger step sizes, leading to more efficient and accurate numerical methods.

One of the critical questions in developing EF methods is how to choose the frequencies to maximize their benefits. In previous studies, [157, 162, 163], an algorithm was presented to tune the frequencies optimally for systems of ODEs using EF multistep methods. The optimal frequencies were derived by considering the expression of the error, which depends on higher-order derivatives of the solution.

Therefore, the exponential fitting technique remains valuable for solving problems with oscillatory or periodic solutions. The development of optimal frequency selection algorithms continues to be an active area of research. The present chapter focuses on a general class of EF two-step peer methods [73, 80] of the form (5.1.2) for the numerical integration of ODEs (5.1.1) with oscillatory solutions. In this chapter, we make an essential contribution by investigating Ixaru's frequency evaluation algorithm for adapted EF peer methods and presenting new frequency formulae based on the behavior of the leading term of the error.

The chapter begins with a brief review of EF peer methods in Section 5.1, laying the foundation for the rest of the chapter. Then, Section 5.2 explores the fundamental concepts of frequency evaluation and the development of an EF peer method frequency assessment algorithm. The estimation of derivatives is also discussed in Section 5.3. To demonstrate the effectiveness of the new frequency assessment algorithm, numer-

ical examples are presented in Section 5.4. Finally, the chapter concludes with some conclusions drawn in Section 5.5.

5.1 EF peer methods

We consider systems of ODEs of the form

$$y'(t) = f(t, y(t)), \quad y(t_0) = y_0 \in \mathcal{R}^d, \quad t \in [t_0, T], \tag{5.1.1}$$

where $f : \mathcal{R} \times \mathcal{R}^d \to \mathcal{R}^d$ is sufficiently smooth to ensure that the solution exists and it is unique. In addition, we assume that the problem (5.1.1) possesses an oscillatory solution. Let $\{t_n := t_0 + nh,\ n = 0, \ldots, N\}$ be a discretization of the interval $[t_0, T]$ with fixed stepsize $h > 0$, $0 \leqslant c_1 \leqslant \ldots \leqslant c_s = 1$ be fixed distinct nodes and define $t_{ni} = t_n + c_i h$, $i = 1, \ldots, s$. Two-step peer methods can be formulated as follows:

$$Y_n = (B \otimes \mathbb{I})\, Y_{n-1} + h\,(A \otimes \mathbb{I})\, F(Y_{n-1}) + h\,(R \otimes \mathbb{I})\, F(Y_n), \tag{5.1.2}$$

where $h > 0$ is the stepsize, $\mathbb{I}$ is the identity matrix of dimension d, $A = [a_{ij}]_{i,j=1}^{s}$, $B = [b_{ij}]_{i,j=1}^{s}$ and $R = [r_{ij}]_{i,j=1}^{s}$ are the coefficient matrices. The stages vector $Y_n = [Y_{ni}]_{i=1}^{s}$ contains the approximations $Y_{ni} \approx y(t_{ni})$ and $F(Y_n) = [f(t_{ni}, Y_{ni})]_{i=1}^{s}$. As $c_s = 1$, Y_{ns} is the approximation of the solution at grid point t_{n+1}.
The procedure for the construction of EF peer methods is a crucial step in the development of efficient numerical methods for solving problems with oscillatory or periodic solutions. This procedure is described in detail in Chapter 3, Section 3.1, and Section 3.2. In order to provide a clear and concise overview, the authors have compiled the procedure into an algorithm, which is briefly reviewed below.

The algorithm outlines the steps involved in constructing EF peer methods, including selecting a suitable exponential function, calculating coefficients, and implementing the method. It is important to note that the construction of EF peer methods is an iterative process, and the algorithm provides a clear and concise guide for this process and can help simplify the development of EF peer methods.

Algorithm 1 : Construction of EF peer methods

Start: Choose the fitting space:

$$\mathcal{F} = \{1, t, t^2, \ldots, t^K, e^{\pm\mu t}, t\, e^{\pm\mu t}, t^2 e^{\pm\mu t}, \ldots, t^P e^{\pm\mu t}\}, \tag{5.1.3}$$

with $\mu = i\,\omega$ where $\omega \in \mathbb{R}$ is problem's oscillating frequency.

Use: Define the linear difference operator

$$\begin{aligned}\mathcal{L}_i[h, \mathbf{w}]\; y(t) = y(t + c_i\, h) - \sum_{j=1}^{s} b_{ij}\; y(t + (c_j - 1)\, h) - h \sum_{j=1}^{s} a_{ij}\; y'(t + (c_j - 1)\, h) \\ - h \sum_{j=1}^{i} r_{ij}\; y'(t + c_j\, h),\; i = 1, \ldots, s,\end{aligned} \tag{5.1.4}$$

where the vector $\mathbf{w}$ contains all the coefficients of the method (5.1.2). The coefficient matrices A, B and R of peer methods (5.1.2) are obtained by imposing that the operator (5.1.4) annihilates when the function y belongs to the fitting space (5.1.3).

Step 1: Construct the classic moments and the dimensionless classic moments:

$$\mathcal{L}^*_{i\,m}(h, \mathbf{w}) = \frac{1}{h^m} \mathcal{L}_i[h, \mathbf{w}] t^m|_{t=0} \text{ for } \; i = 1, \ldots, s, \quad m = 0, 1, \ldots, M - 1. \tag{5.1.5}$$

which have the form:

$$\begin{aligned}\mathcal{L}^*_{i\,m}(h, \mathbf{w}) = c_i^m - \sum_{j=1}^{s} b_{ij}\; (c_j - 1)^m - m \sum_{j=1}^{s} a_{ij}\; (c_j - 1)^{m-1} - m \sum_{j=1}^{i} r_{ij}\; c_j^{m-1}, \\ \text{for } \; i = 1, \ldots, s, \quad m = 0, 1, \ldots, M - 1.\end{aligned} \tag{5.1.6}$$

Step 2: We now look for the maximum value M that ensures the compatibility of the system

$$\mathcal{L}^*_{i\,m}(h, \mathbf{w}) = 0, \quad i = 1, \ldots, s, \quad m = 0, 1, \ldots, M - 1, \tag{5.1.7}$$

which is equivalent to annihilating the difference operator (5.1.4) on polynomials with a degree less or equal to $M - 1$. This system corresponds to the simplifying condition (4.1.5) with $q = M$.

$$\begin{aligned}\text{AB}(M) = c_i^m - \sum_{j=1}^{s} b_{ij}\; (c_j - 1)^m - m \sum_{j=1}^{s} a_{ij}\; (c_j - 1)^{m-1} \\ - m \sum_{j=1}^{i} r_{ij}\; c_j^{m-1} = 0, i = 1, \ldots, s, \quad m = 0, \ldots, M - 1.\end{aligned} \tag{5.1.8}$$

Therefore, we may construct an s-order peer method if $M = s+1$, due to the Theorem 15 and Corollary 4.1.1.

Step 3: Construct the formal expressions of

$$E^*_{i\,m}(z, \mathbf{w}) = \frac{1}{h^m}\mathcal{L}_i[h, \mathbf{w}]t^m e^{\mu t}|_{t=0} = 0, \quad i = 1, \ldots, s, \tag{5.1.9}$$

$$G_i^{\pm(m)}(Z, \mathbf{w}) = 0, \quad m = 0, 1, \ldots, P, \quad i = 1, \ldots, s,$$

where $Z = z^2$ and $G_i^{\pm(m)}(Z, \mathbf{w})$ are the $G-$functions at each stage i

$$G_i^+(Z, \mathbf{w}) = \frac{E^*_{i0}(z, w) + E^*_{i0}(-z, w)}{2},\ G_i^-(Z, \mathbf{w}) = \frac{E^*_{i0}(z, w) - E^*_{i0}(-z, w)}{2z}, \tag{5.1.10}$$

Step 4: Construct the possible expressions for the fitting space (5.1.3) taking into account that $M = s + 1$ and the self-consistency condition $K + 2P = M - 3$ has to be verified. The number of stages s and the dimension M of the system (5.1.7) are of different parities, so the number $K + 1 = s - 1 - 2P$ of classic functions in the fitting space is odd or even if s is even or odd.

Step 5: Solve formally the linear systems

$$\mathcal{L}^*_{i\,m}(h, \mathbf{w}) = 0, \quad i = 1, \ldots, s, \quad m = 0, \ldots, K,$$
$$G_i^{\pm(m)}(Z, \mathbf{w}) = 0, \quad i = 1, \ldots, s, \quad m = 0, \ldots, P.$$

with Z dependent coefficients. The numeric values of a_{ij} and b_i are computed either for real or imaginary μ-values.

Step 6: Compute the leading term of the local truncation error for CL and EF peer methods (Choices for K and P summarized in Table 5.1):

$$(lte_{ef})_i = (-1)^{P+1}h^{s+1}\frac{\mathcal{L}^*_{i,K+1}(h, \mathbf{w})}{(K+1)!\,Z^{P+1}}\ D^{K+1}(D^2 - \mu^2)^{P+1}y(t), \quad i = 1, \ldots, s,$$

where we denote D the derivative with respect to time.

5.2 Frequency evaluation

5.2.1 Basic elements

The question of how frequencies need to be tuned to achieve maximum benefit from EF methods has not been answered for a long time. Ixaru et al. [157, 162, 163], and Vanden Berghe et al. [301, 302] have proposed a frequency evaluation algorithm for EF multistep methods and EF Runge-Kutta methods (respectively) which enable to tune of the frequency μ in the way that the principal local truncation error vanishes. Therefore, the analysis of the error behavior is a required step. We refer to the articles [157, 162, 163, 301, 302] for technical information and even some practical points and we restrict the discussion to only three relevant cases: $A0$, $A1$, and $A2$ algorithms that exactly incorporate all linear combinations from the reference set of functions.

- Algorithm $A0$: $\{1, t, t^2, \ldots, t^K\}$,
- Algorithm $A1$: $\{1, t, t^2, \ldots, t^K, e^{\mu t} \,|\, \mu \in \mathbb{R}\}$,
- Algorithm $A2$: $\{1, t, t^2, \ldots, t^K, e^{\pm \mu t} \,|\, \mu \in \mathbb{R}\, or\, \mu \in i\mathbb{R}\}$,

where K is specified by the considered method. The choice $A0$ covers the purely algebraic classical method; Algorithm $A1$ is especially of importance whenever the solution exhibits a purely exponential behavior, while Algorithm $A2$ describes oscillatory solutions if μ is strictly imaginary.

As said, for the investigation of frequency, analyzing the behavior of the error is a necessary stage. We compute the expression of the leading term of the error (lte) for these algorithms by using the general procedure described in Section 5.1 and appropriate options for K and P in the fitting space based on the above algorithms.

Method	K	P
CL peer, (Algorithm $A0$)	s	-1
EF peer, with s even or odd (Algorithm $A1$)	$s-1$	0
EF peer, with s even or odd (Algorithm $A2$)	$s-2$	0

Table 5.1: Choices for K and P in the fitting space (5.1.3)

5.2.2 Frequency evaluation for adapted EF peer methods

To start, we consider EF peer methods derived in Algorithm 1 to the scalar equation $y'(t) = f(t, y(t))$, then the leading term of their error (lte) assumes the form

$$(lte_{ef})_i = (-1)^{P+1} h^{s+1} \frac{\mathcal{L}^*_{i,K+1}(h, \mathbf{w})}{(K+1)!\, Z^{P+1}}\, D^{K+1}(D^2 - \mu^2)^{P+1} y(t), \quad i = 1, \ldots, s. \quad (5.2.11)$$

When we apply three types of algorithms $A0$, $A1$ and $A2$ to the scalar equation (5.1.1) and assume appropriate options for K and P in the fitting space summarized in Table 5.1 and by attention to Eq. (5.2.11) the lte is derived as follows.

- Algorithm $A0$: in this case $K = s$ and $P = -1$, therefore lte is described as follows
$$(lteA0) = \frac{h^{s+1}}{(s+1)!} D^{s+1} y(t); \tag{5.2.12}$$
- Algorithm $A1$: in this case $K = s-1$ and $P = 0$ and lte is given by the following expressions assuming s even or odd.
  - if $s = 2$, then $K = 1, P = 0$
$$(lteA1)_i = \frac{-h^3}{2!} \frac{\mathcal{L}^*_{i,2}(h, \mathbf{w})}{Z} D^2(D^2 - \mu^2) y(t); \quad i = 1, 2, \tag{5.2.13}$$
  - if $s = 3$, then $K = 2, P = 0$
$$(lteA1)_i = \frac{-h^4}{3!} \frac{\mathcal{L}^*_{i,3}(h, \mathbf{w})}{Z} D^3(D^2 - \mu^2) y(t), \quad i = 1, 2, 3. \tag{5.2.14}$$
- Algorithm $A2$: for this case with $K = s - 2$ and $P = 0$, assuming that s is even or odd, the following expressions provide lte.
  - $s = 2$, then $K = 0, P = 0$
$$(lteA2)_i = -h^3 \frac{\mathcal{L}^*_{i,1}(h, \mathbf{w})}{Z} D(D^2 - \mu^2) y(t); \quad i = 1, 2, \tag{5.2.15}$$
  - $s = 3$, then $K = 1, P = 0$
$$(lteA2)_i = \frac{-h^4}{2!} \frac{\mathcal{L}^*_{i,2}(h, \mathbf{w})}{Z} D^2(D^2 - \mu^2) y(t), \quad i = 1, 2, 3. \tag{5.2.16}$$

Our principal purpose is to determine the μ value that guarantees maximum accuracy when the classical $A0$ case is replaced by one of the two EF Algorithms. For the calculation of parameter μ, we restrict discussion to the expressions for the lte of $A1$ and $A2$ cases especially for $s = 2$ and $s = 3$:

$$\begin{aligned}
(lte\mathrm{A1}, s = 2) &= \frac{-h^3}{2} \frac{\mathcal{L}^*_{i,2}(h, \mathbf{w})}{Z} \Big(y^{(4)}(t) - \mu^2 y''(t) \Big), \ \ i = 1, 2, \\
(lte\mathrm{A1}, s = 3) &= \frac{-h^4}{3!} \frac{\mathcal{L}^*_{i,3}(h, \mathbf{w})}{Z} \Big(y^{(5)}(t) - \mu^2 y^{(3)}(t) \Big), \ \ i = 1, 2, 3, \\
(lte\mathrm{A2}, s = 2) &= -h^3 \frac{\mathcal{L}^*_{i,1}(h, \mathbf{w})}{Z} \Big(y^{(3)}(t) - \mu^2 y'(t) \Big), \ \ i = 1, 2, \\
(lte\mathrm{A2}, s = 3) &= \frac{-h^4}{2} \frac{\mathcal{L}^*_{i,2}(h, \mathbf{w})}{Z} \Big(y^{(4)}(t) - \mu^2 y''(t) \Big), \ \ i = 1, 2, 3.
\end{aligned} \tag{5.2.17}$$

In all cases, we see that the lte consists of a product of three factors, i.e.

- a general h^3 (in the case $s = 2$) or general h^4 factor (in the case $s = 3$),
- a function depending on Z which tends to the classical value when Z tends to zero.
- a factor that involves two derivatives of the solution.

The important thing for our studies is the different behavior of the third factor. This differential factor can make a real difference in accuracy. Let us then introduce the following functionals:

$$\mathcal{D}_1[y(t),\mu,s=2]=\left(y^{(4)}(t)-\mu^2 y^{''}(t)\right),\quad \mathcal{D}_1[y(t),\mu,s=3]=\left(y^{(5)}(t)-\mu^2 y^{(3)}(t)\right)$$

$$\mathcal{D}_2[y(t),\mu,s=2]=\left(y^{(3)}(t)-\mu^2 y^{'}(t)\right),\quad \mathcal{D}_2[y(t),\mu,s=3]=\left(y^{(4)}(t)-\mu^2 y^{''}(t)\right)$$

If a μ exists such that $\mathcal{D}_1$ identically vanishes on the quoted interval then the version $A1$ corresponding to that μ will be exact. The reason is that identically vanishing $\mathcal{D}_1$ is equivalent to looking at the differential equation $y^{(4)}(t)-\mu^2 y^{''}(t)=0$ and $y^{(5)}(t)-\mu^2 y^{(3)}(t)=0$ for $s=2$ and $s=3$, respectively.
In general, no constant μ can be found such that $\mathcal{D}_1$ identically vanishes but it makes sense to address the problem of finding that value of μ which ensures that the values of $\mathcal{D}_1$ are kept as close to zero as possible for t_n in the considered interval. When $\mathcal{D}_1$ is held close to zero, the optimal μ are given by

$$\mu_{A1,s=2}=\pm\sqrt{\frac{y^{(4)}(t_n)}{y^{''}(t_n)}},\quad \mu_{A1,s=3}=\pm\sqrt{\frac{y^{(5)}(t_n)}{y^{(3)}(t)}}. \tag{5.2.18}$$

In $A1$ case the frequency must be real.

For algorithm $A2$, the same considerations can be repeated for $\mathcal{D}_2$. The reason is that identically vanishing $\mathcal{D}_2$ are equivalent to looking at the differential equation $y^{(3)}(t)-\mu^2 y^{'}(t)=0$ and $y^{(4)}(t)-\mu^2 y^{''}(t)=0$ for $s=2$ and $s=3$, respectively. When $\mathcal{D}_2$ is held close to zero, the optimal μ are given by

$$\mu_{A2,s=2}=\pm\sqrt{\frac{y^{(3)}(t_n)}{y^{'}(t_n)}},\quad \mu_{A2,s=3}=\pm\sqrt{\frac{y^{(4)}(t_n)}{y^{''}(t_n)}}. \tag{5.2.19}$$

The frequencies are either real or imaginary if Algorithm $A2$ is chosen.
We have succeeded in proposing formulae for the optimal $\mu=\mathrm{i}\omega$ (ω is frequency)

value in (5.2.18)-(5.2.19). Having found the optimal value for μ, we have the optimal frequency ω.

5.3 Estimation of the derivatives

The evaluation of the optimal μ value and then optimal frequency ω requires knowing the total derivatives appearing in the expressions of the formulae (5.2.18)-(5.2.19). At first, it seems like a very simple task: the first-order derivative is equivalent to the right-hand sides of the equation (5.1.1) i.e. $f(t, y(t))$, after that, it is very straightforward to calculate the higher-order derivatives. This technique works well on many problems, but in [157], authors demonstrate this should be avoided on stiff problems. They also demonstrate that it is sufficient to use finite difference approximations of the derivatives. Since the expressions of the formulae (5.2.18)-(5.2.19) contain derivatives of orders three and four (for $s = 2$) and four and five (for $s = 3$), we will estimate the derivatives in each integration point t_n with five points finite difference formulae for $s = 2$ and six points finite difference formulae for $s = 3$.

Since in [304], the author has shown approximation of the derivatives by five points finite difference formulae, in this work we just mention the formulae of the six points finite difference with data at $t_{n-4}, t_{n-3}, t_{n-2}, t_{n-1}, t_n$ and t_{n+1} for the input.

$$
\begin{aligned}
y^{'} &\simeq \frac{3\,y_{n-4} - 20\,y_{n-3} + 60\,y_{n-2} - 120\,y_{n-1} + 65\,y_n + 12\,y_{n+1}}{60h},\\
y^{''} &\simeq \frac{y_{n-4} - 6\,y_{n-3} + 14\,y_{n-2} - 4\,y_{n-1} - 15\,y_n + 10\,y_{n+1}}{12h^2},\\
y^{(3)} &\simeq \frac{-\,y_{n-4} + 7\,y_{n-3} - 22\,y_{n-2} + 34\,y_{n-1} - 25\,y_n + 7\,y_{n+1}}{4h^3},\\
y^{(4)} &\simeq \frac{-\,y_{n-4} + 6\,y_{n-3} - 14\,y_{n-2} + 16\,y_{n-1} - 9\,y_n + 2\,y_{n+1}}{h^4},\\
y^{(5)} &\simeq \frac{-\,y_{n-4} + 5\,y_{n-3} - 10\,y_{n-2} + 10\,y_{n-1} - 5\,y_n + \,y_{n+1}}{h^5}.
\end{aligned}
$$

The data y_{n-4}, y_{n-3}, y_{n-2}, y_{n-1}, y_n for the input points are the value of the numerical solution at $t_{n-4}, t_{n-3}, t_{n-2}, t_{n-1}, t_n$. The estimation for the y_{n+1} at t_{n+1} is determined by Milne-Simpson two-step formulae [157] as follows:

$$
y_{n+1} = y_{n-1} + \frac{h}{3}\big(f(t_{n-1}, y_{n-1}) + 4\,f(t_n, y_n) + f(t_{n+1}, y_{n+1})\big).
$$

It is necessary that we make this approximation with a method that has a higher or the same order as the EF peer method. Therefore it is sufficient to choose Milne-Simpson's

two-step formulae. We only use the result for the calculation of the derivatives and not for the propagation of the solution.

Case $s = 2$:

If t_n is a root of $y^{''}(t)$, the algorithm $A1$ is not defined, while $A2$ is not defined when t_n is a root of $y^{'}(t)$. In a very special case, when t_n is a root of both $y^{'}(t)$ and $y^{''}(t)$ EF algorithms are not suitable and so the classic $A0$ Algorithm must be activated. In general, a logical way to choose between $A1$ and $A2$ involves comparing $|y^{'}(t)|$ and $|y^{''}(t)|$. If $|y^{'}(t_n)| < |y^{''}(t_n)|$ then $A1$ is selected, otherwise $A2$.

Case $s = 3$:

In this case, if t_n is a root of $y^{(3)}(t)$, the algorithm $A1$ is not defined, whereas $A2$ when t_n is a root of $y^{''}(t)$, not defined. It happens that both $y^{''}(t)$ and $y^{(3)}(t)$ change the sign with the same time interval, neither the two EF algorithms are not suitable, so the classic $A0$ should be enabled. In general, as in the previous case, there is a reasonable way to choose between $A1$ and $A2$ involves comparing $|y^{''}(t)|$ and $|y^{(3)}(t)|$. If $|y^{''}(t_n)| < |y^{(3)}(t_n)|$ then algorithm $A1$ otherwise $A2$ is selected.

5.4 Numerical experiments

In this section we present numerical experiments showing the behaviour of the new "optimal EF peer methods", with Z-dependent coefficients whose are computed for optimal μ-values in (5.2.18)-(5.2.19). In the following examples, we apply the described optimal EF peer methods and the classic and EF peer methods to solve the test cases. We compare errors of the optimal EF implicit peer methods with errors of classic and EF implicit peer methods of [80] in Examples 4 and 5 , and we also compare achieved results from Example 6 with reported results by Ixaru et al. in [157].

The error will be estimated as the infinite norm of the difference between the numerical solution and the exact solution at the endpoint and reported in the tables. In addition, we will use the following notation to represent the used numerical methods:

- CL = classic,
- EF = exponentially fitted,
- IM P2 = implicit peer method of order 2.

In the following examples, we use the notation reported in [80]. We consider $s = 2$. In this case $K = 0$ and $P = 0$. We fix $c_1 = 0$, $c_2 = 1$. According to $Z = \mu^2 h^2 = -\omega^2 h^2$,

the numerical values of a_{ij} and b_i are computed either for real or imaginary μ-values. The corresponding optimal EF IM peer method and EF IM peer method are:

$$B = \begin{bmatrix} 0 & 1 \\ 0 & 1 \end{bmatrix}, R = \begin{bmatrix} 1 & 0 \\ 0 & 1 \end{bmatrix},$$
$$A = \begin{bmatrix} 0 & -1 \\ \frac{1-\eta_{-1}(Z)}{Z\eta_0(Z)} + 1 & \frac{\eta_{-1}(Z)}{Z\eta_0(Z)}(\eta_0(Z) - 1 - (Z\eta_0(Z) - \eta_{-1}(Z))) + \eta_0(Z) - 1 \end{bmatrix}.$$

Example 4. *Let us consider the Prothero-Robinson problem*

$$\begin{aligned} y'(t) &= \lambda\,(\,y(t) - \sin(51\,t)\,) + (51)\,\cos(51\,t), \quad t \in \left[0, \frac{\pi}{2}\right], \\ y(0) &= 0, \end{aligned} \tag{5.4.20}$$

whose exact solution is

$$y(t) = \sin(51\,t) = \sin(50\,t)\,\cos(t) + \cos(50\,t)\,\sin(t).$$

The oscillating behavior of the exact solution leads us to utilize the EF methods with the parameter μ characterizing the functions belonging to the fitting space equal to $\mu = \mathrm{i}\,\omega$. So the problem is integrated by the EF peer methods, where the parameter ω is chosen equal to the frequency of the exact solution, i. e. $\omega = 50$.

We also consider the case in which the oscillatory frequency ω is not known exactly. Therefore by finding the frequency from the formulae (5.2.18)-(5.2.19) and denoting with ω_{op}, we employ the EF peer methods whose coefficients are computed in correspondence of a frequency ω_{op} and $\mu = i\,\omega_{op}$ value.

We used the initial conditions and carried out with CL, EF IM peer methods, and optimal EF IM peer methods, whose algorithms are constructed by the procedure described in Algorithm 1. We consider interval $[0, \frac{\pi}{2}]$ with different grid points $N = 320, 640, 1280$. Tables 5.2, 5.3 represent the absolute errors from the considered methods, for $\lambda = -1$ (non stiff case) and $\lambda = -10^6$ (stiff case). We see that the optimal EF IM peer method works much better than CL and is close to EF IM peer methods, irrespective of whether the problem is stiff or non-stiff.
For additional confirmation, we present some graphs for both cases $\lambda = -1$ and $\lambda = -10^6$. In Fig. 5.1, we depict the variation of ω_{op} at each integration point for the problem when the A2 algorithm is chosen. It is seen from Figs. 5.2, (as expected) the obtained ω_{op} is close to $\omega = 50$. It is instructive to mention that Fig. 5.2 shows the efficiency curve for this problem obtained by the CL IM, EF IM, and optimal EF IM peer methods.

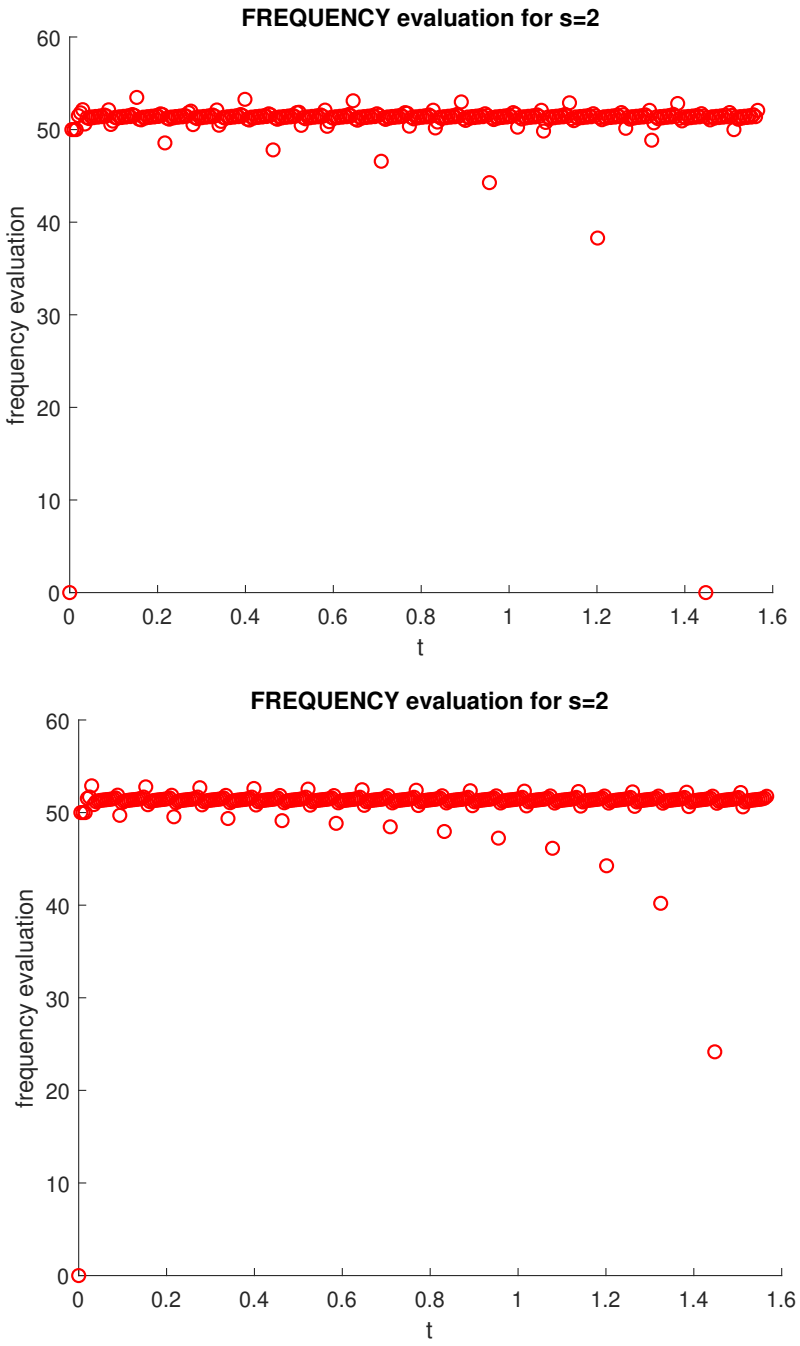

Figure 5.1: Plot of calculated ω_{op} for problem (5.4.20) with $\lambda = -1$ (up),$\lambda = -10^6$ (below), $N = 320$ grid point for Example 4.

		N		
Methods	ω	320	640	1280
CL IM P2	$--$	$3.78e-02$	$9.33e-03$	$2.31e-03$
EF IM P2	50	$1.45e-03$	$3.62e-04$	$8.98e-05$
Optimal EF IM P2	ω_{op}	$7.89e-04$	$6.23e-05$	$5.83e-06$

Table 5.2: Comparison of errors for the problem (5.4.20) with $\lambda = -1$, N grid points and fixed and optimal frequency ω for Example 4.

		N		
Methods	ω	320	640	1280
CL IM P2	$--$	$2.16e-7$	$2.55e-8$	$3.15e-09$
EF IM P2	50	$9.73e-10$	$1.36e-10$	$1.22e-10$
Optimal EF IM P2	ω_{op}	$9.49e-09$	$3.08e-10$	$9.62e-12$

Table 5.3: Comparison of errors for the problem (5.4.20) with $\lambda = -10^6$, N grid points and fixed and optimal frequency ω for Example 4.

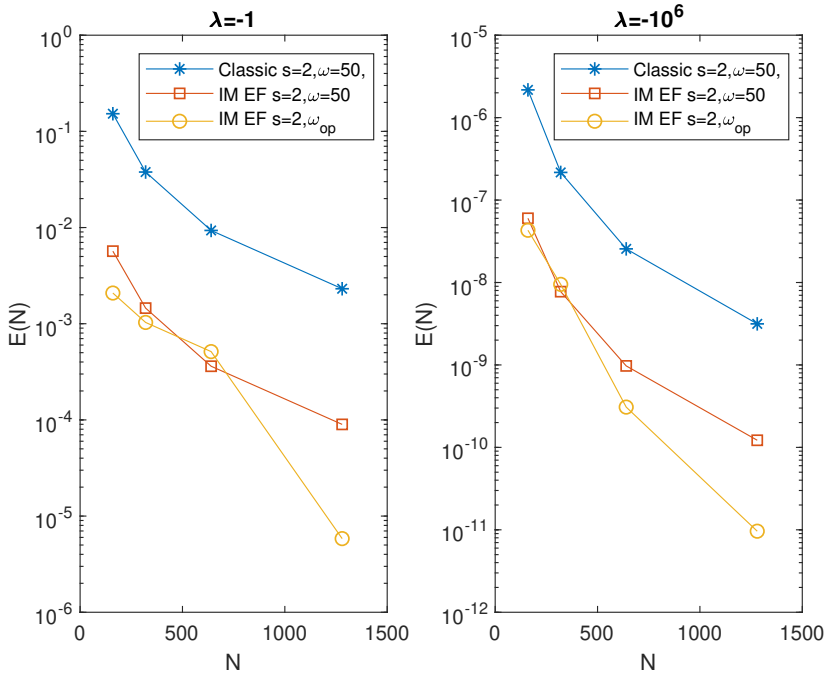

Figure 5.2: Plots of errors of the considered methods (5.4.20) with $\lambda = -1$ (left), $\lambda = -10^6$ (right), N grid points and fixed and optimal frequency ω for Example 4.

Example 5. *Consider the Prothero-Robinson problem*

$$\begin{aligned} y'(t) &= \lambda\,(\,y(t) - \sin(101\,t)\,) + (101)\,\cos(101\,t), \quad t \in \left[0, \frac{\pi}{2}\right], \\ y(0) &= 0, \end{aligned} \tag{5.4.21}$$

where exact solution is

$$y(t) = \sin(101\,t) = \sin(100\,t)\,\cos(t) + \cos(100\,t)\,\sin(t).$$

The oscillating behavior of the exact solution leads us to utilize the EF methods with the parameter $\mu = \mathrm{i}\,\omega$. This system is integrated by the EF peer methods, where the parameter ω is chosen equal to the frequency of the exact solution, i. e. $\omega = 100$. In this example, we also consider the case in which the oscillatory frequency ω is not known exactly and we integrate the system by the optimal EF peer methods with ω_{op}. In detail, we utilized the initial conditions and performed the experiments with CL and EF IM peer methods, as well as optimal EF IM peer methods, whose algorithms are constructed in the process outlined in Algorithm 1. We examine the interval $[0, \frac{\pi}{2}]$ with various grid points $N = 320, 640, 1280$. The absolute errors from the considered approaches are listed in the tables 5.4, 5.5 for $\lambda = -1$ (non-stiff case) and $\lambda = -10^6$ (stiff case).

Whether the problem is stiff or non-stiff, the optimal EF IM peer methods perform much better than CL IM and are close to EF IM peer methods. We offer some graphs for both scenarios $\lambda = -1$ and $\lambda = -10^6$ for extra validation. In Fig. 5.4, we depict the variation of ω_{op} at each integration point for the problem when the A2 algorithm is chosen. As predicted, it is obvious from Fig. 5.4, the obtained ω_{op} is close to $\omega = 100$. It is instructive to mention that Fig. 5.3 shows the efficiency curve for this problem obtained by the CL, EF, and optimal EF IM peer methods.

		N		
Methods	ω	320	640	1280
CL IM P2	$--$	$1.31e-01$	$3.45e-02$	$8.81e-03$
EF IM P2	100	$2.53e-03$	$6.77e-04$	$1.73e-04$
Optimal EF IM P2	ω_{op}	$8.41e-03$	$4.96e-05$	$1.93e-05$

Table 5.4: Comparison of errors for the problem (5.4.21) with $\lambda = -1$, N grid points and fixed and optimal frequency ω for Example 5.

		N		
Methods	ω	320	640	1280
CL IM P2	$--$	$2.16e-7$	$7.51e-08$	$4.90e-08$
EF IM P2	100	$5.78e-08$	$7.52e-09$	$9.48e-10$
Optimal EF IM P2	ω_{op}	$4.61e-07$	$1.27e-08$	$5.78e-10$

Table 5.5: Comparison of errors for the problem (5.4.21) with $\lambda = -10^6$, N grid points and fixed and optimal frequency ω for Example 5.

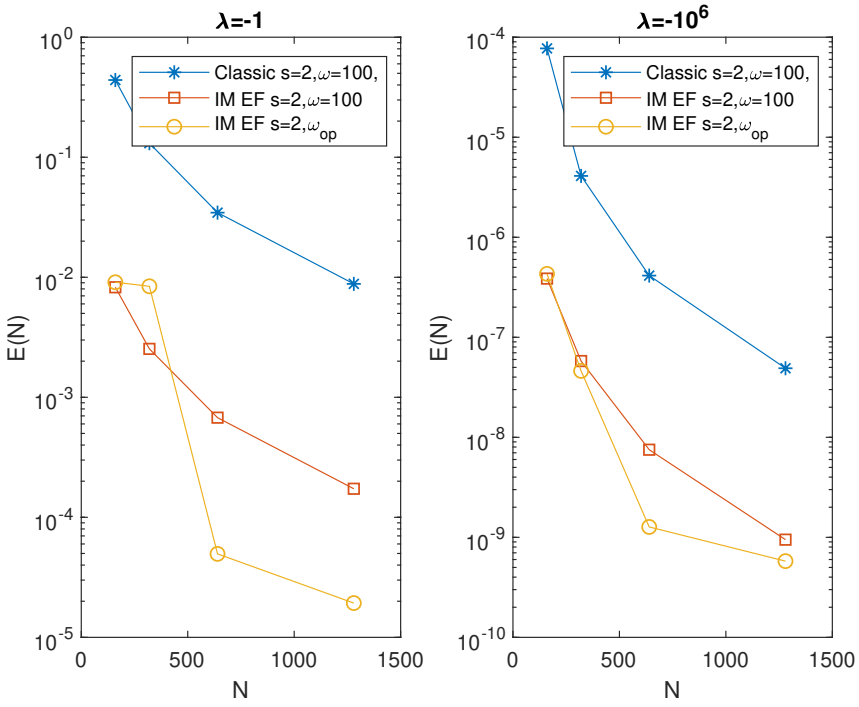

Figure 5.3: Plots of errors of the considered methods on problem (5.4.21) with $\lambda = -1, -10^6$, N grid points and different values for the frequency ω for Example 5.

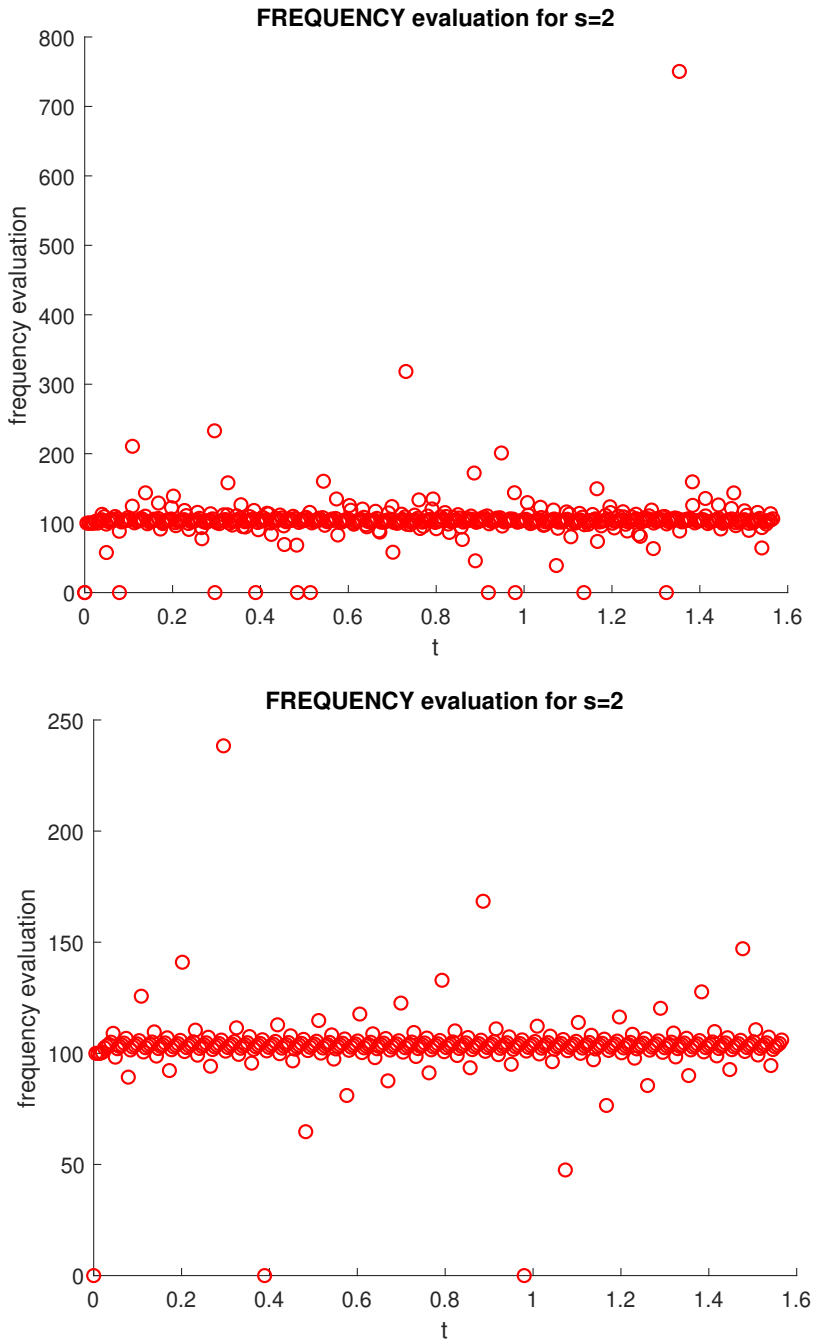

Figure 5.4: Plot of calculated ω_{op} for problem (5.4.21) with $\lambda = -1(up), -10^6(below)$, $N = 320$ grid point for Example 5.

Example 6. *Consider the following test case*

$$y' = 1 - t + \frac{1}{2}t^2, \qquad t > 0, \quad y(0) = 1, \tag{5.4.22}$$

with the exact solution

$$y(t) = 1 + t - \frac{1}{2}t^2 + \frac{1}{6}t^3.$$

This is a simple differential equation, and it helps to illustrate some exciting aspects when (5.4.22) is approached by optimal EF IM peer methods (with Z-dependent coefficients whose are computed for optimal μ-values) introduced in this work. We can construct the optimal μ value for both $A1$ and $A2$ algorithms by using formulae (5.2.18) and (5.2.19). For instance, when $s = 2$, by using formulae (5.2.18) the optimal μ value for $A1$ is the constant representation

$$\varphi_1(t) = \mu^2 = \frac{y^{(4)}(t_n)}{y''(t_n)} = 0$$

while by using formulae (5.2.19) the optimal μ^2 value for $A2$ is

$$\varphi_2(t) = \mu^2 = \frac{y^{(3)}(t_n)}{y'(t_n)} = \frac{1}{1 - t + \frac{t^2}{2}}$$

.

It follows that by using the $A1$ algorithm when $s = 2$, we don't have all of the data to construct the optimal μ value. For this reason, in this test case, we construct the solution by the $A2$ algorithm along with the whole interval. In Fig. 5.5, we depict the variation of optimal μ^2 at each integration point for the problem. As predicted, it is evident from Fig. 5.5, $\mu^2 \simeq 0.024$ when $t = 10$, $s = 2$, $h = 0.0125$, as the theoretically expected value 0.024 is also given from $\varphi_2(10)$.

This test case has been employed by Ixaru et al. in [157]. They used EF multistep methods for Eq. (5.4.22). In Table 5.6, we report the absolute errors at $t = 1, t = 5$ and $t = 10$, with the fixed stepsize $h = 0.0500, 0.0250$ and $h = 0.0125$ by optimal EF IM peer methods and compare them with reported results in [157]. From this table, we observe that for $s = 2$, the optimal EF IM peer methods have the same accuracy behavior concerning with EF multistep methods [157].

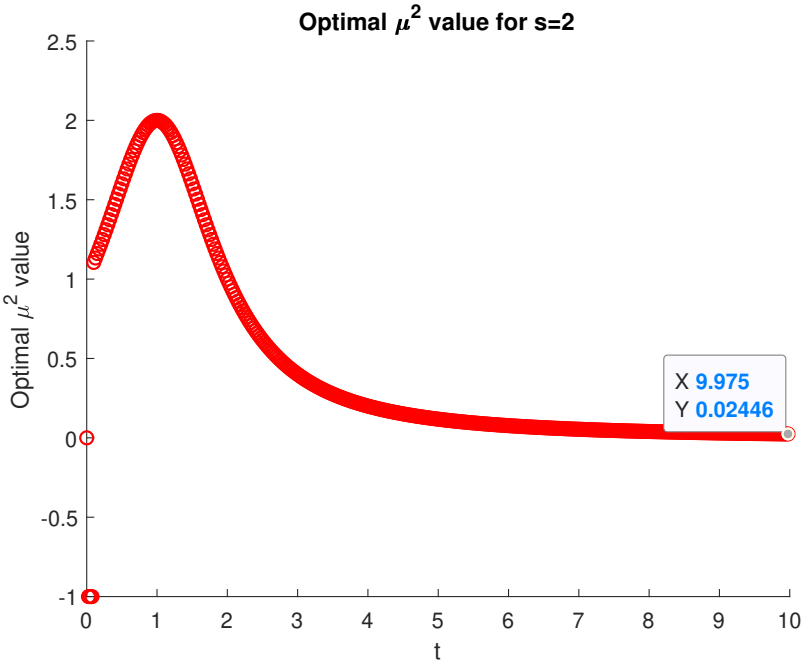

Figure 5.5: Plot of calculated optimal μ^2 value for problem (5.4.22) for $s = 2$, $h = 0.0125$ for Example 6.

t=1			
	$h = 0.0500$	$h = 0.0250$	$h = 0.0125$
Classical A0 [157]	$-8.15e-04$	$-2.06e-04$	$-5.18e-05$
EF multistep [157]	$-1.61e-05$	$-2.08e-06$	$-2.73-07$
optimal EF IM P2	$4.86e-04$	$5.78e-05$	$7.06e-06$
t=5			
	$h = 0.0500$	$h = 0.0250$	$h = 0.0125$
Classical A0 [157]	$-4.15e-03$	$-1.04e-03$	$2.60e-04$
EF multistep [157]	$1.68e-05$	$1.80e-06$	$2.16e-07$
optimal EF IM P2	$4.14e-04$	$5.25e-05$	$6.62e-06$
t=10			
	$h = 0.0500$	$h = 0.0250$	$h = 0.0125$
Classical A0 [157]	$-8.31e-3$	$-2.08e-03$	$-5.21e-04$
EF multistep [157]	$2.53e-05$	$2.87e-06$	$3.49e-07$
optimal EF IM P2	$4.01e-04$	$5.11e-05$	$6.46e-06$

Table 5.6: Comparison of errors for the problem (5.4.22) for Example 6.

5.5 Conclusion

In this chapter, we applied EF peer methods for the numerical solution of first-order ODEs and examined the problem of how the frequencies should be tuned to obtain the maximal benefit from the exponential fitting versions. To answer this question, we analyzed the error behavior of EF peer methods. We have succeeded in proposing formulae for optimal μ values. Under this condition and with the determination of optimal μ values, we achieved the "optimal EF peer methods". The introduced methods were tested on some examples, and the efficiency of optimal EF peer methods was shown.

Part II

Numerical solution of Volterra integral equations

Chapter 6

Numerical solution of delay Volterra functional integral equations with variable bounds

In recent decades, the numerical treatment of integral equations has attracted considerable interest. VIEs are significant in modeling phenomena in many applicable fields, including engineering, mechanics, physics, chemistry, astronomy, biology, economics, potential theory, and electrostatics, among others [24, 32, 222].

Since it is typically challenging to solve VIEs analytically, numerical approaches are employed. In the numerical computation of integral and differential equations, spectral methods have grown in popularity [46, 52, 67, 68, 274]. Various numerical approaches based on spectral methods and orthogonal polynomials have been employed to solve VIEs [127, 248, 222, 307]. When the solution to the problem is infinitely smooth, spectral methods have excellent error characteristics and provide exponential rates of convergence.

This chapter proposes a new numerical method to solve delay VIEs of the form

$$\sum_{k=0}^{m_1} P_k(x) y(\alpha_k x + \beta_k) = f(x) + \sum_{r=0}^{m_2} \lambda_r \int_{u_r(x)}^{v_r(x)} K_r(x,t) \mathcal{F}(y(\mu_r t + \gamma_r)) dt, \qquad (6.0.1)$$

where $P_k(x)$, $f(x)$, $K_r(x,t)$, $u_r(x)$ and $v_r(x)$ are continuous functions on the interval $[a,b]$, $a \leqslant u_r(x) \leqslant v_r(x) \leqslant b$ and α_k,β_k,λ_k,μ_k and γ_k are appropriate constants. $\mathcal{F}(y(\mu_r t + \gamma_r))$ is a function of unknown function of $y(x)$.

The classical orthogonal polynomials belong to the discrete/continuous orthogonal polynomials category. The idea of using discrete orthogonal polynomials is due to the projection approach. Examples of discrete polynomials include Charlier, Meixner, Krwtchouk, and Hahn. The chapter focuses on using Hahn polynomials $\mathcal{H}_n[x, \alpha, \beta, N]$,

which are discrete orthogonal polynomials, to solve Volterra integral equations (VIEs). The Hahn polynomials, invented by W. Hahn [131] in 1949, are discrete orthogonal polynomials of degree n on the interval $[0, N]$ in the variable x with parameters $\alpha, \beta > -1$.

The chapter is organized as follows: Section 6.1 introduces the Hahn polynomials and some of their characteristics. Section 6.2 examines the Hahn coefficients and provides proof of their spectral accuracy and convergence. In Section 6.3, the operational matrix of integration, derivation, and product for the Hahn polynomials has been derived. Section 6.4 proposes a collocation approach based on Hahn polynomials and their associated operational matrices to solve VIEs (6.0.1). The numerical experiments in Section 6.5 validate the correctness of the approach. Finally, the chapter concludes in Section 6.6 with a discussion of the results. The use of Hahn polynomials in this chapter is based on the collocation approach and has been referred to as the HPs approach. The chapter aims to demonstrate the effectiveness of Hahn polynomials in solving VIEs.

6.1 Hahn polynomials and properties

This section briefly describes Hahn polynomials, including their formulae and characteristics. The Hahn polynomials $\mathcal{H}_n[x, \alpha, \beta, N]$ were introduced in 1949 by W. Hahn [131]. They are discrete orthogonal polynomials of degree n and $\alpha, \beta > -1$ on the range $[0, N]$ in the variable x. For further information about Hahn polynomials, please see [124, 171, 317].

Definition 6.1.1. *For arbitary complex numbers a_i, $i = 1, 2, 3$ and $b_j \neq 0$, $j = 1, 2$ the generalized hypergeometric series ${}_3F_2(a_1, a_2, a_3; b_1, b_2; z)$ is defined as*

$$ {}_3F_2(a_1, a_2, a_3; b_1, b_2; z) = \sum_{k=0}^{\infty} \frac{(a_1)_k (a_2)_k (a_3)_k}{(b_1)_k (b_2)_k} . \frac{z^k}{k!} $$

where

$$ \begin{aligned} &(a_i)_0 = 1, \\ &(a_i)_k = a_i(a_i + 1)...(a_i + k - 1), \quad k \geqslant 1. \end{aligned} \tag{6.1.2} $$

The series terminates if one of the a_i is zero or a negative integer.

Definition 6.1.2. *The Hahn polynomials $\mathcal{H}_n(x) = \mathcal{H}_n(x; \alpha, \beta, N), n = 0, 1, ..., N$ when N is positive integer and for real $\alpha, \beta > -1$ are defined by*

$$ \mathcal{H}_n(x) = {}_3F_2(-n, -x, n + \alpha + \beta + 1; \alpha + 1, -N; 1). \tag{6.1.3} $$

$\mathcal{H}_n(x)$ is a polynomials on the interval $[0, N]$ in the variable x of degree n.

By using (6.1.3) and generalized hypergeometric series ${}_3F_2$, the explicit formula of Hahn polynomials is as follows:

$$ \mathcal{H}_n(x) = \sum_{k=0}^{n} \frac{(-n)_k (n + \alpha + \beta + 1)_k (-x)_k}{(\alpha + 1)_k (-N)_k k!}, \qquad n = 0, 1, ...N. \tag{6.1.4} $$

Remark 3. *Hahn polynomials are orthogonal on* $[0, N]$. *The orthogonality relation of these polynomials as follows:*

$$\langle \mathcal{H}_n(x), \mathcal{H}_n(x) \rangle = \sum_{x=0}^{N} \mathcal{H}_n(x)\mathcal{H}_n(x)w(x) = \frac{(-1)^n(n+\alpha+\beta+1)_{N+1}(\beta+1)_n n!}{(2n+\alpha+\beta+1)(-N)_n(\alpha+1)_n N!} \tag{6.1.5}$$

and if $n \neq m$

$$\langle \mathcal{H}_n(x), \mathcal{H}_m(x) \rangle = 0$$

where $w(x)$ *is the weight function and defined as*

$$w(x) = \begin{pmatrix} \alpha+x \\ x \end{pmatrix} \begin{pmatrix} \beta+N-x \\ N-x \end{pmatrix} = \frac{\Gamma(\alpha+x+1)\Gamma(\beta+N-x+1)}{\Gamma(x+1)\Gamma(N-x+1)\Gamma(\alpha+1)\Gamma(\beta+1)}.$$

By using of expansion of Hahn polynomials in terms of Taylor basis, relation (6.1.4) can be written the following form

$$\mathcal{H}_n(x) = \sum_{k=0}^{n} a_{k,n} x^k, \qquad n = 0, 1, ...N,$$

such that

$$a_{k,n} = \sum_{i=k}^{n} (-1)^i \frac{(-n)_i (n+\alpha+\beta+1)_i \, S_k^i}{(\alpha+1)_i (-N)_i i!}$$

where

$$S_k^i = \frac{1}{i!} \sum_{r=0}^{i} (-1)^{i-r} \begin{pmatrix} i \\ r \end{pmatrix} r^k.$$

Remark 4. *The polynomials solve the eigenvalue equation*

$$\gamma_n \, \mathcal{H}_n(x) = B(x) \, \mathcal{H}_n(x+1) - [B(x) + D(x)] \mathcal{H}_n(x) + D(x) \, \mathcal{H}_n(x-1) \tag{6.1.6}$$

with eigenvalues $\gamma_n = n(n+\alpha+\beta+1)$, $B(x) = (x+\alpha+1)(x-N)$ *and* $D(x) = x(x-\beta-N-1)$. *By using the difference operators*

$$\triangle f(x) := f(x+1) - f(x), \ \bigtriangledown f(x) := f(x) - f(x-1)$$

and their identities

$$\begin{aligned} &\triangle f(x) = \bigtriangledown f(x+1), \\ &\triangle [f(x)g(x)] = f(x) \triangle g(x) + g(x+1) \triangle f(x) \\ &\bigtriangledown [f(x)g(x)] = f(x-1) \bigtriangledown g(x) + g(x) \bigtriangledown f(x) \end{aligned} \tag{6.1.7}$$

we can reshape equation (6.1.6) in the following self-adjoint form

$$\triangle \left[-D(x) \, w(x) \, \bigtriangledown \mathcal{H}_n(x) \right] + \gamma_n \, w(x) \, \mathcal{H}_n(x) = 0 \tag{6.1.8}$$

with weight function w.

Function approximation:

Any function $f(x)$, defined over the interval $[0,1]$, may be approximated by the Hahn polynomials as follows:

$$f(x) \simeq \sum_{i=0}^{N} c_i \mathcal{H}_i(x) = C^T \Psi(x), \tag{6.1.9}$$

such that

$$\Psi(x) = [\mathcal{H}_0(x), \mathcal{H}_1(x), ..., \mathcal{H}_N(x)]^T, \quad C^T = [c_0, c_1, ..., c_N]^T \tag{6.1.10}$$

6.2 Convergence analysis

Covergence analysis and spectral accuracy of the Hahn polynomials expansion are investigated thoroughly in [124, 125]. Spectral accuracy/convergence indicates that the i-th coefficient in the expansion of a smooth function decays to zero faster than any power of i. In this part, the behavior of the Hahn coefficients is examined. It is inaccurate to speak of spectral convergence in this context because all coefficients c_i are either equal to zero for $i > N$ or are undefined. Consequently, we use the term spectral accuracy in the following sense: Accuracy is spectral if there exists an index n_1 such that the absolute values of c_i, $N \geqslant i > n_1$, decrease faster than any power of i. Nonetheless, we examine the interval $I = [0, N]$ using a $(N+1)$-equidistant grid. Transformation to any compact interval $[a, b]$ is conceivable and follows similarly. For Hahn polynomials, spectral accuracy derives immediately from Theorem 18.

Theorem 18. *Let $\alpha, \beta > -1$, m, $N \in \mathbf{N}$ with $m \leqslant N$, $I = [0, N]$ and $f \in C^{\infty}([-1, N+1])$. $\mathcal{H}_i(x)$ are the normalized Hahn polynomials of degree i. The Hahn projection of f with degree m is given by*

$$P_m f(x) = \sum_{i=0}^{m} c_i \mathcal{H}_i(x),$$

with the coefficient

$$c_i = \langle \mathcal{H}_i, f \rangle_w$$

and weight function w. It holds

$$|c_i| \leqslant \frac{1}{i^{2k}} \Big(\sum_{j=0}^{N} w(j) (\boldsymbol{L}_{disk} f(j))^2 \Big)^{\frac{1}{2}} \tag{6.2.11}$$

for all $k \in N0$, where $\boldsymbol{L}_{disk} := \frac{1}{w(j)} \triangle [-D(j) w(j) \triangledown]$ is the discrete difference operatator.

Proof. The proof follows directly from [[124], Theorem 3.1, page 4] □

Remark 5. *For fixed N and $f \in C^{\infty}$, the sum $\frac{1}{i^{2k}} \Big(\sum_{j=0}^{N} w(j) (\boldsymbol{L}_{disk} f(j))^2 \Big)^{\frac{1}{2}}$ is well-defined and independent of i. The decay behavior of c_i is characterized by $\frac{1}{i^{2k}}$ for $i \leqslant N$. If $i > N$ then c_i is equal to zero.*

The following Theorem provides conditions that ensure that the series expansion of a function by the discrete Hahn polynomials converges.

Theorem 19. *The series expansion* $\sum_{k=0}^{n} \frac{\langle f, \mathcal{H}_k \rangle}{\langle \mathcal{H}_k, \mathcal{H}_k \rangle} \mathcal{H}_k(x)$ *of a function* f *by the discrete Hahn polynomials converges pointwise, if the series expansion of the function* f *by the Jacobi polynomials converges pointwise and if* $\frac{n^{3+\alpha+max\{1,\alpha\}}}{N} \longrightarrow 0$ *as* $n, N \longrightarrow \infty$.

Proof. The proof follows directly from [[125], Theorems 1.1, 2.1 and 2.2]. □

6.3 Operational matrices based on Hahn orthogonal polynomials

Here, we provide explicit formulae for the Hahn polynomials' ordinary differentiation and integration and delay product operational matrices. First, we assume that $\Psi(x)$ is the Hahn polynomials vector. For more details about operational matrices based on orthogonal polynomials, refer to [71, 213].

$$\Psi(x) = [\mathcal{H}_0(x), \mathcal{H}_1(x), ..., \mathcal{H}_N(x)].$$

6.3.1 Ordinary integral matrix for Hahn polynomials

Lemma 6.3.1. *Suppose that, for a positive real number* s*, the inner product of the* n*th Hahn polynomial* $H_n(t)$ *and* x^s *is denoted by* $\lambda_(n, s)$*. It can be derived as*

$$\lambda_(n, s) = \langle \mathcal{H}_n(x), x^s \rangle_w = \sum_{r=0}^{N} \sum_{k=0}^{n} \frac{a_{k,n} r^{s+k} \Gamma(\alpha + r + 1) \Gamma(\beta + N - r + 1)}{\Gamma(r+1)\Gamma(N-r+1)\Gamma(\alpha+1)\Gamma(\beta+1)} \tag{6.3.12}$$

Proof. From the definition of the discrete inner product $\langle ., . \rangle_w$ in (6.1.5), we have:

$$\lambda_(n, s) = \sum_{r=0}^{N} \mathcal{H}_n(r)\, r^s\, w(r) = \sum_{r=0}^{N} \Big(\sum_{k=0}^{n} a_{k,n} r^k \Big) r^s \begin{pmatrix} \alpha + r \\ r \end{pmatrix} \begin{pmatrix} \beta + N - r \\ N - r \end{pmatrix} = \sum_{r=0}^{N} \sum_{k=0}^{n} \frac{a_{k,n} r^{s+k} \Gamma(\alpha + r + 1) \Gamma(\beta + N - r + 1)}{\Gamma(r+1)\Gamma(N-r+1)\Gamma(\alpha+1)\Gamma(\beta+1)}. \tag{6.3.13}$$

□

Theorem 20. *If* $\Psi(x)$ *is the Hahn polynomials vector, then the Ordinary integration of Hahn polynomial vector is given by*

$$\mathcal{I}\Psi(x) = \mathcal{G}\Psi(x) \tag{6.3.14}$$

where $\mathcal{G}$ is the $(N+1)\times(N+1)$ matrix. In fact, the (i,j)-th element of this matrix is obtained by:

$$\mathcal{G}_{i,j}=\sum_{k=0}^{i-1}\frac{a_{k,i-1}\lambda(j,k+1)}{(k+1)\rho_j},\qquad i=1,2,...,N+1,\ j=0,...,N.$$

where

$$\rho_j=(-1)^j\frac{(j+\alpha+\beta+1)_{N+1}(\beta+1)_j j!}{(2j+\alpha+\beta+1)(\alpha+1)_j(-N)_j N!}.$$

Proof. Assume that the i-th element of the vector $\Psi(x)$ is $\mathcal{H}_{i-1}(x)$. Applying the analytical form of $\mathcal{H}_{i-1}(x)$, the ordinary integration for this function can be written as

$$\mathcal{I}\mathcal{H}_{i-1}(x)=\sum_{k=0}^{i-1}\frac{a_{k,i-1}x^{k+1}}{(k+1)} \tag{6.3.15}$$

Now the term of $x^{k+1}$by expanding exactly with Hahn polynomials as

$$x^{k+1}=\sum_{j=0}^{N}u_{k,j}\mathcal{H}_j(x) \tag{6.3.16}$$

in which $u_{k,j}$ can be derived by using Lemma 6.3.1 as

$$u_{k,j}=\frac{1}{\rho_j}\big\langle\mathcal{H}_j(x),x^{k+1}\big\rangle_w=\frac{\lambda(j,k+1)}{\rho_j} \tag{6.3.17}$$

By putting Eqs. (6.3.16) and (6.3.17) in (6.3.15), we have:

$$\mathcal{I}\mathcal{H}_{i-1}(x)=\sum_{j=0}^{N}\Big(\sum_{k=0}^{i-1}\frac{a_{k,i-1}\lambda(j,k+1)}{(k+1)\rho_j}\Big)\mathcal{H}_j(x),$$

therfore the desired result is derived. □

6.3.2 Ordinary differentiation matrix for Hahn polynomials

Theorem 21. *If $\Psi(x)$ is the Hahn polynomials vector, then the Ordinary differentiation of Hahn polynomial vector is given by*

$$\mathcal{D}\Psi(x)=\Phi\mathcal{H}(x) \tag{6.3.18}$$

where Φ is the $(N+1)\times(N+1)$ matrix. In fact, the (i,j)-th element of this matrix is obtained by:

$$\Phi_{i,j}=\sum_{k=0}^{i-1}\frac{k\,a_{k,i-1}\lambda(j,k-1)}{\rho_j},\qquad i=1,2,...,N+1,\ j=0,...,N.$$

where

$$\rho_j=(-1)^j\frac{(j+\alpha+\beta+1)_{N+1}(\beta+1)_j j!}{(2j+\alpha+\beta+1)(\alpha+1)_j(-N)_j N!}.$$

Proof. Assume that the i-th element of the vector $\Psi(x)$ is $\mathcal{H}_{i-1}(x)$. Applying the analytical form of $\mathcal{H}_{i-1}(x)$, the ordinary differentiation for this function can be written as

$$\mathcal{D}\mathcal{H}_{i-1}(x) = (\mathcal{D}\sum_{k=0}^{i-1} a_{k,i-1}x^k)$$

Therefore

$$\mathcal{D}\mathcal{H}_{i-1}(x) = \sum_{k=0}^{i-1} a_{k,i-1}k\,x^{k-1} \tag{6.3.19}$$

Now the term of $x^{k-1}$by expanding exactly with Hahn polynomials as

$$x^{k-1} = \sum_{j=0}^{N} q_{k,j}\mathcal{H}_j(x) \tag{6.3.20}$$

in which $q_{k,j}$ can be derived by using Lemma6.3.1 as

$$q_{k,j} = \frac{1}{\rho_j}\big\langle \mathcal{H}_j(x), x^{k-1}\big\rangle_w = \frac{\lambda(j,k-1)}{\rho_j} \tag{6.3.21}$$

By putting Eqs. (6.3.20) and (6.3.21) in (6.3.19), we have:

$$\mathcal{D}\mathcal{H}_{i-1}(x) = \sum_{j=0}^{N}\Big(\sum_{k=0}^{i-1}\frac{k\,a_{k,i-1}\lambda(j,k-1)}{\rho_j}\Big)\mathcal{H}_j(x), \tag{6.3.22}$$

therfore the desired result is derived. □

Remark 6. *Let $\Psi(x)$ be the $(N+1)$ Hahn vector defined in (6.1.10) and V be an arbitrary $(N+1)$ vector. Then, we can write*

$$\Psi(x)\Psi^T(x)V = \tilde{V}\Psi(x), \tag{6.3.23}$$

where $\tilde{V}$ is the $(N+1)\times(N+1)$ product operational matrix and its (i,j)th element can be defined as

$$\tilde{V}_{i+1,j+1} = \frac{1}{\rho_j}\sum_{k=0}^{N} V_k\,\langle \mathcal{H}_k(t)\mathcal{H}_i(x), \mathcal{H}_j(x)\rangle_w, \quad i,j = 0,1,...,N.$$

6.4 Numerical approach

Consider the delay VIEs (6.0.1). First, we approximate $y(x), f(x)$ and $k(x,t)$ in terms of the HPs as follows

$$y(x) \simeq C^T\Psi(x) = \Psi^T(x)C, \tag{6.4.24}$$

$$f(x) \simeq F^T\Psi(x) = \Psi^T(x)F, \tag{6.4.25}$$

$$P_k(x) \simeq P_k^T\Psi_k(x) = \Psi^T(x)P_k, \tag{6.4.26}$$

$$K_r(x,t) \simeq \Psi(x)^T\mathbf{K}_r\,\Psi(t) = \Psi(t)^T\mathbf{K}_r^T\Psi(x), \tag{6.4.27}$$

where C, P and F are the HPs coefficient vectors and $\mathbf{K}_r$ is the HPs coefficient matrix that is obtained by the following relations:

$$\mathbf{K}_r = [k_{i,j}^r],\;\; k_{i,j}^r = \langle \mathcal{H}_j(x), \langle K_r(x,t), \mathcal{H}_i(t)\rangle\rangle \quad i,j = 0,1,2,...,N.$$

Hence, by using (6.4.24), the functions $y(\alpha_k x + \beta_k)$ and $\mathcal{F}(y(\mu_r t + \gamma_r))$ can be derived as:

$$y\left(\alpha_k x + \beta_k\right) \approx C^T\Psi(\alpha_k x + \beta_k) = \Psi^T(\alpha_k x + \beta_k)C$$

and

$$\mathcal{F}(y\left(\mu_r t + \gamma_r\right)) \approx Z^T\Psi(t) = \Psi^T(t)Z$$

These delay function can be expanded as

$$y\left(\alpha_k x + \beta_k\right) \approx C^T\Omega_k\Psi\left(x\right) + V_k^T\Psi\left(x\right), \tag{6.4.28}$$

where V_k is known $(N+1)$ vector, whereas Ω_k is known $(N+1)\times(N+1)$ matrix which depends on the delay parameters α_k, β_k, respectively. Substituting Eqs. (6.4.25)-(6.4.26)-(6.4.27) and (6.4.28) in the VIEs (6.0.1), we get

$$\sum_{k=0}^{m_1} P_k^T\Psi(x)\Psi^T(x)(C\Omega_k^T + V_k) = F^T\Psi(x) + \sum_{r=0}^{m_2}\lambda_r\Big(\int_{u_r(x)}^{v_r(x)} Z^T\Psi(t)\Psi^T(t)dt\Big)\,\mathbf{K}_r^T\Psi(x),$$

Now by applying product operation matrix for HPs defined in Remark 33, we have:

$$\sum_{k=0}^{m_1} \Psi^T(x)\tilde{P}_k(C\Omega_k^T + V_k) = F^T\Psi(x) + \sum_{r=0}^{m_2}\lambda_r\Big(\int_{u_r(x)}^{v_r(x)} \Psi^T(t)dt\Big)\,\tilde{Z}\mathbf{K}_r^T\Psi(x),$$

$\tilde{P}_k$ and $\tilde{Z}$ are the product operation matrices. Now by applying operational matrix of integration $\mathcal{Q}_r$ for HPs defined in Theorem 6.3.14, we have the residual function $R(x)$ for the VIE (6.0.1) can be derived as:

$$R(x) = \sum_{k=0}^{m_1}\Big(\tilde{P}_k(C\Omega_k^T + V_k) \;-\; F^T - \sum_{r=0}^{m_2}\lambda_r\mathcal{Q}_r\,\tilde{Z}\mathbf{K}_r^T\Big)\Psi(x), \tag{6.4.29}$$

In order to approximate solution of the VIEs (6.0.1), we collocate the residual system (6.4.29) at the $N+1$ zeros of shifted Chebyshev polynomials in the interval $[0,1]$, as follow:

$$R(r_j) = 0, \quad i = 1,2...,N+1. \tag{6.4.30}$$

Eqs. (6.4.30) generate a system of $N+1$ algebraic equations for $N+1$ unknown coefficients of the vector C. This system of algebraic equations can be solved for unknown coefficients of the vector C. For nonlinear cases, the Newton-Raphson method can be applied to solve the nonlinear system. Consequently, unknown function $y(x)$ can be obtained by substituting the vector C in Eq. (6.4.24).

The accuracy of the approximate solutions is determined by substituting the solutions into the Eq. (6.0.1)

$$E_N(x) = |\sum_{k=0}^{m_1} P_k(x)y(\alpha_k x+\beta_k) - \Big(f(x) + \sum_{r=0}^{m_2}\lambda_r \int_{u_r(x)}^{v_r(x)} K_r(x,t)\mathcal{F}(y(\mu_r t+\gamma_r))dt\Big)| \tag{6.4.31}$$

We anticipate that $E_N(x) = 0$ on the collocation points. Whenever $y(x) \simeq y_N(x)$ then $E_N(x) \simeq 0$. The accuracy of the approximate solutions may not provide any information about the absolute errors. Thus, we can estimate the absolute errors using the residual correction approach [65, 66, 226, 273].

We now will provide an error estimation for the HPs approach based on the residual function. Using the residual function, we have

$$R_N(x) = \sum_{k=0}^{m_1} P_k(x)y(\alpha_k x+\beta_k) - \Big(f(x) + \sum_{r=0}^{m_2}\lambda_r \int_{u_r(x)}^{v_r(x)} K_r(x,t)\mathcal{F}(y(\mu_r t+\gamma_r))dt\Big). \tag{6.4.32}$$

The error function $e_N(x)$ can be defined as $e_N(x) = y(x) - y_N(x)$, where $y(x)$ is the exact solution of problem6.0.1 and also $y_N(x)$ is the approximate solution.
By adding Eq. (6.4.32) into the both side of Eq. (6.0.1), we have

$$-R_N = \sum_{k=0}^{m_1} P_k(x)e_N(\alpha_k x+\beta_k) - \sum_{r=0}^{m_2}\lambda_r \int_{u_r(x)}^{v_r(x)} K_r(x,t)\mathcal{F}(y(\mu_r t+\gamma_r) - y_N(\mu_r t+\gamma_r))dt. \tag{6.4.33}$$

On the other hand, using the residual function described by $R_N(x)$, the solution's accuracy can be evaluated, and error can be estimated. If $R_N(x) \longrightarrow 0$ when N is sufficiently large enough, then error decrease.
Using the error equation (6.4.33), we obtain the approximation $e_{N,M}(x)$ to $e_N(x)$, $(M \geqslant N)$

$$e_{N,M}(x) = \sum_{k=0}^{M} a_k \mathcal{H}_k(x),$$

where , $e_{N,M}(x)$ is the Hahn polynomial solution of the error equation (6.4.33). So, we establish the error function $e_N(x) = y(x) - y_N(x)$, the estimated error function $e_{N,M}(x)$ and the corrected Hahn polynomial solution is

$$E_{N,M}(x) = e_N(x) - e_{N,M}(x) = y(x) - y_{N,M}(x).$$

6.5 Numerical experiments

In this section, five examples demonstrate how well Hahn polynomials perform in solving the linear and nonlinear delay VIEs. The accuracy of the numerical solution is examined using the Root Mean Squared Error (RMSE). Assume that the function $y(x)$ is approximated by $\tilde{y}(x)$. In the examples, actual absolute error is shown by $e_N(x) = |\tilde{y}(x) - y_N(x)|$, estimated absolute error is demonstrated by $e_{N,M}$ and corrected absolute error is defined by $E_{N,M}(x)$.All findings were calculated using Maple 17 with a precision of 16 digits and $\alpha = 1$, $\beta = 1$.

For this approximate function $\tilde{y}(t)$, the RMSE can be calculated as follows:

$$\|y - \tilde{y}\|_2 = \sqrt{\frac{\sum_{i=1}^{m} |y(x_i) - \tilde{y}(x_i)|^2}{N}}. \tag{6.5.34}$$

Example 7. *Assume the following delay VIEs:*

$$y(x) + xe^{-x}y(\frac{1}{2}x) - \int_0^x e^{x-t}y(t)dt = f(x), \tag{6.5.35}$$

where $f(x) = (x+1)e^x + xe^{\frac{x}{2}}$. *This equation has exact solution* $\tilde{y}(x) = e^x$.

The presented HPs method has been used to solve this delay VIEs. Comparison between actual absolute errors with the estimated and corrected absolute errors for $x = 0, 0.2, 0.4, 0.6, 0.8, 1, 1.1$ *and different values of* N, M *are listed in Table 6.1. The absolute errors acquired by the published results and our method are compared in Table 6.2. The numerical examples show that for different values of* N*, the approach outperforms all other methods, such as the Legendre collocation method, the Lagrange collocation method, the Chebyshev collocation method, the VIM method, and Taylor collocation method. In addition, Fig. 6.1 shows the comparison between absolute errors for different N. Fig. 6.2 shows the errors of approximation solution y(x). From these results, we conclude that the presented method is an effective tool for solving the delay VIEs and that the RMSE of the approximate solutions significantly decreases as the number of basis functions increases. According to Fig. 6.2, numerical errors will decay at an exponential rate. The errors exhibit an exponential decrease, as expected because the error variations in this semi-log representation are practically linear versus the degrees of the polynomial. The elapsed CPU time (in second) for different values of N is provided in Table 6.3.*

x_i	Actual absolute errors $N=4$, $e_4(x_i)$		Estimated absolute errors $N=4$, $M=6$, $e_{4,6}(x_i)$		Corrected absolute errors $N=4$, $M=6$, $E_{4,6}(x_i)$	
	HPs	[127]	HPs	[127]	HPs	[127]
0.0	0	0	0	0	0	0
0.2	$0.356494e-5$	$0.161717e-4$	$0.352973e-5$	$0.161129e-4$	$0.352052e-9$	$0.588529e-7$
0.4	$0.183943e-4$	$0.175270e-4$	$0.184318e-4$	$0.175071e-4$	$0.375707e-9$	$0.199332e-7$
0.6	$0.315997e-4$	$0.258794e-3$	$0.315600e-4$	$0.258772e-3$	$0.397138e-9$	$0.221217e-7$
0.8	$0.459194e-8$	$0.949598e-3$	$0.500791e-8$	$0.949614e-3$	$0.415973e-9$	$0.163145e-7$
1.0	$0.265482e-4$	$0.137166e-2$	$0.265931e-4$	$0.137166e-2$	$0.449127e-9$	$0.248660e-6$
1.1	$0.342140e-3$	$0.896502e-3$	$0.343941e-3$	$0.896502e-3$	$0.180041e-5$	$0.598131e-7$
x_i	Actual absolute errors $N=5$, $e_5(x_i)$		Estimated absolute errors $N=5$, $M=7$, $e_{5,7}(x_i)$		Corrected absolute errors $N=5$, $M=7$, $E_{5,7}(x_i)$	
	HPs	[127]	HPs	[127]	HPs	[127]
0.0	0	0	0	0	0	0
0.2	$0.874173e-8$	$0.288997e-5$	$0.874657e-8$	$0.288713e-5$	$0.483213e-11$	$0.284325e-8$
0.4	$0.676526e-8$	$0.320749e-5$	$0.676478e-8$	$0.320842e-5$	$0.481330e-12$	$0.927994e-9$
0.6	$0.468135e-8$	$0.630605e-4$	$0.468085e-8$	$0.630614e-4$	$0.504941e-12$	$0.834475e-9$
0.8	$0.116701e-5$	$0.433426e-3$	$0.116757e-5$	$0.433428e-3$	$0.557997e-11$	$0.165510e-8$
1.0	$0.178320e-5$	$0.249601e-2$	$0.178458e-5$	$0.249602e-2$	$0.138734e-10$	$0.683476e-8$
1.1	$0.268999e-4$	$0.512460e-2$	$0.270031e-4$	$0.512466e-2$	$0.103263e-8$	$0.608253e-7$

Table 6.1: Comparison of numerical results for different N, M, Example 7.

	$N=3$	$N=4$	$N=5$
[20]	$4.60e-004$	$7.30e-007$	$1.10e-007$
[32]	$2.20e-004$	$9.20e-006$	$4.10e-007$
[127]	$1.00e-004$	$3.00e-007$	$5.80e-008$
HPs	$3.48e-004$	$6.868e-007$	$4.03e-008$

Table 6.2: Comparison RMSE for different values of N, Example 7.

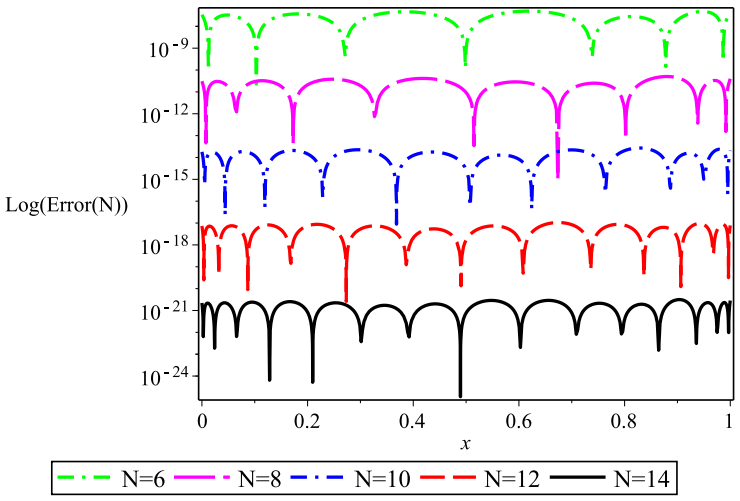

Figure 6.1: Comparison of absolute errors for different N, Example 7

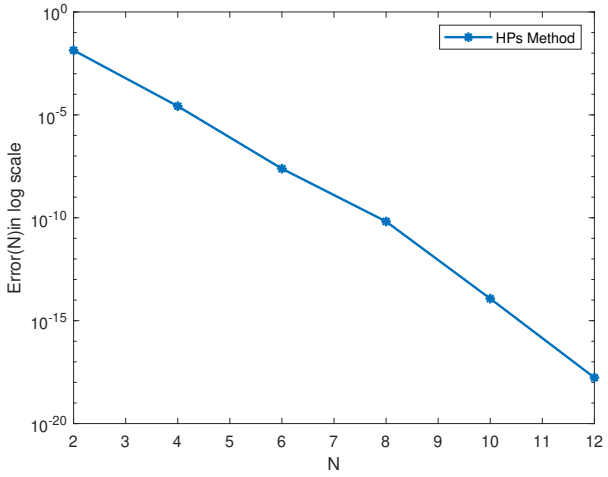

Figure 6.2: The errors of approximation solution y(x) for Example 7

	N		
	4	6	8
$Wall\ clock\ time(s)$	0.906	1.047	1.031

Table 6.3: CPU times for different N of Example 7.

Example 8. *Consider the following delay VIEs:*

$$x^2y(x) + e^xy(2x) - \int_0^{2x} e^{x+t}y(t)dt + \int_0^1 e^{x-2t}y(2t)dt = f(x), \tag{6.5.36}$$

where

$$f(x) = -\frac{e^x}{4} - \frac{1}{4}e^{x-2}\cos 2 + \frac{1}{2}e^{3x}\cos 2x - \frac{1}{4}e^{x-2}\sin 2 - \frac{1}{2}e^{3x}\sin 2x + x^2\sin x + e^x\sin 2x.$$

This equation has exact solution $\tilde{y}(x) = sin(x)$.
The proposed HPs method has been employed to solve this delay VIEs. The absolute errors acquired by the published results and our method are compared in Table 6.4. The method provides a better approximation than all other methods, including the Legendre collocation method, the Lagrange collocation method, the Chebyshev collocation method, the VIM method, and Taylor collocation method for different values of N, *as can be seen from the numerical examples. Additionally, Table 6.5 displays the comparison of the actual absolute errors with the estimated and corrected absolute errors for* $x = 0, 0.2, 0.4, 0.6, 0.8, 1$ *and different values of* N, M. *Fig. 6.3 compares absolute errors for different N. In summary, the results show that the proposed method is a useful tool for solving the delay VIEs and that the RMSE of the approximations drops noticeably*

with the number of basis functions. Furthermore, in Fig. 6.4, we exhibit the numerical errors for various values of N to demonstrate the high accuracy and convergence of the proposed method. These results illustrate that our method provides a good approximation and produces an exponential rate of convergence. The elapsed CPU time (in second) for different values of N is provided in Table 6.6.

	$N = 2$	$N = 5$	$N = 8$	$N = 9$
[127]	$- - - - -$	$1.40e-004$	$7.40e-009$	$2.40e-010$
[196]	$- - - - -$	$2.93e-005$	$3.94e-008$	$2.29e-009$
[196]	$3.41e-002$	$3.68e-004$	$1.24e-005$	$3.46e-007$
[308]	$7.87e-002$	$6.23e-005$	$1.89e-008$	$2.35e-008$
[309]	$7.87e-002$	$6.23e-005$	$1.77e-007$	$7.21e-006$
HPs	$3.87e-002$	$4.90e-005$	$5.07e-009$	$3.60e-010$

Table 6.4: Comparison RMSE for different values of N, Example 8.

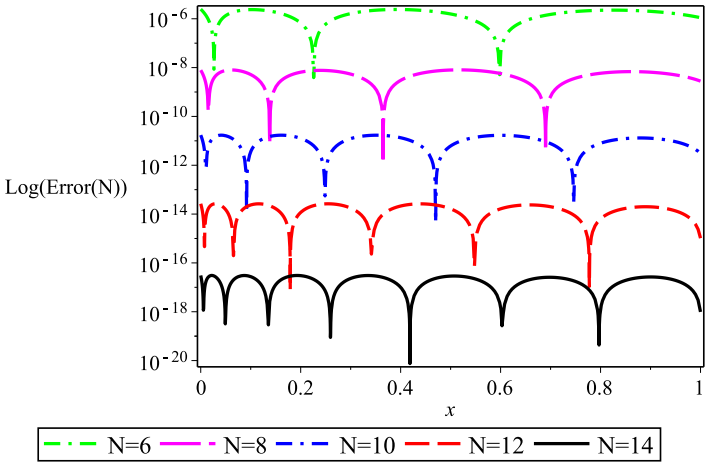

Figure 6.3: Comparison of absolute errors for different N, Example 8

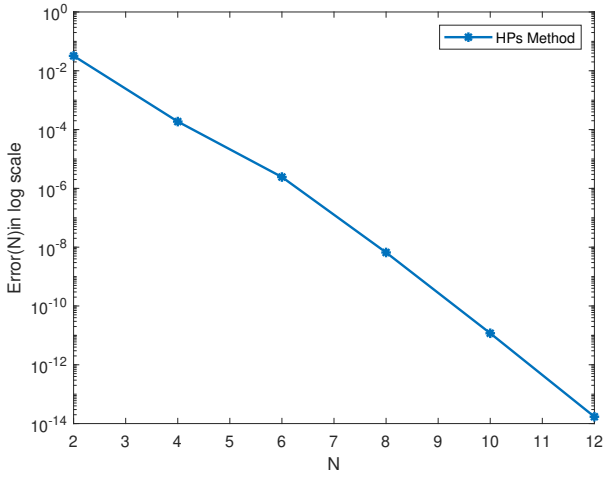

Figure 6.4: The errors of approximation solution y(x) for Example 8

x_i	Actual absolute errors $N = 8, e_8(x_i)$		Estimated absolute errors $N = 8, M = 10,\ e_{8,10}(x_i)$		Corrected absolute errors $N = 8, M = 10, E_{8,10}(x_i)$	
	HPs	[127]	HPs	[127]	HPs	[127]
0.0	$0.786197e-10$	$0.166857e-4$	$0.787897e-10$	$0.166840e-4$	$0.170019e-12$	$0.173027e-8$
0.2	$0.649202e-10$	$0.677028e-6$	$0.647776e-10$	$0.675149e-6$	$0.142549e-12$	$0.187909e-8$
0.4	$0.300124e-10$	$0.253054e-4$	$0.298293e-10$	$0.253029e-4$	$0.183106e-12$	$0.245143e-8$
0.6	$0.570982e-10$	$0.203764e-4$	$0.572993e-10$	$0.203731e-4$	$0.201106e-12$	$0.327117e-8$
0.8	$0.5861108e-10$	$0.351658e-4$	$0.587918e-10$	$0.351610e-4$	$0.180781e-12$	$0.478454e-8$
1.0	$0.278791e-10$	$0.557315e-4$	$0.276729e-10$	$0.557239e-4$	$0.206177e-12$	$0.762705e-8$
x_i	Actual absolute errors $N = 9, e_9(x_i)$		Estimated absolute errors $N = 9,\ M = 11,\ e_{9,11}(x_i)$		Corrected absolute errors $N = 9,\ M = 11,\ E_{9,11}(x_i)$	
	HPs	[127]	HPs	[127]	HPs	[127]
0.0	$0.5094913e-11$	$0.252523e-5$	$0.5104291e-11$	$0.252528e-5$	$0.937864e-14$	$0.435909e-10$
0.2	$0.519600e-11$	$0.400632e-5$	$0.519755e-11$	$0.400637e-5$	$0.154924e-14$	$0.537286e-10$
0.4	$0.529117e-11$	$0.433152e-5$	$0.528033e-11$	$0.433158e-5$	$0.108388e-13$	$0.686267e-10$
0.6	$0.209963e-11$	$0.637944e-5$	$0.208680e-11$	$0.637953e-5$	$0.1282759e-13$	$0.928910e-10$
0.8	$0.382958e-11$	$0.893953e-5$	$0.383205e-11$	$0.893966e-5$	$0.246816e-14$	$0.134946e-9$
1.0	$0.400643e-11$	$0.144296e-4$	$0.402344e-11$	$0.144298e-4$	$0.170102e-13$	$0.214906e-9$

Table 6.5: Comparison of numerical results for different N, M, Example 8.

	N		
	4	6	8
Wall clock time(s)	1.000	1.062	1.156

Table 6.6: CPU times for different N of Example 8.

Example 9. *Consider the delay VIEs:*

$$y(x) + e^{-x}y(0.8x) + \int_{-1}^{1} e^{x-t}y(t)dt = f(x) \tag{6.5.37}$$

where $f(x) = 3e^{-x} + e^{3-0.8x}$. *This equation has exact solution* $\tilde{y}(x) = e^{x}$.
This delay VIEs has been resolved using the suggested HPs approach. The comparison of the actual absolute errors with the estimated and corrected absolute errors for $x = -1, -0.6, -0.2, 0, 0.2, 0.6, 1$ *and different values of* N, M *is also shown in Table 6.7. The absolute error comparison for various* N *is shown in Fig. 6.5. In conclusion, the findings demonstrate that the suggested approach is a helpful tool for resolving delay VIEs and that the RMSE of the approximations decreases significantly with the number of basis functions. These outcomes show that our approach yields accurate approximations and an exponential convergence rate. The elapsed CPU time (in second) for different values of* N *is provided in Table 6.8.*

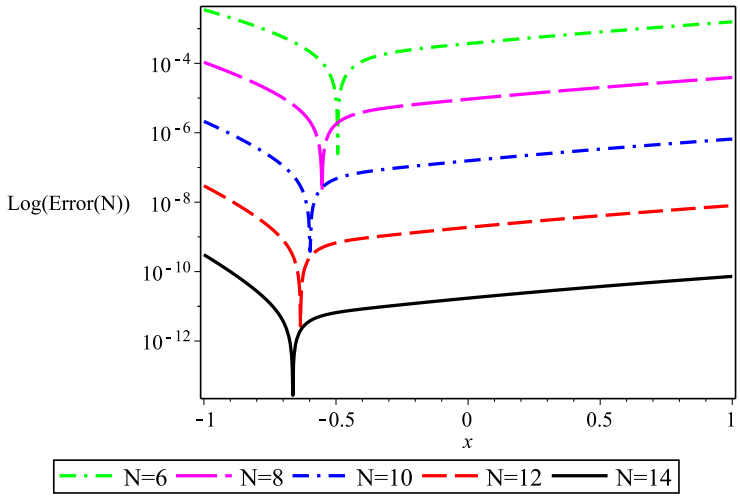

Figure 6.5: Comparison of absolute errors for different N, Example 9

Example 10. *Consider the nonlinear delay VIEs:*

$$y(x) - \int_{0}^{x} 2e^{-x}y^{2}(t)dt = f(x) \tag{6.5.38}$$

x_i	Actual absolute errors $N = 10$, $e_{10}(x_i)$		Estimated absolute errors $N = 10, M = 10$, $e_{10,12}(x_i)$		Corrected absolute errors $N = 10, M = 10$, $E_{10,12}(x_i)$	
	HPs	[127]	HPs	[127]	HPs	[127]
-1.0	$0.0213245e-5$	$0.364e-7$	$0.209132e-5$	$0.367e-7$	$0.411295e-9$	$0.147e-12$
-0.6	$0.102876e-10$	$0.542e-9$	$0.535040e-11$	$0.741e-10$	$0.493721e-11$	$0.436e-14$
-0.2	$0.110353e-8$	$0.818e-9$	$0.1.10352e-8$	$0.427e-9$	$0.340561e-14$	$0.325e-13$
0.0	$0.155889e-8$	$0.100e-8$	$0.155889e-8$	$0.600e-9$	$0.860343e-19$	$0.476e-13$
0.2	$0.215293e-8$	$0.137e-8$	$0.215293e-8$	$0.828e-9$	$0.751331e-19$	$0.671e-13$
0.6	$0.660083e-8$	$0.247e-8$	$0.388293e-8$	$0.166e-9$	$0.432497e-19$	$0.135e-13$
1.0	$0.278791e-8$	$0.563e-7$	$0.660083e-8$	$0.555e-7$	$0.873861e-19$	$0.227e-12$
x_i	Actual absolute errors $N = 14$, $e_{14}(x_i)$		Estimated absolute errors $N = 14$, $M = 16$, $e_{14,16}(x_i)$		Corrected absolute errors $N = 14$, $M = 16$, $E_{14,16}(x_i)$	
	HPs	[127]	HPs	[127]	HPs	[127]
-1.0	$0.307047e-11$	$0.100e-9$	$0.295285e-11$	$0.130e-11$	$0.117622e-12$	$0.460e-18$
-0.6	$0.374663e-13$	$0.150e-10$	$0.370333e-13$	$0.570e-14$	$0.433044e-15$	$0.350e-19$
-0.2	$0.121881e-12$	$0.220e-10$	$0.1.21881e-12$	$0.130e-13$	$0.350602e-19$	$0.640e-19$
0.0	$0.172013e-12$	$0.750e-10$	$0.172013e-12$	$0.190e-13$	$0.110900e-25$	$0.910e-19$
0.2	$0.237523e-12$	$0.160e-9$	$0.237523e-12$	$0.260e-13$	$0.487724e-24$	$0.120e-18$
0.6	$0.428388e-12$	$0.400e-9$	$0.428388e-12$	$0.490e-13$	$0.450163e-24$	$0.210e-18$
1.0	$0.728241e-12$	$0.490e-9$	$0.728241e-12$	$0.160e-11$	$0.272505e-24$	$0.440e-18$

Table 6.7: Comparison of numerical results for different N, M, Example 9.

	N		
	4	6	8
Wall clock time(s)	0.844	0.891	1.063

Table 6.8: CPU times for different N of Example 9.

where $f(x) = -e^{-x}$. *This equation has exact solution* $\tilde{y}(x) = e^x$.
The suggested HPs technique has been used to resolve this nonlinear delay VIEs. Table 6.9 compares the actual absolute errors with the estimated and corrected absolute errors for $x = 0, 0.2, 0.4, 0.6, 0.8, 1$ *and various values of* N, M. *Fig. 6.6 displays the absolute error comparison for various* N. *The results show that the recommended strategy is a valuable tool for resolving delay VIEs and that the RMSE of the approximations dramatically lowers with the number of basis functions. Furthermore, CPU times have been given to show the efficiency of the method. The elapsed CPU time (in second) for different values of* N *is provided in Table 6.10.*

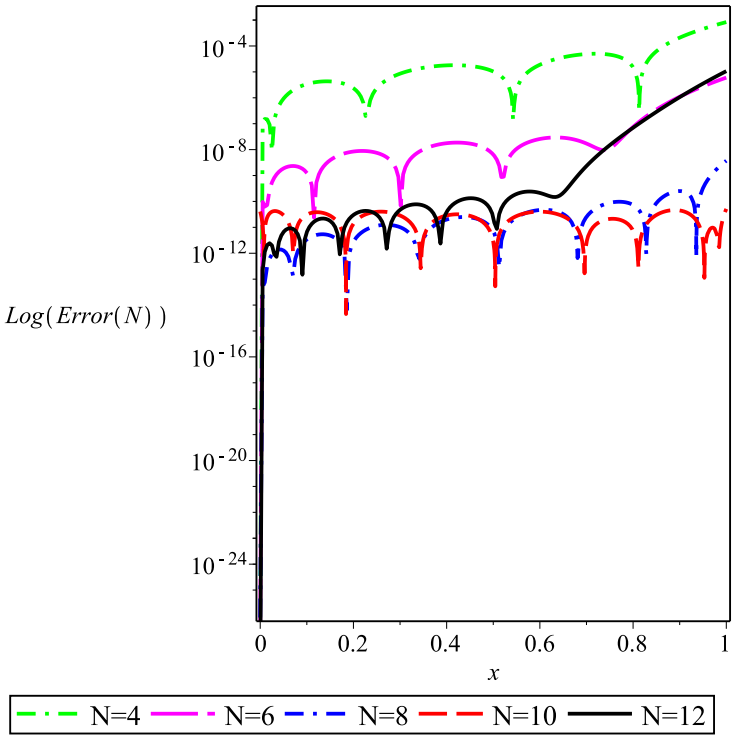

Figure 6.6: Comparison of absolute errors for different N, Example 10

	x_i					
Errors	0	0.2	0.4	0.6	0.8	1
$e_5(x_i)$	0	$1.7932e-7$	$1.1893e-8$	$8.7149e-7$	$3.0828e-4$	$5.2387e-3$
$e_{5,7}(x_i)$	0	$1.7872e-7$	$1.1697e-8$	$8.7090e-7$	$2.9883e-6$	$4.8023e-5$
$E_{5,7}(x_i)$	0	$5.9496e-10$	$1.96268e-10$	$5.9405e-10$	$9.4489e-8$	$4.3641e-4$
$e_9(x_i)$	0	$6.9560e-10$	$1.3780e-9$	$1.7720e-9$	$4.3584e-8$	$9.1656e-4$
$e_{9,11}(x_i)$	0	$6.7893e-10$	$1.0892e-9$	$1.0614e-9$	$1.7477e-8$	$4.3370e-7$
$E_{9,11}(x_i)$	0	$1.6668e-11$	$2.8881e-10$	$7.1054e-10$	$6.1062e-8$	$8.7319e-4$

Table 6.9: Numerical results for different N, M for Example 10.

	N		
	4	6	8
Wall clock time(s)	0.906	0.922	1.297

Table 6.10: CPU times for different N of Example 10.

Example 11. *Consider the nonlinear delay VIEs:*

$$y(x) - \int_0^x y^3(t)dt = f(x) \tag{6.5.39}$$

where $f(x) = e^x - \frac{1}{3}e^{3x} + \frac{1}{3}$. *This equation has exact solution* $\tilde{y}(x) = e^x$.
This nonlinear delay VIEs has been solved using the indicated HPs approach. For $x = 0, 0.2, 0.4, 0.6, 0.8, 1$ *and various values of* N, M, *Table 6.11 compares the actual absolute errors with the estimated and corrected ones. The absolute error comparison for different* N *is shown in Fig. 6.7. The findings demonstrate that the suggested approach is a valuable tool for resolving nonlinear delay VIEs and that the number of basis functions significantly impacts the approximations' accuracy. In addition, CPU times have been given to show the efficiency of the method. The elapsed CPU time (in second) for different values of* N *is provided in Table 6.12.*

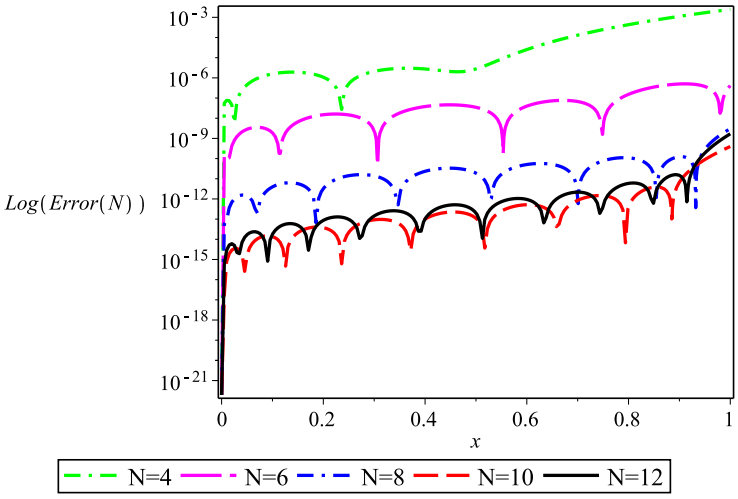

Figure 6.7: Comparison of absolute errors for different N, Example 11

	x_i					
Errors	0	0.2	0.4	0.6	0.8	1
$e_5(x_i)$	0	$2.2991e-7$	$2.4853e-7$	$1.5468e-4$	$1.1769e-4$	$4.7640e-3$
$e_{5,7}(x_i)$	0	$2.2975e-10$	$2.4849e-10$	$1.5467e-6$	$1.1750e-6$	$4.7595e-5$
$E_{5,7}(x_i)$	0	$1.6036e-10$	$4.0380e-11$	$8.4491e-11$	$1.8949e-9$	$4.5005e-8$
$e_8(x_i)$	0	$1.4907e-8$	$3.7929e-8$	$3.9737e-8$	$1.5273e-7$	$4.1273e-7$
$e_{8,10}(x_i)$	0	$1.4902e-8$	$3.7903e-8$	$3.9683e-8$	$1.5268e-7$	$4.1120e-7$
$E_{8,10}(x_i)$	0	$4.7886e-12$	$2.5968e-11$	$5.3967e-11$	$5.5293e-11$	$1.5385e-9$

Table 6.11: Numerical results for different N, M for Example 11.

	N		
	4	6	8
$Wall\ clock\ time(s)$	1.515	2.985	7.890

Table 6.12: CPU times for different N of Example 11.

6.6 Conclusion

In this chapter, a direct numerical method based on discrete orthogonal polynomials is proposed to approximate the solution of delay VIEs (linear and nonlinear). By using the properties of proposed polynomials, explicit formulations for their integration and product operational matrices were derived. A numerical approach was suggested to solve delay VIEs using collocation methods and these matrices. An instrument for residual correction is also provided to calculate the estimated and corrected absolute errors. The current method is applied to several problems that were previously studied in the literature and the error analysis is carried out. Several illustrative examples were considered to confirm the accuracy of the proposed method. The method has advantages such as:

- The presented method is accurate and effective for the numerical solution of linear and nonlinear delay VIEs. we can calculate the approximate solutions and absolute errors in a short time.
- Application of discrete Hahn polynomials is less time-consuming and less complex in comparison with continuous polynomials. As these polynomials are orthogonal with respect to a discrete norm, the implementation of the proposed numerical method is more efficient and less complex in comparison to similar methods in which continuous polynomials are used. The complexity and required CPU time of continuous polynomials increase significantly as the number of basis functions increases.
- Tables and figures have shown that the error decreases when N and M increase.
- Furthermore, CPU times have been given to show the efficiency of the method.
- As a result, the technique can be applied to a particular type of mathematical models, such as differential functional integral equations with delay, nonlinear differential functional integral equations with delay, and fractional Volterra integro-differential equations, but some modifications are required.

Chapter 7

Optimal control of system governed by nonlinear Volterra integral and derivative equations

Optimal Control (OC) is used in various engineering fields such as aerospace, mechanics, robotics, electronics, chemical processes, medical engineering, and sub-branches. The OC was first introduced by Newton and Leibniz. They could express dynamic processes by defining concepts such as differential and integral in the 17th century. But the OC in its present form has been considered since the 1950s. In the 1970s, with the significant development of software and hardware of digital computers and numerical algorithms, it became possible to provide very complex methods based on numerical calculations to solve optimal control problems. Several applications of optimal control problems in different scientific fields will be mentioned in the following.

Medical Engineering: The human body is highly complex and nonlinear, yet has highly regulated and adaptive physiological control systems. Therefore, there is a close relationship between control theory and physiology. Effective preventive measures and controlling the spread of infectious diseases are among the most important concerns worldwide. The control strategy in modeling the control of the spread of infectious diseases is vaccination (provided that the vaccine is readily available in the market).

Cancer tumor treatment: The simulation of the problem of treating a cancer tumor is studied to check the efficiency of optimal control in diseased tissue. The population of different cells as effective species, the effect of immune cells, chemotherapy drugs, and some important factors have been considered. After choosing the model, presenting a treatment program that can suggest a suitable process to reduce the number of cancer cells and, at the same time, cause the least damage to the patient's body is one of the issues raised in the field of optimal control. In this regard, it is important to consider various biological limitations, including the need to limit the dose of the injected drug and maintain the healthy cell population of a tissue.

Rehabilitation of disabled patients: The process of strengthening the muscles to bring them to normal values (rehabilitation) is a time-consuming task and requires high cost and precision. There are many exercise machines for rehabilitation purposes. Most of these machines are used in a limited and special way for various reasons. An optimal algorithm for designing an intelligent system for rehabilitating human lower limbs can be done using a parallel robot. Due to their high stiffness and fast reactions, parallel robots have recently attracted the attention of many researchers for medical applications and low-cost pharmaceutical activities. These robots generally have two circular plates of fixed and movable shape, connected using several flexible and removable links. The length of the links is controlled to reach the desired position and direction. Estimation and optimization of control parameters using neural networks and genetic algorithms. The use of the neural network in the control of rehabilitation robots arose from the fact that the results of experiments have shown that there are training centers in the spinal cord of adult mammals that activate and control the motor neurons responsible for walking. In the genetic algorithm, quantitative coding is used for chromosomes, and classical optimal control strategies can be used to find the least deviation from the desired path.

Car control systems: By using anti-lock brakes and slip and stability control, the safety of cars has been transformed by control technology. The invention of mechanical control for car suspension led to victory in car racing for the first time. Also, collision avoidance systems are used in air traffic management based on control and estimation algorithms. Also, optimal control has been used to design and solve various problems-described in this section.

Optimal Control Problems (OCPs) are widely used in several fields, such as aerospace, economy and finance, medical engineering, automotive systems, etc.

They are essentially related to identifying state trajectories for a dynamical system over a time interval that optimizes a specific performance index by achieving the best possible outcome through endogenous control of a parameter within a mathematical model of the system itself. The associated problem is characterized by a cost or objective function, depending on the state and control variables, and by a group of constraints. There are two essential types of OCPs, respectively, subjected to differential equations and integral equations. The classical optimal control theory was initially conceived to solve systems of controlled ordinary differential equations, referring to the first type. However, the second type of OCPs recently gained significant success for handling a broad class of phenomena and mathematical models, such as, for example, technological, physical, economic, biological, and network control problems, as reported in Figure 7.1.

Figure 7.1: Some applications of optimal control problem in real life

OCPs are typically nonlinear and hence do not admit analytic solutions, especially when they are ruled by Volterra integral or Volterra integral derivative systems (second type). To overcome the difficulties related to obtaining an analytical solution to these problems, several authors have suggested different techniques to provide a numerical solution.

Belbas described iterative methods with their convergence by assuming some conditions on the kernel of the integral equations involved to solve optimal control of nonlinear Volterra integral equations (VIEs) [27]. Also, he discovered a technique to solve OCPs for VIEs based on approximating the controlled VIEs by systems of controlled ordinary differential equations[28, 29]. The existence and uniqueness of solutions for OCPs governed by VIEs can be found in [11].

In addition, orthogonal functions have been leveraged to find the solution OCPs for VIEs. An iterative numerical method for solving optimal control using triangular functions is described in [198]. Maleknejad and Ebrahimzadeh introduced a collocation approach based on rationalized Legendre wavelets to approximate optimal control and state variables in [199]. In [296], Tohidi and Samadi investigated the use of Lagrange polynomials in solving OCPs for systems governed by VIEs and also analyzed the convergence of their proposed solution, characterized by a significant efficiency, mainly for problems characterized by smooth solutions. Hybrid functions consisting of block-pulse functions and a Bernoulli polynomial method for OCPs described by integro-differential equations has been investigated by Mashayekhi et al. in [205]. In [241], the authors proposed hybrid approaches leveraging the steepest descent and two-step Newton methods for achieving optimal control and the associated optimal state. Some other methods have been described in [106, 185, 200].

In a recent paper, Khanduzi et al. [174] proposed a novel revised method based on teaching-learning-based optimization (MTLBO) to gain an approximate solution of OCPs subjected to nonlinear Volterra integro-differential systems.

As said, the OCPs, which is the minimization of a performance index subject to the dynamical system is one of the most practical subjects in science and engineering. As a generalization of the classical OCPs and Fractional Optimal Control Problems (FOCPs) involve the minimization of a performance index subject to dynamical systems in which fractional derivatives or integrals are used (See [214] and references therein). Even if fractional calculus is almost as old as normal integer order calculus, its application in various fields of science has gained increasing attention in the last three decades. In related literature, considerable attention has been paid to fractional calculus to have a better description of the behavior of the natural processes [23, 225, 261, 289].

Centered on the approach reported in [174, 199] and considering the interest in fractional calculus that has grown over the past few years, the main aim of this analysis is to establish a new computational method for solving the OCPs ruled by Nonlinear Volterra Integro-Fractional Differential systems (NVIFs):

$$\min \mathcal{J} = \int_0^1 \mathcal{L}(t, y(t), u(t))dt \tag{7.0.1}$$

subjected to the NVIFs

$$\begin{array}{l} D^{\alpha}y(t) + a(t)y(t) - b(t)u(t) - c(t)\int_0^t \mathcal{G}(t, s, \varphi(s))ds = 0,, \quad 0 < \alpha \leqslant 1, \\ y(0) = y_0. \end{array} \tag{7.0.2}$$

where $y(t)$ and $u(t)$ are the state and control functions, $D^{\alpha}y(t)$ denotes the fractional derivative of $y(t)$ in the Caputo sense, $a(t)$, $b(t)$ and $c(t)$ are functions and φ is a linear or nonlinear function. Moreover, $\mathcal{L}$ and $\mathcal{G}$ are continuously differentiable operators.

This chapter considers a new type of orthogonal polynomial, which Chelyshkov has described for the first time. First, the $D^{\alpha}(y)$ is expanded using Chelyshkov polynomials vector with unknown coefficients. The fractional integral operational matrix is employed to find the approximate solution of OCPs (7.0.1) subject to the dynamic system (7.0.2). By increasing the number of basis functions, the accuracy of numerical results is enhanced.

The novelty of this work is that in the dynamic system (7.0.2), we have considered the order as a fractional, while in the reported works (see [173, 174, 199] and references therein), the order of the dynamic system is considered $\alpha = 1$. We have proposed a new formulation for OCPs subject to nonlinear Volterra integral equations. One of the big advantages of this approach is that by setting $\alpha = 1$, our scheme can easily be applied

to OCPs for NVIFs considered for examples in the work of Khanduzi et al. [174] and Maleknejad et al.[199], and to other similar methods. To verify this notable inference, the new technique is compared with MTLBO, TLBO, Legendre wavelet methods, and GWO and local methods [173, 174, 199] when $\alpha = 1$. Comparing the results of this work with the other relevant ones available in the related literature, as those reported by [173, 174, 199], revealed that the newly proposed formulation provides better performances concerning the previous ones.

The chapter aims to comprehensively analyze Chelyshkov polynomials and their applications in solving NVIFs. Section 7.1 describes the Chelyshkov polynomials and highlights their essential properties. The integration matrix, which plays a crucial role in solving these differential systems, is evaluated in Section 7.2. Section 7.3 proposes a computational optimization approach that can efficiently solve NVIFs. The accuracy of the proposed method is demonstrated through three numerical examples in Section 7.4. Finally, the chapter concludes with a summary of the key points and insights in Section 7.5.

7.1 Chelyshkov polynomials

In this section, we will report the definition and some properties of Chelyshkov polynomials. These polynomials were introduced in 2006 by Chelyshkov [69]. They constitute a family of new orthogonal polynomials defined by:

$$\chi_n(t) = \sum_{j=0}^{N-n} \gamma_{j,n} t^{n+j}, \qquad n = 0, 1, ...N, \tag{7.1.3}$$

in which

$$\gamma_{j,n} = (-1)^j \begin{pmatrix} N-n \\ j \end{pmatrix} \begin{pmatrix} N+n+j+1 \\ N-n \end{pmatrix}. \tag{7.1.4}$$

Moreover, the orthogonality condition for these polynomials is described as follow:

$$\int_0^1 \chi_p(t)\chi_q(t)dt = \frac{\delta_{pq}}{p+q+1},$$

where δ_{pq} represents Kronecker delta.

Remark 7. *By paying attention to the definition of the Chelyshkov polynomials, we conclude that the main difference between the these polynomials and other orthogonal polynomials in the interval* $[0, 1]$*, where the* n*-th polynomial has a degree* n*.*

Function approximation

Any function $\mathfrak{f}(t)$ which is integrable on $[0,1)$ can be approximated by applying the Chelyshkov polynomials as

$$\mathfrak{f}(t) \simeq \sum_{i=0}^{N} c_i \chi_i(t) = C^T \Upsilon(t), \tag{7.1.5}$$

where $\Upsilon(t)$ and C are $(N+1)$ vectors given by

$$C = [c_0, c_1, ..., c_N]^T, \quad \Upsilon(t) = [\chi_0(t), \chi_1(t), ..., \chi_N(t)]^T. \tag{7.1.6}$$

and the coefficients $c_i, i = 0, 1, ...N$ can be derived by means of the expression:

$$c_i = \frac{\langle \mathfrak{f}(t), \chi_i(t) \rangle_*}{\langle \chi_i(t), \chi_i(t) \rangle_*} = \frac{\int_0^1 \chi_i(t)\mathfrak{f}(t)dt}{\int_0^1 \chi_i(t)\chi_i(t)dt} = (2i+1)\int_0^1 \chi_i(t)\mathfrak{f}(t)dt. \tag{7.1.7}$$

7.2 Operational matrices

This section concerns processing operational matrices of the Chelyshkov polynomials vector $\Upsilon(t)$. In the following, some explicit formulations for the fractional integration operational matrix in the Riemann-Liouville sense and the product operational matrix for the Chelyshkov polynomials vectors will be given.

Theorem 22. *The fractional integration of order α of Chelyshkov polynomials vector can be obtained by*

$$I^\alpha \Upsilon(t) \simeq \Omega^{(\alpha)} \Upsilon(t), \tag{7.2.8}$$

where $\Upsilon(t)$ is $(N+1)$ Chelyshkov polynomials vector, $\Omega^{(\alpha)} \in \mathbb{R}^{N+1}$ is the fractional integration operational matrix of $\Upsilon(t)$ and each element of this matrix can be computed as

$$\Omega_{i,j}^{(\alpha)} = \sum_{r=0}^{N-i+1} \sum_{s=0}^{N-j} \frac{(2j+1)\Gamma(i+r)\gamma_{r,i-1}\gamma_{s,j}}{(\alpha+r+i+j+s)\Gamma(i+r+\alpha)}, \quad i = 1, 2..., N+1,\ j = 0, ..., N.$$

Proof. Let us consider the i-th element of the vector $\Upsilon(t)$. The fractional integral of order α for $\chi_{i-1}(t)$, can be obtained as

$$I^\alpha \Upsilon_i(t) = \mathcal{I}^\alpha \chi_{i-1}(t) = I^\alpha \sum_{r=0}^{N-i+1} \gamma_{r,i-1} t^{r+i-1} = \sum_{r=0}^{N-i+1} \frac{\Gamma(i+r)\gamma_{r,i-1}}{\Gamma(i+r+\alpha)} t^{\alpha+r+i-1}, \tag{7.2.9}$$

we expand by using the Chelyshkov polynomials the expression $t^{\alpha+r+i-1}$, then we have

$$t^{\alpha+r+i-1} \simeq \sum_{j=0}^{N} \theta_{r,j} \chi_j(t), \tag{7.2.10}$$

where $\theta_{r,j}$ can be obtained as

$$\theta_{r,j} = (2j+1)\int_0^1 \chi_j(t)t^{\alpha+r+i-1}dt$$

$$= (2j+1)\sum_{s=0}^{N-j}\gamma_{s,j}\int_0^1 t^{\alpha+r+i+j+s-1}dt = (2j+1)\sum_{s=0}^{N-j}\frac{\gamma_{s,j}}{\alpha+r+i+j+s}. \quad (7.2.11)$$

Now, by substituting (9.2.11) and (9.2.12) in (7.2.9) we have:

$$I^{\alpha}\Upsilon_i(t) \simeq \sum_{j=0}^{N}\left(\sum_{s=0}^{N-j}\sum_{r=0}^{N-i+1}\frac{(2j+1)\Gamma(i+r)\gamma_{r,i-1}\gamma_{s,j}}{(\alpha+r+i+j+s)\Gamma(i+r+\alpha)}\right)\chi_j(t).$$

Therefore the desired outcome is extracted. □

Theorem 23. *Let $Y \in \mathbb{R}^{N\times 1}$ be an arbitrary vector.*

$$\Upsilon(t)\Upsilon^T(t)Y = \tilde{Y}\Upsilon(t), \quad (7.2.12)$$

where $\Upsilon(t) \in \mathbb{R}^{N+1}$ is the Chelyshkov polynomial vector introduced in (7.1.6) and the (i,j)-th element of the product operational matrix $\tilde{Y}$ can be obtained as:

$$\tilde{Y}_{i,j} = \sum_{k=1}^{N} Y_k\int_0^1 \Upsilon_k(t)\Upsilon_i(t)\Upsilon_j(t)dt, \quad i,j = 1,2,...,N+1.$$

Proof. Consider two Chelyshkov polynomial vectors $\Upsilon(t)$ and $\Upsilon^T(t)$. The product of these two vectors is a matrix described as follows:

$$\Upsilon(t)\Upsilon^T(t) = \begin{bmatrix} \chi_0(t)\chi_0(t) & \chi_0(t)\chi_1(t) & \dots & \chi_0(t)\chi_N(t) \\ \chi_1(t)\chi_0(t) & \chi_1(t)\chi_1(t) & \dots & \chi_1(t)\chi_N(t) \\ \vdots & \vdots & \ddots & \vdots \\ \chi_N(t)\chi_0(t) & \chi_N(t)\chi_1(t) & \dots & \chi_N(t)\chi_N(t) \end{bmatrix}_{(N+1)\times(N+1)}.$$

As a consequence, the relation (7.2.12) can be represented as:

$$\sum_{k=0}^{N}\chi_k(t)\chi_i(t)Y_{k+1} = \sum_{k=0}^{N}\chi_k(t)\tilde{Y}_{i+1,k+1}, \quad i = 0,1,...,N. \quad (7.2.13)$$

By multiplying $\chi_j(t)$ on both sides of the relation (7.2.13) and integrating results over $[0,1]$, we have:

$$\sum_{k=0}^{N}Y_k\int_0^1\chi_k(t)\chi_i(t)\chi_j(t)dt = \sum_{k=0}^{N}\tilde{Y}_{i,k}\int_0^1\chi_k(t)\chi_j(t)dt, \quad i,j = 0,1,...,N.$$

Finally, the (i,j)-th element of product operational matrix $\tilde{Y}$ provided by

$$\tilde{Y}_{i,j} = \sum_{k=0}^{N}Y_k\int_0^1\chi_k(t)\chi_i(t)\chi_j(t)dt, \quad i,j = 0,1,...,N.$$

□

7.3 Description of the proposed numerical method

Consider the NVIFs (7.0.1) with initial conditions (7.0.2). First of all, all functions involved in NVIFs are approximated as follows:

$$D_t^\alpha y(t) \simeq Y^T \Upsilon(t), \tag{7.3.14}$$

$$y_0(t) \simeq O^T \Upsilon(t), \quad \varphi(s) \simeq \varepsilon^T \Upsilon(s), \tag{7.3.15}$$

$$a(t) \simeq A^T \Upsilon(t), \quad b(t) \simeq B^T \Upsilon(t), \quad c(t) \simeq C^T \Upsilon(t), \tag{7.3.16}$$

where $\Upsilon(t)$ is a vector defined as in relation (7.1.6). Moreover, O, A, B and C are known coefficient vectors that can be determined as described in (7.1.5) and Y represents the unknown vector to be determined. By (2.1.7) we have:

$$I^\alpha D_t^\alpha y(t) = y(t) - y_0(t). \tag{7.3.17}$$

Moreover, from Eq. (7.2.8) along with Eq. (7.3.14), we also have:

$$I^\alpha D_t^\alpha y(t) \simeq Y^T \mathcal{Q}^\alpha \Upsilon(t), \tag{7.3.18}$$

where $\mathcal{Q}^\alpha$ is the fractional derivative operational matrix.
In virtue of Eqs. (7.3.17)-(7.3.18), we get

$$y(t) \simeq Y^T \mathcal{Q}^\alpha \Upsilon(t) + O^T \Upsilon(t), \tag{7.3.19}$$

Applying of Eqs. (11.3.2), (7.3.15), (7.3.16) and (7.3.19) in relation (7.0.2), we have:

$$\begin{aligned} u(t) \simeq \frac{1}{B^T \Upsilon(t)} (&Y^T \Upsilon(t) + A^T \Upsilon(t)(Y^T \mathcal{Q}^\alpha \Upsilon(t) + O^T \Upsilon(t)) \\ &- C^T \Upsilon(t) \int_0^t \mathcal{G}(t, s, \varepsilon^T \Upsilon(s)) ds) \end{aligned}$$

Continuing, we can re-write $u(t)$ in the following format by using the Gauss-Legendre quadrature formula on $[0, 1]$:

$$\begin{aligned} u(t) \simeq \frac{1}{B^T \Upsilon(t)} \Big(&Y^T \Upsilon(t) + A^T \Upsilon(t)(Y^T \mathcal{Q}^\alpha \Upsilon(t) + O^T \Upsilon(t)) - (C^T \Upsilon(t)) \\ &(\frac{t}{2} \sum_{k=1}^{M} w_k \mathcal{G}(t, \frac{t}{2} s_k + \frac{t}{2}, \varepsilon^T \Upsilon(\frac{t}{2} s_k + \frac{t}{2})))) \Big) \end{aligned} \tag{7.3.20}$$

where s_k and w_k are Gauss-Legendre quadrature weights and nodes, respectively. Therefore, the performance index (7.0.1) is approximated as follows:

$$\mathcal{J}\left[y_0, y_1, ..., y_N\right] \simeq \int_0^1 \Psi\left(t, Y\right) dt,$$

where

$$\Psi(t,Y) = L\Big(t, Y^T\mathcal{Q}^\alpha\Upsilon(t) + O^T\Upsilon(t), \frac{1}{B^T\Upsilon(t)}(Y^T\Upsilon(t) + A^T\Upsilon(t)(Y^T\mathcal{Q}^\alpha\Upsilon(t)$$
$$O^T\Upsilon(t)) - C^T\Upsilon(t)(\frac{t}{2}\sum_{k=1}^{M} w_k\mathcal{G}(t, \frac{t}{2}s_k + \frac{t}{2}, \varepsilon^T\Upsilon(\frac{t}{2}s_k + \frac{t}{2}))))\Big).$$

Additionally, the performance indicator $\mathcal{J}\left[y_0, y_1, ..., y_N\right]$ can be approximated by implementing the Gauss-Legendre quadrature formula on $[0, 1]$, as follows:

$$\mathcal{J}\left[y_0, y_1, ..., y_N\right] \simeq \sum_{k=1}^{M} \mathbf{w}_k \Psi\left(t_k, Y\right), \tag{7.3.21}$$

where $\mathbf{w}_k$ and t_k are Gauss-Legendre quadrature nodes and weights, respectively. Ultimately, the conditions required for the optimal performance indicator are:

$$\frac{\partial \mathcal{J}}{\partial y_i} = 0, \qquad i = 0, 1, ..., N. \tag{7.3.22}$$

We solve the algebraic equation systems for the unknown vector Y to determine the optimal coefficient values y_i with $i = 0, 1, ..., N$. Next, we use Newton's iterative method to evaluate the coefficients of this modified problem, which is an algebraic equation system for the unknown vector Y. By identifying the vector Y and inserting vector Y in Eqs. (7.3.19) and (7.3.20), the state and control functions $y(t)$ and $u(t)$ can be approximated, respectively.

7.4 Numerical experiments

In this section, to investigate the proposed method's effectiveness, the numerical results based on three examples are exhibited. In these examples, the exact solutions are compared with the numerical solutions. Moreover, the obtained results are compared with the results of the method suggested in [173, 174, 199]. All the algorithms have been implemented using Maple 17 with 16 digits and M (number of Gauss-Legendre quadrature nodes and weights).

Example 12. *Consider the following NVIFs: minimize the performance indicator*

$$\min \mathcal{J} = \int_0^1 ((y(t) - e^{t^2})^2 + (u(t) - (1 + 2t))^2)dt,$$

subjected to the initial dynamical system

$$D^{\alpha}y(t) + y(t) - u(t) - \int_0^t (t(1+2t)e^{s(t-s)}y(s))ds = 0,$$
$$y(0) = 1.$$

For $\alpha = 1$, $\tilde{y}(t) = e^{t^2}, \tilde{u}(t) = 1 + 2t$ *are the exact solutions. Hence, the solution of these NVIFs using the presented Chelyshkov polynomials-based approach for various values of* N *and* α *has been approximated. As it can be seen from Figure 7.2 the approximate solutions (for* $N = 8$, $M = N + 2$ *and* $\alpha = 0.45, 0.55, 0.65, 0.75, 0.85, 0.95, 1$*) have been determined. The absolute errors of the numerical solution for* $y(t)$ *and* $u(t)$ *for* $\alpha = 1, N = 10$ *are also shown in Figure 7.3.*

Table 7.1 summarizes the results obtained using the presented method and the ones reported in other papers [174, 199] with various values of N*, where* $\alpha = 1$ *and* $M = N+2$*. In addition, as* α *approaches* 1*, the numerical solutions converge to the exact one and agree well with it. As the fractional order* α *approaches* 1*, the optimal performance indicator* J *gets close to the optimal value (*$J = 0$*) of the integer-order* $\alpha = 1$*. Based on the results, it can be concluded that the approach has successfully solved the above problem and outperformed the other analyzed techniques.*

Table 7.1: Comparison between indicator $\mathcal{J}$ of the obtained numerical solutions and other reported results for various value of N and $\alpha = 1$ in Example 12.

		N		
Methods	2	4	6	8
our method	$2.68e-02$	$2.11e-07$	$2.23e-10$	$2.48e-14$
MTLBO[174]	$3.59e-05$	$1.24e-06$	$3.29e-09$	$3.40e-13$
TLBO[174]	$1.94e-04$	$8.40e-05$	$4.50e-08$	$1.32e-12$
Legendr wavelet [199]	$9.33e-03$	$5.19e-04$	$7.46e-08$	$4.57e-12$

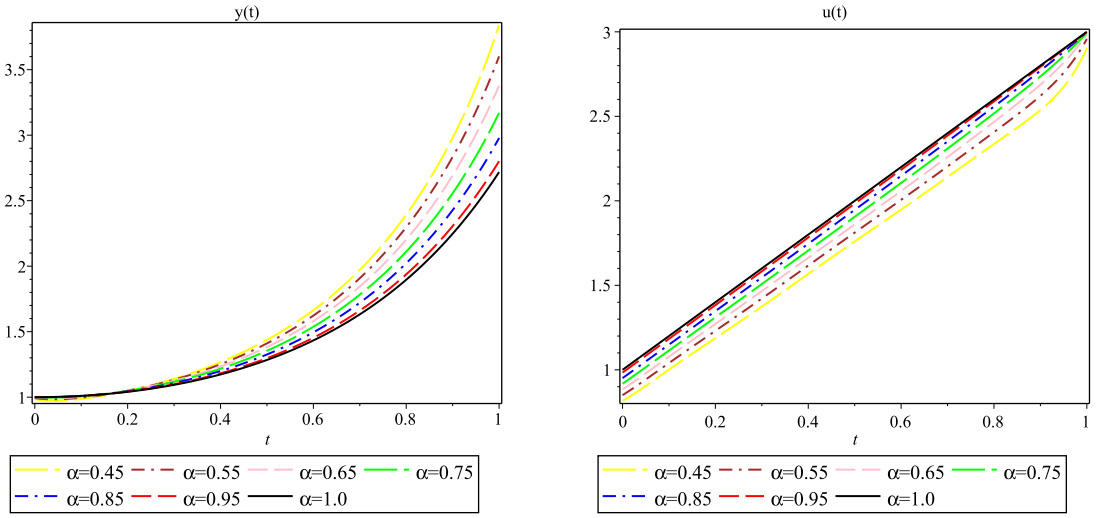

Figure 7.2: Numerical results for various values of α and $N = 8$ for y(t) and u(t) in Example 12.

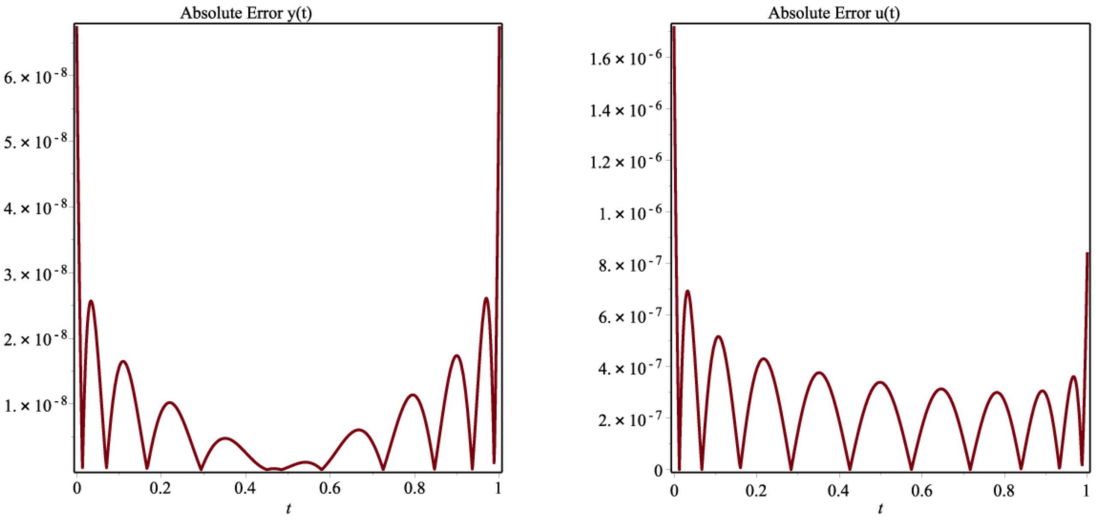

Figure 7.3: The absolute errors of numerical results for y(t) and u(t) for $\alpha = 1, N = 10$ Example 12.

Example 13. *Consider the following NVIFs: minimize the performance indicator*

$$\min \mathcal{J} = \int_0^1 ((y(t)-t)^2 + (u(t)-(1-te^{t^2}))^2)dt,$$

subjected to the initial dynamical system

$$\begin{aligned} &D^\alpha y(t) - y(t) - u(t) + 2\int_0^t (tse^{-y^2(s)})ds = 0, \\ &y(0) = 0 \end{aligned}$$

where $\tilde{y}(t) = t, \tilde{u}(t) = 1 - te^{t^2}$ are the exact solutions. The resulting plot of the approximate solutions (related to $N = 8$, $M = N+2$ and $\alpha = 0.45, 0.55, 0.65, 0.75, 0.85, 0.95, 1$) considering both state and control functions together is shown in Figure 7.4, whereas the absolute errors for $\alpha = 1$ and $N = 10$ are plotted in Figure 7.5. The solution of these NVIFs using the presented Chelyshkov polynomials approach for various values of N and α has been approximated. A comparison between the obtained optimal performance indicator J results obtained with the presented method and the others referred to in [174, 199] with different values of N, where $\alpha = 1$ and $M = N + 2$ are reported in Table 7.2.
Based on the numerical findings presented in these Tables, the utility of the method for solving NVIFs is obvious. In contrast to other approaches, the implementation of Chelyshkov polynomials is effective and accurate. In addition, as α approaches 1, the numerical solutions converge to the exact one and agree well with it. That is, as the fractional order α approaches 1, the optimal performance indicator J get close to the optimal value ($J = 0$) of the integer-order $\alpha = 1$. From the outcome of our investigation, it is possible to conclude that also this experiment has given good results.

Table 7.2: Comparison between indicator $\mathcal{J}$ of the obtained numerical solutions and other reported results for various value of N and $\alpha = 1$ in Example 13.

		N		
Methods	2	4	6	8
our method	$7.29e-22$	$4.68e-23$	$1.68e-23$	$2.00e-24$
MTLBO[174]	$5.02e-16$	$1.05e-16$	$8.98e-17$	$9.25e-18$
TLBO[174]	$3.72e-13$	$7.51e-15$	$5.26e-16$	$1.41e-17$
Legendr wavelet [199]	$3.94e-06$	$5.98e-10$	$2.47e-14$	$8.67e-17$

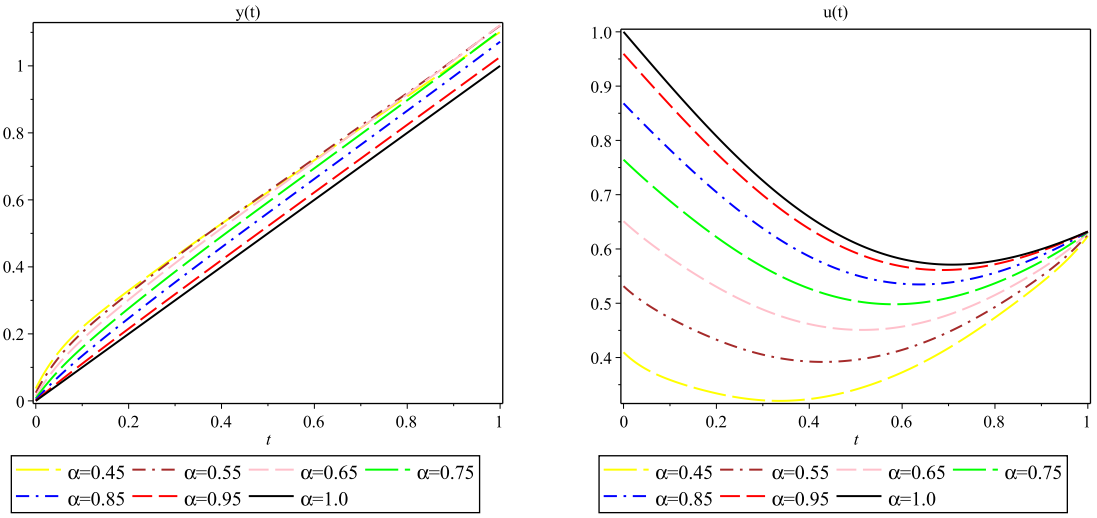

Figure 7.4: Numerical results for various values of α and $N = 8$ for y(t) and u(t) in Example 13.

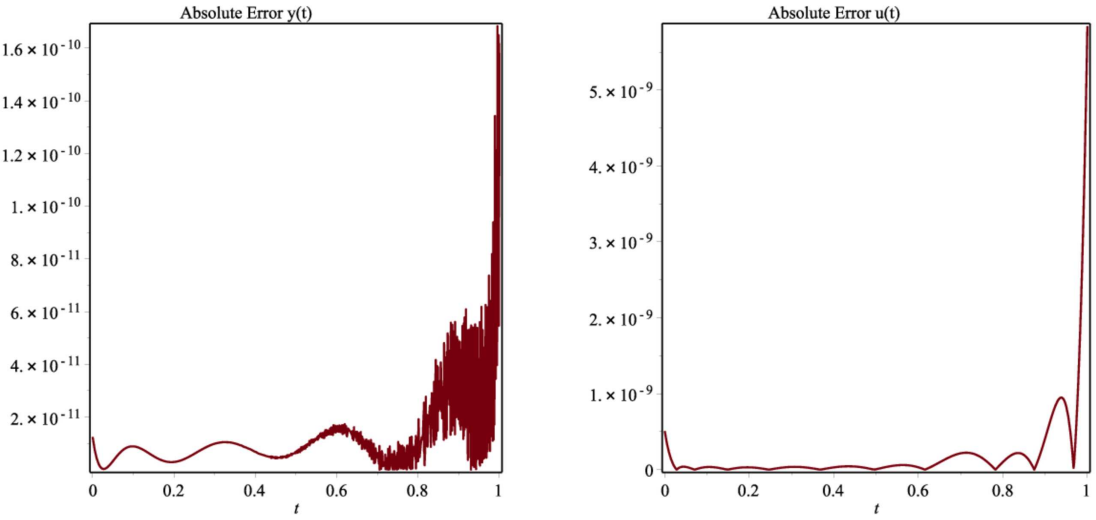

Figure 7.5: The absolute errors of numerical results for y(t) and u(t) for $\alpha = 1, N = 10$ Example 13.

Example 14. *Now, consider the following NVIFs: minimize the performance indicator*

$$\min \mathcal{J} = \int_0^1 ((y(t) - e^t)^2 + (u(t) - e^{3t})^2)dt,$$

subjected to the initial dynamical system

$$D^\alpha y(t) - \tfrac{3}{2}y(t) + \tfrac{1}{2}u(t) - \int_0^t (e^{(t-s)}y^3(s))ds = 0,$$
$$y(0) = 1.$$

where $\tilde{y}(t) = e^t, \tilde{u}(t) = e^{3t}$ are the exact solutions. The approximate solutions (related to $N = 6$, $M = N + 2$ and $\alpha = 0.45, 0.55, 0.65, 0.75, 0.85, 0.95, 1$) are shown in Figure 7.6 for both state and control functions. The absolute errors of the numerical solution for $y(t)$ and $u(t)$ for $\alpha = 1, N = 10$ are also shown in Figure 7.7.
Hence, the solution of these NVIFs using the suggested Chelyshkov polynomials approach for various values of N and α has been approximated. A comparison between the obtained optimal performance indicator J obtained with the suggested method and the other ones reported in [174, 199] with different values of N, where $\alpha = 1$ and $M = N + 2$ is reported in Tables 7.3.
Based on the presented results, the utility of the method for solving NVIFs is obvious, and in contrast to other approaches, the implementation of Chelyshkov polynomials is efficient and accurate. In addition, as α approaches 1, the numerical solutions converge to the exact one and agree well with it. That is, as the fractional order α approaches 1, the optimal performance indicator J get close to the optimal value ($J = 0$) of the integer-order $\alpha = 1$. The findings of our research are quite convincing, and thus it is possible to assert that the method is accurate and successful.

Table 7.3: Comparison between indicator $\mathcal{J}$ of the obtained numerical solutions and other reported results for various value of N and $\alpha = 1$ in Example 14.

		N		
Methods	2	4	6	8
our method	$8.43e-05$	$1.25e-09$	$1.49e-15$	$3.04e-22$
MTLBO[174]	$9.09e-05$	$1.39e-07$	$8.02e-09$	$1.95e-15$
TLBO[174]	$2.39e-04$	$1.80e-07$	$8.45e-09$	$6.10e-14$
Legendre wavelet [199]	$1.05e-02$	$1.98e-07$	$1.17e-11$	$2.73e-12$

In the end, a comparison between the obtained optimal performance indicator J with the suggested method and the other ones reported in [173] for $N = 7$, where $\alpha = 1$ and $M = N + 2$ is reported in Table 7.4 (for Examples 1, 2 and 3). As can be seen, the superiority of the method for solving NVIFs is clear, and the implementation of Chelyshkov polynomials is efficient and accurate.

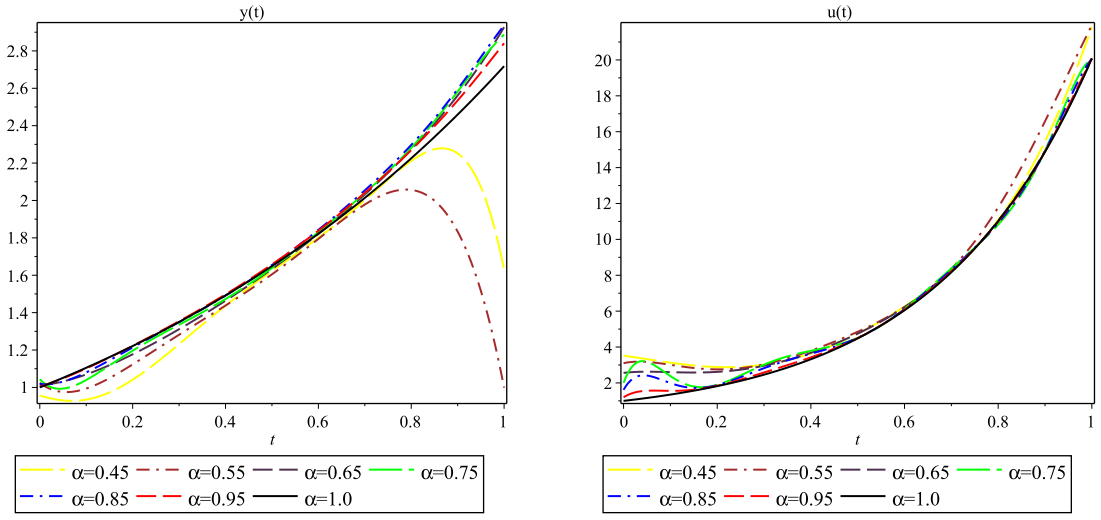

Figure 7.6: Numerical results for various values of α and $N = 8$ for y(t) and u(t) in Example 14

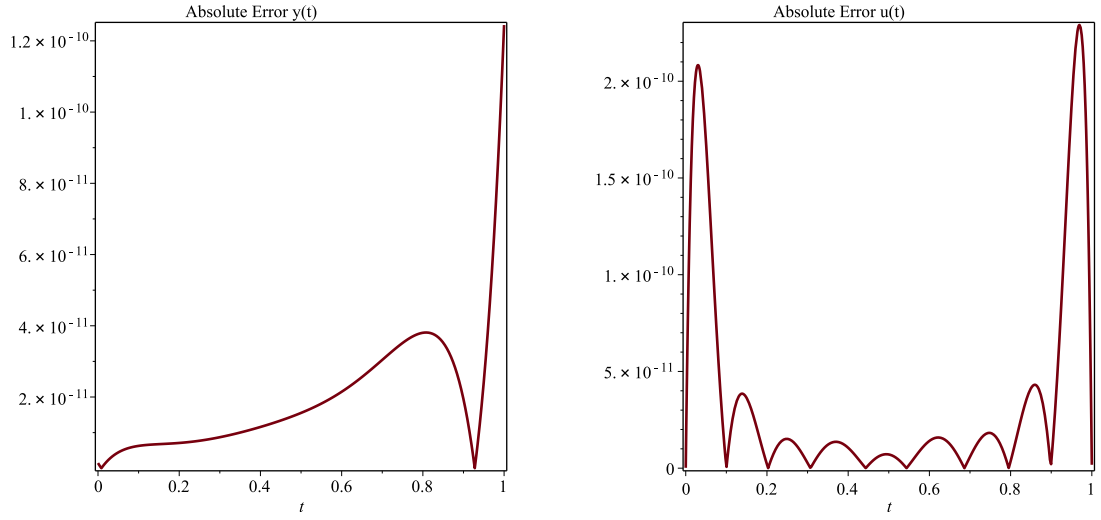

Figure 7.7: The absolute errors of numerical results for y(t) and u(t) for $\alpha = 1, N = 10$ Example 14.

Table 7.4: Comparison between indicator $\mathcal{J}$ of the obtained numerical solutions and other reported results for $N = 7, \alpha = 1$ in Examples 12, 13, 14.

Methods	**Our method**	**GWO algorithm**[173]	**Local method**[173]
*Example*12	$1.70e-12$	$7.40e-12$	$1.29e-11$
*Example*13	$8.15e-17$	$2.12e-14$	$8.84e-14$
*Example*14	$1.65e-23$	$7.74e-12$	$4.17e-11$

7.5 Conclusion

In this chapter, a practical approach was introduced in order to approximate solutions of systems of Volterra fractional integral equations. The essential characteristic of the proposed method is based on new polynomials named Chelyshkov polynomials and their fractional operational matrix and it helps reduce the Volterra fractional integral equations system into systems of algebraic equations to obtain approximate solutions. Three Examples illustrating the usefulness and precision of the suggested method have been presented. In addition, a summary of our numerical findings and the numerical solutions obtained with some other methods already show that the Chelyshkov method of polynomials is more precise than other approaches. The obtained results by the proposed Chelyshkov polynomials emphasized that:

- The main contribution is that a new type of polynomials is applied to obtain numerical solutions.
- Chelyshkov polynomials are efficient and successful in solving NVIFs.
- Application of Chelyshkov polynomials is accurate, and the results, as α approach to 1, are better than other reported results.
- The current strategy has ended well and with good results.

Chapter 8

Collocation methods or nonlinear Volterra integral equations with oscillatory kernel

Numerous mathematical problems in physics, biology, and engineering can be solved utilizing integral equations. These equations cannot often be solved analytically. Thus, numerically solving integral equations has attracted considerable interest [36, 67, 143, 144, 188]. In this chapter, we consider VIEs with a highly oscillatory kernel. Due to the oscillation factor, standard techniques may be costly. Therefore, specific numerical approaches are needed to discretize the highly oscillatory integral of the VIEs. For example, the steepest descent approach [145], the Filon type method [153], the exponential fitting method [158], the Levin type method [183], and other works [88, 191, 228, 318].

Some research has been reported on numerical approaches for VIEs with periodic solutions. The mixed collocation method, which differs from the polynomial collocation approach, is one of them. It includes additional trigonometric functions for approximating solutions. The mixed collocation approach was developed by Brunner [37] to solve problems with periodic solutions. Cardone et al. also developed the Exponential Fitting (EF) approach, which solved these VIEs using the EF quadrature formula [54]. Zhao et al. propose and demonstrate the EF collocation method for VIEs and global convergence based on EF interpolation [333].

In actuality, numerical solutions to integral equations with highly oscillatory kernels are the subject of very few publications. Xiang et al. studied VIEs with a Bessel kernel [319] by employing analytical expressions and a Filon-type technique. The author in [309] obtained a numerical solution by using a Filon-type method directly to the integral problem. In [186], the authors employed an improved Levin approach for solving Fredholm oscillatory integral equations.

There exists a category of numerical methods whose error acts asymptotically like a negative frequency power ω. Such methods have asymptotic order α if their error

is $O(\omega^{-\alpha})$ for $\omega \gg 1$, where α can be any positive number. Xiang et al. presented linear collocation techniques based on the Filon method for weakly singular VIEs of the second class with Bessel kernel in [320]. They confirmed that the methods have an asymptotic order. Asymptotic order is desirable for highly oscillatory problems. Zhao et al. proposed collocation methods based on the Filon method for the second kind VIEs with an oscillatory kernel in [335]. Based on an asymptotic solution analysis, they studied the convergence of the technique. For other schemes based on the Filon-type technique, please refer to [139, 192] and the references therein. Notably, the focus of the abovementioned articles is mainly on the asymptotic order , i.e., on the relationship between the error and the frequency. Less focus has been on the exact relationship between error and step size.

In this chapter, we consider second-kind Nonlinear Volterra Integral Equations (NVIEs) with a highly oscillatory kernel having the form

$$u(t) = f(t) + \int_0^t K(t, s, u(s)) e^{i\omega g(t,s)} ds, \quad (\omega \gg 1),\ t \in I = [0, T]\ (T < \infty) \tag{8.0.1}$$

where $u(t)$ is the unknown function and $f(t)$ is a given continuous function on I. The function $K = K(t, s, u)$ is assumed to be defined and continuous on $\Omega_B := \{(t, s, y) : (t, s) \in D,\ u \in \mathbb{R}\ \ |u - f(t)| \leqslant B, \}$, where $D := \{(t, s) : 0 \leqslant s \leqslant t \leqslant T\}$. The oscillating frequency ω is a real positive fixed parameter. Brunner [38, 39] has studied the oscillatory behavior of solutions for separable oscillators, i.e., $g(t, s) = g_0(t) - g_0(s)$. In this chapter, we are concerned with the NVIEs for $g(t, s) = s$.

Following the approach of [36] and based on a similar strategy extended to solve VIEs with the oscillatory kernel in [335], we employ the conventional collocation approach with predetermined collocation points for (3.1.1) to develop approaches for such highly oscillatory cases. The oscillatory integrals in the exact collocation are then discretized using a Filon-type method to produce an utterly discrete scheme. The theoretical part examines the asymptotic property and derivative of the solution. The error estimates for exact and discrete collocation are then calculated. Our results demonstrate the combined influence of step size h and frequency on error. The approach converges with step size h, and adding collocation points enhances the classical order. The approach has an asymptotic order if the frequency is substantial. Numerous cases in the numerical part support the theoretical results.

This chapter is structured into four sections. Section 8.1 describes the collocation approach for NVIEs of the second kind and applies the Filon technique for NVIEs. Section 8.2 contains theorems and lemmas that are useful for analyzing the solution's asymptotic property and the approach's convergence. Section 8.3 illustrates numerical experiments. In the final, Section 8.4 discusses conclusions.

8.1 Collocation method for second kind of NVIE

The exact collocation method and its fully discrete version are presented in this section. The first description is based on Brunner's classical approach [36]. The integrals in the exact collocation are then discretized using a Filon-type technique. Just for simplicity, we will use a uniform mesh. Discretize the interval $I = [0, T]$ by

$$I_h := \{t_n := nh,\ n = 0, ..., N,\ h \geqslant 0, Nh = T\}. \tag{8.1.2}$$

Let $\sigma_n := (t_n, t_{n+1}]$. Define the collocation points

$$T_h := \{t = t_{n,j} := t_n + c_j h,\ \ 0 \leqslant c_1 \leqslant ... \leqslant c_m \leqslant 1\,(0 \leqslant n \leqslant N-1)\}. \tag{8.1.3}$$

with c_j being collocation parameters. Now, we aim to identify a collocation solution for (8.0.1) in the space of piecewise polynomials.

$$S_{m-1}^{(-1)}(I_h) := \left\{P(s) : P(s)|_{\sigma_n} \in \pi_{m-1}\,(0 \leqslant n \leqslant N-1)\right\}, \tag{8.1.4}$$

where π_{m-1} represents the space of all polynomials of degree less than or equal to $m-1$. Brunner discusses how selecting $c_1 = 0$ and $c_m = 1$ would result in a continuous numerical solution on the I [36].

8.1.1 The exact collocation scheme

The collocation solution u_h, for (8.0.1) is specifically defined:

$$u_h(t) = f(t) + \int_0^t K(t, s, u_h(s))e^{i\omega s}ds \tag{8.1.5}$$

From another point of view, if we consider $U_{n,i} := u_h(t_{n,i})$, the collocation $u_h(t)$ on σ_n could also be expressed as

$$u_h(t) = u_h(t_n + sh) = \sum_{j=1}^{m} L_j(s)\, U_{n,j}, \quad s \in (0, 1], \tag{8.1.6}$$

where $L_j(s)$ represents the Lagrange basis functions.

$$L_j(s)\ := \prod_{k\neq j}^{m} \frac{s - c_k}{c_j - c_k}. \tag{8.1.7}$$

For $t = t_{n,j}$ the collocation equation (8.1.5) could be expressed as follows:

$$\begin{aligned}
&u_h(t) = f(t) + \textstyle\int_0^{t_n + c_j h} K(t, s, u_h(s))e^{i\omega s}ds \\
&= f(t) + \sum_{l=0}^{n-1} \textstyle\int_{t_l}^{t_{l+1}} K(t, s, u_h(s))e^{i\omega s}ds\ + \int_{t_n}^{t_n + c_j h} K(t, s, u_h(s))e^{i\omega s}ds \\
&= f(t) + \sum_{l=0}^{n-1} h\, e^{i\omega t_l} \textstyle\int_0^1 K(t, t_l + sh, u_h(t_l + sh))e^{i\omega sh}ds \\
&+h\, e^{i\omega t_n} \textstyle\int_0^{c_j} K(t, t_n + sh, u_h(t_n + sh))e^{i\omega sh}ds
\end{aligned} \tag{8.1.8}$$

Putting the local representation (8.1.6) of u_h into (8.1.8) and expressing it in terms of $U_{n,j}$ yields

$$\begin{aligned} U_{n,j} = f(t_{n,j}) + \sum_{l=0}^{n-1} h\, e^{i\omega t_l} \int_0^1 K(t_{n,j}, t_l + sh, \sum_{k=1}^{m} L_k(s)\, U_{l,k}) e^{i\omega sh} ds + \\ h\, e^{i\omega t_n} \int_0^{c_j} K(t_{n,j}, t_n + sh, \sum_{k=1}^{m} L_k(s)\, U_{n,k}) e^{i\omega sh} ds \end{aligned} \tag{8.1.9}$$

8.1.2 The fully discrete scheme

Due to the highly oscillatory integrals, the scheme in the last section could not always be applicable in practice. We need a fully discrete system ready to utilize for numerical simulation from a computational viewpoint. In order to deal with the highly oscillatory integral, we use a Filon-type technique. We recommend citing for additional information about oscillatory quadrature [118, 145, 153, 318, 333]. The new collocation equation supposes

$$\hat{u}_h(t) = f(t) + \int_0^{t_n + c_j h} K(t, s, \hat{u}_h(s)) e^{i\omega s} ds, \quad t \in T_h, \tag{8.1.10}$$

where $\hat{u}_h(t) \in S_{m-1}^{(-1)}(I_h)$ is the fully discrete collocation solution and $\int_0^t K(t, s, \hat{u}_h(s)) e^{i\omega s} ds$ is the Filon-type approximation of $u_h(t) = f(t) + \int_0^{t_n + c_j h} K(t, s, u_h(s)) e^{i\omega s} ds$. In fact, we use

$$\sum_{j=1}^{m} w_j(\nu)\, K(t, t_n + \nu c_j h, u_h(t_n + \nu c_j h)) \tag{8.1.11}$$

for the integrals

$$\int_0^{\nu} K(t, t_n + sh, u_h(t_n + sh)) e^{i\omega sh} ds \tag{8.1.12}$$

where $w_j(\nu) := \nu \int_0^1 e^{i\omega\nu sh} ds$ could be found using the incomplete Gamma function [153]. Replace the integrals in (8.1.8) with the previous quadrature approximations and disregard the quadrature errors to obtain the appropriate fully discrete collocation equation. The local representation of $\hat{u}_h$ on σ_h that is identical to (8.1.6) is

$$\hat{u}_h(t_n + sh) = \sum_{j=1}^{m} L_j(s)\, \hat{U}_{n,j}, \quad s \in (0, 1], \tag{8.1.13}$$

with $\hat{U}_{n,j} := \hat{u}_h(t_{n,j})$. Therefore, the fully discrete version is

$$\begin{aligned} \hat{U}_{n,j} = f(t_{n,j}) + \sum_{l=0}^{n-1} h\, e^{i\omega t_l} \sum_{k=1}^{m} w_k(1) K(t_{n,j}, t_l + c_k h, \sum_{k=1}^{m} L_k(c_k)\, \hat{U}_{l,k}) + \\ h\, e^{i\omega t_n} \sum_{l=1}^{m} w_l(c_j) K(t_{n,j}, t_n + c_l c_j h, \sum_{k=1}^{m} L_k(c_l c_j)\, \hat{U}_{n,k}) \end{aligned} \tag{8.1.14}$$

8.2 Convergence analysis

The existence and uniqueness of the solution for NVIEs (8.0.1), are indicated within the taking after lemma and theorem which can be found in [36].

Lemma 8.2.1. *Suppose that $z, g \in C(I), k \in C(I)$ and let $I := [0, T]$ with $k(t) \geqslant 0$. If z satisfies the inequality*

$$z(t) \leqslant g(t) + \int_0^t k(s)\, z(s)\, ds, \quad t \in I. \tag{8.2.15}$$

Then

$$z(t) \leqslant g(t) + \int_0^t k(s)\, g(s) \cdot exp\Big(\int_0^t k(\nu) d\nu\Big)\, ds, \quad for\ all\ t \in I. \tag{8.2.16}$$

If g is non-decreasing on I the above inequality reduces to

$$z(t) \leqslant g(t) \cdot exp\Big(\int_0^t k(s) ds\Big), \quad for\ all\ t \in I. \tag{8.2.17}$$

Theorem 24. *Set $\Omega_B := \{(t, s, u) :\ (t, s) \in D,\ u \in \mathbb{R}\, and\, |u - f(t)| \leqslant B\}$ and $M_B := \max\{|k(t, s, u)| :\ (t, s, u) \in \Omega_B\}$. Assume:*

a) $f \in C(I)$

b) $k \in C(\Omega_B)$

c) K *satisfies the Lipschitz condition for all* $(t, s, u), (t, s, z) \in \Omega_B$

Then

- *The Picard iterates $u_n(t)$ exist for all $n \geqslant 1$. They are continuous on the interval $I_0 := [0, \sigma_0]$, where*
$$\sigma_0 := min\,\{T, \frac{T}{M_B}\}$$
and they converge uniformly on I_0 to a solution $u \in C(I_0)$ of the NVIEs (8.0.1).
- *This solution u is the unique continuous solution on I_0.*

Proof. **Uniqueness:** Assume that (8.0.1) possesses two continuous solutions u_1 and u_2 on the interval I_0. Thus, by (c),

$$\begin{array}{l} |u_1(t) - u_2(t)| \leqslant \int_0^t |k(t, s, u_1(s)) - k(t, s, u_2(s))| ds \\ \leqslant L_B \int_0^t |u_1(s) - u_2(s)|\, ds, \quad t \in I_0 \end{array} \tag{8.2.18}$$

It follows from the continuity of $|u_1 - u_2|$ and from Lemma 8.2.1 that

$$|u_1(t) - u_2(t)| \leqslant 0 \cdot \exp(L_B t) = 0, \qquad for\ all\ \ t \in I_0 \tag{8.2.19}$$

Hence, $\|u_1 - u_2\|_{0,\infty} := max t_{t\in I_0} |u_1(t) - u_2(t)| = 0$, implying that the two solutions are identical on I_0.

Existence: The Picard iterates defined in (8.0.1) satisfy

$$|u_n(t) - f(t)| \leqslant M_B t \leqslant B, \qquad for\ all\ \ t \in I_0 \tag{8.2.20}$$

Since this statement is definitely true for $n = 0$, suppose it is true for n. This means that $k(t, s, u_n(s)) \in \Omega_B$ when $t \in I_0$. Hence, $k(t, s, u_n(s))$ is well defined and we have

$$|k(t, s, u_n(s))| \leqslant M_B, \qquad for\,(t, s) \in D. \tag{8.2.21}$$

This gives results

$$|u_n(t) - f(t)| \leqslant \left|\int_0^t k(t, s, u_n(s))ds\right| \leqslant M_B t \leqslant B, \qquad for\ \ t \in I_0. \tag{8.2.22}$$

Therefore, $u_{n+1}(t)$ is defined on I_0, and results from the continuity of f and k on I and Ω_B that $u_{n+1} \in C(I_0)$.

The sequence $\{u_n(t)\}$ defined by Picard iteration (8.0.1) is a Cauchy sequence on I_0. Hence, let $z_n(t) := u_{n+1}(t) - u_n(t)$. It is easily verified that

$$|z_n(t)| \leqslant \frac{M_B L_B t^{n+1}}{(n+1)!}, \qquad t \in I_0\ (n \geqslant 0) \tag{8.2.23}$$

Therefore,

$$u_{n+m}(t) - u_n(t) = \sum_{j=0}^{m-1} [u_{n+j+1}(t) - u_{n+j}(t)] \tag{8.2.24}$$

implies that, for all $t \in I_0$,

$$|u_{n+m}(t) - u_n(t)| \leqslant |z_{n+j}(t)| \leqslant M_B \sum_{j=0}^{m-1} \frac{L_B^{n+j} t^{n+j+1}}{(n+j+1)!} = M_B \sum_{j=n+1}^{n+m} \frac{L_B^{j-1} t^j}{(j)!}. \tag{8.2.25}$$

Thus, $\lim\limits_{n\to\infty} u_n(t) =: u(t)$ uniformly on I_0, with limit $u \in C(I_0)$. Using the Lipschitz condition for $k(t, s, u)$ with respect to u (assuming (c)), we obtain

$$\left|\int_0^t k(t, s, u_n(s)) - k(t, s, u(s))ds\right| \leqslant L_B \int_0^t |u_n(s) - u(t)| \longrightarrow 0, \quad t \in I_0 \tag{8.2.26}$$

as $n \to \infty$. This allows us to do the last step of proving existence, that is, to show that u solves the nonlinear integral equation (8.0.1) in I_0:

$$\begin{aligned} &\left|\textstyle\int_0^t k(t, s, u_n(s)) - k(t, s, u(s))ds\right| \leqslant L_B \int_0^t |u_n(s) - u(t)| \\ &= f(t) + \textstyle\int_0^t k(t, s, \lim\limits_{n\to\infty} u_{n-1}(s)) = f(t) + \int_0^t k(t, s, u(s))ds, \quad t \in I_0 \end{aligned} \tag{8.2.27}$$

The proof is now complete. □

We now introduce some lemmas that are used to estimate highly oscillating integrals.

Lemma 8.2.2. *[293] Suppose $q(t)$ is real-valued and smooth in (a,b), and that $|q^{(k)}(t)| \geqslant 1$ for all $t \in (a,b)$. Then*

$$\left|\int_a^b e^{i\omega q(t)}\right| \leqslant c(k)\,\omega^{-1/k} \tag{8.2.28}$$

holds when:

- *1) $k \geqslant 2$, or*
- *2) k=1 and $q^{'}(t)$ is monotonic.*

The bound $c(k)$ is independent of q and ω and $c(k) = 5 \cdot 2^{k-1} - 2$.

Lemma 8.2.3. *[293] Under the assumptions on $q(t)$ in Lemma 8.2.2, we can conclude that*

$$\left|\int_a^b e^{i\omega q(t)}\phi(t)dx\right| \leqslant c(k)\omega^{-1/k}\left[|\phi(b)| + \int_a^b \left|\phi^{'}(t)\right|dt\right]. \tag{8.2.29}$$

Following the idea of [318],the following theorem is proposed for oscillating integrals with a specific $\phi(t)$, i.e., $\phi(t)$ has some zero points.

Theorem 25. *Suppose $\phi(t) \in C^1$, $q(t)$ satisfies the assumptions in Lemma 8.2.3 and there exists a point $t_0 \in [a,b]$ making $\phi(t_0) = 0$. Then we have*

$$\left|\int_a^b e^{i\omega q(t)}\phi(t)dt\right| \leqslant 2\,c(k)\,\frac{\left\|\phi^{'}(t)\right\|_\infty}{\omega^{1/k}}(b-a). \tag{8.2.30}$$

Moreover, if $\phi(t) \in C^2$, $q(t) \in C^3$ with $k = 1$ and $\phi(a) = \phi(b) = 0$, it can be concluded that

$$\left|\int_a^b e^{i\omega q(t)}\phi(t)dt\right| \leqslant \min\left\{C_1\frac{b-a}{\omega^2}, C_2\frac{(b-a)^2}{\omega},\right\} \tag{8.2.31}$$

where $C_1 = 6\left\|\left(\dfrac{\phi(t)}{u^{'}(t)}\right)^{''}\right\|_\infty$, $C_2 = 3\left\|\phi^{''}(t)\right\|_\infty$.

Proof. With the constant t $in[a,b]$, we consider

$$\psi(x) = \phi(t) - \frac{\phi(t)}{t-t_0}(x-t_0). \tag{8.2.32}$$

Clearly, $\psi(x) \in C^1$ and it satisfies $\psi(t) = \psi(t_0) = 0$. Pursuant to Rolle's theorem, there exists a $\eta \in (a,b)$ such that

$$\psi^{'}(\eta) = \phi^{'}(\eta) - \frac{\phi(t)}{t-t_0} = 0. \tag{8.2.33}$$

That means $\phi(t) = \phi^{'}(\eta)(t - t_0)$. Then, by Lemma 8.2.3, we get

$$\begin{aligned}
&\left|\int_a^b e^{i\omega q(t)}\phi(t)dt\right| \leqslant c(k)\omega^{-1/k}\left[|\phi(b)| + \int_a^b |\phi^{'}(t)|dt\right] \\
&\leqslant \frac{c(k)}{\omega^{1/k}}\left(|\phi^{'}(\eta)|(b-a) + \left\|\phi^{'}(t)\right\|_\infty (b-a)\right) \\
&\leqslant 2c(k)\frac{\left\|\phi^{'}(t)\right\|_\infty}{\omega^{1/k}}(b-a).
\end{aligned} \tag{8.2.34}$$

This complete the first part.

For the second part, the result is very similar to [318]. Integration by parts produces

$$\int_a^b e^{i\omega q(t)}\phi(t)dt \;\; = -\frac{1}{i\omega}\int_a^b \left(\frac{\phi(t)}{q'(t)}\right)^{'} e^{i\omega q(t)}dt, \tag{8.2.35}$$

where $\phi(a) = \phi(b) = 0$. According to Rolle's theorem, there exists at least one c in (a, b) such that $(\phi(t)/q'(t))'|_{t=c} = 0$. Like the procedure of the first part, the inequality

$$\left|\int_a^b e^{i\omega q(t)}\phi(t)dt\right| = \frac{1}{\omega}\left|\int_a^b \left(\frac{\phi(t)}{q'(t)}\right)^{'} e^{i\omega q(t)}dt\right| \leqslant C_1\frac{b-a}{\omega^2} \tag{8.2.36}$$

holds for $k = 1$, where $C_1 := 6\left\|\left(\dfrac{\phi(t)}{q'(t)}\right)^{''}\right\|_\infty$.

In other words,

$$\begin{aligned}
&\left|\int_a^b e^{i\omega q(t)}\phi(t)dt\right| \leqslant c(1)\omega^{-1}\left[|\phi(b)| + \int_a^b |\phi'(t)|\,dt\right] \\
&= \frac{c(1)}{\omega}\int_a^b |\phi'(t)|\,dt \\
&\leqslant C_2\frac{(b-a)^2}{\omega}
\end{aligned} \tag{8.2.37}$$

where $C_2 := 3\left\|\phi^{''}(t)\right\|_\infty$. Finally, the combination of (8.2.36) and (8.2.37) results (8.2.31). □

8.2.1 Convergence of collocation solution u_h

Suppose $1 \leqslant d \leqslant m$ and $y \in C^d(I)$. According to Peano's Theorem [36], on σ_n

$$u(t_n + sh) = \sum_{j=1}^{m} L_j(s)u(t_{n,j}) + h^d R_{d,n}(s), \quad s \in (0, 1], \tag{8.2.38}$$

where

$$R_{d,n}(s) := \int_0^1 K_d(s, z)u^{(d)}(t_n + zh)dz, \tag{8.2.39}$$

with

$$K_d(s,z)=\frac{1}{(d-1)!}[(s-z)_+^{d-1}-\sum_{j=1}^{m}L_j(s)(c_j-z)_+^{d-1}],\quad z\in(0,1], \tag{8.2.40}$$

$(s-z)_+^p=0$ for $s<z$ and $(s-z)_+^p=(s-z)^p$ for $s\geqslant z$. Therefore, the error $e_h:=u-u_h$ has the local representation for the exact collocation solution

$$e_h(x_n+sh)=\sum_{j=1}^{m}L_j(s)\varepsilon_{n,j}+h^dR_{d,n}(s), \tag{8.2.41}$$

at $t=t_{n,j}$

$$\begin{aligned}
&e_h(t_{n,j})=\textstyle\int_0^{t_{n,j}}K(t_{n,j},s,u(s))e^{i\omega s}ds-\int_0^{t_{n,j}}K(t_{n,j},s,u_h(s))e^{i\omega s}ds\\
&=\textstyle\int_0^{t_n}K(t_{n,j},s,u(s))e^{i\omega s}ds+\int_{t_n}^{t_{n,j}}K(t_{n,j},s,u(s))e^{i\omega s}ds\\
&-\textstyle\int_0^{t_n}K(t_{n,j},s,u_h(s))e^{i\omega s}ds-\int_{t_n}^{t_{n,j}}K(t_{n,j},s,u_h(s))e^{i\omega s}ds\\
&=\textstyle\sum_{l=0}^{n-1}he^{i\omega t_l}\int_0^1(K(t_{n,j},t_l+sh,u(t_l+sh))-K(t_{n,j},t_l+sh,u_h(t_l+sh)))e^{i\omega sh}ds\\
&+he^{i\omega t_n}\textstyle\int_0^{c_j}(K(t_{n,j},t_n+sh,u(t_n+sh))-K(t_{n,j},t_n+sh,u_h(t_n+sh)))e^{i\omega sh}ds
\end{aligned} \tag{8.2.42}$$

As to $u_h=u-e_h$, we can write it in the form

$$\begin{aligned}
&e_h(t_{n,j})=\textstyle\sum_{l=0}^{n-1}he^{i\omega t_l}\int_0^1K_u(t_{n,j},t_l+sh,z_l(s))e_h(t_l+sh)e^{i\omega sh}ds\\
&+he^{i\omega t_n}\textstyle\int_0^{c_j}(K_u(t_{n,j},t_n+sh,z_n(s))e_h(t_n+sh)e^{i\omega sh}ds\\
&=\textstyle\sum_{l=0}^{n-1}he^{i\omega t_l}\int_0^1K_u(t_{n,j},t_l+sh,z_l(s))(\sum_{k=1}^{m}L_k(s)\varepsilon_{l,k}+h^dR_{d,l}(s))e^{i\omega sh}ds\\
&+he^{i\omega t_n}\textstyle\int_0^{c_j}(K_u(t_{n,j},t_n+sh,z_n(s))(\sum_{k=1}^{m}L_k(s)\varepsilon_{n,k}+h^dR_{d,n}(s))e^{i\omega sh}ds
\end{aligned} \tag{8.2.43}$$

assuming $K_u(t,s,.)$ is continuous and bounded. The functions z_l $(l\leqslant n)$ are the arguments arising in the Taylor remainder terms.

Then $\varepsilon_{n,j}:=u(t_{n,j})-u_h(t_{n,j})$ implies that

$$\begin{aligned}
&\varepsilon_{n,j}-he^{i\omega t_n}\textstyle\sum_{k=1}^{m}\int_0^{c_j}K_u(t_{n,j},t_n+sh,z_n(s))L_k(s)e^{i\omega sh}ds\varepsilon_{n,k}\\
&=\textstyle\sum_{l=0}^{n-1}he^{i\omega t_l}\sum_{k=1}^{m}\int_0^1K_u(t_{n,j},t_l+sh,z_l(s))L_k(s)e^{i\omega sh}ds\varepsilon_{l,k}\\
&+\textstyle\sum_{l=0}^{n-1}h^{d+1}e^{i\omega t_l}\sum_{k=1}^{m}\int_0^1K_u(t_{n,j},t_l+sh,z_l(s))R_{d,l}(s)e^{i\omega sh}ds\\
&+h^{d+1}e^{i\omega t_n}\textstyle\int_0^{c_j}K_u(t_{n,j},t_n+sh,z_n(s))R_{d,n}(s)e^{i\omega sh}ds
\end{aligned} \tag{8.2.44}$$

for $j=1,...,m$. Define the matrices

$$B_n^l:=\left(\sum_{k=1}^{m}\int_0^1K_u(t_{n,j},t_l+sh,z_l(s))L_k(s)e^{i\omega sh}ds\right)_{j,k=1,...,m},\quad (0\leqslant l<n\leqslant N-1), \tag{8.2.45}$$

$$B_n := \left(\sum_{k=1}^{m} \int_0^{c_j} K_u(t_{n,j}, t_n + sh, z_n(s)) L_k(s) e^{i\omega sh} ds \right)_{j,k=1,...,m}, \tag{8.2.46}$$

$$\rho_n^l := \left(e^{i\omega t_l} \sum_{k=1}^{m} \int_0^{1} K_u(t_{n,j}, t_l + sh, z_l(s)) R_{d,l}(s) e^{i\omega sh} ds \right)_{j=1,...,m}^{T}, \quad (l < n), \tag{8.2.47}$$

and

$$\rho_n := \left(e^{i\omega t_n} \int_0^{c_j} K_u(t_{n,j}, t_n + sh, z_n(s)) R_{d,n}(s) e^{i\omega sh} ds \right)_{j=1,...,m}^{T} \tag{8.2.48}$$

and let $\xi_n := (\varepsilon_{n,1}, ..., \varepsilon_{n,m})^T$. The Eq. (8.2.44) then assume the form

$$\left[I_m - h e^{i\omega t_n} B_n \right] \xi_n = \sum_{l=0}^{n-1} h\, e^{i\omega t_l} B_n^l\, \xi_l + \sum_{l=0}^{n-1} h^{d+1} \rho_n^l + h^{d+1} \rho_n, \quad 0 \leqslant N-1 \tag{8.2.49}$$

Here, I_m denotes the identity matrix.

If the kernel function $K(t, s, .)$ is continuous, we can ensure that each element in the matrices B_n is bounded. According to the Neumann Lemma [232], the inverse of the matrix $I_m - h e^{i\omega t_n} B_n$ exists whenever $h \left\| e^{i\omega t_n} B_n \right\| < 1$ for some matrix norm. This holds when h is small enough. In other words, for any mesh I_h with $h \in (0, \bar{h})$ where $\bar{h}$ is suitably small, each matrix $I_m - h e^{i\omega t_n} B_n$ has uniformly bounded inverse. Then,

$$\left\| I_m - h e^{i\omega t_n} B_n \right\|_1 \leqslant D_0 \tag{8.2.50}$$

for sufficient small h and $0 \leqslant n \leqslant N-1$. Also, we suppose $\left\| B_n^{(l)} \right\|_1 \leqslant D_1$ for $l < n \leqslant N-1$.

Paying attention to $R_{d,l}(c_1) = ... = R_{d,l}(c_m) = 0$ gives

$$\left| \int_0^{1} K_u(t_{n,j}, t_l + sh, z_l(s)) R_{d,l}(s) e^{i\omega sh} ds \right| \leqslant C \frac{M_d}{\omega h} \tag{8.2.51}$$

given $a = 0$, $b = 1$, $q(t) = t$ in Theorem 25, where $M_d := \left\| u^{(d)}(t) \right\|_\infty$. From now on, we apply C to represent a constant that may have different values in different places, but does not depend on h and ω. In addition, if $d \geqslant 2$ and $c_1 = 0$, $c_m = 1$ which means that $R_{d,l}(0) = ... = R_{d,l}(1) = 0$, then we have

$$\left| \int_0^{1} K_u(t_{n,j}, t_l + sh, z_l(s)) R_{d,l}(s) e^{i\omega sh} ds \right| \leqslant C\, M_d \min \left\{ \frac{1}{\omega^2 h^2}, \frac{1}{\omega h} \right\}. \tag{8.2.52}$$

We can deduce in a similar way

$$\left| \int_0^{c_j} K_u(t_{n,j}, t_n + sh, z_n(s)) R_{d,n}(s) e^{i\omega sh} ds \right| \leqslant C \frac{M_d}{\omega h} \tag{8.2.53}$$

and, for $d \geqslant 2$ and $c_1 = 0$,

$$\left| \int_0^{c_j} K_u(t_{n,j}, t_n + sh, z_n(s)) R_{d,n}(s) e^{i\omega sh} ds \right| \leqslant C M_d \min \left\{ \frac{1}{\omega^2 h^2}, \frac{1}{\omega h} \right\}. \tag{8.2.54}$$

Then we have the estimate

$$\begin{aligned} \left\| \rho_n^{(l)} \right\|_1 &\leqslant \sum_{j=1}^{m} \left| \int_0^1 K_u(t_{n,j}, t_l + sh, z_l(s)) R_{d,l}(s) e^{i\omega sh} ds \right| \\ &\leqslant C\, M_d \begin{cases} \min \left\{ \dfrac{1}{\omega^2 h^2}, \dfrac{1}{\omega h} \right\}, & for\ d \geqslant 2\ and\ \ c_1 = 0,\ c_m = 1, \\ \dfrac{1}{\omega h} & otherwise \end{cases} \end{aligned} \tag{8.2.55}$$

For $\|\rho_n\|_1$, we have

$$\|\rho_n\|_1 \leqslant C M_d \begin{cases} \min \left\{ \dfrac{1}{\omega^2 h^2}, \dfrac{1}{\omega h} \right\}, & for\ d \geqslant 2\ and\ \ c_1 = 0, \\ \dfrac{1}{\omega h} & otherwise \end{cases} \tag{8.2.56}$$

Then, (8.2.49) gives

$$\|\varepsilon_n\|_1 \leqslant D_0 D_1 \sum_{l=0}^{n-1} h \|\varepsilon_l\|_1 + D_0 \left(\sum_{l=0}^{n-1} h^{d+1} \left\| \rho_n^{(l)} \right\|_1 + h^{d+1} \|\rho_n\|_1 \right). \tag{8.2.57}$$

With the discrete Gronwall inequality in general [36], we estimate

$$\begin{aligned} \|\varepsilon_n\|_1 &\leqslant D_0 \left(\sum_{l=0}^{n-1} h^{d+1} \left\| \rho_n^{(l)} \right\|_1 + h^{d+1} \|\rho_n\|_1 \right) \exp\left(D_0 D_1 T\right) \\ &\leqslant C M_d \begin{cases} \dfrac{h^{d-1}}{\omega} \min\left\{ \frac{1}{\omega h}, 1 \right\}, & for\ d \geqslant 2\ and\ \ c_1 = 0,\ c_m = 1, \\ \dfrac{h^{d-1}}{\omega} & otherwise \end{cases} \end{aligned} \tag{8.2.58}$$

In other words, we have

$$\begin{aligned} \left\| \rho_n^{(l)} \right\|_1 &\leqslant \sum_{j=1}^{m} \left| e^{i\omega t_l} \int_0^1 K_u(t_{n,j}, t_l + sh, z_l(s)) R_{d,l}(s) e^{i\omega sh} ds \right| \\ &\leqslant \sum_{j=1}^{m} \int_0^1 |K_u(t_{n,j}, t_l + sh, z_l(s)) R_{d,l}(s)| ds \\ &\leqslant m\, \bar{K} k_d M_d, \end{aligned} \tag{8.2.59}$$

and

$$\|\rho_n\|_1 \leqslant m\, \bar{K} k_d M_d, \tag{8.2.60}$$

where $k_d := \max\limits_{s\in[0,1]} \int_0^1 |K_d(s,z)|\, dz$ and $\bar{K} := \max\limits_{t\in I} \int_0^t |K_u(t,s,.)|\, ds$. Taking them into (8.2.57) leads

$$\|\varepsilon_n\|_1 \leqslant C M_d h^d \tag{8.2.61}$$

To conclude this subsection, we summarize the above analysis in the following theorem.

Theorem 26. *Assume the functions $f(t)$ and $K(t,s,.) \in C^d$ in (8.0.1) with $1 \leqslant d \leqslant m$. Then numerical solution defined by (8.1.14) is estimated by*

$$\begin{aligned}&\max_{t\in X_h} |u(t) - u_h(t)| \\ &\leqslant CM_d \begin{cases} \min\left\{h^d, \dfrac{h^{d-1}}{\omega}, \dfrac{h^{d-2}}{\omega^2}\right\}, & for\ d \geqslant 2\ and\ \ c_1 = 0,\ c_m = 1, \\ \min\left\{h^d, \dfrac{h^{d-1}}{\omega}\right\} & otherwise \end{cases}\end{aligned} \tag{8.2.62}$$

with $M_d := \left\|u^{(d)}(t)\right\|_\infty$.

Proof. Pursuant to Theorem 24, we infer that $u(t) \in C^d$. Thus, the regularity condition for $u(t)$ at the begin of this subsection is satisfied and the above method can be done successfully. Combining (8.2.58) and (8.2.61) completes the proof. □

8.2.2 Convergence of collocation solution $\hat{u}_h$

By taking the quadrature error of (8.1.11), we have

$$E_n^l(t,\nu) := \int_0^\nu K(t, t_n + sh, u_h(t_l + sh))e^{i\omega sh}ds - \sum_{j=1}^m w_j(\nu)\, K(t, t_n + \nu c_j h, u_h(t_n + \nu c_j h)) \tag{8.2.63}$$

By reducing (8.1.11) from (8.1.12) for fixed $\nu > 0$, we have

$$\begin{aligned}&E_n^l(t,\nu) \\ &:= \nu \int_0^1 \Big(K(t, t_n + \nu sh, u_h(t_l + \nu sh)) - \sum_{j=1}^m w_j(\nu)\, K(t, t_n + \nu c_j h, u_h(t_n + \nu c_j h))\Big)e^{i\omega sh}ds.\end{aligned} \tag{8.2.64}$$

In (8.2.64), the expression in the brackets is the interpolation error for $p(s) := K(t, t_n + \nu sh, u_h(t_n + \nu sh))$.Thus, by Peano's Theorem, we have

$$E_n^l(t,\nu) = \nu h^d \int_0^1 \hat{R}_{d,n}(s)\, e^{i\omega sh}ds. \tag{8.2.65}$$

with

$$\hat{R}_{d,n}(s) := \nu h^d \int_0^1 \hat{K}_d(s,z) p^{(d)}(t_n + zh)dz. \tag{8.2.66}$$

Then, we have $|E_n^l(t,\nu)| \leqslant Ch^d$. Furthermore, it holds $\hat{R}_{d,n}(c_1) = ... = \hat{R}_{d,n}(c_m) = 0$. Similar to (8.2.51) and (8.2.52), quadrature error (8.2.65) has the estimate

$$\left|E_n^l(t,\nu)\right| \leqslant C \begin{cases} \min\left\{h^d, \dfrac{h^{d-1}}{\omega}, \dfrac{h^{d-2}}{\omega^2}\right\}, & for\ d \geqslant 2\ and\ \ c_1 = 0,\ c_m = 1, \\ \min\left\{h^d, \dfrac{h^{d-1}}{\omega}\right\} & otherwise \end{cases} \tag{8.2.67}$$

where the same idea of the last subsection is applied. For $\nu = 0$, the above result is obvious.

Theorem 27. *Assume that the given functions $f(t)$ and $K(t,s,u) \in C^d$ in (8.0.1) with $1 \leqslant d \leqslant m$. Then the numerical solution defined by (8.1.14) has an estimate*

$$\begin{aligned}&\max_{t\in T_h} |u(t) - \hat{u}_h(t)| \\ &\leqslant C\gamma_d \begin{cases} \min\left\{h^d, \dfrac{h^{d-1}}{\omega}, \dfrac{h^{d-2}}{\omega^2}\right\}, & for\ d \geqslant 2\ and\ \ c_1 = 0,\ c_m = 1, \\ \min\left\{h^d, \dfrac{h^{d-1}}{\omega}\right\} & otherwise \end{cases}\end{aligned} \tag{8.2.68}$$

with $\gamma_d := max\{M_d,\, 1\}$.

Proof. Due to

$$|u(t) - \hat{u}_h(t)| \leqslant |u(t) - u_h(t)| \,+\, |u_h(t) - \hat{u}_h(t)|\,. \tag{8.2.69}$$

The result is conducted in a way that is similar to the last subsection, then we estimate $|u_h(t) - \hat{u}_h(t)|$.
Let $z_h(t) := u_h(t) - \hat{u}_h(t)$. Then, on σ_n,

$$z_h(t_n + sh) := u_h(t_n + sh) - \hat{u}_h(t_n + sh) = \sum_{j=1}^{m} L_j(s) Z_{n,j}, \tag{8.2.70}$$

with $Z_{n,j} := U_{n,j} - \hat{U}_{n,j}$. Due to the (8.1.9) and (8.1.14), we have

$$\begin{aligned} Z_{n,j} = &\sum_{l=0}^{n-1} h\, e^{i\omega t_l} \sum_{k=1}^{m} \textstyle\int_0^1 K_u(t_{n,j}, t_l + sh, z_l(s)) L_k(s)\, Z_{l,k} e^{i\omega sh} ds + \\ &h\, e^{i\omega t_n} \sum_{l=1}^{m} \textstyle\int_0^{c_j} K_u(t_{n,j}, t_n + sh, z_n(s))\, L_k(s)\, Z_{n,k} e^{i\omega sh} ds + \epsilon_n(t_{n,j}), \end{aligned} \tag{8.2.71}$$

where

$$\epsilon_n(t_{n,j}) := \sum_{l=0}^{n-1} h\, e^{i\omega t_l} E_n^l(t, 1) + h\, e^{i\omega t_n} E_n^n(t, c_j)$$

and the functions z_l $(l \leqslant n)$ are the arguments arising in the Taylor remainder terms.

Recalling the definition of B_n^l and B_n in the last section, the system can be written as

$$\left[I_m - he^{i\omega t_n} B_n\right] \mathbf{Z}_n = \sum_{l=0}^{n-1} h\, e^{i\omega t_l} B_n^l\, \mathbf{Z}_l + \chi_n \tag{8.2.72}$$

where $\mathbf{Z} := (Z_{n,1}, ..., Z_{n,m})^T$ and $\chi_n := (\epsilon_{n,1}, ..., \epsilon_{n,m})^T$. This structure is as the same structure (8.2.49) but different from the term inhomogeneous. It therefore leads to

similar inequality as follow (8.2.57). For χ_n, we have

$$\begin{aligned}
\|\chi_n\|_1 &= \sum_{j=1}^{m} \left| \sum_{l=0}^{n-1} h e^{i\omega t_l} E_n^l(t_{n,j}, 1) + h e^{i\omega t_n} E_n^n(t_{n,j}, c_j) \right| \\
&\leqslant \sum_{j=1}^{m} \left(\sum_{l=0}^{n-1} h \left| E_n^l(t_{n,j}, 1) \right| + h \left| E_n^n(t_{n,j}, c_j) \right| \right) \\
&\leqslant C \begin{cases} \min \left\{ h^d, \dfrac{h^{d-1}}{\omega}, \dfrac{h^{d-2}}{\omega^2} \right\}, & for\ d \geqslant 2\ and\ c_1 = 0,\ c_m = 1, \\ \min \left\{ h^d, \dfrac{h^{d-1}}{\omega} \right\}, & otherwise. \end{cases}
\end{aligned} \tag{8.2.73}$$

Therefore, the following inequality is established

$$\|\mathbf{Z}_n\|_1 \leqslant C \begin{cases} \min \left\{ h^d, \dfrac{h^{d-1}}{\omega}, \dfrac{h^{d-2}}{\omega^2} \right\}, & for\ d \geqslant 2\ and\ c_1 = 0,\ c_m = 1, \\ \min \left\{ h^d, \dfrac{h^{d-1}}{\omega} \right\}, & otherwise. \end{cases} \tag{8.2.74}$$

Combination of inequality (8.2.69), Theorem 26 and (8.2.74) give us Theorem 27. □

The method converges for a fixed ω as the step length h approaches 0. This theorem demonstrates that our strategy may produce superior results compared to the classical collocation method. If M_d is bounded by ω, our technique will have asymptotic order 1, and it may reach 2 if $d \geqslant 2$ and $c_1 = 0$, $c_m = 1$. As ω increases, numerical findings will become more accurate under such conditions. In conformity with Theorem 24, $d = 1$ will yield a technique with one asymptotic order.

8.3 Numerical experiments

As demonstrated in the previous section, Filon's approaches are practical for solving NVIEs with highly oscillatory kernels. According to Theorem 27, the errors generated by these approaches decrease significantly as the frequency increases. This section focuses on two examples to illustrate the effectiveness of the strategy. In our experiments, we always take $T = 1$. We fix the parameters $\omega = 100$ and $N = 64, 128, 256, 512, 1024$ and plot figures to show the corresponding classical orders. We can get that the asymptotic order of the error eh is α if the absolute error is scaled by ω^α, i.e., $\omega^\alpha |e_h|$ is bounded as $\omega \longrightarrow \infty$. $N = 3$ is used to plot the asymptotic orders. Moreover, the following notation will be used to denote the numerical approach employed:

- CC = classical collocation method,
- CF = proposed method,

Example 15. *Consider the NVIE*

$$u(t) = e^t - \frac{1}{(i\omega+2)}(e^{(i\omega+2)t} - 1) + \int_0^t e^{i\omega s}(u(s))^2\, ds \tag{8.3.75}$$

such that the exact solution is $u(t) = e^t$.

For this example, we want to illustrate that the classical order is 1 *when* $m = 2$. *For parameters* $c_1 = \frac{1}{3}, c_2 = 1$ *and* $c_1 = 0, c_2 = 1$, *the right pictures of Figures 8.1 and 8.2 indicate that the classical order is* 1. *We fix the parameters* $\omega = 100$, *and* $N = 64, 128, 256, 512, 1024$. *These figures show the corresponding classical orders along with the slope line. By taking* $d = 1$, *to demonstrate the asymptotic order behaviour for parameters* $c_1 = \frac{1}{3}, c_2 = 1$, *we investigate the left picture of Figure 8.1. In the left picture of Figure 8.1, the absolute errors scaled by* ω *are bounded, confirming that the asymptotic order is* 1, *which is consistent well with Theorem 27. For parameters* $c_1 = 0, c_2 = 1$, *Theorem 27 predicts that the asymptotic order could be reached to* 2 *with* $d \geqslant 2$. *Here,* g *is continuous and dependent on* ω, *so the solution* $y = y(t, \omega)$ *behaves like* $u(t) - f(t) = O(\omega)$ *as* $\omega \longrightarrow \infty$, *so* $\|u^{(2)}(t)\|_\infty = O(\omega)$. *In the left picture of Figure 8.2, the absolute errors scaled by* ω *are bounded, confirming that the asymptotic order is* 1. *Our method could be easily adapted to solve the equation. This match well with Theorem 27. A large sample of numerical findings from the Figures demonstrates that these approaches are more effective and accurate as frequency increases.*

The boundedness of the errors scaled by ω *in the figures indicates that it is* 1 *for the asymptotic order. To confirm the effectiveness, we compare CF with the CC method in [36] and the numerical findings are compared in Table 8.1 for* $\omega = 20$. *One can observe that the method converges concerning* h. *Figure 8.3 shows the superiority of the CF method in comparison with the CC method. However, our strategy improves the conventional one with the same settings for collocation. The absolute errors are displayed in Tables 8.2 and 8.3. The data in Tables 8.2 and 8.3 indicate that our technique is convergent concerning* h. *The numerical findings show the scheme's effectiveness, and our theoretical analysis is precise. They inform us that the proposed approach suits oscillatory NVIEs, particularly* $\omega \gg 1$.

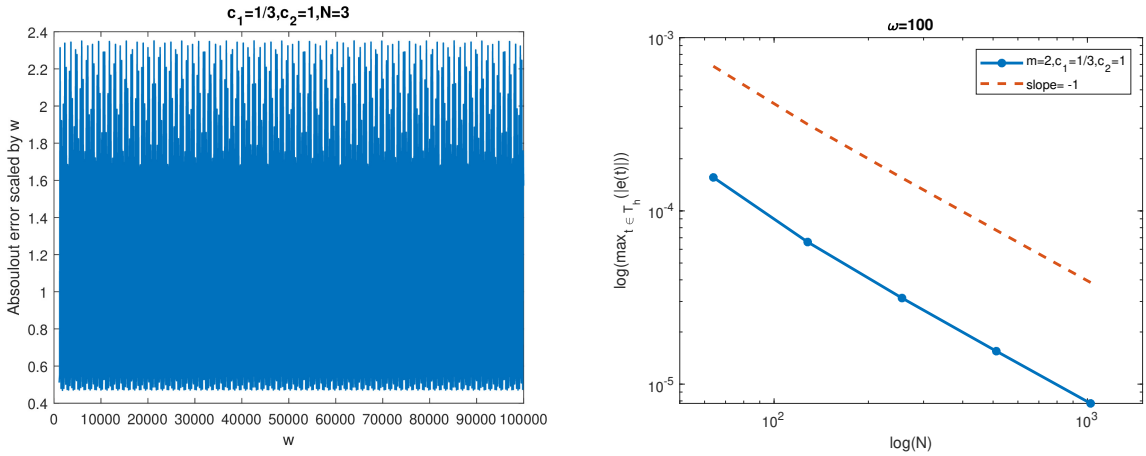

Figure 8.1: The asymptotic order and the classical order with $c_1 = \frac{1}{3}, c_2 = 1$ for Example 15

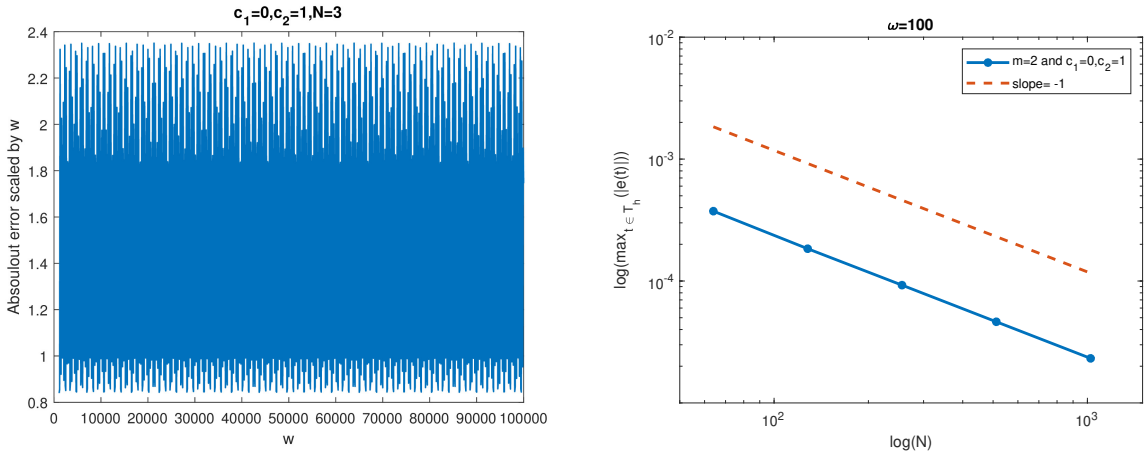

Figure 8.2: The asymptotic order and the classical order with $c_1 = 0, c_2 = 1$ for Example 15

Table 8.1: Comparison of absolute errors with $\omega = 20$ for Example 15.

		N				
Parameters	*Methods*	64	128	256	512	1024
$c_1 = \frac{1}{3}$, $c_2 = 1$	CC	$7.63e-03$	$3.81e-03$	$1.91e-03$	$9.54e-04$	$4.74e-04$
	CF	$7.66e-04$	$3.80e-04$	$1.90e-04$	$9.51e-05$	$4.75e-05$
$c_1 = 0$, $c_2 = 1$	CC	$2.22e-02$	$1.13e-02$	$5.69e-03$	$2.85e-03$	$1.43e-03$
	CF	$2.23e-03$	$1.13e-03$	$5.67e-04$	$2.84e-04$	$1.42e-04$

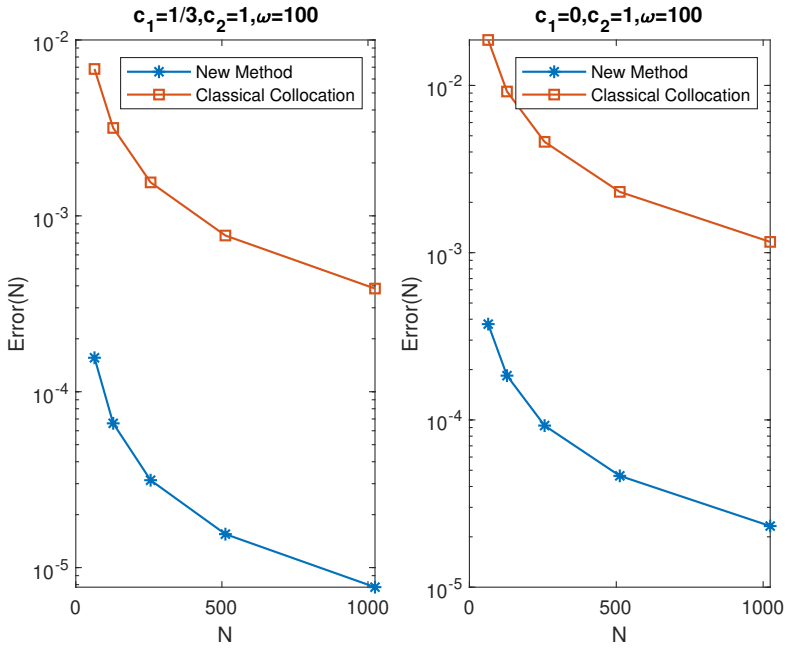

Figure 8.3: Comparison of absolute errors with $\omega = 100$ for Example 15

Table 8.2: The absolute errors with $c_1 = \frac{1}{3}$, $c_2 = 1$ for Example 15.

	N				
ω	64	128	256	512	1024
50	$2.57e-04$	$1.23e-04$	$6.09e-05$	$3.04e-05$	$1.52e-05$
100	$1.56e-04$	$6.61e-05$	$3.14e-05$	$1.55e-05$	$7.74e-06$
200	$2.24e-04$	$4.22e-05$	$1.77e-05$	$8.39e-06$	$4.14e-06$
400	$5.04e-03$	$6.27e-05$	$1.23e-05$	$5.11e-06$	$2.42e-06$

Table 8.3: The absolute errors with $c_1 = 0$, $c_2 = 1$ for Example 15.

	N				
ω	64	128	256	512	1024
50	$7.16e-04$	$3.61e-04$	$1.81e-04$	$9.08e-05$	$4.55e-05$
100	$3.74e-04$	$1.84e-04$	$9.25e-05$	$4.63e-05$	$2.32e-05$
200	$3.87e-04$	$1.01e-04$	$4.96e-05$	$2.47e-05$	$1.23e-05$
400	$5.04e-03$	$1.05e-04$	$2.95e-05$	$1.44e-05$	$7.13e-06$

To test its performance for some equations with oscillatory solutions, we also report the following examples.

Example 16. *Consider the NVIE*

$$u(t) = \sqrt{t} - e^{i\omega t}\left(\frac{t}{i\omega} + \frac{1}{\omega^2}\right) + \frac{1}{\omega^2} + \int_0^t e^{i\omega s}(u(s))^2\, ds \tag{8.3.76}$$

such that the exact solution is $u(t) = \sqrt{t}$.

For this example, we want to demonstrate that the classical order is 1 *when* $m = 2$. *For parameters* $c_1 = \frac{1}{3}, c_2 = 1$ *and* $c_1 = 0, c_2 = 1$, *the right pictures of Figures 8.1 and 8.2 tell that the classical order is* 1. *These figures show the corresponding classical orders along with the slope line for fixing the parameters* $\omega = 100$ *and* $N = 64, 128, 256, 512, 1024$. *By taking* $d = 1$ *in Theorem 27, the asymptotic order of the method is* 1 *for* $c_1 = \frac{1}{3}$ *and* $c_2 = 1$ *as well , and it is confirmed by the left picture of Figure 8.4. Noticing* $M_2 := \|u^{(2)}(t)\|_\infty = O(\omega)$, *Theorem 27 predicts that the asymptotic order is* 1 *with* $c_1 = 0$ *and* $c_2 = 1$ *and it is confirmed by the left picture of Figure 8.5. The findings confirm that the method is more efficient and accurate as the frequency increases.*

We also compare the CF and CC approaches to investigate superiority. The numerical results are given in Table 8.4 for $\omega = 20$. *It can be seen that the method converges concerning* h. *To verify the superiority, Figure 8.6 shows the CF method's superiority compared to the CC method. However, our method outperforms the classical one with the same collocation parameters. The absolute errors are presented in Tables 8.5 and 8.6. Tables 8.5 and 8.6 describe the convergence of the procedure concerning* h *and the order* 2 *is verified by the right pictures of Figures 8.4 and 8.5. The numerical results demonstrate the scheme's effectiveness, and our theoretical analysis is incisive. They inform us that the approach shown here is suited for oscillatory NVIEs, particularly* $\omega \gg 1$.

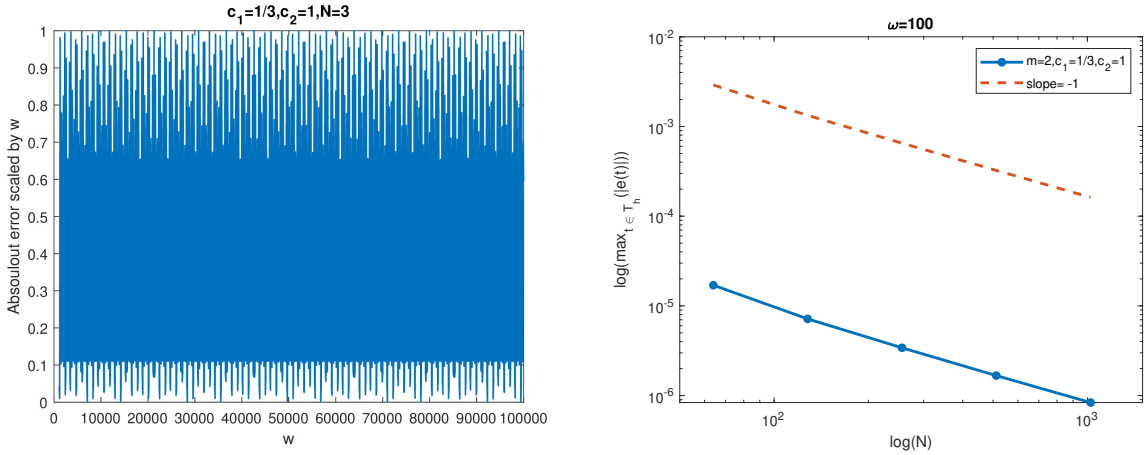

Figure 8.4: The asymptotic order and the classical order with $c_1 = \frac{1}{3}, c_2 = 1$ for Example 16

Table 8.4: Comparison of absolute errors with $\omega = 20$ for Example 16.

		N				
Parameters	*Methods*	64	128	256	512	1024
$c_1 = \frac{1}{3}$, $c_2 = 1$	CC	$2.73e-03$	$1.36e-03$	$6.82e-04$	$3.40e-04$	$1.70e-04$
	CF	$1.53e-04$	$7.62e-05$	$3.81e-04$	$1.90e-05$	$9.52e-06$
$c_1 = 0$, $c_2 = 1$	CC	$8.11e-03$	$4.07e-03$	$2.04e-03$	$1.02e-03$	$5.11e-04$
	CF	$4.54e-04$	$2.28e-04$	$1.14e-04$	$5.71e-05$	$2.85e-05$

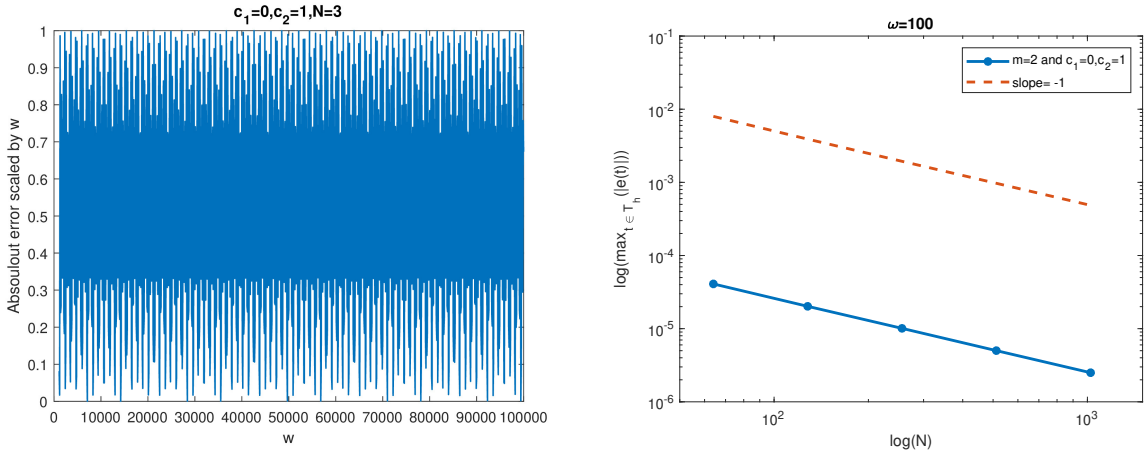

Figure 8.5: The asymptotic order and the classical order with $c_1 = 0, c_2 = 1$ for Example 16

Table 8.5: The absolute errors with $c_1 = \frac{1}{3}$, $c_2 = 1$ for Example 16.

	N				
ω	64	128	256	512	1024
50	$1.36e-05$	$4.49e-06$	$3.21e-06$	$1.60e-06$	$7.99e-07$
100	$1.70e-05$	$7.16e-06$	$3.41e-06$	$1.67e-06$	$8.36e-07$
200	$1.58e-06$	$8.40e-06$	$3.51e-06$	$1.66e-06$	$8.21e-07$
400	$2.06e-03$	$1.21e-05$	$3.66e-06$	$1.52e-06$	$7.22e-07$

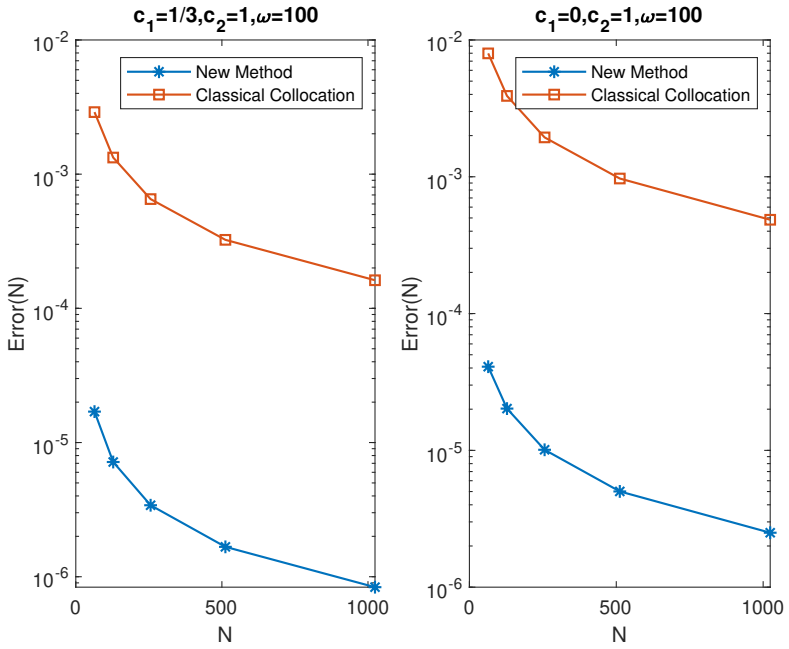

Figure 8.6: Comparison of absolute errors with $\omega = 100$ for Example 16

Table 8.6: The absolute errors with $c_1 = 0$, $c_2 = 1$ for Example 16.

	N				
ω	64	128	256	512	1024
50	$3.81e-05$	$1.90e-05$	$9.56e-06$	$4.79e-06$	$2.41e-06$
100	$4.09e-05$	$2.02e-05$	$1.01e-05$	$5.01e-06$	$2.50e-06$
200	$3.19e-05$	$2.02e-05$	$9.87e-06$	$4.91e-06$	$2.45e-06$
400	$2.06e-03$	$2.08e-05$	$8.81e-06$	$4.29e-06$	$2.14e-06$

8.4 Conclusion

This chapter presented efficient collocation methods using the Filon-type method for NVIEs with an oscillatory kernel. Based on the solution's asymptotic analysis, the method's convergence has been achieved by applying the inequalities shown here. The theorem demonstrates that the approach has a classical order and, for high-frequency values, an asymptotic order. In addition, by increasing the number of collocation parameters, the classical order could be raised, and in some cases, the asymptotic order 2 can be reached. The theoretical analysis and numerical tests confirmed that these methods are efficient and become more accurate as the frequency increases.

Part III

Numerical solution of fractional integral/differential equations

Chapter 9

A Galerkin approach for fractional delay differential equations using Hybrid Chelyshcov basis functions

Fractional derivatives and integrals have been practical tools for characterizing memory and hereditary properties in various materials and processes. For instance, fractional differential equations are employed to explain a range of natural phenomena in physics, chemistry, fluid mechanics, and mathematics [243].

Unlike ODEs, Delay Differential Equations (DDEs) incorporate addition derivatives from earlier-time, making the mathematical model closer to real-world occurrence. Biology, economics, medicine, chemistry, control, and electrodynamics are only a few of the topics where delay differential equations have been widely used for analysis, and prediction [221, 4]. As a generalization, Fractional Delay Differential Equations (FDDEs) deal with differential equations governed by fractional differential operators. In the last two decades, numerical approaches based on orthogonal polynomials have been commonly used to approximate the solution of fractional differential and integral equations. The primary characteristic of these methods is that they convert fractional problems to a system of algebraic equations that can be solved more conveniently using the orthogonal properties of polynomials and typical spectral methods.

Several numerical methods have been applied to solve DDEs. For instance, Chebyshev polynomials [272], Bernoulli polynomials [295], variational iteration method [324], one-leg θ-method [310], Adomian decomposition method [110], hybrid of block-pulse functions and Taylor series [204], Legendre wavelet [257], etc. However, not many studies focus on finding numerical solutions to FDDEs. Some of these works are Hermite wavelet method [258], spectral-collocation method [322], Legendre pseudospectral method [172], Adams-Bashforth-Moulton method, and the linear interpolation method [311], finite difference method [209] and Bernoulli wavelets method [246].

This chapter developed a novel idea for an efficient numerical method to approximate the solution to the FDDEs presented below, using a combination of block-pulse functions and Chelyshkov polynomials. Consider

$$\begin{cases} D^{\alpha}q(t) = p(t, q(t), q(t-\tau)), \quad 0 \leqslant t \leqslant 1, r-1 < \alpha \leqslant r, 0 < \tau < 1, \\ q^{(i)}(0) = \lambda_i, \qquad\qquad i = 0, 1, ..., r-1, \\ q(t) = \xi(t), \qquad\qquad\qquad t < 0. \end{cases} \tag{9.0.1}$$

$$\begin{cases} D^{\alpha}q(t) = p(t, q(t), q(t\tau)), \ 0 \leqslant t \leqslant 1, r-1 < \alpha \leqslant r, 0 < \tau < 1, \\ q^{(i)}(0) = \mu_i, \qquad\qquad i = 0, 1, ..., r-1, \end{cases} \tag{9.0.2}$$

where p is an analytical function, τ is delay, λ_i, μ_i, $i = 0, 1, ..., r-1$, are real constants, $\xi(t)$ is an arbitrary known function, q is the solution to be determined, and $D^{\alpha}, (r-1 < \alpha \leqslant r)$ is the fractional derivative in the Caputo sense [246, 261]. The goal of this work is to get a direct numerical method that is based on hybrid Chelyshkov orthogonal polynomials for solving a system of FDDEs (9.0.1) and (9.0.2).

Initially, to solve FDDEs, we shall discuss hybrid Chelyshkov polynomials and the properties of these polynomials. After that, the Galerkin method was applied to solve FDDEs utilizing the fractional integration operational matrix of the hybrid Chelyshkov polynomials. The most notable benefit of using hybrid Chelyshkov orthogonal polynomials and the Galerkin technique for the problem of solving FDDEs is the ability to convert the problem to a set of algebraic equations with unknown coefficients. Numerical examples demonstrate that the provided numerical method is accurate and efficient.

The components of this chapter are organized as follows: In Section 9.1, an overview of the hybrid Chelyshkov polynomial is presented. Three subsections make up Section 9.5. First, we are given an overview of the definition of Chelyshkov polynomials. The second is linked to the hybrid Chelyshkov functions (HCFs) and the transformation and fractional operational matrices for HCFs. A numerical method for solving FDDEs will be presented in Section 9.3, and it will be based on HCFs and the operational matrices of the problem. In Section 9.4, the proposed approach based on HCFs is applied to the resolution of specific numerical cases. We will provide some concluding remarks in Section 9.5.

9.1 Hybrid of the Chelyshkov polynomials and block-pulse Functions

This section will focus on the fundamental definition of HCFs and some of the aspects associated with them. These polynomials are part of a family of orthogonal polynomials and were introduced by Vladimir. S. Chelyshkov [69]. The Chelyshkov orthogonal polynomials are very significant in the performance of HCFs. The previous chapter

discussed the general features of these polynomials, including the fundamental definition, formulation, and explicit formulas for operational matrices. After introducing the Chelyshkov orthogonal polynomials, HCFs will be built by mixing these orthogonal polynomials with block-pulse functions [206]. The procedure for using Chelyshkov orthogonal polynomials is described in detail in Section 7.1 and Section 7.2 of Chapter 7.

Chelyshkov polynomials are defined explicitly by

$$\rho_{M,k}(t) = \sum_{j=k}^{M} \mathbf{z}_{k,j}^{M} t^j, \quad k = 0, 1, ...M, \qquad \mathbf{z}_{k,j}^{M} = (-1)^{j-k} \left(\begin{array}{c} M-k \\ j-n \end{array} \right) \left(\begin{array}{c} M+j+1 \\ M-k \end{array} \right) \tag{9.1.3}$$

The hybrid of Chelyshkov polynomials and block pulse functions, $\phi_{nm}(t)$, $n = 1, 2, ..., N$, $m = 0, 1, 2, ..., M$ are defined on the interval $[0, 1]$ as

$$\phi_{nm}(t) = \begin{cases} \sqrt{N}\rho_{N,m}(Nt - n + 1) & t \in [\frac{n-1}{N}, \frac{n}{N}] \\ 0 & otherwise, \end{cases} \tag{9.1.4}$$

where $\rho_{N,m}$ denotes the Chelyshkov polynomials of degree m defined in (9.1.3).

Function approximation:

The set of $\{\phi_{nm}(t), n = 1, 2, ..., N, m = 0, 1, 2, ..., M\}$ constitutes an orthogonal basis over $[0, 1)$ and every square inegrable function $p(t)$ in interval $[0, 1)$ may be enlarged as

$$p(t) \simeq \sum_{n=1}^{N} \sum_{m=0}^{M} c_{nm}\phi_{nm}(t) = C^T \Phi(t) \tag{9.1.5}$$

where

$$\Phi(t) = \left[\phi_{10}(t), \phi_{20}(t), ..., \phi_{N0}(t), \phi_{11}(t), \phi_{21}(t), ..., \phi_{N1}(t), ..., \phi_{1M}(t), \phi_{2M}(t), ..., \phi_{NM}(t)\right]^T, \tag{9.1.6}$$

$$C = \left[c_{10}, c_{20}, ..., c_{N0}, c_{11}, c_{21}, ..., c_{N1}, ..., c_{1M}, c_{2M}, ..., c_{NM}\right]^T. \tag{9.1.7}$$

The vectors $\Phi(t)$ and C in series (9.1.5) can be rewritten as

$$p(t) \simeq \sum_{i=1}^{\hat{m}} c_i \phi_{nm}(t) = C^T \Phi(t),$$

where

$$\Phi(t) = \left[\phi_1(t), \phi_2(t), ..., \phi_{\hat{m}}(t)\right], \tag{9.1.8}$$

and

$$C = \left[c_1, c_2, ..., c_{\hat{m}}\right].$$

Also $c_i = c_{nm}$, $\phi_i(t) = \phi_{nm}(t)$, $i = (n-1)(M+1) + m + 1$, $\hat{m} = (M+1)N$.

9.2 Operational matrices

The solution of variable-order fractional differential or integral equations is accomplished using an operational matrix technique. The primary idea behind this part is to generate the operational integration matrix using hybrid Chelyshkov functions.

Theorem 28. *[71, 213, 113] Given that $\Psi(t)$ represents the Chelshkov polynomial vectors, the Riemann-Liouville fractional integral of order α of the Chelyshkov polynomial vector can be expressed as:*

$$I^{\alpha}\Psi(t) = \Theta^{(\alpha)}\Psi(t), \tag{9.2.9}$$

where $\Theta^{(\alpha)}$ indicates the fractional integral matrix of order α and has the dimensions $(M+1)\times(M+1)$. The (i,j)-th element of this matrix is generated by the following operations:

$$\Theta_{i,j}^{(\alpha)} = \sum_{r=i-1}^{M}\sum_{s=j}^{M}\frac{\mathbf{z}_{j,s}\mathbf{z}_{i-1,r}\Gamma(r+1)(2j+1)}{\Gamma(r+\alpha+1)(r+\alpha+s+1)}, \qquad i=1,2,...,M+1,\ j=0,...,M.$$

Proof. The i-th element of the vector $\Psi(t)$ is $\rho_{i-1}(t)$. So, by applying the fractional integration I^{α} in its analytical form we have

$$I^{\alpha}\rho_{i-1}(t) = I^{\alpha}\left(\sum_{r=i-1}^{M}\mathbf{z}_{i-1,r}t^{j}\right) = \sum_{r=i-1}^{M}\frac{\mathbf{z}_{i-1,r}\Gamma\left(r+1\right)}{\Gamma\left(r+\alpha+1\right)}t^{r+\alpha}, \tag{9.2.10}$$

by expanding the term $t^{j+\alpha}$ by the Chelyshkov polynomials we get

$$t^{r+\alpha} \simeq \sum_{j=0}^{M}\beta_{r,j}\rho_{j}(t), \tag{9.2.11}$$

in which $\beta_{j,r}$ can be obtained as

$$\beta_{r,j} = (2j+1)\int_{0}^{1}\rho_{j}(t)t^{r+\alpha}dt$$

$$= (2j+1)\sum_{s=j}^{M}\mathbf{z}_{j,s}\int_{0}^{1}t^{s+r+\alpha}dt = (2j+1)\sum_{s=j}^{M}\frac{\mathbf{z}_{j,s}}{s+r+\alpha+1}. \tag{9.2.12}$$

Now, by inserting Eqs. (9.2.11) and (9.2.12) in Eq. (9.2.10) we get

$$I^{\alpha}\rho_{i-1}(t) = \sum_{j=0}^{M}\left(\sum_{r=i-1}^{M}\sum_{s=j}^{M}\frac{\mathbf{z}_{j,s}\mathbf{z}_{i-1,r}\Gamma(r+1)(2j+1)}{\Gamma(r+\alpha+1)(r+\alpha+s+1)}\right)\rho_{j}(t),$$

which leads to the desired results. □

Lemma 9.2.1. *[71, 213, 113] The $\hat{m}$ HCFs vector $\Phi(t)$ can be convert into the $(M+1)$ Chelyshkov polynomials vector $\Psi(t)$ by expanding as follows:*

$$\Phi(t) = \Lambda\Psi(t), \tag{9.2.13}$$

where Λ is a $\hat{m} \times (M+1)$ matrix,

$$\Lambda_{ij} = (2j+1)\sum_{r=j}^{M}\sum_{s=m}^{M}\sum_{k=0}^{r}\frac{\left(\begin{array}{c} r \\ k \end{array}\right)(n-1)^{r-k}\,N^{-\frac{1}{2}-r}\mathbf{z}_{r,j}\mathbf{z}_{s,m}}{r+s+1},$$

and $i = 1, ..., \hat{m},\ j = 0, ..., M$.

Proof. According to (9.1.8), the i-th element of HCFs vector $\Phi(t)$ is $\phi_i(t)$ which can be defined by Chelyshkov polynomials as

$$\phi_i(t) = \sum_{j=0}^{M}\Lambda_{ij}\rho_j(t).$$

The coefficient Λ_{ij} can be obtained from

$$\Lambda_{ij} = (2j+1)\int_0^1 \phi_i(t)\rho_j(t)dt.$$

By substituting the analytical form of $\rho_j(t)$ from Eq. (9.1.3), the coefficient Λ_{ij} can be derived as

$$\Lambda_{ij} = (2j+1)\sum_{r=j}^{M}\mathbf{z}_{r,j}\int_0^1\phi_i(t)t^r dt = (2j+1)\sum_{r=j}^{M}\sqrt{N}\mathbf{z}_{r,j}\int_{\frac{n-1}{N}}^{\frac{n}{N}} t^r\rho_m\left(Nt-n+1\right)dt,$$

where $i = (n-1)(M+1)+m+1$. Now, by changing the variable $z = Nt-n+1$ we have

$$\Lambda_{ij} = (2j+1)\sum_{r=j}^{M}N^{-\frac{1}{2}-r}\mathbf{z}_{r,j}\int_0^1\left(z+n-1\right)^r\rho_m\left(z\right)dz$$

$$= (2j+1)\sum_{r=j}^{M}\sum_{s=m}^{M}N^{-\frac{1}{2}-r}\mathbf{z}_{r,j}\mathbf{z}_{s,m}\int_0^1\left(z+n-1\right)^r z^s dz$$

$$= (2j+1)\sum_{r=j}^{M}\sum_{s=m}^{M}\sum_{k=0}^{r}\frac{\mathbf{z}_{r,j}\mathbf{z}_{s,m}N^{-\frac{1}{2}-r}\left(\begin{array}{c} r \\ k \end{array}\right)(n-1)^{r-k}}{r+s+1}.$$

This completes the proof. □

Theorem 29. *[71, 213, 113] Consider the $(M+1)$ Chelyshkov polynomials vector to be denoted by $\Psi(t)$. Then, the HCFs representation of $\Psi(x)$ can be developed as follows:*

$$\Psi(t) = \Pi\Phi(t), \tag{9.2.14}$$

where Π is $(M+1)\times\hat{m}$ matrix and

$$\Pi_{i,j} = \sum_{r=i-1}^{M}\sum_{s=m}^{M}\sum_{k=0}^{r}\frac{\mathbf{z}_{r,i-1}\mathbf{z}_{s,m}N^{-\frac{1}{2}-r}\begin{pmatrix} r \\ k \end{pmatrix}(n-1)^{r-k}}{k+s+1}.$$

Proof. The proof is similar to Lemma 9.2.13. □

Theorem 30. *[71, 213, 113] Using $\Phi(t)$ as the HCFs vector, the fractional integration of order α for this vector can be written as:*

$$I^{\alpha}\Phi(t) = \mathcal{P}^{(\alpha)}\Phi(t), \tag{9.2.15}$$

where $\mathcal{P}^{(\alpha)} = \Lambda\Theta^{(\alpha)}\Pi$ is a $\hat{m}\times\hat{m}$ matrix, and Λ and Π are transformation matrices derived in equations (9.2.13) and (9.2.14), respectively. In addition, Θ^{α} is the operational matrix of fractional integration for HCFs vector $\Phi(t)$.

Proof. Consider the HCFs vector $\Phi(t)$. By using the transformation matrix Λ, it can be written as

$$\Psi(t) = \Lambda\Phi(t),$$

applying the fractional integration operator I^{α} and using (9.2.9), we get

$$I^{\alpha}\Phi(t) = \Lambda I^{\alpha}\Psi(t) = \Lambda\Theta^{\alpha}\Psi(t),$$

now the transformation matrix Λ results

$$I^{\alpha}\Phi(t) = \Lambda J^{\alpha}\Psi(t) = \Lambda\Theta^{\alpha}\Pi\Phi(t),$$

which yields (9.2.15) and completes the proof. □

9.3 Problem statement and approximation scheme

In this section, we solve FDDEs (9.0.1) and (9.0.2) by employing the Galerkin method and the fractional integration operational matrices of the HCFs.

Problem(1)

Consider the FDDEs (9.0.1). To solve this problem, we approximate $D^{\alpha}q(t)$ via HCFs basis $\phi_i(t), i = 0, 1, 2, ..., \hat{m}$, as

$$D^{\alpha}q(t) = C^{T}\Phi(t), \tag{9.3.16}$$

where C is an unknown vector that can be acquired. By utilizing (9.2.9), we obtain:

$$q(t) \simeq I^{\alpha}\left(C^{T}\Phi(t)\right) + \sum_{i=0}^{r-1}\frac{\lambda_i}{i!}t^{i} = C^{T}\mathcal{P}^{(\alpha)}\Phi(t) + d^{T}\Phi(t). \tag{9.3.17}$$

In other words, for the problem (9.0.1), we get:

$$q\left(t-\tau\right) = \begin{cases} \xi\left(t-\tau\right), & 0 \leqslant t \leqslant \tau \\ C^{T}\mathcal{P}^{(\alpha)}\Phi\left(t-\tau\right) + d^{T}\Phi\left(t-\tau\right), & \tau \leqslant t \leqslant 1 \end{cases} = C_{\tau}^{T}\Phi\left(t\right).$$

to

(9.3.19)

We can obtain the following residual function by substituting Eqs. (9.3.16)-(9.3.18) for the original equations in problem (9.0.1).

$$R(t) = C^{T}\Phi(t) - p\left(t, C^{T}\mathcal{P}^{(\alpha)}\Phi(t) + d^{T}\Phi(t), C_{\tau}^{T}\Phi\left(t\right)\right). \tag{9.3.20}$$

To obtain the answer $q(t)$, we must first identify the residual $R(t)$ at the $\hat{m}+1$ points. As demonstrated below, we use the roots of shifted Chebyshev polynomials to determine appropriate collocates.

$$R(t_j) = 0, j = 1, 2, ...\hat{m}+1. \tag{9.3.21}$$

It is possible to find the solution to this problem using the vector C coefficients that are unknown. Consequently, we can obtain the numerical solution by substituting the resulting vector C into the Eq. (9.3.17).

Problem(2)

We use a method that was employed for the previous problem (9.0.1) to solve the FDDEs (9.0.2). Replacing Eqs. (9.3.16) and (9.3.17) in (9.0.2), we have the following residual function:

$$R(t) = C^{T}\Phi(t) - p\left(t, C^{T}\mathcal{P}^{(\alpha)}\Phi(t) + d^{T}\Phi(t), C^{T}\mathcal{P}^{(\alpha)}\Phi(\tau t) + d^{T}\Phi(\tau t)\right). \tag{9.3.22}$$

As shown follows, we then compute the residual value $R(t)$ at the $\hat{m}+1$ roots of the shifted Chebyshev polynomials.

$$R(t_j) = 0, \quad j = 1, 2, ...\hat{m}+1. \tag{9.3.23}$$

These equations are then solved for unknown coefficients of the vector C. As a result, by solving these systems by determining C, we obtain the numerical solution to this problem (9.0.2).

9.4 Numerical experiments

This section will examine three different example scenarios to highlight the usefulness and advantages of the proposed technique.

Example 17. *Consider the FDDEs*

$$\begin{cases} D^{\alpha}q(t) = q(t-\tau) - q(t) + \frac{2t^{2-\alpha}}{\Gamma(3-\alpha)} - \frac{t^{1-\alpha}}{\Gamma(2-\alpha)} + 2t\tau - \tau^2 - \tau, \ 0 \leqslant t \leqslant 1, \ 0 < \alpha \leqslant 1, \\ q(t) = 0, \qquad\qquad\qquad\qquad\qquad\qquad\qquad\qquad\qquad\qquad\qquad\qquad t \leqslant 0. \end{cases}$$

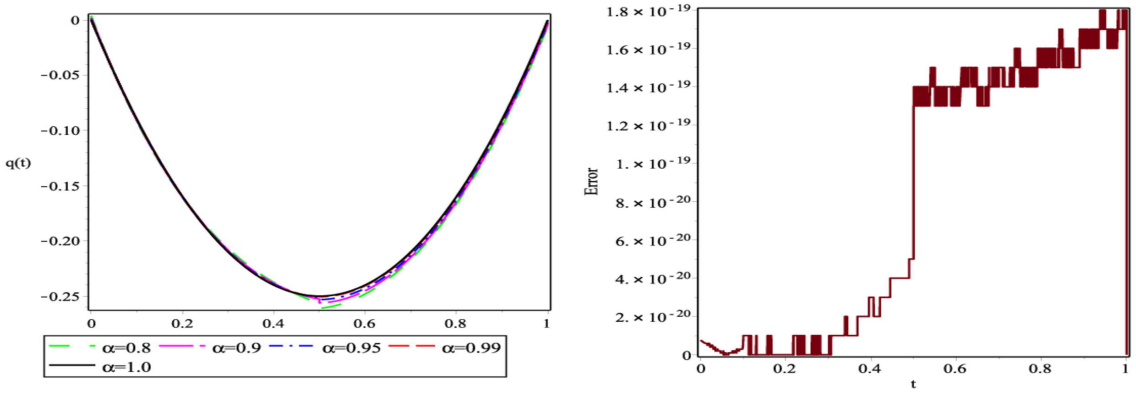

Figure 9.1: The approximate solution for various values of α (Left) and absolute error for $\alpha = 1$ (Right), Example 17.

In the case where $\alpha = 1$, the exact solution to this system is $q(t) = t^2 - t$. The approximate solutions for several different values of α and the absolute error for $\alpha = 1$ are displayed in Fig. 9.1 for the case in which $M = 2$, $N = 2$, and $\tau = 0.01$ are the input values. When utilizing the current approach with $\hat{m} = 6$, the RMSE for various values

of t is displayed in the table referenced by Table 9.1. As anticipated, the outcomes of this example get closer and closer to the exact solution as the fractional order α approaches 1.

Table 9.1: The RMSE ($\|q - \tilde{q}\|_2$) for different values of t in Example 17.

Methods	$t = 0.2$	$t = 0.4$	$t = 0.6$	$t = 0.8$
[9]	7.58×10^{-14}	3.90×10^{-14}	1.45×10^{-14}	7.96×10^{-14}
[19]	3.46×10^{-16}	2.35×10^{-16}	3.46×10^{-16}	9.69×10^{-17}
[246]	0	1.11×10^{-16}	3.15×10^{-14}	3.23×10^{-14}
[283]	1.19×10^{-14}	1.63×10^{-15}	7.29×10^{-15}	4.64×10^{-15}
HCFs	0	2.00×10^{-16}	1.00×10^{-16}	0

Example 18. *Consider the following FDDEs*

$$\begin{cases} D^{\alpha}q(t) = -q(t-0.3) - q(t) + e^{-t+0.3}, \quad 0 \leqslant t \leqslant 1, \quad 2 < \alpha \leqslant 3 \\ q(0) = 1, \quad q'(0) = -1, \quad q''(0) = 1, \\ q(t) = e^{-t}, t < 0. \end{cases}$$

$q(t) = e^{-t}$ *that provides an exact solution for the present test problem for* $\alpha = 3$. *The approximate solutions for several different values of* α *and the absolute error for* $\alpha = 3$ *are displayed in Fig. 9.2, when* $M = 8, N = 2$, *and* $\tau = 0.3$ *are the input variables. The approximate solutions obtained by applying the current approach with* $\hat{m} = 14$ *are displayed in Table 9.2. As the fractional-order* α *approaches* 3, *these results demonstrate that the approximate solutions converge to the precise solution.*

Table 9.2: The approximate solutions for different values of t in Example 18.

Methods	$t = 0.2$	$t = 0.4$	$t = 0.6$	$t = 0.8$
[170]	0.8187	0.6703	0.5488	0.4493
[290]	0.8187	0.6703	0.5488	0.4494
[246]	0.8187	0.6703	0.5488	0.4494
HCFs	0.8187	0.6703	0.5488	0.4494

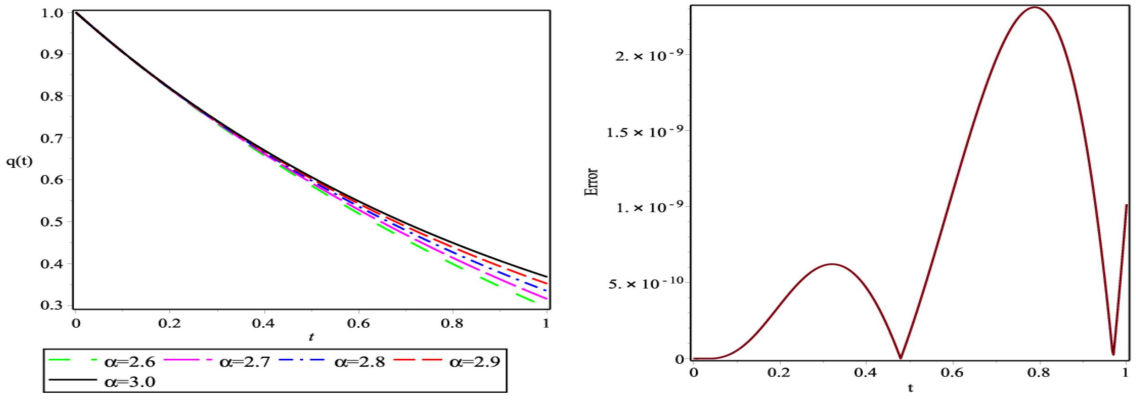

Figure 9.2: The approximate solution for various values of α (Left) and absolute error for $\alpha = 3$ (Right), Example 18.

Example 19. *Consider the following FDDEs*

$$\begin{cases} D^{\alpha}q(t) = 1 - 2\,q^2(\frac{1}{2}t), \quad 0 \leqslant t \leqslant 1, \quad 1 < \alpha \leqslant 2, \\ q(0) = 1, \quad q'(0) = 0. \end{cases}$$

In this example, the exact solution is $q(t) = \cos(t)$ *when* $\alpha = 2$. *The approximate solutions for several different values of* α *and the absolute error for* $\alpha = 2$ *are displayed in Fig. 9.3 for the case when* $M = 6$ *and* $N = 2$. *The RMSE is shown for different values of* t *in Table 9.3, which uses the current approach and has* $\hat{m} = 14$. *Based on the information obtained, we can conclude: that the approximate solution will eventually converge to the exact solution as the fractional order* α *goes closer and closer to* 2.

Table 9.3: The RMSE ($\|q - \tilde{q}\|_2$) for different values of t and N in Example 19.

Methods	$t = 0.2$	$t = 0.4$	$t = 0.6$	$t = 0.8$
[246]	3.21×10^{-11}	3.81×10^{-11}	1.31×10^{-06}	1.82×10^{-06}
HCFs	3.20×10^{-11}	3.81×10^{-11}	8.90×10^{-11}	6.21×10^{-11}

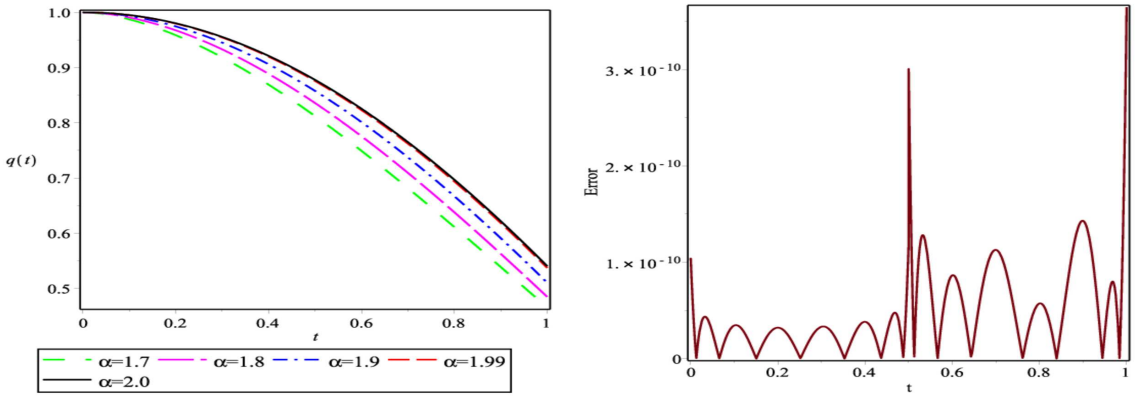

Figure 9.3: The approximate solution for various values of α (Left) and absolute error for $\alpha = 2$ (Right), Example 19.

9.5 Conclusion

This chapter presented a new and effective method for performing the numerical technique on hybrid Chelyshkov orthogonal polynomials. In the HCFs strategy, the operational matrix of fractional integration for HCFs is the first and most significant aspect of solving the system of FDDEs that we experience, as we have seen in Section , these matrices were derived. To solve FDDEs, these matrices, in addition to the Galerkin method, are utilized. As in the final step of the procedure, the robustness and efficiency of the suggested method are evaluated using numerical examples of FFDEs.

Chapter 10

Discrete Chebyshev polynomials for solving fractional variational problems

In the last two decades, numerical approaches based on orthogonal polynomials have been frequently used to approximate the solution of fractional differential, and integral equations [111, 175, 211, 210, 259]. The essential characteristic of these approaches is that, by using the orthogonal properties of the polynomials and the typical spectral methods, they reduce such fractional equations to a system of algebraic equations which can be solved easier. According to the defined inner product in the solution space, orthogonal polynomials are usually classified into two main classes: continuous and discrete. For continuous orthogonal polynomials such as Legendre, Chebyshev, Hermite, and Laguerre, one has to evaluate an integral in the inner product. In contrast, discrete orthogonal polynomials come with a discrete scalar product; hence, the integral becomes a sum [326, 327]. Although continuous orthogonal polynomials have been more frequently used to approximate the solution of functional equations, there are some advantages of using discrete orthogonal polynomials. For example, using discrete orthogonal polynomials, the Fourier coefficients can be calculated with a summation, and the obtained coefficients are exact. Consequently, compared to continuous cases, the implementation of discrete orthogonal polynomials is more efficient and less complex [125, 321]. Moreover, there is a close connection between stochastic processes and discrete orthogonal polynomials which motivated many researchers to consider them to solve stochastic differential equations [16, 321].

In the field of optimization theory, the calculus of variations is concerned with the problem of optimizing a real-valued functional over a set of functions [7, 195, 41, 328]. The functional is usually defined as definite integrals involving functions and their derivatives. Developing the calculus of variations started with Johann Bernoulli and his well-known "brachistochrone" problem. After that, this subject was developed by the works of Jakob Bernoulli, Newton, Leibniz, Euler, Lagrange, Legendre, Jacobi, Weierstrass, and Hilbert [41]. Recently, the calculus of variations has been found in many applications in areas such as quantum mechanics, medicine, economics, aerodynamics, environmental engineering, and biology [7, 22, 112, 201, 252, 253]. As a generalization

of the calculus of variations, the Fractional Calculus of Variations (FCV) deals with variational functionals depending on fractional derivatives instead of integer ones [7]. The subject of FCV was introduced in 1996 with the work of Riewe [252]. He used fractional derivatives to formulate the problem of the calculus of variations and obtained the respective Euler-Lagrange equations. Nowadays, FCV is under development due to its many applications in physics, and engineering [7, 22, 112, 201, 253]. The main purpose of this chapter is to present a comparative study of numerical solution of the following fractional variational problems:

$$Min.\ \mathcal{J}(x) = \int_a^b \mathcal{F}\left(t, x(t), {}_0^C D_t^\alpha x(t), u(t)\right) dt, \tag{10.0.1}$$

in which the variable $u(t)$ is described by

$$u(t) = \int_a^t \mathcal{K}\left(s, x(s), {}_0^C D_t^\alpha x(s)\right) ds, \quad a \leqslant t \leqslant b, \tag{10.0.2}$$

subject to the following boundary conditions

$$x(a) = \alpha, \quad x(b) = \beta. \tag{10.0.3}$$

The functions $\mathcal{F}$ and $\mathcal{K}$ are continuously differentiable, x is absolutely continuous functions, such that its fractional derivative of order α, i.e. ${}_0^C D_t^\alpha x(t)$, exists and is continuous on $[a, b]$. First, the general formulation of DCPs and their properties are investigated briefly. Then, DCPs and their operational matrix of fractional integration are used to approximate the solution of FVP (10.0.1)-(10.0.3). The numerical results and the required CPU time were compared to the previously acquired results by the classical Chebyshev polynomials in Ref. [112]. The comparison reveals that the presented DCPs method is more efficient and less complex than the Chebyshev polynomials method.

This chapter contains five sections. Section 10.1 defines discrete Chebyshev polynomials and their properties. Section 10.2 presents the operational matrices based on the discrete Chebyshev polynomials. Section 10.3 deals with the numerical solution of FVPs. Section 10.4gives some illustrative examples to verify the superiority of the discrete Chebyshev polynomials. Finally, some concluding remarks are given in Section 10.5.

10.1 Discrete Chebyshev polynomials

The discrete Chebyshev polynomials belong to a rich family of orthogonal polynomials which introduced by Chebyshev. In this section, we restrict our attention to the basic definition, formula and properties of these polynomials. For more details and some applications of these polynomials one can refer to Refs. [126, 218].

Definition 10.1.1. *Let N be a positive integer number. The discrete Chebyshev polynomials $\mathcal{T}_{n,N}(x)$ may be defined as follow:*

$$\mathcal{T}_{n,N}(x) = \sum_{k=0}^{n} (-1)^k \binom{n+k}{n} \binom{N-k}{n-k} \binom{x}{k}, \quad n = 0, 1, ..., N. \tag{10.1.4}$$

Orthogonality:

The set of discrete Chebyshev polynomials $\{\mathcal{T}_{n,N}, n = 0, 1, ..., N\}$ is orthogonal on the interval $[0, N]$ with respect to the following discret norm:

$$\langle f, g \rangle = \sum_{r=0}^{N} f(r)g(r). \tag{10.1.5}$$

Moreover, the orthogonality condition for these polynomials is as follow:

$$\langle \mathcal{T}_{m,N}, \mathcal{T}_{n,N} \rangle = \sum_{r=0}^{N} \mathcal{T}_{m,N}(r)\mathcal{T}_{n,N}(r) = \mu_n \delta_{mn},$$

where δ_{mn} is the Kronecker delta and μ_n can be defined as:

$$\mu_n = \frac{(N+n+1)!}{(2n+1)(N-n)!(n!)^2}. \tag{10.1.6}$$

Recurrence relation:

The set of discrete Chebyshev polynomials $\{\mathcal{T}_{n,N},\ n = 0, 1, ..., N\}$ can be determined with the aid of the following recurrence formulae for $n = 0, 1, ..., N$:

$$\alpha_n \mathcal{T}_{n+1,N}(x) = \frac{(N-k)\,(\alpha_n + \beta_n - x)}{k+1} \mathcal{T}_{n,N}(x) - \frac{(N-k+1)(N-k)\beta_n}{k(k+1)} \mathcal{T}_{n-1,N}(x).$$

where $\mathcal{T}_{0,N}(x) = 1,\ \mathcal{T}_{1,N}(x) = N - 2x$ and

$$\alpha_n = \frac{(N-n)(n+1)^2}{(2n+1)(2n+2)}, \qquad \beta_n = \frac{N^2(N+n+1)}{2n(2n+1)}.$$

Explicit formula:

By using the relation (10.1.4), the discrete Chebyshev polynomial $\mathcal{T}_{n,N}$ can be written as follow:

$$\mathcal{T}_{n,N}(x) = \sum_{k=0}^{n} \frac{(-1)^k \binom{n+k}{n} \binom{N-k}{n-k}}{k!} x(x-1)...(x-k+1)$$

$$= \sum_{k=0}^{n} \frac{(-1)^k \binom{n+k}{n} \binom{N-k}{n-k}}{k!} \sum_{i=0}^{k} s(k,i) x^i, \quad n = 0, 1, ...N, \tag{10.1.7}$$

in which $s(k,i)$ are the Stirling numbers of the first kind [291, 251]. Therefore, the analytical form of $\mathcal{T}_{n,N}(x)$ can be derived as follow:

$$\mathcal{T}_{n,N}(x) = \sum_{k=0}^{n} a_{j,n} x^k, \quad n = 0, 1, ...N, \tag{10.1.8}$$

where

$$a_{j,n} = \sum_{r=j}^{n} \frac{(-1)^r \binom{n+r}{n} \binom{N-r}{n-r} s(r,i)}{r!}. \tag{10.1.9}$$

Shifted discrete Chebyshev polynomials:

In order to use the discrete Chebyshev polynomials on the interval $[0,1]$, we define the shifted discrete Chebyshev polynomials (SDCPs) by introducing a change of variable $x = Nt$. Let nth shifted discrete Chebyshev polynomial, i.e. $\mathcal{T}_{n,N}(Nt)$, is denoted by $\mathfrak{T}_{n,N}(t)$. Then, the set of SDCPs $\{\mathfrak{T}_{n,N}, n = 0, 1, ..., N\}$ are orthogonal on the interval $[0,1]$ with respect to the following discrete norm:

$$\langle f, g \rangle_* = \sum_{r=0}^{N} f\left(\frac{r}{N}\right) g\left(\frac{r}{N}\right). \tag{10.1.10}$$

Also, the orthogonality condition for SDCPs can be defined as follow:

$$\langle \mathfrak{T}_{m,N}(t), \mathfrak{T}_{n,N}(t) \rangle_* = \sum_{r=0}^{N} \mathfrak{T}_{m,N}\left(\frac{r}{N}\right) \mathfrak{T}_{n,N}\left(\frac{r}{N}\right) = \mu_n \delta_{mn}, \tag{10.1.11}$$

where μ_n is defined in relation (10.1.6).

Function approximation:

Any function $f(t)$, defined over the interval $[0,1]$ may be expanded by the SDCPs as

$$f(t) \simeq \sum_{i=0}^{N} c_i \mathfrak{T}_{i,N}(t) = C^T \Psi(t), \tag{10.1.12}$$

where C and $\Phi(x)$ are $(N+1)$ vectores given by

$$C^T = [c_0, c_1, ..., c_N]^T, \tag{10.1.13}$$

$$\Psi(t) = \left[\mathfrak{T}_{0,N}(t), \mathfrak{T}_{1,N}(t), ..., \mathfrak{T}_{N,N}(t)\right]^T, \tag{10.1.14}$$

and the coefficients c_i can be derived as follow

$$c_i = \frac{\langle f(t), \mathfrak{T}_{i,N}(t)\rangle_*}{\mu_i}, \quad i = 0, 1, ...N. \tag{10.1.15}$$

Convergence analysis:

The discrete Chebyshev polynomials $\mathcal{T}_{n,N}(x)$ are special case of the well-known Hahn polynomials $Q_n(x; \alpha, \beta, N)$ with $\alpha = \beta = 0$ [125]. The following Theorem provides conditions that ensure the series expansion of a function by the discrete Chebyshev polynomials converges.

Theorem 31. *The series expansion* $\sum_{k=0}^{n} \frac{\langle f, \mathcal{T}_{k,N}\rangle}{\langle \mathcal{T}_{k,N}, \mathcal{T}_{k,N}\rangle} \mathcal{T}_{k,N}(x)$ *of a function* f *by the discrete Chebyshev polynomials converges pointwise, if the series expansion of the function* f *by the Jacobi polynomials converges pointwise and if* $\frac{n^4}{N} \to 0$ *as* $n, N \to \infty$.

Proof. The proof follows directly from Theorems 1.1, 2.1, and 2.2 in Ref. [125]. □

10.2 Operational matrices

Now, some explicit formulations for operational matrix of fractional integration, in the Riemann-Liouville sense, for the SDCPs will be obtained. Moreover, the product operational matrix for the SDCPs vector is defined.

Lemma 10.2.1. *For a positive number* r *the inner product of the* $\mathfrak{T}_{n,N}(t)$ *and* t^r, *denoted by* $\beta(n, r)$, *can be derived as:*

$$\beta(n, r) = \frac{1}{N^r} \sum_{j=0}^{N} \sum_{k=0}^{n} a_{j,n} j^{k+r}. \tag{10.2.16}$$

where $a_{j,n}$ *is defined in relation (10.1.9).*

Proof. By using definition of the discrete inner product $\langle ., . \rangle_*$ in (10.1.11), we get:

$$\beta(n, r) = \langle t^r, \mathfrak{T}_{n,N}(t)\rangle_* = \sum_{j=0}^{N} \mathfrak{T}_{n,N}\left(\frac{j}{N}\right) \frac{j^r}{N^r} = \frac{1}{N^r} \sum_{j=0}^{N} \mathcal{T}_{n,N}(j) j^r.$$

Now, the analytical form of the discrete Chebyshev polynomial $\mathcal{T}_{n,N}$ in relation (10.1.8) results (10.2.16). □

Theorem 32. *Let $\Psi(t)$ be the SDCPs vector as defined in (10.1.14). Then its fractional integral of order α in the Riemann-Liouville sense is given by*

$$ {}_0I_t^{\alpha}\Psi(t) = \mathcal{P}^{(\alpha)}\Psi(t) \tag{10.2.17} $$

where $\mathcal{P}^{(\alpha)}$ is the operational matrix of fractional integration and its (i,j)th element can be derived as

$$ \mathcal{P}_{i,j}^{(\alpha)} = \sum_{k=0}^{i-1} \frac{\beta(k+\alpha,j)\Gamma(k+1)N^k a_{k,i-1}}{\mu_j \Gamma(\alpha+k+1)}, \quad i = 1,2,...,N+1, j = 0,..,N. \tag{10.2.18} $$

Proof. The ith element of the vector $\Psi(t)$ is $\mathfrak{T}_{i-1,N}(t)$. Therefore, its fractional integration of order α may be written as

$$ {}_0I_t^{\alpha}\mathfrak{T}_{i-1,N}(t) = {}_0I_t^{\alpha}\sum_{k=0}^{i-1} N^k a_{k,i-1}t^k = \sum_{k=0}^{i-1} N^k a_{k,i-1}\left({}_0I_t^{\alpha}t^k\right) = \sum_{k=0}^{i-1} \frac{\Gamma(k+1)N^k a_{k,i-1}}{\Gamma(\alpha+k+1)}t^{k+\alpha} \tag{10.2.19} $$

Now by expanding the term $t^{k+\alpha}$ we get

$$ t^{k+\alpha} \simeq \sum_{j=0}^{N} b_{k,j}\mathfrak{T}_{j,N}(t), \tag{10.2.20} $$

in which $b_{k,j}$ can be derived as

$$ b_{k,j} = \frac{\left\langle x^{k+\alpha}, \mathfrak{T}_{j,N}(t)\right\rangle_*}{\left\langle \mathfrak{T}_{j,N}(t), \mathfrak{T}_{j,N}(t)\right\rangle_*} = \frac{\beta(k+\alpha,j)}{\mu_j}. \tag{10.2.21} $$

By putting Eqs. (10.2.21) and (10.2.20) in (10.2.19), we have:

$$ {}_0I_t^{\alpha}\mathfrak{T}_{i-1,N}(t) = \sum_{j=0}^{N}\left(\sum_{k=0}^{i-1} \frac{\beta(k+\alpha,j)\Gamma(k+1)N^k a_{k,i-1}}{\mu_j\Gamma(\alpha+k+1)}\right)\mathfrak{T}_{j,N}(t). \tag{10.2.22} $$

Accordingly, the desired result is derived. □

Theorem 33. *Let $\Psi(t)$ be the SDCPs vector defined in (10.1.14) and V be an arbitrary $(N+1)$ vector. Then, we can write*

$$ \Psi(t)\Psi^T(t)V = \tilde{V}\Psi(t), \tag{10.2.23} $$

where $\tilde{V}$ is the $(N+1)\times(N+1)$ product operational matrix and its (i,j)-th element can be defined as

$$ \tilde{V}_{i+1,j+1} = \frac{1}{\mu_j}\sum_{k=0}^{N} V_k \left\langle \mathfrak{T}_{k,N}(t)\mathfrak{T}_{i,N}(t), \mathfrak{T}_{j,N}(t)\right\rangle_*, \quad i,j = 0,1,...,N. $$

Proof. The product of two SDCPs vectors $\Psi(t)$ and $\Psi^T(t)$ is a $(N+1)\times(N+1)$ matrix as follow

$$\Psi(t)\Psi^T(t) = \begin{bmatrix} \mathfrak{T}_{0,N}(t)\mathfrak{T}_{0,N}(t) & \mathfrak{T}_{0,N}(t)\mathfrak{T}_{1,N}(t) & \dots & \mathfrak{T}_{0,N}(t)\mathfrak{T}_{N,N}(t) \\ \mathfrak{T}_{1,N}(t)\mathfrak{T}_{0,N}(t) & \mathfrak{T}_{1,N}(t)\mathfrak{T}_{1,N}(t) & \dots & \mathfrak{T}_{1,N}(t)\mathfrak{T}_{N,N}(t) \\ \vdots & \vdots & \ddots & \vdots \\ \mathfrak{T}_{N,N}(t)\mathfrak{T}_{0,N}(t) & \mathfrak{T}_{N,N}(t)\mathfrak{T}_{1,N}(t) & \dots & \mathfrak{T}_{N,N}(t)\mathfrak{T}_{N,N}(t) \end{bmatrix}.$$

As a result, the relation (10.2.23) can be rewritten as:

$$\sum_{k=0}^{N} \mathfrak{T}_{k,N}(t)\mathfrak{T}_{i,N}(t)V_{k+1} = \sum_{k=0}^{N} \mathfrak{T}_{j,N}(t)\tilde{V}_{i+1,k+1}, \quad i = 0,1,...,N.$$

Now, by multiplying both sides of the above relation by $\mathfrak{T}_{j,N}(t)$ and using the defined inner product in (10.1.10), we get:

$$\sum_{k=0}^{N} \langle \mathfrak{T}_{k,N}(t)\mathfrak{T}_{i,N}(t), \mathfrak{T}_{i,N}(t)\rangle_* V_{k+1} = \langle \mathfrak{T}_{j,N}(t), \mathfrak{T}_{j,N}(t)\rangle_* \tilde{V}_{i+1,j+1}, \quad i,j = 0,1,...,N.$$

Therefore, the matrix $\tilde{V}$ may be given by

$$\tilde{V}_{i+1,j+1} = \frac{\sum_{k=0}^{N} V_k \langle \mathfrak{T}_{k,N}(t)\mathfrak{T}_{i,N}(t), \mathfrak{T}_{j,N}(t)\rangle_*}{\langle \mathfrak{T}_{j,N}(t), \mathfrak{T}_{j,N}(t)\rangle_*} = \frac{1}{\mu_j}\sum_{k=0}^{N} V_k \langle \mathfrak{T}_{k,N}(t)\mathfrak{T}_{i,N}(t), \mathfrak{T}_{j,N}(t)\rangle_*.$$

□

10.3 The numerical approach

In this section, we will apply the SDCPs and thier operational matrix to solve the FVP (10.0.1)-(10.0.2) with boundary conditions (10.0.3). First, we approximate ${}_0^C D_t^\alpha x(t)$ via SDCPs as follows:

$${}_0^C D_t^\alpha x(t) \simeq C^T \Psi(t), \tag{10.3.24}$$

where $\Psi(t)$ is the SDCPs vector as defined in relation (10.1.14) and C is unknown coefficient vector defined as:

$$C = \begin{pmatrix} c_1 \\ c_2 \\ \vdots \\ c_N \end{pmatrix}. \tag{10.3.25}$$

By applying the fractional Riemann-Liouville operator ${}_0I_t^\alpha$ on both sides of the relation (10.3.24), we have:

$$x(t) \simeq {}_0I_t^\alpha C^T \Psi(t) + \alpha = C^T \mathcal{P}^{(\alpha)} \Psi(t) + d^T \Psi(t), \tag{10.3.26}$$

in which d is the SDCPs coefficient vector for α and $P^{(\alpha)}$ is the operational matrix of fractional integration of the SDCPs vector $\Psi(t)$ derived in Theorem 32. So, the boundary condition in relation (10.0.3) can be written as follows:

$$C^T \mathcal{P}^{(\alpha)} \Psi(b) + d^T \Psi(b) - \beta \simeq 0, \tag{10.3.27}$$

Moreover, by inserting the relations (10.3.24) and (10.3.26) the function $u(t)$ in (10.0.2) can be approximated as a function of unknown vector C, namely:

$$u\left[t, C\right] \simeq \int_a^t \mathcal{K}\left(s, C^T \mathcal{P}^{\alpha} \Psi(s) + d^T \Psi(s), C^T \Psi(s)\right) ds. \tag{10.3.28}$$

Therefore, the performance index (10.0.1) can be derived as follows:

$$\mathcal{J}_N[C] \simeq \int_a^b \mathcal{F}\left(t, C^T \mathcal{P}^{\alpha} \Psi(s) + d^T \Psi(s), C^T \Psi(s), u\left[t, C\right]\right) dt. \tag{10.3.29}$$

Finally, by applying the necessary conditions for optimality of the performance index $\mathcal{J}_N[C]$ we are able to write

$$\frac{\partial \mathcal{J}_N}{\partial c_i} = 0, \qquad i = 0, 1, ..., N-1. \tag{10.3.30}$$

Eqs. (10.3.27) along with (10.3.30) generate a set of $(N+1)$ nonlinear equations that can be solved by the Newton's iterative method to find the coefficients $c_i, i = 0, 1, ..., N$.

Main features of the SDCPs method

Using the SDCPs, which are orthogonal concerning a discrete norm, a numerical scheme has been proposed for the approximate solution of FVPs. The implementation of this method is more efficient and less complex in comparison with similar methods such as the classical Chebyshev polynomials method in which continuous norm is used. Moreover, the need for using a Lagrange multiplier during the solution procedure is eliminated.

10.4 Numerical experiments

In order to verify the efficiency and superiority of the SDCPs method, we will consider some examples in this section. Let $e(t) = x(t) - \tilde{x}(t)$ be the error function of the approximate solution $\tilde{x}(t)$. The maximum absolute error (MAE) for the obtained numerical solution will be estimated as follow:

$$\left\|e\right\|_{\infty} = \underset{0 \leqslant t \leqslant 1}{Max} \left|e(t)\right|.$$

All computations are carried out using MAPLE 17 with 30 digits precision.

Example 20. *As first example, we consider the following FVP*

$$Min.\ \mathcal{J}(x) = \int_0^1 \left[\left({}_0^C D_t^\alpha x(t) - t\Gamma(\alpha+2) \right)^2 + u(t) \right] dt, \quad 0 < \alpha \leqslant 1,$$

in which

$$u(t) = \int_0^t (x(s) - s^{\alpha+1})^2 ds, \quad 0 \leqslant t \leqslant 1,$$

subject to the boundary conditions

$$x(0) = 0, \quad x(1) = 1.$$

The exact solution for this problem is $x(t) = t^{\alpha+1}$. The proposed DCPs method has been applied to solve this FVP for various values α. Fig. 10.1 shows the obtained approximate solution $x(t)$ and the absolute error functions for different choices of α and $N = 10$. The MAE for the approximate solutions with different values of N and α are provided in Table 10.1. Moreover, in Table 10.2, the obtained optimal values $\mathcal{J}$ and the required CPU time (in seconds) are compared with those achieved by the classical Chebyshev polynomials in Ref. [112]. From these results, we can conclude that both discrete and classical Chebyshev polynomials efficiently solve this FVP. In contrast, the discrete polynomials method requires less CPU time when compared to the contentious one. Moreover, as the number of basis functions, i.e. N increases, and the complexity and required CPU time of the contentious Chebyshev polynomials method increases significantly.

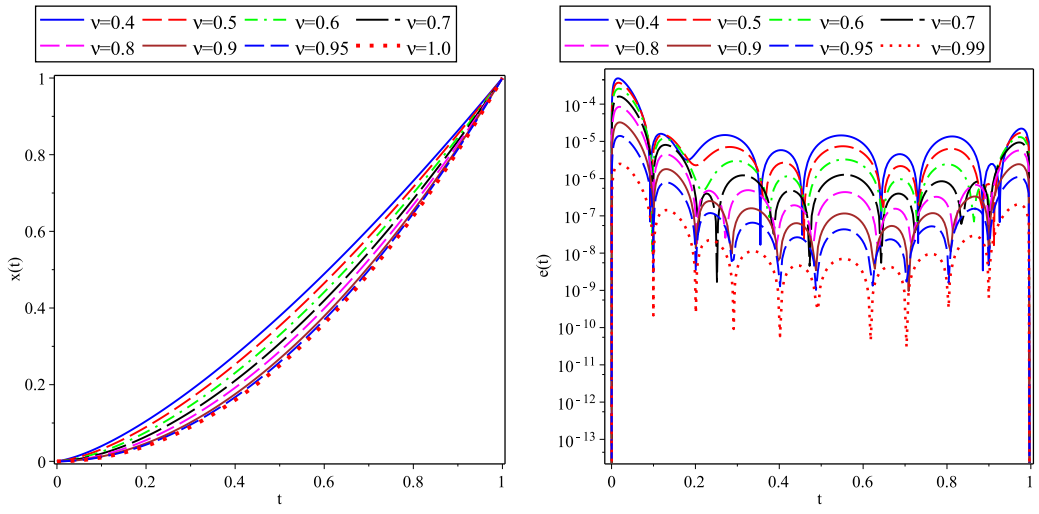

Figure 10.1: The obtained approximate solutions (Left) and the absolute error functions (Right) for different values of α and $N = 10$ in Example 20.

Table 10.1: The MAE of the approximate solution $\tilde{x}(t)$ in Example 20.

α	$N = 6$	$N = 8$	$N = 12$
$\alpha = 0.50$	1.7×10^{-3}	6.2×10^{-4}	2.2×10^{-4}
$\alpha = 0.70$	5.6×10^{-4}	2.5×10^{-4}	1.0×10^{-4}
$\alpha = 0.80$	3.3×10^{-4}	1.4×10^{-4}	5.1×10^{-5}
$\alpha = 0.90$	1.2×10^{-4}	5.3×10^{-5}	1.8×10^{-5}
$\alpha = 0.95$	5.8×10^{-5}	2.5×10^{-5}	8.2×10^{-6}
$\alpha = 0.99$	1.2×10^{-5}	4.5×10^{-6}	1.4×10^{-6}

Table 10.2: The optimal values $\mathcal{J}$ and required CPU time (in seconds) for different values of α and N in Example 20.

$N = 6$				
	$\mathcal{J}$		CPU time	
	Chebyshev polynomial [112]	DCPs	Chebyshev polynomials	DCPs
$\alpha = 0.50$	7.677×10^{-9}	1.052×10^{-8}	8.078	2.469
$\alpha = 0.70$	3.329×10^{-9}	2.175×10^{-8}	8.063	2.343
$\alpha = 0.90$	2.588×10^{-10}	9.133×10^{-10}	8.063	2.782
$\alpha = 0.99$	1.986×10^{-12}	7.811×10^{-12}	8.297	2.438
$N = 8$				
	$\mathcal{J}$		CPU time	
	Chebyshev polynomial [112]	DCPs	Chebyshev polynomials	DCPs
$\alpha = 0.50$	8.338×10^{-10}	2.246×10^{-9}	17.203	4.735
$\alpha = 0.70$	3.076×10^{-10}	3.785×10^{-10}	18.843	4.641
$\alpha = 0.90$	1.928×10^{-11}	1.631×10^{-11}	17.688	4.454
$\alpha = 0.99$	1.336×10^{-13}	1.034×10^{-13}	18.828	4.703
$N = 10$				
	$\mathcal{J}$		CPU time	
	Chebyshev polynomial [112]	DCPs	Chebyshev polynomials	DCPs
$\alpha = 0.50$	1.458×10^{-10}	7.286×10^{-9}	25.891	7.500
$\alpha = 0.70$	4.739×10^{-11}	1.021×10^{-10}	26.765	9.609
$\alpha = 0.90$	2.512×10^{-12}	3.861×10^{-12}	25.500	9.547
$\alpha = 0.99$	1.608×10^{-14}	2.258×10^{-13}	26.063	9.625

Example 21. *Now, we consider the following FVP*

$$Min.\ \mathcal{J}(x) = \int_0^1 \left[\left({}_0^C D_t^\alpha x(t) - 1 \right)^2 + u(t) \right] dt, \quad 0 < \alpha \leqslant 1,$$

in which

$$u(t) = \int_0^t \left(x(s) - \frac{s^{\alpha+1}}{\Gamma(\alpha+2)} \right)^2 ds, \quad 0 \leqslant t \leqslant 1,$$

subject to the boundary conditions

$$x(0) = 1, \quad x(1) = \frac{1}{\Gamma(\alpha+1)}.$$

The exact solution is $x(t) = \dfrac{t^\alpha}{\Gamma(\alpha+1)}$. *The described DCPs method in Section 10.3 with different values of* N *and* α *have been applied to solve this problem. The approximate solutions* $x(t)$ *and their absolute error functions for* $N = 10$ *and various values of* α *are plotted in Fig. 10.2. Moreover, the MAE of the approximate solution* $\tilde{x}(t)$ *for various values of* N *and* α *are listed in Table 10.3. In order to verify the superiority and efficiency of the DCPs method, in Table 10.4, the obtained optimal values* $\mathcal{J}$ *and the required CPU time (in seconds) were compared to those achieved by the classical Chebyshev polynomials in Ref. [112]. These resultsshow that the proposed DCPs method is efficient and accurate for solving FVPs. In addition, it can be concluded that the application of DCPs is less time-consuming and complex in comparison with the classical Chebyshev polynomials.*

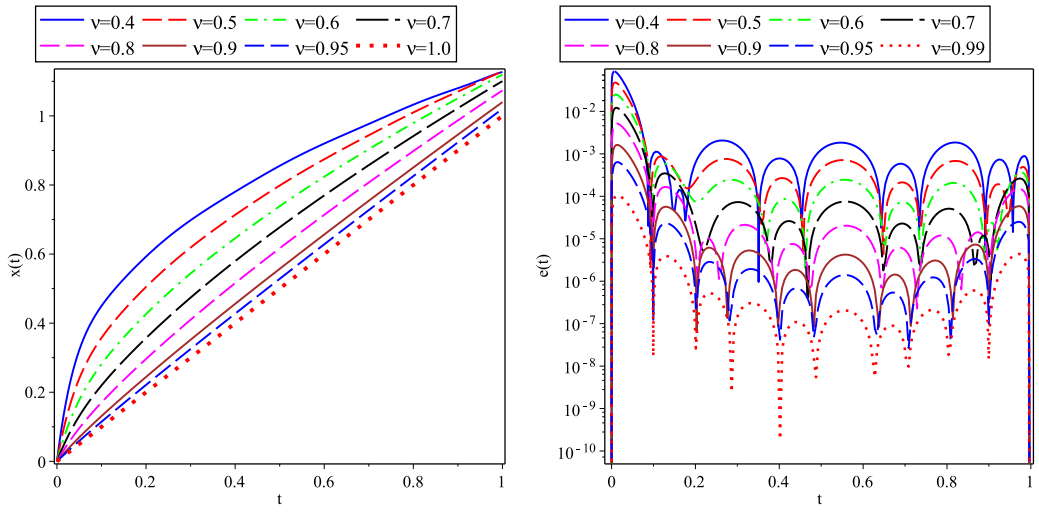

Figure 10.2: The obtained approximate solutions (Left) and the absolute error functions (Right) for different values of α and $N = 10$ in Example 21.

Table 10.3: The MAE of the approximate solution $\tilde{x}(t)$ in Example 21.

α	$N = 8$	$N = 10$	$N = 12$
$\alpha = 0.50$	5.7×10^{-2}	8.7×10^{-2}	4.1×10^{-2}
$\alpha = 0.70$	1.5×10^{-2}	1.2×10^{-2}	1.0×10^{-2}
$\alpha = 0.80$	6.6×10^{-3}	5.1×10^{-3}	4.2×10^{-3}
$\alpha = 0.90$	2.3×10^{-3}	1.6×10^{-3}	1.2×10^{-3}
$\alpha = 0.95$	8.6×10^{-4}	6.3×10^{-4}	5.1×10^{-4}
$\alpha = 0.99$	1.4×10^{-4}	1.1×10^{-4}	8.3×10^{-5}

Table 10.4: The optimal values $\mathcal{J}$ and required CPU time (in seconds) for different values of α and N in Example 21.

$N = 8$				
	$\mathcal{J}$		CPU time	
	Chebyshev polynomial [112]	DCPs	Chebyshev polynomials	DCPs
$\alpha = 0.50$	2.427×10^{-6}	1.19×10^{-5}	28.578	9.344
$\alpha = 0.70$	4.548×10^{-7}	9.195×10^{-7}	29.250	9.922
$\alpha = 0.99$	7.611×10^{-11}	8.553×10^{-11}	29.094	10.454
$N = 10$				
	$\mathcal{J}$		CPU time	
	Chebyshev polynomial [112]	DCPs	Chebyshev polynomials	DCPs
$\alpha = 0.50$	9.933×10^{-7}	6.476×10^{-6}	59.110	19.531
$\alpha = 0.70$	1.647×10^{-7}	4.533×10^{-7}	58.453	20.922
$\alpha = 0.99$	2.171×10^{-11}	3.573×10^{-11}	57.829	21.093
$N = 12$				
	$\mathcal{J}$		CPU time	
	Chebyshev polynomial [112]	DCPs	Chebyshev polynomials	DCPs
$\alpha = 0.50$	4.845×10^{-7}	3.751×10^{-6}	82.532	32.640
$\alpha = 0.70$	7.166×10^{-7}	9.504×10^{-7}	96.938	38.031
$\alpha = 0.99$	7.713×10^{-12}	1.760×10^{-12}	98.297	39.921

Example 22. *Consider the following FVPs*

$$Min.\ \mathcal{J}(x) = \int_0^1 \left[2 \left({}_0^C D_t^\alpha x(t) - \frac{\Gamma(\alpha+4)}{\Gamma(4)} t^3 - \frac{\Gamma(\alpha+3)}{\Gamma(3)} t^2 \right)^2 + 5u(t) \right] dt, \quad 0 < \alpha \leqslant 1,$$

in which

$$u(t) = \int_0^t \left(x(s) - s^{\alpha+3} - s^{\alpha+2}\right)^2 ds, \quad 0 \leqslant t \leqslant 1,$$

subject to the boundary conditions

$$x(0) = 0, \ x(1) = 2, \quad 0 \leqslant t \leqslant 1.$$

For $0 < \alpha \leqslant 1$ the exact solution of this problem is $x(t) = t^{\alpha+3} + t^{\alpha+2}$. The solution of this FVP has been approximated by using the proposed DCPs method for various values of N and α. The approximate solutions $\tilde{x}(t)$ and their absolute error functions for $N = 10$ and various values of α are plotted in Fig. 10.3. The MAE of the solution functions $x(t)$ for different choices of N and α are presented in Table 10.5. Furthermore, Table 10.6 provides a comparison between the obtained optimal values $\mathcal{J}$ and their required CPU time (in seconds) and those derived by the classical Chebyshev polynomials in Ref. [112]. According to the presented results, it is clear that both DCPs and classical Chebyshev polynomials methods are efficient in solving FVPs, while the application of DCPs is less time-consuming and complex compared to the typical Chebyshev polynomials method. Moreover, it is easy to conclude that the classical Chebyshev polynomials method's complexity and required CPU time increase significantly as the number of basis functions N increases.

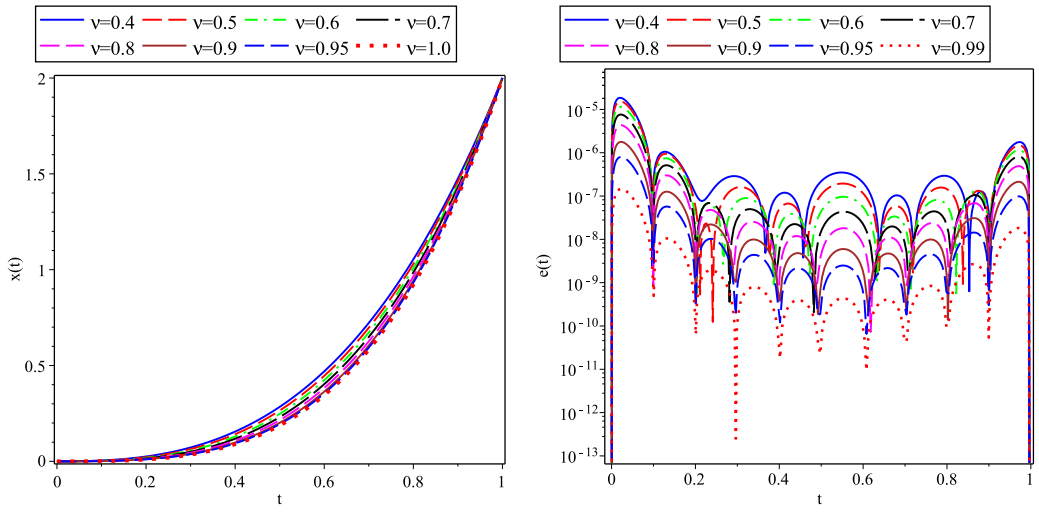

Figure 10.3: The obtained approximate solutions (Left) and the absolute error functions (Right) for different values of α and $N = 10$ in Example 22.

Table 10.5: The MAE of the approximate solution $\tilde{x}(t)$ in Example 22.

	$N = 6$	$N = 8$	$N = 12$
$\alpha = 0.50$	8.7×10^{-5}	3.7×10^{-5}	7.7×10^{-6}
$\alpha = 0.70$	4.8×10^{-5}	1.6×10^{-5}	3.9×10^{-6}
$\alpha = 0.80$	2.9×10^{-5}	1.1×10^{-5}	2.3×10^{-6}
$\alpha = 0.90$	1.2×10^{-5}	4.0×10^{-6}	2.2×10^{-7}
$\alpha = 0.95$	5.6×10^{-6}	1.8×10^{-6}	3.8×10^{-7}
$\alpha = 0.99$	1.6×10^{-7}	3.8×10^{-7}	6.8×10^{-8}

Table 10.6: The optimal values $\mathcal{J}$ and required CPU time (in seconds) for different values of α and N in Example 22.

$N = 5$				
	$\mathcal{J}$		CPU time	
	Chebyshev polynomials [112]	DCPs	Chebyshev polynomials	DCPs
$\alpha = 0.5$	2.855×10^{-10}	1.960×10^{-9}	17.109	3.438
$\alpha = 0.7$	1.366×10^{-10}	5.882×10^{-10}	17.875	3.438
$\alpha = 0.9$	9.337×10^{-12}	3.740×10^{-11}	18.922	3.406
$N = 7$				
	$\mathcal{J}$		CPU time	
	Chebyshev polynomials [112]	DCPs	Chebyshev polynomials	DCPs
$\alpha = 0.5$	1.291×10^{-11}	1.615×10^{-10}	24.344	5.922
$\alpha = 0.7$	6.855×10^{-12}	4.592×10^{-11}	24.344	6.484
$\alpha = 0.9$	6.061×10^{-13}	3.001×10^{-12}	24.125	6.078
$N = 9$				
	$\mathcal{J}$		CPU time	
	Chebyshev polynomials [112]	DCPs	Chebyshev polynomials	DCPs
$\alpha = 0.5$	8.479×10^{-13}	2.156×10^{-12}	68.532	10.750
$\alpha = 0.7$	4.035×10^{-13}	5.438×10^{-12}	64.797	11.312
$\alpha = 0.9$	3.089×10^{-14}	3.127×10^{-13}	64.891	11.235

10.5 Conclusion

This chapter proposed a new type of discrete orthogonal polynomials basis. Using these orthogonal polynomials and their fractional operational matrix, a numerical method is developed to solve FVPs. As these polynomials are orthogonal concerning a discrete

norm, implementation of the presented method is more efficient and less complex in comparison with similar methods in which continuous orthogonal polynomials are used. Application of the proposed method for some test problems verified that:

1. The discrete orthogonal polynomials are efficient for solving FVPs.
2. The application of discrete Chebyshev polynomials is less time-consuming and complex than the classical Chebyshev polynomials.
3. The complexity and required CPU time of classical Chebyshev polynomials increase significantly as the number of basis functions increases.
4. The need for using a Lagrange multiplier during the solution procedure is eliminated.

Chapter 11

Comparison between Protein- Protein interaction network CD^+4 and CD^+8 and a numerical approach for fractional HIV infection of CD^+4 T-cell

A lentivirus, the human immunodeficiency virus (HIV), causes acquired immunodeficiency syndrome (AIDS). Alterations distinguish HIV infection in the function of T cells and homeostasis and the extreme heterogeneity between infected people and those untreated. On average, most patients infected with HIV develop AIDS in 10 to 20 years. Variations in HIV infection clinical outcomes may be due to genetic differences in HIV strains, host genetic differences, or differences in virus-specific inflammatory responses. The first HIV case was confirmed in 1980. Due to the latest count, more than 35 million people have died due to HIV, and over 37 million people have this virus in their bodies, posing a threat to the rest of the world. They will also convey this danger through mother-to-child transfer, unsafe sex, and other ways.

Several mathematical models have already been developed to research the within-host dynamics of HIV infection [17, 220, 312]. Virus-to-cell infection was the focus of the majority of these models. Direct cell-to-cell transmission is also a possibility for the virus to spread. An ODE model of the HIV spread in a well-mixed compartment, like the bloodstream, was proposed by Perelson [238, 239]. Within the mathematical modeling of HIV infection, this model has had a considerable effect. Several other approaches have been suggested based on the Perelson model [9, 12, 87, 133, 178, 187, 216, 229, 247, 294, 323]. However, most HIV infection modeling research has focused on integer-order ordinary differential equations [18, 208, 230, 325].

Fractional calculus has recently been widely used in various fields. Many applied

scientists and mathematicians have attempted to use fractional calculus to model real-world processes. Fractional kinetics in complex systems, reported in [217]. The fractional order dynamics in botanical impedances were studied in [169]. A mathematical fractional-order model of human root dentin was presented in [240]. In biology, it has been determined that biological organisms' cell membranes have fractional-order electrical conductance, which is then categorized into non-integer order models. Fractional derivatives represent essential characteristics of cell-rheological conduct and have had the best achievement in the area of rheology [86]. Furthermore, it has been demonstrated that the behavior modeling by FDEs for the vestibule oculomotor neurons has more benefits than the classical integer-order modeling [10]. FDEs is intrinsically linked to systems found in all biological systems. They are also associated with fractals, typically found in biological systems. In this study, we propose a FDEs system for modeling HIV and a numerical method for solving it.

The following is the chapter's structure. The primary objective of selecting FDEs for modeling HIV infection of CD4$^+$T cells is described in Section 11.1. In this section, we present and compare the protein-protein interaction network of cell infection. The mathematical model will be outlined in Section 11.2. The numerical solution of HIV infection of CD4$^+$T cells is discussed in section 11.3. Section 11.4 describes illustrative examples that show the DCP's superiority. Finally, in Section 11.5, the main concluding remark is summarized.

11.1 Comparison protein-protein interaction networks CD4$^+$T and CD8$^+$T

CD4$^+$T lymphocytes are a kind of white blood cell and a lymphocyte. A helper T cell is also a T cell that assists other cells. CD4$^+$ T cells primarily serve as a type of T cell that helps other T cells resist virus infection. In contrast, CD8$^+$ cells are widely distributed on the surface of suppressor and cytotoxic T lymphocytes during HIV infection. The researchers concluded that HIV infection caused severe immune system problems, including the loss of CD4$^+$ T cells and a reduction in the $\frac{CD4^+}{CD8^+}$T cell ratio.

In the peripheral group of healthy adults, the $\frac{CD4^+}{CD8^+}$T ratio is about 2:1, and an abnormal ratio may signify disorders related to autoimmunity or immunodeficiency. An inverted $\frac{CD4^+}{CD8^+}$T ratio (i.e., less than $\frac{1}{1}$) means that the immune system is compromised. As a result, it is critical to look into the differences between CD4$^+$ and CD8$^+$T cells at various stages of HIV infection. AIDS is caused by the pathogen HIV, which is well-known. The researchers reasoned that analyzing the differences in mutual differentially expressed genes between CD4$^+$ and CD8$^+$Tcells at different phases of disease would reveal more about HIV.

Few studies examine the systemic features of CD4$^+$ T cells at various levels of

HIV infection or the differences between $CD4^+$ and $CD8^+$ T cells at the same level. Moreover, this topic is beyond the scope of this article's discussion. In this study, we compare and contrast the construction of protein-protein interaction (PPI) networks in $CD4^+$ and $CD8^+$ T cells after HIV infection. We investigate the overlapping differentially expressed genes in $CD4^+$ cells and those in $CD8^+$ T cells in two PPI networks and compare two PPI networks Fig. 11.1, to comprehend the differentially expressed between $CD4^+$ and $CD8^+$ from a network perspective.

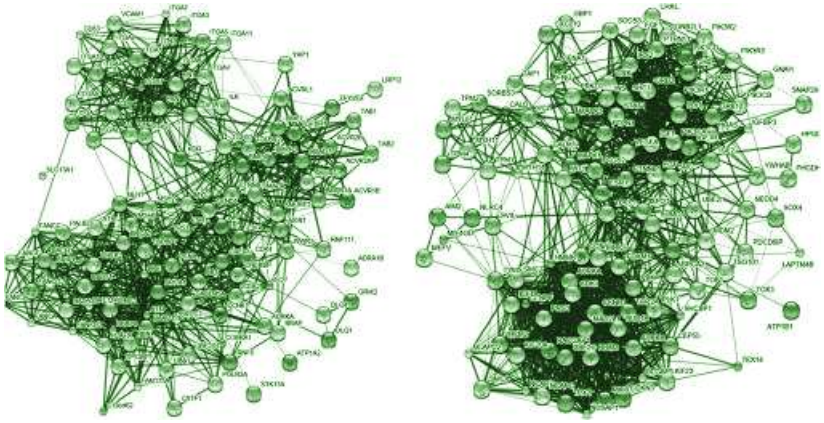

Figure 11.1: PPI network constructed in $CD8^+$ T cells (right) and $CD4^+$ T cells (left)

The overlap of differentially expressed genes in each cell type is extremely high. The two PPI networks shown in Fig. 11.1 are far too convoluted to provide important network information. As a result, we compare the functional modules from each PPI network in separate networks to assess the differences between two HIV-infected cells, respectively (11.2-11.3). The immune responses of $CD4^+$ and $CD8^+$ T cells at various stages after HIV infection are diverse, as shown in Figs. 11.2-11.3. According to research, specific $CD8^+$ T cells play a key role in directly combating HIV infection, while $CD4^+$ T cells primarily serve to support $CD8^+$ T cells.

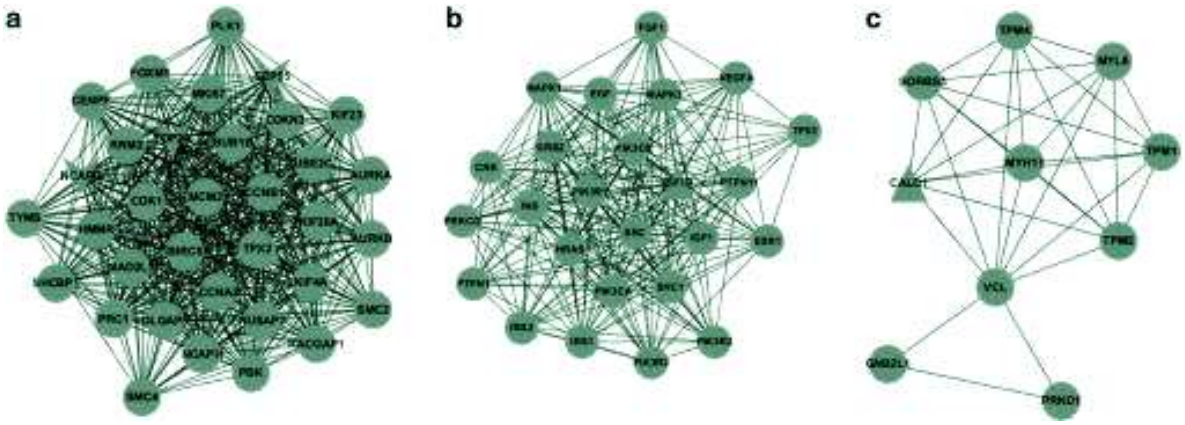

Figure 11.2: (a-c) Function modules obtained by the PPI network in $CD8^+$T cells.

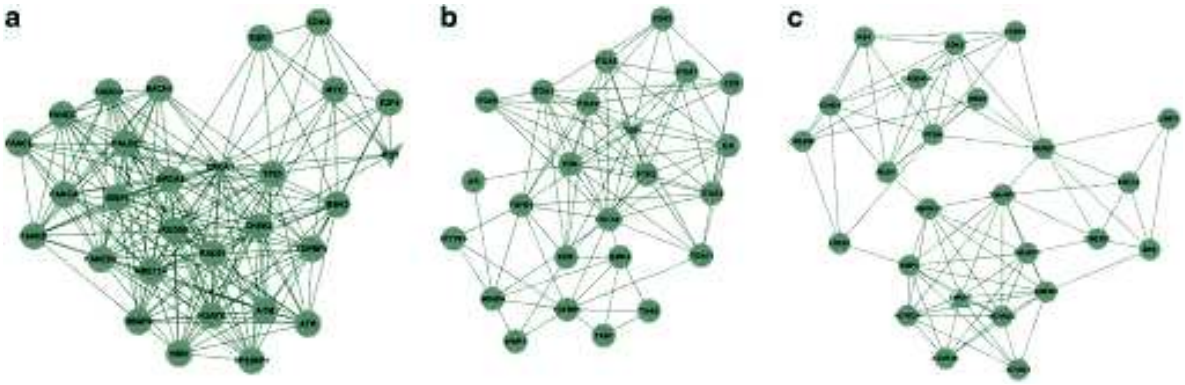

Figure 11.3: (a-c) Functional modules obtained by the PPI network in CD4$^+$T cells.

It has been validated by comparing networks and prior research that CD4$^+$T cells undergo gradual depletion after HIV infection. That virus reproduction (more than 99 %) happened primarily in CD4$^+$T cells in the peripheral blood and lymphoid tissue. HIV infection can also stop CD4$^+$T cells from proliferating. As a consequence, HIV is a retrovirus that primarily infects CD4$^+$T cells. CD4$^+$T cells will develop new virions after being infected, leading to more cell infection and viral development (See Fig. 11.4). Therefore, for researchers, studying these cells is critical. We want to introduce a mathematical model of fractional HIV infection of CD4$^+$T cells and find a numerical solution for it in this chapter.

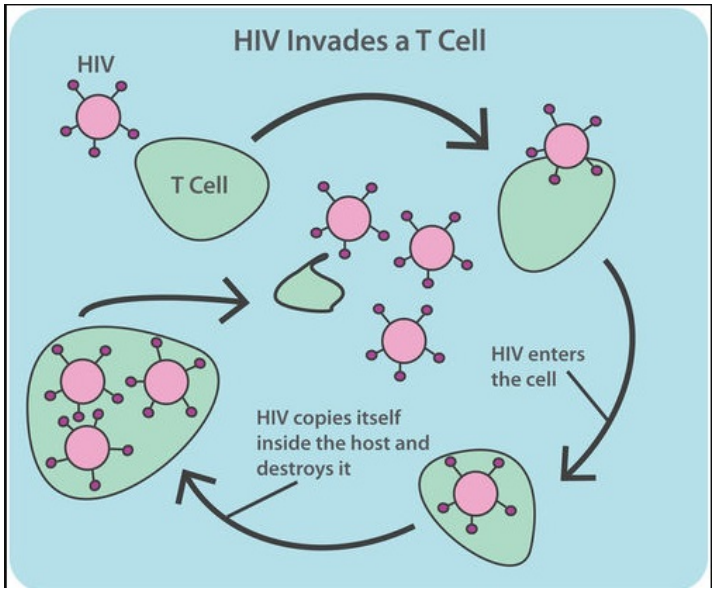

Figure 11.4: HIV virus invades T cell.

11.2 Mathematical model information

Now we present the HIV infection model in CD4$^+$T cells with fractional-order. The following FDE is used to characterize the new system:

$$\begin{aligned} &\mathbf{D}^{\alpha}T = q - \eta T + rT(1 - \tfrac{T+1}{T_{\max}}) - kVT, \\ &\mathbf{D}^{\alpha}I = kVT - \beta I, \\ &\mathbf{D}^{\alpha}V = \mu\beta I - \gamma V, \end{aligned} \tag{11.2.1}$$

where $T(0) = r_1,\ I(0) = r_2,\ V(0) = r_3,\ 0 \leqslant t \leqslant R < \infty$.

Where $V(t)$, $I(t)$, and $T(t)$ represent free HIV particles within the blood, CD4$^+$T cells contaminated by HIV, and the concentration of susceptible CD4$^+$T cells, respectively. R is any positive constant. The terms η, γ, and β indicate the normal circulation rates of non-infected T cells, virus particles, and infected T cells, respectively. $1 - \frac{T+1}{T_{\max}}$ depicts the logistic growth of healthy CD4$^+$T cells while ignoring the proliferation of infected CD4$^+$T cells. The term kVT reflects the occurrence of HIV infection of healthy CD4$^+$T cells when $k > 0$ is the infection rate. During its lifetime of CD4$^+$T cell, each infected CD4$^+$T cell is expected to generate l virus particles. The body is attempted to make CD4$^+$T cells at a constant rate q from precursors in the bone marrow and thymus. Whenever T cells are stimulated by antigen or mitogen, they multiply at a rate of r via mitosis. The maximum CD4$^+$T cell concentration in the body is denoted by $T_{\max}$.

11.3 The numerical method

In this section, we will focus on presenting the numerical approach based on a large family of orthogonal polynomials, namely discrete Chebyshev polynomials introduced by P.L. Chebyshev [126, 218]. The considerations of the previous chapter referred to the general features of the discrete Chebyshev polynomials, the fundamental definition, formulation, and explicit formulas for operational matrices of Riemann-Liouville fractional integration vector's product operational matrix for SDCPs. For the procedure described in the previous chapter (Chapter 10), we refer to Section 10.1 and Section 10.2.

To start the procedure, SDCPs approximate the solution of fractional HIV infection of CD4$^+$T cells. Consider the FODE (11.2.1) and $\mathbf{D}^{\alpha}T(t), \mathbf{D}^{\alpha}I(t)$ and $\mathbf{D}^{\alpha}V(t)$ involved in, as follows:

$$\mathbf{D}^{\alpha}T(t) \simeq F^T\Psi(t),\ \ \mathbf{D}^{\alpha}I(t) \simeq G^T\Psi(t),\ \ \mathbf{D}^{\alpha}V(t) \simeq H^T\Psi(t), \tag{11.3.2}$$

where $\Psi(t)$ is the SDCPs vector specified in (10.1.14). Furthermore, F, G, H are unknown vectors that should be determined. By using of fractional Riemann-Liouville operator $\mathbf{I}^{\alpha}$, we have:

$$\begin{cases} T \simeq \mathbf{I}^{\alpha} F^T \Psi(t) + \sum_{k=0}^{m-1} T^{(k)}(0)\frac{t^k}{k!} = F^T \mathcal{P}^{(\alpha)} \Psi(t) + d_1 \Psi(t), \\ I \simeq \mathbf{I}^{\alpha} G^T \Psi(t) + \sum_{k=0}^{m-1} I^{(k)}(0)\frac{t^k}{k!} = G^T \mathcal{P}^{(\alpha)} \Psi(t) + d_2 \Psi(t), \\ V \simeq \mathbf{I}^{\alpha} H^T \Psi(t) + \sum_{k=0}^{m-1} V^{(k)}(0)\frac{t^k}{k!} = H^T \mathcal{P}^{(\alpha)} \Psi(t) + d_3 \Psi(t), \end{cases} \tag{11.3.3}$$

where $\mathcal{P}^{(\alpha)}$ is the fractional operational matrix of SDCPs vector derived in (10.2.17). Substituting (11.3.2)-(11.3.3) in FODE (11.2.1), we have the following residual functions as:

$$\begin{cases} E_1(t) \simeq (F^T \Psi(t)) - q - \eta(F^T \mathcal{P}^{(\alpha)} \Psi(t) + d_1 \Psi(t)) + r(F^T \mathcal{P}^{(\alpha)} \Psi(t) + d_1 \Psi(t)) \\ (1 - \frac{(F^T \mathcal{P}^{(\alpha)} \Psi(t) + T(0)) + 1}{T_{\max}}) - k(H^T \mathcal{P}^{(\alpha)} \Psi(t) + d_2 \Psi(t))(F^T \mathcal{P}^{(\alpha)} \Psi(t) + d_1 \Psi(t)), \\ \\ E_2(t) \simeq (G^T \Psi(t)) - k(H^T \mathcal{P}^{(\alpha)} \Psi(t) + d_2 \Psi(t))(F^T \mathcal{P}^{(\alpha)} \Psi(t) + d_1 \Psi(t) + \\ \beta(G^T \mathcal{P}^{(\alpha)} \Psi(t) + d_3 \Psi(t)), \\ \\ E_3(t) \simeq (H^T \Psi(t)) - \mu\beta(G^T \mathcal{P}^{(\alpha)} \Psi(t) + d_3 \Psi(t)) + \gamma(H^T \mathcal{P}^{(\alpha)} \Psi(t) + d_2 \Psi(t)). \end{cases} \tag{11.3.4}$$

Now, to find the solution $T(t), I(t)$ and $V(t)$, we must first collocate the residual functions $E_i(t)$, $i = 1, 2, 3$ at the $N + 1$ points. We use roots of shifted Chebyshev polynomials to find appropriate collocates, as shown below:

$$E_i(t_j) = 0, \quad i = 1, 2, 3, \ j = 1, 2, ...N + 1. \tag{11.3.5}$$

Solve the system of algebraic equations to achieve unknown coefficients of the vectors F, G, H. Finally, we obtain the numerical solution by inputting the acquired vectors F, G, H in Eq. (11.2.1).

11.4 Numerical experiments

The effectiveness of the shifted discrete Chebyshev polynomials method for solving fractional HIV infection of CD4$^+$T cells is proved in this section. In the following, one example is given to demonstrate the properties of the new model.

- SDCPM=Shifted discrete chebyshev polynomials method
- All computations are carried out using MAPLE 17 with 16 digits precision

Example 23. *In the $t \in [0, 1]$, we used the described method for FODEs (11.2.1) with the initial conditions $T(0) = 0.1, I(0) = 0$, and $V(0) = 0.1$. $q = 0.1, \eta = 0.02, \beta = 0.3, r = 3, \gamma = 2.4, k = 0.0027, T_{max} = 1500, \mu = 10$ were used in this article.*

Approximate solutions population of healthy $CD4^+$ T cells, infected $CD4^+$ T cells, and free HIV particle for $N = 8$ and different α in $[0, 1]$ are represented in Figs. 11.5, 11.6, and 11.7, respectively. Can be seen in Figs. 11.8, 11.9, and 11.10, that $T(t)$, the concentration of susceptible $CD4^+$ T cells, increases rapidly, $I(t)$, the amount of $CD4^+$ T cells infected by the HIV increases significantly for $N = 8$, and $V(t)$, the number of free HIV particles in the blood decrease in a short time after infection.

For $N = 8$ and $\alpha = 1$, Figs. 11.11, 11.12, and 11.13 display the error functions obtained with an accuracy of the solutions by utilizing the mentioned strategy given by Eqs. (11.3.5). The numerical values of the approximate solutions $T(t)$, $I(t)$, and $V(t)$ of the present method for $N = 8$ in the interval $[0, 1]$ are compared with the Legendre Wavelet Collocation strategy [18], the Runge-Kutta strategy [18], the variational iteration strategy [208], the modified variational iteration strategy [208], the Laplace Adomian decomposition-pade strategy [230]. The Bessel collocation [325] in Tables 11.1, 11.2, and 11.3. To compare error functions provided by Eqs. (11.3.5) for $T(t)$, $I(t)$, and $V(t)$ of the current method for $N = 8$ in the interval $[0, 1]$ are reported in Tables 11.4, 11.5, and 11.6. These results lead to the conclusion that the numerical solutions of the present method are better than those obtained with other methods since the absolute errors have gotten by the current strategy are superior to other methods.

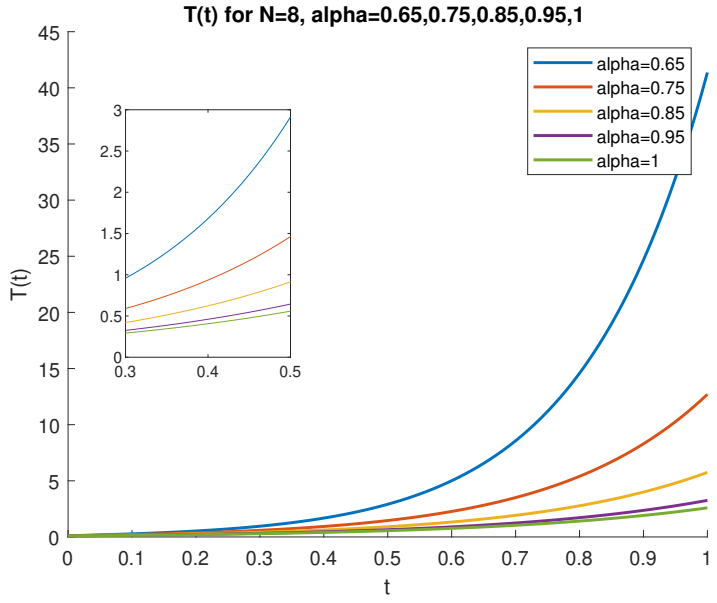

Figure 11.5: Numerical results comparison $T(t)$ for $N = 8$ and different α in $[0, 1]$ in Example 23.

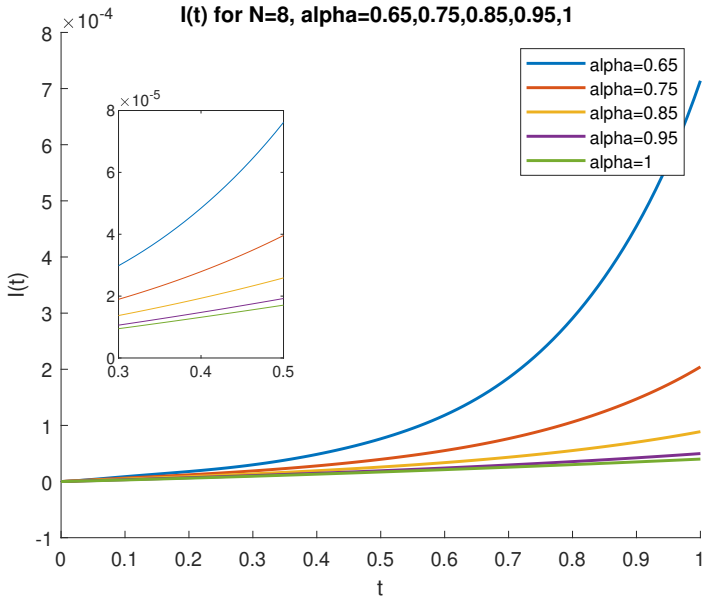

Figure 11.6: Numerical results comparison $I(t)$ for $N = 8$ and different α in $[0, 1]$ in Example 23.

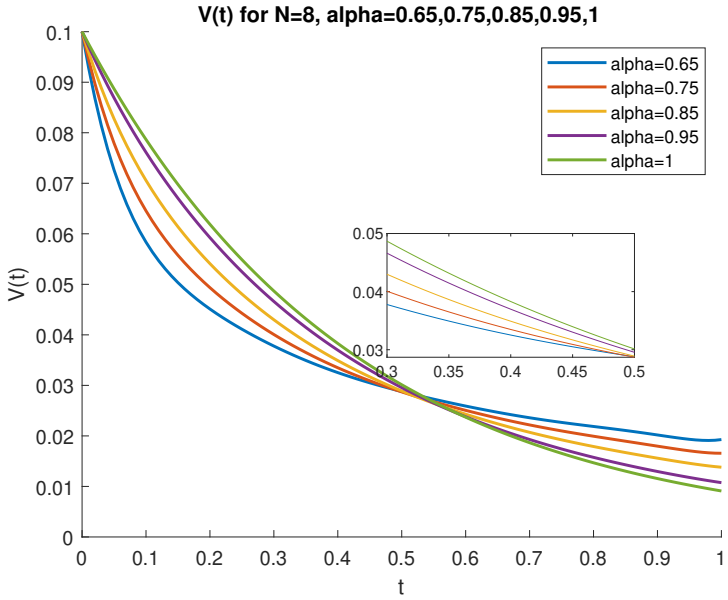

Figure 11.7: Numerical results comparison $V(t)$ for $N = 8$ and different α in $[0, 1]$ in Example 23.

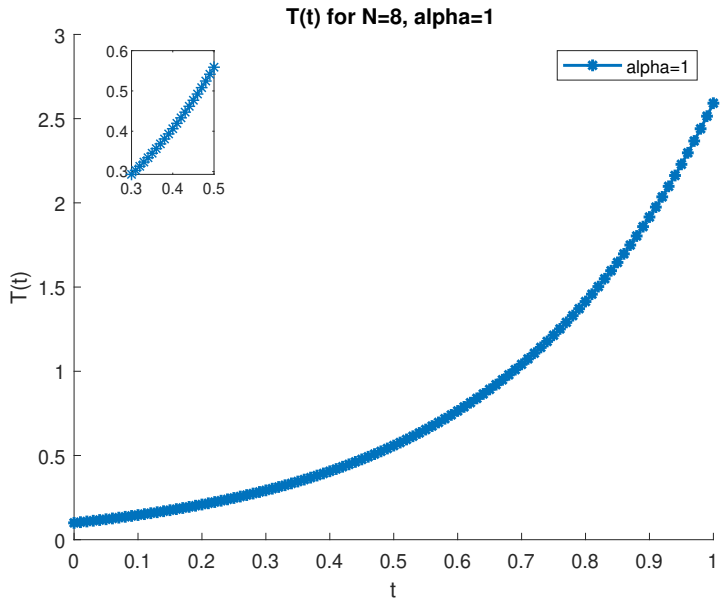

Figure 11.8: Numerical result $T(t)$ for $N = 8$ and $\alpha = 1$ in $[0, 1]$ in Example 23.

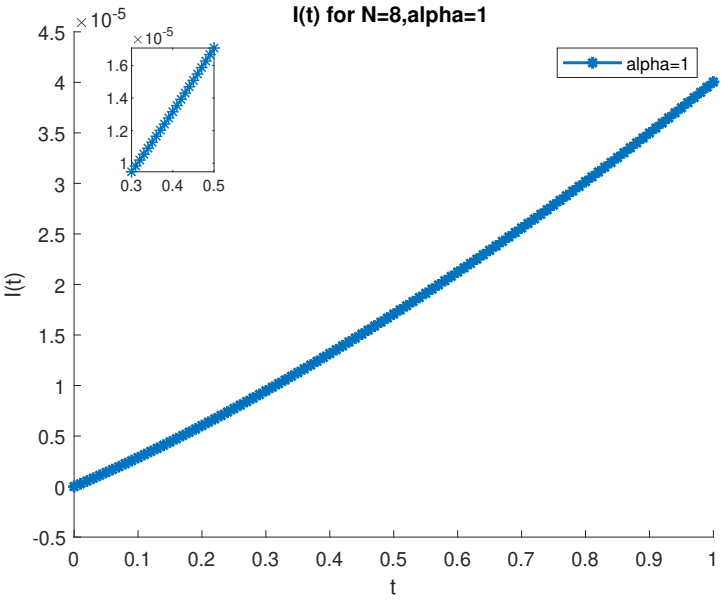

Figure 11.9: Numerical result $I(t)$ for $N = 8$ and $\alpha = 1$ in $[0, 1]$ in Example 23.

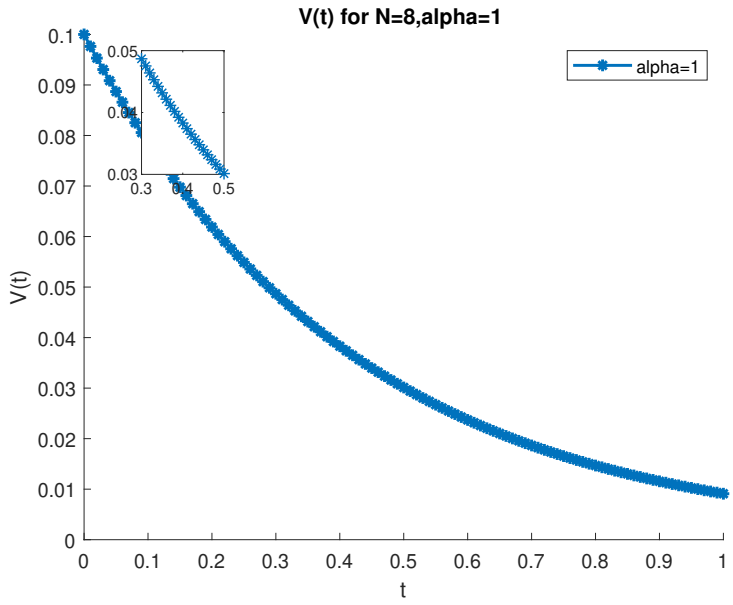

Figure 11.10: Numerical result $V(t)$ for $N = 8$ and $\alpha = 1$ in $[0, 1]$ in Example 23.

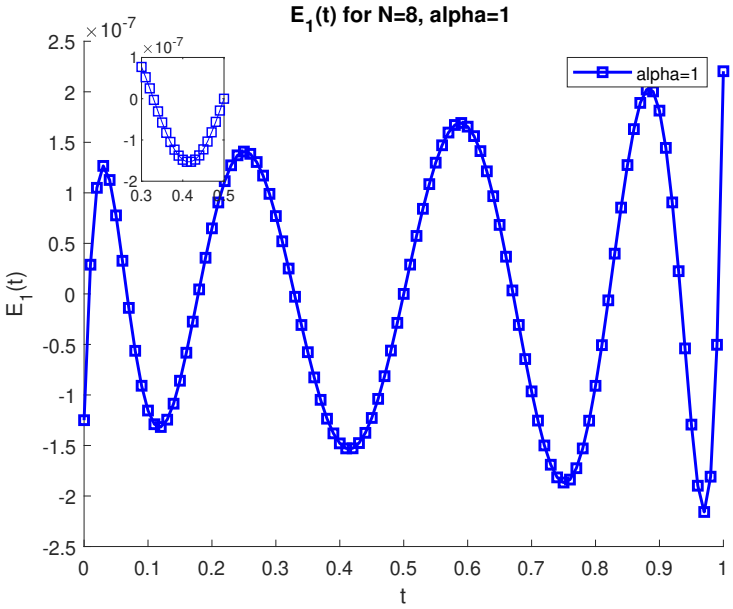

Figure 11.11: Error function of $E_1(t)$ for $N = 8$ and $\alpha = 1$ in Example 23.

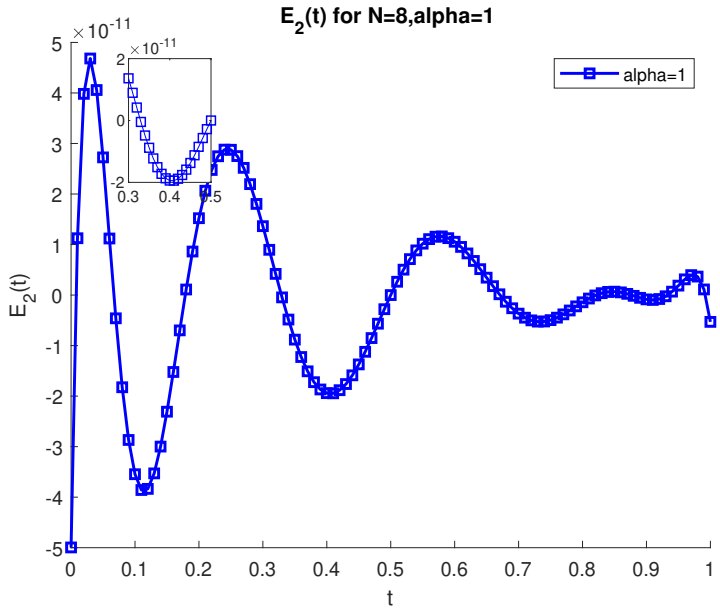

Figure 11.12: Error function of $E_2(t)$ for $N = 8$ and $\alpha = 1$ in Example 23.

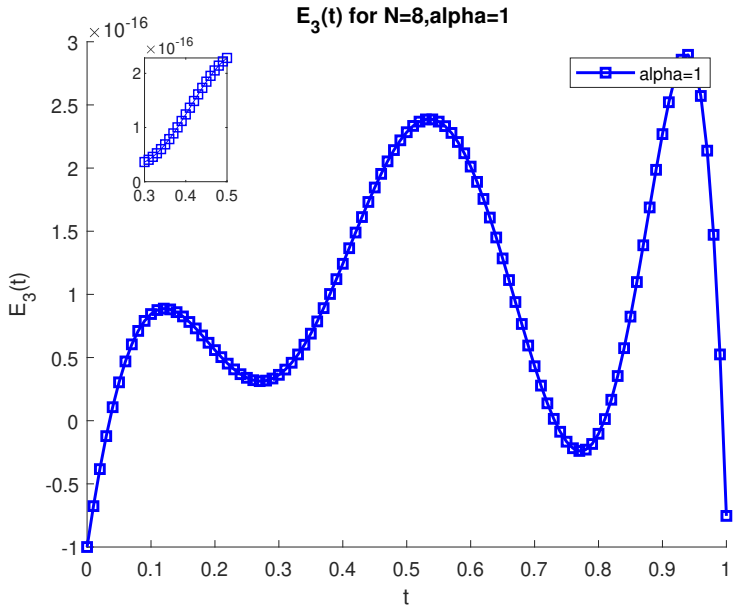

Figure 11.13: Error function of $E_3(t)$ for $N = 8$ and $\alpha = 1$ in Example 23.

Table 11.1: Numerical results comparison for $T(t)$ in Example 23.

Method	$t = 0.2$	$t = 0.4$	$t = 0.6$	$t = 0.8$	$t = 1.0$
Runge-kutta [18]	0.208808	0.406240	0.764423	1.414046	2.591594
MVIM [208]	0.208808	0.406240	.764428	1.414094	2.208808
VIM [208]	0.208807	0.406134	0.762453	1.397880	2.506746
LADM-Pade[230]	0.208807	0.406105	0.761146	1.377319	2.329169
Bessel [325]	0.203861	0.380330	0.695462	1.275962	2.383227
SDCPM	0.208807	0.406240	0.764422	1.414045	2.591592

Table 11.2: Numerical results comparison for $I(t)$ in Example 23.

Method	$t = 0.4$	$t = 0.6$	$t = 0.8$	$t = 1.0$
Runge-kutta [18]	$0.131583e-4$	$0.212237e-4$	$0.301774e-4$	$0.400378e-4$
MVIM [208]	$0.131583e-4$	$0.212233e-4$	$0.301745e-4$	$0.400254e-4$
VIM [208]	$0.131487e-4$	$0.210141e-4$	$0.279513e-4$	$0.243156e-4$
LADM-Pade[230]	$0.131591e-4$	$0.212683e-4$	$0.300691e-4$	$0.398736e-4$
Bessel [325]	$0.129355e-4$	$0.203526e-4$	$0.283730e-4$	$0.369084e-4$
SDCPM	$0.131583e-4$	$0.212237e-4$	$0.301773e-4$	$0.400377e-4$

Table 11.3: Numerical results comparison for $V(t)$ in Example 23.

Method	$t = 0.2$	$t = 0.4$	$t = 0.6$	$t = 0.8$	$t = 1.0$
Runge-kutta [18]	0.061879	0.038294	0.023704	0.014680	0.009100
MVIM [208]	0.061879	0.038295	0.023710	0.014700	0.009157
VIM [208]	0.061879	0.038308	0.023920	0.016217	0.016084
LADM-Pade[230]	0.061879	0.038313	0.024391	0.009967	0.003305
Bessel [325]	0.061879	0.038294	0.023704	0.014679	0.023704
SDCPM	0.061879	0.038294	0.023704	0.014680	0.009100

Table 11.4: Comparison error results for $T(t)$ in Example 23.

Method	$t = 0.2$	$t = 0.4$	$t = 0.6$	$t = 0.8$	$t = 1.0$
LWCM [18]	$7.50e-06$	$2.70e-05$	$7.34e-05$	$1.77e-04$	$3.98e-04$
MVIM [208]	$7.85e-05$	$3.00e-04$	$8.49e-04$	$2.14e-03$	$5.14e-03$
VIM [208]	$7.78e-05$	$1.94e-04$	$1.13e-03$	$1.41e-02$	$8.00e-02$
LADM-Pade[230]	$7.77e-05$	$1.65e-04$	$2.43e-03$	$3.46e-02$	$2.58e-01$
Bessel [325]	$4.87e-03$	$2.56e-02$	$6.81e-02$	$1.36e-01$	$2.04e-01$
SDCPM	$6.48e-08$	$1.47e-07$	$1.65e-07$	$9.09e-08$	$2.20e-07$

Table 11.5: Comparison error results for $I(t)$ in Example 23.

Method	$t = 0.2$	$t = 0.4$	$t = 0.6$	$t = 0.8$	$t = 1.0$
LWCM [18]	$8.36e-10$	$1.95e-09$	$3.20e-09$	$4.63e-09$	$6.44e-09$
MVIM [208]	$1.19e-09$	$5.29e-09$	$1.27e-08$	$2.27e-08$	$3.12e-08$
VIM [208]	$1.12e-09$	$4.23e-09$	$1.96e-07$	$2.20e-06$	$1.57e-05$
LADM-Pade[230]	$1.20e-09$	$6.15e-09$	$5.78e-08$	$8.26e-08$	$1.21e-07$
Bessel [325]	$2.16e-07$	$2.17e-07$	$8.58e-07$	$1.78e-06$	$3.09e-06$
SDCPM	$1.52e-11$	$1.94e-11$	$1.05e-11$	$1.42e-12$	$5.30e-12$

Table 11.6: Comparison error results for $V(t)$ in Example 23.

Method	$t = 0.2$	$t = 0.4$	$t = 0.6$	$t = 0.8$	$t = 1.0$
LWCM [18]	$1.00e-10$	$1.24e-06$	$1.15e-06$	$9.50e-07$	$7.61e-07$
MVIM [208]	$5.61e-08$	$1.06e-06$	$5.75e-06$	$2.01e-05$	$5.64e-05$
VIM [208]	$1.00e-07$	$1.33e-05$	$2.16e-04$	$1.54e-03$	$6.98e-03$
LADM-Pade[230]	$1.08e-07$	$1.84e-05$	$6.87e-04$	$4.71e-03$	$5.80e-03$
Bessel [325]	$6.59e-08$	$3.79e-08$	$2.31e-07$	$7.87e-07$	$1.46e-02$
SDCPM	$2.06e-16$	$9.64e-17$	$6.47e-17$	$2.12e-16$	$8.01e-17$

11.5 Conclusion

This chapter looked at the design of protein-protein interaction (PPI) networks and compared them. Besides, the mathematical model of fractional HIV infection of $CD4^+T$ cells was introduced, which refers to a class of nonlinear differential equation structures. The SDCPM was suggested for finding approximate solutions to the HIV infection model of $CD4^+T$ cells. With the help of an example, the precision and reliability of the current procedure were illustrated. All calculations were done with the aid of a Maple 17 computer program.

Part IV

General conclusion and future research

This thesis focused on mathematical modeling, specifically differential equations, to study various problems in science, engineering, business, and management. Specifically, the thesis considered using exponential fitting and spectral methods to solve ODEs, VIEs, and fractional integral/differential equations. The thesis presented the numerical methods for solving ODEs with oscillatory solutions, using an adapted numerical integration based on an exponential fitting strategy and peer methods in Part I, and numerical methods for solving VIEs and fractional integral/differential equations, using spectral methods with new orthogonal functions and operational matrices as significant tools in Parts II, III.

Classical numerical integrators could require a very small step size to follow the oscillations, especially when the frequency increases. To develop efficient and accurate numerical methods, we proposed an adapted numerical integration based on exploiting a-priori known information about the behavior of the exact solution, utilizing exponential fitting strategy. EF algorithms were designed to overcome the limitations of classical algorithms, which require very small step sizes for accuracy when the oscillation frequency is high. With the EF technique, the same level of accuracy can be achieved with larger step sizes, leading to more efficient and accurate numerical methods. We combined this feature with the usage of peer methods, which represent a highly structured subclass of General Linear Methods and are identified with several distinct stages, such as Runge-Kutta methods. One of the main advantages of EF peer methods is their ability to efficiently and accurately approximate the solution of differential equations with oscillatory behavior, which often arise in many fields of science and engineering, such as physics, chemistry, electrical engineering, and mechanical engineering. These methods have a wide range of applications, for example, studying dynamic systems, control systems, signal processing, and other fields where oscillatory behavior is present. In terms of future developments, researchers are developing new techniques and algorithms to improve the performance of EF peer methods. This includes developing new techniques to efficiently solve high-dimensional and multi-scale problems and new methods to improve the accuracy of the solution.

This study proposed new methods based on spectral methods to solve VIEs and fractional integral/differential equations. We have demonstrated the effectiveness of new methods through numerical experiments. The results of the proposed methods have been compared with existing methods, and it has been shown that the proposed methods provide more accurate and efficient solutions for the problems considered in

this thesis.

Spectral methods are a powerful and efficient approach to solving complex mathematical problems and have a wide range of applications in many different fields, such as physics, engineering, finance, fluid dynamics, electromagnetism, quantum mechanics, and many other areas. Spectral methods are known for their fast convergence rate and ability to approximate solutions with high accuracy, meaning that the numerical solution obtained using spectral methods approaches the exact solution more quickly than other methods. One of the reasons for the fast convergence of spectral methods is the use of basis functions such as orthogonal polynomials. These polynomials can approximate the solution of a problem with high accuracy, and the error in the numerical solution decreases rapidly as the number of discretization points or the degree of the polynomials increases. Spectral methods have some limitations, particularly regarding problems with discontinuities or singularities. They may also be computationally expensive and less easy to implement for large-scale problems. Spectral methods are more suitable for smooth problems and problems with global solutions.

Bibliography

[1] Abdou, M. A.; Badr, A. A. On a method for solving an integral equation in the displacement contact problem, *Appl. Math. Comput.* 127 (2002), no. 1, 65-78.

[2] Acary, V.; Brogliato, B. Numerical Methods for Nonsmooth Dynamical Systems, Applications in Mechanics and Electronics. Springer Verlag Berlin Heidelberg, Lecture Notes in Applied and Computational Mechanics, vol. 35, 2008.

[3] Ahmad, W. M.; El-khazali, R. Fractional-order dynamical models of love, Chaos Solitons Fractals33, (2007), 1367-1375.

[4] Ajello, W. G.; Freedman, H. I.; and Wu, J. A model of stage structured population growth with density depended time delay, *SIAM. J. Appl. Math.* 52 (1992), 855-869.

[5] Ali, K. K.; El Salam, M. A. A.; Mohamed, E. M. Chebyshev operational matrix for solving fractional order delay-differential equations using spectral collocation method, *Arab. J. Basic Appl. Sci.,* 26 (2019), 342-353.

[6] Almeida, R.; Bastos. N. R.; Monteiro M. T. T. Modeling some real phenomena by fractional differential equations Math, *Methods Appl. Sci.,* 39 (16) (2016), 4846-4855.

[7] Almeida, R.; Torres, D. F. M. Calculus of variations with fractional derivatives and fractional integrals, *Appl. Math. Lett.* 22 (12) (2009), 1816-1820.

[8] Alfieri, R.; Mosca, E.; Merelli, I.; Milanes, L. Parameter Estimation for Cell Cycle Ordinary Differential Equation (ODE) Models using a Grid Approach, *Stud. Health Technol. Inform.* 126 (2007), 93-102.

[9] Ali, N.; Ahmad, S.; Aziz, S.; Zaman, G. The adomian decomposition method for solving HIV infection model of latently infected cells. *Matrix. Sci. Math.* 3 (2019), 5-8 .

[10] Anastasio, T. J. The fractional-order dynamics of bainstem vestibulo-oculomotor neurons. Biological Cybernetics 72 (1994), 69-79.

[11] Angell, T. S. On the optimal control of systems governed by nonlinear Volterra equations, Journal of Optimization Theory and Applications, 19 (1976), 29-45.

[12] Angulo, J.; Cuesta, T.; Menezes, E.; Pedroso, C.; Brites, C. A systematic review on the influence of HLA-B polymorphisms on HIV-1 mother to child transmission, *Braz. J. Infec. Dis.* 23 (2019), 53-9.

[13] Aris, R. On the dispersion of a solute in a fluid flowing through a tube, Proc R Soc Lond A. 235 (1200) (1956) 67-77.

[14] Ascher, U.M.; Ruuth, S.J.; Wetton, B.Tr. Implicit-explicit methods for time-dependent partial differential equations, SIAM *J. Numer. Anal.* 32 (1995) 797-823.

[15] Ascher, U.M.; Ruuth, S.J.; Spiteri, R.J. Implicit-explicit Runge-Kutta methods for time-dependent partial differential equations, *Appl. Numer. Math.* 25 (1997) 151-167.

[16] Asli, B. H. S.; Flusser, J. New discrete orthogonal moments for signal analysis, Signal Processing, 141 (2017), 57-73.

[17] Asquith, B.; Bangham,C.R.M. The dynamics of T-cell fratricide: application of a robust approach to mathematical modelling in immunology, *J. Theoret. Biol.* 222 (2003), 53-69.

[18] Attaullah, Sohaib, M. Mathematical modeling and numerical simulation of HIV infection model, Results in Applied Mathematics, 7 (2020), 100-118 (2020).

[19] Avcı, I.; Numerical Simulation of Fractional Delay Differential Equations Using the Operational Matrix of Fractional Integration for Fractional-Order Taylor Basis, Fractal and Fractional, 6 (2022), no. 1-10. https://doi.org/10.3390/fractalfract6010010

[20] Babolian, E.; Abbasbandy, S.; Fattahzadeh, F. A numerical method for solving a class of functional and two dimensional integral equations, *Appl. Math. Comput.* 198 (2008), 35-43.

[21] Baillie, R. T. Long memory processes and fractional integration in econometrics, J. Econ. 73 (1996), 5-59 .

[22] Baleanu, D.; Muslih, S. I. Lagrangian formulation of classical fields within Riemann-Liouville fractional derivatives, *Phys. Scripta.* 72(3) (2005), 119-121.

[23] Baleanu, D.; Diethelm, K.; Scalas, E.; Trujillo, J. J. Fractional Calculus: Models and Numerical Methods, World Scientific, 2016.

[24] Banas, J.; Knap, Z. Integrable solutions of a functional-integral equations: Revista Mathematica, 2(1) (1989) 31-38.

[25] Beck, S.; Gonzalez-Pinto, S.; Perez-Rodriguez, S.; Weiner, R. A comparison of AMF-and Krylov-methods inmatlabfor large stiff ode systems, *J. Comput. Appl. Math.* 262 (2014) 292-303.

[26] Beck, S.; Weiner, R.; Podhaisky, H.; Schmitt, B. Implicit parallel peer methods for large stiff ode systems, *J. Appl. Math. Comput.* 38 (2012), 389-406,.

[27] Belbas, S. A. Iterative schemes for optimal control of Volterra integral equations, *Nonlinear Anal.* 37 (1999), 57-79.

[28] Belbas, S. A. A new method for optimal control of Volterra integral equations. Applied Mathematics and Computation, 189(2) (2007), 1902-1915.

[29] Belbas, S. A. A reduction method for optimal control of Volterra integral equations. Applied Mathematics and Computation, 197(2) (2008), 880-890.

[30] Beuter, A.; Glass, L.; Mackey, M. C.; Titcombe, M. S. Nonlinear Dynamics in Physiology and Medicine, Springer, 2002.

[31] Bhrawy, A. H.; Doha, E. H.; Baleanu, D.; and Ezz-Eldien, S. S. An accurate numerical tech nique for solving fractional optimal control problems. Differential equations 15 (2015), 23.

[32] Bloom, F. Asymptotic bounds for solutions to a system of damped integro-differential equations of electromagnetic theory, *J. Math. Anal. Appl.* 73 (1980) 524-542.

[33] Boscarino, S. Error analysis of IMEX Runge-Kutta methods derived from differential-algebraic systems, SIAM *J. Numer. Anal.* 45 (2007) 1600-1621.

[34] Boscarino, S. On an accurate third order implicit-explicit Runge-Kutta method for stiff problems, *Appl. Numer. Math.* 59 (7) (2009) 1515-1528.

[35] Bras, M.; Izzo, G.; Jackiewicz, Z. Accurate implicit-explicit general linear methods with inherent Runge-Kutta stability, *J. Sci. Comput.* 70 (2017) 1105-1143.

[36] Brunner, H. Coitocatioa methods for Volterra integral and related functional differential equations, volume 15 of Cambridge Monographs on Applied and Complexional Mathematics. Cambridge University Press, Cambridge, 2004.

[37] Brunner, H.; Makroglou, A.; Miller, R, K. On mixed collocation methods for Volterra integral equations with periodic solution, *Appl. Numer. Math.* 24 (1997) 115-130.

[38] Brunner, H. On Volterra integral operators with highly oscillatory kernels, *Discrete Conlin. Dyn. Syst.* 34 (2014) 915-929.

[39] Brunner, H. Volterra integral equations, volume 30 of Cambridge Monographs on Applied and Computational Mathematics. Cambridge University Press. Cambridge, 2017. An introduction to theory and applications.

[40] Brunner, H.; van der Houwen, P. J. The Numerical Solution of Volterra Equations, CWI Monographs, 3, North-Holland Publishing, Amsterdam, 1986.

[41] Brunt, B. V. The Calculus of Variations, Springer-Verlag, New York, 2004.

[42] Burrage, K.; Cardone, A.; D'Ambrosio, R.; Paternoster, B. Numerical solution of time fractional diffusion systems, *Appl. Numer. Math.* 116 (2017), 82-94.

[43] Butcher, J. C. The Numerical Analysis of Ordinary Differential Equations. Runge-Kutta and General Linear Methods, John Wiley Sons, Chichester, New York, 1987.

[44] Butcher, J. C. Numerical Methods for Ordinary Differential Equations, 2nd Edition, John Wiley Sons, Chichester, 2008.

[45] Butcher, J. C. General linear methods, *Acta Numer.* 15 (2006) 157-256.

[46] Canuto, C.; Hussaini, M.; Quarteroni, A.; Zang, T. Spectral methods fundamentals in single domains. Springer, Heidelberg (2006).

[47] Calvo, M.; Franco, J. M.; Montijano, J. I.; Rndez, L. Sixthorder symmetric and symplectic exponentially fitted modified Runge-Kutta methods of Gauss type. Computer Physics Communications 178, 10 (2008), 732-744.

[48] Calvo, M.; Franco, J. M.; Montijano, J. I.; Rndez, L. Structure preservation of exponentially fitted Runge-Kutta methods. Journal of Computational and Applied Mathematics 218, 2 (2008), 421-434.

[49] Calvo, M.; Franco, J. M.; Montijano, J. I.; Rndez, L. Sixthorder symmetric and symplectic exponentially fitted Runge-Kutta methods of the Gauss type. Journal of Computational and Applied Mathematics 223, 1 (2009), 387-398.

[50] Calvo, M.; Franco, J. M.; Montijano, J. I.; Rndez, L. Explicit Runge-Kutta methods for initial value problems with oscillating solutions, *J. Comput. Appl. Math.* 76 (1-2)(1996), 195-212.

[51] Calvo, M.; Montijano, J. I.; Rández, L.; Van Daele, M. Exponentially fitted fifth-order two step peer explicit methods, *AIP Conf. Proc.* 1648 (2015), 150015-1-150015-4.

[52] Canuto, C.; Hussaini, M.; Quarteroni, A.; Zang, T. Spectral methods. Evolution to complex geometries and applications to fluid dynamics. Springer, Heidelberg, 2007.

[53] Capobianco, G.;Conte, D.; Paternoster, B. Construction and implementation of two-step continuous methods for Volterra Integral Equations, *Appl. Numer. Math.* 119 (2017), 239-247.

[54] Cardone, A.; D'Ambrosio, R.; Patenoster, B. High order exponentially fitted methods for Volterra integral equations with periodic solution. *Appl. Numer. Math.* 114 (2017), 18-29.

[55] Cardone, A.; Ferro, M.; Ixaru, L. Gr.; Paternoster, B. A Family of exponential fitting direct quadrature methods for volterra integral equations, *AIP Conf. Proc.* 1281 (2010), 2204-2207.

[56] Cardone, A.; Ixaru, L. Gr.; Paternoster, B. Exponential fitting direct quadrature methods for volterra integral equations, *Numer. Algorithms* 55 (2010), 467-480.

[57] Cardone, A.; Ixaru, L. Gr.; Paternoster, B.; Santomauro, G. Ef-Gaussian direct quadrature methods for volterra integral equations with periodic solution, *Math. Comput. Simulat.* 110 (C) (2015), 125-143.

[58] Cardone, A.; Patenoster, B.; Santomauro, G. Exponential-fitting quadrature rule for functional equations, *AIP Conf. Proc.* 1479 Springer, (2012), 1169-1172, .

[59] Cardone, A.; D'Ambrosio, R.; Patenoster, B. Exponentially fitted IMEX methods for advection-diffusion problems, *J. Comput. Appl. Math.* 316 (2017), 100-108.

[60] Cardone, A.; Ixaru, L.Gr.; Patenoster, B. Exponential fitting direct quadrature methods for Volterra integral equations, *Numer. Algorithms.* 55 (2010), 467-480.

[61] Cardone, A.; D'Ambrosio, R.; Patenoster, B. A spectral method for stochastic fractional differential equations, Applied Numerical Mathematics 139 (2019), 115-119.

[62] Cardone, A.; Conte, D.; Patenoster, B. A family of Multistep Collocation Methods for Volterra Integro-Differential Equations, AIP Conf. Proc., 1168 (1) (2009), 358–361.

[63] Cardone, A.; Conte, D.; Patenoster, B. Two-step collocation methods for fractional differential equations, *Discr. Cont. Dyn. Sys.* - B 23(7) (2018), 2709-2725.

[64] Carr, J.; Duncan, D. B.; Walshaw, C. H. Numerical approximation of a metastable system, *IMA. J. Numer. Anal.* 15 (1995), no. 4, 505-521.

[65] Celik, I. Approximate calculation of eigenvalues with the method of weighted residuals-collocation method, *Appl. Math. Comput.* 160 (2005), 401-410.

[66] Celik, I. Collocation method and residual correction using Chebyshev series, *Appl. Math. Comput.* 174 (2006), 910-920.

[67] Chen, Y.; Tang, T. Spectral methods for weakly singularVolterra integral equations with smooth solutions, *J. Comput. Appl. Math.* 233 (2009), 938-950.

[68] Chen, Y.; Tang, T. Convergence analysis of Jacobi spectral collocation methods for Volterra integral equations with a weakly singular kernel, *Math. Comput.* 79 (2010), 147-167.

[69] Chelyshkov, V. S. Alternative orthogonal polynomials and quadratures, *Electron. Trans. Numer. Anal.* 25(7) (2006), 17-26.

[70] Chihara, T. S. An introduction to orthogonal polynomials, Gordon and Breach, 1978.

[71] Conte, D.; Farsimadan, E.; Moradi, L.; Palmieri, F.; B. Paternoster, B. Time-Delay Fractional Optimal Control Problems: A Survey Based on Methodology. In: Abdel Wahab, M. (eds) Proceedings of the 8th International Conference on Fracture, Fatigue and Wear . FFW 2020 2020. Lecture Notes in Mechanical Engineering. Springer, Singapore. https://doi.org/10.1007/978-981-15-9893-7_ 23.

[72] Conte, D.; Esposito, E.; Ixaru, L. Gr.; Paternoster, B. Some new uses of the $\eta_m(Z)$ functions, *Comput. Phys. Commun.* 181 (2010), 128-137.

[73] Conte, D.; D'Ambrosio, R.; Moccaldi, M.; Paternoster, B. Adapted explicit two-step peer methods, *J. Num. Math.* 27 (2) (2019), 69-83.

[74] Conte, D.; D'Ambrosio, R.; Giordano G.; Ixaru L. Gr.; Paternoster B. User-friendly expressions of the coefficients of some exponentially fitted methods, Computational Science and Its Applications. ICCSA 2020. Lecture Notes in Computer Science(2020), vol 12249. Springer, Cham. https://doi.org/10.1007/978-3-030-58799-4_4.

[75] Conte, D.; D'Ambrosio, R.; Giordano G.; Paternoster, B. Regularized exponentially fitted methods for oscillatory problems, Journal of Physics: Conference Series - IOPscience, 1564 (2020), 012013.

[76] Conte, D.; Ixaru, L. Gr.; Paternoster, B.; Santomauro, G. Exponentially-fitted Gauss-Laguerre quadrature rule for integrals over an unbounded interval, *J. Comput. Appl. Math.* 255(2014), 725-736.

[77] Conte, D.; Moradi L.; Paternoster, B.; Mohammadi F. Construction of exponentially fitted explicit peer methods, International Journal of Circuits, Systems and Signal Processing 13 (2019), 501-506.

[78] Conte, D.; Paternoster, B. Modified Gauss-Laguerre Exponential Fitting Based Formulae, *J. Sc. Comp.* 69 (1)(2016), 227-243.

[79] Conte, D.; Paternoster, B.; Santomauro, G. An exponentially fitted quadrature rule over unbounded intervals, *AIP Conf. Proc.*, 1479 Springer (2012), 1173-1176.

[80] Conte, D.; Mohammadi, F.; Moradi, L.; Paternoster, B. Exponentially fitted two-step peer methods for oscillatory problems, *Comput. Appl. Math.* 39 (2020), 10.1007/s40314-020-01202-x.

[81] Conte, D.; Cardone, A. Stability analysis of spline collocation methods for fractional differential equations, Mathematics and Computers in Simulation, Vol. 178 (2020), 501-514.

[82] Conte, D.; D'Ambrosio, R.; Paternoster, B. On the stability of θ-methods for stochastic Volterra integral equations, *Discr. Cont. Dyn. Sys. - Series* B 23(7) (2018), 2695-2708.

[83] Conte, D.; Califano, G. Optimal Schwarz Waveform Relaxation for fractional diffusion-wave equations, *Appl. Numer. Math.* 127 (2017), 125-141.

[84] Conte, D.; Paternoster, B. Parallel methods for weakly singular Volterra Integral Equations on GPUs, *Appl. Numer. Math.* 114 (2017), 30-37.

[85] Conte, D.; Shahmorad, S.; Talaei, Y. New fractional Lanczos vector polynomials and their application to system of Abel–Volterra integral equations and fractional differential equations, *J. Comput. Appl. Math.* 366 (2020), 112409.

[86] Djordjevi'c, V. D.; Jari'c, J.; Fabry, B.; Fredberg, J. J.; Stamenovi'c, D. Fractional derivatives embody essential features of cell rheological behavior. Annals of Biomedical Engineering 31 (2003), 692-699.

[87] Duro, R.; Pereira, N.; Figueiredo, C.; Pineiro, C.; Caldas, C.; Serrao, R. Routine CD4 monitoring in HIV patients with viral suppression: Is it really necessary? A Portuguese cohort. *J. Microbiol. Immunol. Infect.* 51 (2018), 593-7.

[88] Deano, A.; Huybrechs, D.; Iserles, A. Computing highly oscillatory integrals. Society for Industrial and Applied Mathematics (SIAM), Philadelphia, PA, 2018.

[89] Dabiri, A.; Butcher, E. A.; Nazari, M. Coefficient of restitution in fractional viscoelastic compliant impacts using fractional Chebyshev collocation. Journal of Sound and Vibration, 388 (2017a), 230-244.

[90] D'Ambrosio, R.; Esposito, E.; Paternoster, B. Exponentially fitted two-step hybrid for $y'' = f(x; y)$, *J. Comp. Appl. Math.* 235 (2011), 4888-4897.

[91] D'Ambrosio, R.; Esposito, E.; Paternoster, B. Exponentially fitted two-step Runge-Kutta methods: construction and parameter selection, *Appl. Math. Comput.* 218 (2012), 7468-7480.

[92] D'Ambrosio, R.; Esposito, E.; Paternoster, B. Parameter estimation in exponentially fitted hybrid methods for second order ordinary differential problems, *J. Math. Chem.* 50 (2012), 155-168.

[93] D'Ambrosio, R.; Ferro, M.; Paternoster, B. Trigonometrically fitted two-step hybrid methods for special second order ordinary differential equations, *Math. Comput. Simulat.*, 81 (2011), 1068-1084.

[94] D'Ambrosio, R.; Ferro, M.; Paternoster, B. Two-step hybrid collocation methods for $y'' = f(x; y)$, *Appl. Math. Lett.* 22 (2009), 1076-1080.

[95] D'Ambrosio, R.; Ixaru, L. Gr.; Paternoster, B. Construction of the ef-based Runge-Kutta methods revisited, *Comput. Phys. Commun.* 182 (2011), 322-329.

[96] D'Ambrosio, R., Moccaldi, M., Paternoster, B., Rossi, F.: On the employ of time series in the numerical treatment of differential equations modelling oscillatory phenomena, Communications in Computer and Information Science 708, 179–187, (2017).

[97] D'Ambrosio, R.; Moccaldi, M.; Paternoster, B. Adapted numerical methods for advection–reaction–diffusion problems generating periodic wavefronts, Computers & Mathematics with Applications, Computers and Mathematics with Applications, doi: 10.1016/j.camwa.2017.04.023, (2017).

[98] D'Ambrosio, R.; Paternoster, B. Exponentially fitted singly diagonally implicit Runge-Kutta methods, *J. Comput. Appl. Math.* 263(2014), 277-287, .

[99] D'Ambrosio, R.; Paternoster, B. Numerical solution of a diffusion problem by exponentially fitted finite difference methods, *Springer. Plus.* 3, 425, (2014).

[100] D'Ambrosio, R.; Paternoster, B. Numerical solution of reaction-diffusion systems of λ-ω type by trigonometrically fitted methods, *J. Comput. Appl. Math.* 294 (2016), 436-445.

[101] D'Ambrosio, R.; Paternoster, B.; Santomauro, G. Revised exponentially fitted Runge-Kutta-Nyström methods, *Appl. Math. Lett.* 30 (2014), 56-60.

[102] D'Ambrosio, R.; Moccaldi, M.; Paternoster, B. Parameter estimation in IMEX-trigonometrically fitted methods for the numerical solution of reaction-diffusion problems, Computer Physics Communication. 226 (2018), 55-66.

[103] Durran, D. R.; Blossey, P. N. Implicit-explicit multistep methods for fast-wave-slow-wave problems, *Mon. Weather Rev.* 140 (2012), 1307-1325.

[104] De Meyer, H.; Vanthournout, J.; Vanden Berghe, G. On a new type of mixed interpolation. Journal of Computational and Applied Mathematics 30, 1 (1990), 55-69.

[105] Ejlali, N.; Hosseini, S. M. A Pseudospectral Method for Fractional Optimal Control Problems. Journal of Optimization Theory and Applications, (2016), 1-25.

[106] El-Kady, M.; Moussa, H. Monic Chebyshev approximations for solving optimal control problem with Volterra integro differential equations, *Gen. Math. Notes*, 14(2)(2013), 23-36.

[107] Engheta, N. On fractional calculus and fractional multipoles in electromagnetism. *IEEE. T. Antenn. Propag.* 44 (1996), 554-566.

[108] Engl, G. J.; Ussif, A. Estimation of Trends Using Ordinary Differential Equations: An Application to Occupational Injuries, Casualty Actuarial Society Forum, Fall 2004, pp. 481-496

[109] Engquist, B.; Fokas, A. S.; Hairer, E.; Iserles, A. Highly Oscillatory Problems, London Mathematical Society Lecture Note Series, Cambridge University Press, 2009.

[110] Evans, D. J.; Raslan, K. R. The Adomian decomposition method for solving delay differential equation. *Int. J. comput. Math.* 82 (2005), 49-54.

[111] Ezz-Eldien, S. S.; Hafez, R. M.; Bhrawy, A. H.; Baleanu, D.; El-Kalaawy, A. A. New numerical approach for fractional variational problems using shifted Legendre orthonormal polynomials, *J. Optimiz. Theory App.,* 174(1) (2017), 295-320.

[112] Ezz-Eldien, S. S.; Doha, E. H.; Bhrawy, A. H.; El-Kalaawy, A. A.; Machado, J. A. T. A new operational approach for solving fractional variational problems depending on indefinite integrals, *Commun. Nonlinear. Sci. Numer. Simul.* 57 (2018), 246-263.

[113] Farsimadan, E.; Moradi, L.; Conte, D.; Paternoster, B.; Palmieri, F. Comparison Between Protein-Protein Interaction Networks CD4$^+$T and CD8$^+$T and a Numerical Approach for Fractional HIV Infection of CD4$^+$T Cells. In: , et al. Computational Science and Its Applications. ICCSA 2021. Lecture Notes in Computer Science (LNCS), vol 12949. Springer, Cham, (2021). https://doi.org/10.1007/978-3-030-86653-2_ 6

[114] Fattah, Q.; Hoopes, J. Dispersion in anistropic homogenoeous porous media. *J. Hydraul. Eng.* 111 (1985), 810-27.

[115] Franco, N. B. A Volterra integral equation arising from the propagation of nonlinear waves, *Rev. Mat. Estat.* 17 (1999), 35-49.

[116] Frank, J.; Hundsdorfer, W.; Verwer, J. G. On the stability of IMEX linear multistep methods, *Appl. Numer. Math.* 25 (1997), 193-205.

[117] Galphin, C.; Glembocki, J.; Tompkins, J. Video Tape Counters: The Exponential Measure of Time (available online at `http://people.uncw.edu/lugo/MCP/DIFF_EQ/deproj/deproj.htm`)

[118] Gao. J.; lserles, A. A generalization of Filon-Clenshaw-Curtis quadrature for highly oscillatory integrals, BIT 57 (2017), 943-961.

[119] Gautschi, W. Numerical integration of ordinary differential equations based on trigonometric polynomials, *Numer. Math.* 3 (1961), 381-397.

[120] Gerisch, A.; Lang, J.; Podhaisky, H.; Weiner, R. High-order linearly implicit two-step peer - finite element methods for time-dependent PDEs, *Appl. Numer. Math.* 59 (2009), 634-638.

[121] Gherghiu, C. I, Spectral Methods for differential problems, T. Popoviciu" Institute of Numerical Analysis, Cluj-Napoca, Romania, 2007.

[122] Ghosh, D.; Constantinescu, E. M. Semi-implicit time integration of atmospheric flows with characteristic-based flux partitioning, *SIAM J. Sci. Comput.* 38(3) (2016), A1848-A1875.

[123] Giraldo, F. X.; Kelly, J. F.; Constantinescu, E. M. Implicit-explicit formulations of a three-dimensional nonhydrostatic unified of the atmosphere (NUMA), *SIAM J. Sci. Comput.* 35(5) (2013), B1162–B1194.

[124] Goertz, R.; Öffner, P. Spectral accuracy for the Hahn polynomials, arXiv:1609.07291v1 [math.NA] 2016.

[125] Goertz, R.; Öffner, P. On Hahn polynomial expansion of a continuous function of bounded variation, ArXiv e-prints: arXiv:1610.06748 (2016).

[126] Gogin, N.; Hirvensalo, M. On the generating function of Discrete Chebyshev Polynomials, Journal of Mathematical Sciences, 224(2) (2017).

[127] Gokmen, E.; Yuksel, G.; Sezer, M. A numerical approach for solving Volterra type functional integral equations with variable bounds and mixed delays, *J. Comput. Appl. Math.*, 311 (2017), 354-363.

[128] Gottlieb, D.; Orszag, S. A. Numerical analysis of spectral methods, Society for Industrial and Applied Mathematics, Philadelphia, 1977.

[129] Guardiola, J.; Izzo, G.; Vecchio, A. Simulating the effect of vaccineinduced immune responses on HIV infection, *Hum. Immunol.* 64 (2003), 840-851.

[130] Guvanasen, V.; Volker, R. Numerical solution for solute transport in unconfined aquifers. *Int. J. Numer. Meth. Fluids.* 3 (1983), 103-23.

[131] Hahn, W. Uber Orthogonal polynome, die q-Differenzengleichungen genugen, (German) *Math. Nachr.* 2, (1949), 4-34.

[132] Hall, M.G.; Barrick, T. R. From diffusion-weighted MRI to anomalous diffusion imaging. *Magn. Reson. Med.* 59 (2008), 447-455.

[133] Hallbergc, D.; Kimariob, T.; Mtuyab, C.; Msuyab, M.; Bjorlingc, G. Factors affecting HIV disclosure among partners in morongo. tanzania. *Int. J. Afr. Nurs. Sci.* 10(2019), 49-54.

[134] Hairer, E.; Lubich, C.; Wanner, G. Geometric numerical integration. Structure-preserving algorithms for ordinary differential equations, Second edition, Springer Series in Computational Mathematics 31, Springer-Verlag, Berlin, 2006.

[135] Hairer, E.; Norsett, S. P.; Wanner, G. Solving Ordinary Differential Equations I - Nonstiff Problems, Springer Series in Computational Mathematics 8, Springer-Verlag, Berlin, 2000.

[136] Hairer, E.; Wanner, G. Solving Ordinary Differential Equations II-Stiff and Differential-Algebraic Problems, Springer Series in Computational Mathematics 14, Springer-Verlag, Berlin, 2002.

[137] He, J.nH. Some applications of nonlinear fractional differential equations and their approximations. *Bull. Sci. Technol.* 15 (1999), 86-90.

[138] He, J. H. Approximate analytical solution for seepage flow with fractional derivatives in porous media. Comput. *Methods Appl. Mech. Eng.* 167 (1998), 57-68.

[139] He, G.; Xiang, S.; Xu, Z. A Chehyshev collocation method fora class of Fredholm integral equations with highly oscillatory kernels, *J. Comput. Appl. Math.* 300 (2016), 354-368.

[140] Henrici, P. Discrete variable methods in ordinary differential equations, John Wiley Sons, New York-London, 1962.

[141] Hetcote, H. W.; Tudor, D. W. Integral equation models for endemic infectious diseases, J. Math. Biol., 9 (1980), 37-47.

[142] Hoppensteadt, F. C.; Jackiewicz, Z.; Zubik-Kowal, B. Numerical solution of Volterra integral and integro-differential equations with rapidly vanishing convolution kernels, BIT 47 (2007), no. 2, 325-350.

[143] Huang, C.; Vandewallc, S. Stability of Runge-Kutta-Pouzet methods for Volterra integro-differential equations with delays. *Front. Matb.* China 4 (2009), 63-87.

[144] Huang, C. Stability of linear multistep methods for delay integro-differential equations, *Comput. Math.Appl.* 55 (2008), 2830-2838.

[145] Huybrechs, D.; Vandewalle, S. On the evaluation of highly oscillatory integrals by analytic continuation, *SIAM J. Numer. Anal.* 44 (2006), 1026-1048.

[146] Huang, W.; Li, Y.; Chen, W. Analysis of the dynamic response of a fluid-supported circular elastic plate impacted by a low-velocity projectile, Proceedings of the Institution of Mechanical Engineers. Part C, Journal of mechanical engineering science 214 (2000), no. 5, 719-727.

[147] Hundsdorfer, W.; Ruuth, S. J. IMEX extensions of linear multistep methods with general monotonicity and boundedness properties, *J. Comput. Phys.* 225 (2007), 2016-2042.

[148] Hundsdorfer, W.; Verwer, J. Numerical Solution of Time-Dependent Advection-Diffusion-Reaction Equations, in: Springer Series in Computational Mathematics, vol. 33, Springer-Verlag, Berlin, Heidelberg, 2003.

[149] Hussaini, M. Y.; Kopriva, D. A.; Salas, M. D.; Zang, T. A. Spectral methods for the Euler equations: Part I-Fourier methods and shock capturing. *AIAA Journal,* 23(1) (1985) 64-70.

[150] Hussaini, M. Y.; Streett, C. L.; Zang, T. A. Spectral methods for partial differential equations. ICASE Report No. 83-46; 1983.

[151] Isaacson, E.; Keller, H. B. Analysis of Numerical Methods, Dover Publications, New York, 1994.

[152] Isenberg, J.; Gutfinger, C. Heat transfer to a draining film. *Int. J. Heat. Transfer.* 16 (1972) 505-12.

[153] Iserles. A.; No rsett, S. P. Efficient quadrature of highly oscillatory integrals using derivatives, *Proc. R. Soc. Land. Ser. A Math. Phys. Eng. Sci.* 461 (2005), 1383-1399.

[154] Ixaru, L. Gr. Operations on Oscillatory Functions, *Comput. Phys. Commun.* 105 (1997), 1-19.

[155] Ixaru, L. Gr. Runge-Kutta method with equation dependent coefficients, *Comput. Phys. Commun.* 183 (2012), 63-69, .

[156] Ixaru, L. Gr.; Paternoster B. A Gauss quadrature rule for oscillatory integrands, *Comput. Phys. Commun.* 133(2001), 177-188.

[157] Ixaru, L. Gr.; Vanden Berghe, G.; Meyer, H. De. Frequency evaluation in exponential fitting multistep algorithms for ODEs, *J. Comput. Appl. Math.* 140 (2002), 423-434.

[158] Ixaru, L. Gr.; Vanden Berghe, G. Exponential Fitting, Kluwer, Boston-Dordrecht-London, 2004.

[159] Iannelli, M.; Martcheva, M.; Milner, F. A. Gender-structured Population Modeling : Mathematical Methods, Numerics, and Simulations, SIAM Frontiers in Applied Mathematics, 2005.

[160] Ixaru, L. G.; and Paternoster, B. A conditionally P-stable fourth-order exponential-fitting method for $y\text{J} = f(x, y)$. Journal of Computational and Applied Mathematics 106, 1 (1999), 87-98.

[161] Ixaru, L. Gr., Runge-Kutta method with equation dependent coefficients, *Comput. Phys. Commun.* 183 (2012), 63-69.

[162] Ixaru, L. Gr.; Rizea, M.; De Meyer, H.; Vanden Berghe, G. Weights of the exponential fitting multistep algorithms for ODEs, *J. Comput. Appl. Math.* 132 (2001) 83-93.

[163] Ixaru, L. Gr.; Vanden Berghe, G.; De Meyer, H. Exponentially fitted variable two-step BDF algorithms for first order ODEs, *Comput. Phys. Comm.* 150 (2003) 116-128.

[164] Ixaru, L. Gr.; Vanden Berghe, G.; De Meyer, H.; Van Daele, M. Four-step exponential-fitted methods for nonlinear physical problems, *Comput. Phys. Comm.* 100 (1997) 56-70.

[165] Iyengar, R. Quantitative models of Mammalian Cell Signaling Pathways, *Sci. Signal.* 1 (2008), no. 7.

[166] Jackiewicz, Z. General linear methods for ordinary differntial equations, John Willey and SonsLtd, Chichester, 2009.

[167] Jafari, H.; Ghasempour, S.; Baleanu, D. On comparison between iterative methods for solving nonlinear optimal control problems. Journal of Vibration and Control 22(9) (2016), 2281-2287.

[168] Jamrog, D. C.; Szipro A. A. A Smallpox and an Inhalation Anthrax Model Implemented Using Ordinary Differential Equations Technical Report of Lincoln Laboratory, Massachussetts Insitute of Technology, 2006.

[169] Jesus, I. S.; Machado, J. A. T.; Cunha, J. B. Fractional electrical impedances in botanical elements. Journal of Vibration and Control 14 (2008), 1389-1402.

[170] Jing Du, M. A Specific Method for Solving Fractional Delay Differential Equation via Fraction Taylor's Series. Mathematical Problems in Engineering, 6, (2022). https://doi.org/10.1155/2022/4044039

[171] Karlin, S.; McGregor, J. L. The Hahn polynomials, formulas, and an application, *Scripta. Math.* 26 (1961), 33-46.

[172] Khader, M. M.; Hendy, A. S. The approximate and exact solutions of the fractional-order delay differential equations using Legendre seudospectral method. *Int. J. pure. Appl. Math.* 74 (2012), 287-297.

[173] Khanduzi, R.; Ebrahimzadeh, A.; Panjeh Ali Beikc, S. Optimal control of fractional integro-differential systems based on a spectral method and grey wolf optimizer, An International Journal of Optimization and Control: Theories and Applications, 10(1)(2020), 55-65.

[174] Khanduzi, R.; Ebrahimzadeh, A.; Reza Peyghami, M. A modified teaching-learning-based optimization for optimal control of Volterra integral systems, Methodologies and Application, doi: 10.1007/s00500-017-2933-8.

[175] Khosravian-Arab, H.; Almeida, R. Numerical solution for fractional variational problems using the Jacobi polynomials, *Appl. Math. Model.* 39(21) (2015), 6461-6470.

[176] Kim, J. K.; Cools, R.; Ixaru, L. Gr. Extended quadrature rules for oscillatory integrands, *Appl. Numer. Math.* 46 (2003), 59-73.

[177] Kim, J. K.; Cools, R.; Ixaru, L. Gr. Quadrature rules using first derivatives for oscillatory integrands, *J. Comput. Appl. Math.* 140 (2002), 479-497.

[178] Kirschner, D. E. Using mathematics to understand HIV immune dynamics. Notices of the American Mathematical Society 43 (1996), 191-202.

[179] Kulikov, G. Y.; Weiner, R. Doubly quasi-consistent parallel explicit peer methods with built-in global error estimation, *J. Comput. Appl. Math.* 233 (2010), 2351-2364.

[180] Lambert, J. D. Numerical methods for ordinary differential systems: The initial value problem, John Wiley, Chichester, 1991.

[181] Larter, R.; Speelman, B.; Worth, R. M. A coupled ordinary differential equation lattice model for the simulation of epileptic seizures, Chaos 9 (1999), no. 3, 795-804.

[182] Lederman, C.; Roquejoffre, J. M.; Wolanski, N. Mathematical justification of a nonlinear integrodifferential equation for the propagation of spherical flames. Annali di Matematica Pura ed Applicata, 183 (2004), 173-239.

[183] Levin. D. Procedures for computing one- and two-dimensional integrals of functions with rapid irregular oscillations, *Math. Comp.* 38 (1982), 531-538.

[184] Lewandowski, R.; Chorazyczewski, B. Identification of the parameters of the Kelvin-Voigt and the Maxwell fractional models, used to modeling of viscoelastic dampers. *Comput. Struct.* 88 (2010), 1-17.

[185] Li, Y. Solving a nonlinear fractional differential equation using Chebyshev wavelets, *Commun. Nonlinea.r Sci. Numer. Simul.* 15(9)(2010), 2284-2292.

[186] Li, J.; Wang, X.; Xiao, S.; Wang, T. A rapid solution of a kind of ID Fredhalm oscillatory integral equation, *J. Comput. Appl. Math.* 236 (2012) 2696-2705.

[187] Li, Q.; Xiao, Y. Global dynamics of a virus immune system with virus guided therapy and saturation growth of virus. *Math. Probl. Eng.* (2018), 1-18 .

[188] Liang, H.; Brunner, H. On the convergence of collocation solutions in continuous pieeewise polynomial spaces for Volterra integral equations. BIT 56 (2016), 1339-1367.

[189] Logan, J. D.; Zlotnik, V. The convection-diffusion equation with periodic boundary conditions, *Appl. Math. Lett.* 8 (3) (1995), 55-61.

[190] Ludwin, C. Blood Alcohol Content, Undergrad. *J. Math. Model.*: One + Two 3 (2) 1 (2011).

[191] Ma, Y.; Xu. Y. Computing highly oscillatory integrals, *Math. Comp.* 87 (2018), 309-345.

[192] Ma, J.; Xiang, S. A collocation boundary value method for linear Volterra integral equations, *I. Sci. Comput.* 71 (2017), 1-20.

[193] Magin, R. L. Fractional Calculus in Bioengineering, Begell House Publishers, Redding, 2006.

[194] Mainardi, F. Fractional calculus: Some basic problems in continuum and statistical mechanics. In: Carpinteri, A., Mainardi, F. (eds.) Fractals and Fractional Calculus in Continuum Mechanics. Springer, New York, 291-348, (1997).

[195] Malinowska, A.; Torres, D. Fractional calculus of variations for a combined Caputo derivative, *Fract. Calc. Appl. Anal.* 14(4) (2011), 523-537.

[196] Maleknejad, K.; Mahmoudi, Y. Taylor polynomial solution of high-order nonlinear Volterra-Fredholm integro-differential equations, Applied Mathematics and Computation 145 (2003), 641-653.

[197] Maleknejad, K.; Hashemizadeh, E.; Ezzati, R. A new approach to the numerical solution of Volterra integral equations by using Bernsteins approximation. *Commun. Nonlinear. Sci. Numer. Simulat.* 16 (2011), 647-655.

[198] Maleknejad, K. Almasieh, H. Optimal control of Volterra integral equations via triangular functions, *Math. Comput. Modelling.* 53 (2011), 1902-1909.

[199] Maleknejad, K.; Ebrahimzadeh, A. Optimal control of Volterra integro-differential systems based on Legendre wavelets and collocation method, *Int. J. Math. Comput. Sci.* 1(7)(2014), 50-54.

[200] Maleknejad, K.; Nosrati Sahlan, M.; Ebrahimizadeh, A. Wavelet Galerkin method for the solution of nonlinear Klein-Gordon equations by using B-spline wavelets, The international conference on scientific computing, Las Vegas, Nevada (2012).

[201] Malinowska, A. B.; Odzijewicz, T.; Torres, D. F. Advanced methods in the fractional calculus of variations. Springer, 2015.

[202] Mandelbrot, B. Some noises with $\frac{1}{f}$spectrum, a bridge between direct current and white noise, *IEEE Trans. Inform. Theory.* 13 (1967), 289-298.

[203] Marino, M. A.; Luthin, J. N. Seepage and Groundwater, Elsevier, Amsterdam, 1982.

[204] Marzban, H. R.; Razzaghi, M. Solution of multi-delay systems using hybrid of block-pulse functions and Taylor series. *Sound. Vib.* 292 (2006), 954-963.

[205] Mashayekhi, S.; Ordokhani, Y.; Razzaghi, M. Hybrid functions approach for optimal control of systems described by integro differential equations, *Appl. Math. Model.* 37(5)(2013), 3355-3368.

[206] Mashayekhi, S.; Ordokhani, Y.; Razzaghi, M. Hybrid functions approach for nonlinear constrained optimal control problems. *Commun. Nonl. Sci. Numer. Simul.* 17 (2012), 1831-1843.

[207] Mercier, B. An introduction to the numerical analysis of spectral methods, Springer- Verlag, Berlin 1989.

[208] Merdan, M.; Gökdogan, A.; Yildirim, A. On the numerical solution of the model for HIV infection of CD4+T-cells, *Comput. Math. Appl.* 62 (2011), 118-123.

[209] Moghaddam, B. P.; Mostaghim, Z. S. A numerical method based on finite difference for solving fractional delay differential equations, *J. Taibah Univ. Sci.* 7 (2103), 120-127.

[210] Mohammadi, F.; Mohyud-Din, S. T. A fractional-order Legendre collocation method for solving the Bagley-Torvik equations, *Adv. Differ. Equ.* 269 (2016), 269.

[211] Mohammadi, F.; Cattani, C. A generalized fractional-order Legendre wavelet Tau method for solving fractional differential equations, *J. Comput. Appl. Math.*, (2017).

[212] Montijano, J. I.; Rández, L.; Van Daele, M.; Calvo, M. Functionally Fitted Explicit Two Step peer Methods, *J. Sci. Comput.* 64(3) (2014), 938-958.

[213] Moradi, L.; Conte, D.; Farsimadan, E.; Palmieri, F.; Paternoster, B. Optimal control of system governed by nonlinear volterra integral and fractional derivative equations. *Comp. Appl. Math.* 40, 157 (2021). https://doi.org/10.1007/s40314-021-01541-3.

[214] Moradi, L.; Mohammadi, F. A comparative approach for time-delay fractional optimal control problems: Discrete versus continuous chebyshev polynomials, Asian Journal of Control, Vol. 21(6) (2019), 1-13.

[215] Nerukh, A. G.; Sewell, P.; Benson T. M. Volterra Integral Equations for Nonstationary Electromagnetic Processes in Time-Varying Dielectric Waveguides, *J. Lightwave. Technol.* 22 (2004), no. 5.

[216] Nelson, P. W.; Perelson, A. S. Mathematical analysis of delay differential equation models of HIV-1 infection. Mathematical Bioscience 179 (2002), 73-94.

[217] Nigmatullin, R. R.; Nelson, S. O. Recognition of the fractional kinetics in complex systems: Dielectric properties of fresh fruits and vegetables form 0.01 to 1.8 GHz. Signal Processing 86 (2006), 2744-2759.

[218] Nikiforov, A. F.; Suslov, S. K.; Uvarov, V. B. Classical Orthogonal Polynomials of a Discrete Variable. Springer, Berlin, Heidelberg, 1991.

[219] Norberto, A. M.; Benavente, M. A.; Eguaras, M. A Model in Differential Equations to Describe the Mite Varroa Destructor Population Dynamic in Apis Mellifera Colonies, Foro Red. Mat. 16, 2005.

[220] Nowak, M.; May, R. Mathematical biology of HIV infections: antigenic variation and diversity threshold, *Math. Biosci.* 106 (1991), 1-21.

[221] Ockendon, J. R.; Tayler, A.B. The dynamics of a current collection system for an electric locomotive, *Proc. R. Soc. Lond. Ser. A.* 322 (1971), 447-468.

[222] Oguz, C.; Sezer, M. Chelyshkov collocation method for a class of mixed functional integro- differential equations, *Appl. Math. Comput.* 259 (2015) 943-954.

[223] Oldham, K. B. Fractional differential equations in electrochemistry, *Adv. Eng. Soft.* 41 (2010), 9-12.

[224] Oldham, K.; Spanier, J. The fractional calculus theory and applications of differentiation and integration to arbitrary order, 111, Elsevier, 1974.

[225] Oldham, K. B.; Spanier, J. The Fractional Calculus. Academic Press, New York, 1974.

[226] Oliveira, F. A. Collocation and residual correction, *Numer. Math.* 36 (1980) 27-31.

[227] Oliver C. Ibe, 10-Diffusion Processes, Markov Processes for Stochastic Modeling (Second Edition), Elsevier, (2013), 295-327. https://doi.org/10.1016/B978-0-12-407795-9.00010-4. (https://www.sciencedirect.com/topics/mathematics/fractional-differential-equations)

[228] Olver, S. Moment-free numerical integration of highly oscillatory functions, *IMA J. Nuclei. Anal.* 26 (2006) 213-227.

[229] Omondi, E.; Mbogo, W.; Luboobi, L. A mathematical modeling study of HIV infection in two heterosexual age groups in Kenya. *Infec. Dis. Modell.* 4 (2019),83-98.

[230] Ongun, M. The Laplace adomian decomposition method for solving a model for HIV infection of CD4+ T-cells. *Math. Comput. Modelling.* 63 (2011), 597-603.

[231] Oppenheim, A. V.; Schafer, R. W.; Buck, J. R. Discrete-Time Signal Processing, 2nd edn., Prentice Hall, Upper Saddle River, 1999.

[232] Ortega, J. M. Numerical analysis. A second course. Academic Press, New York-London, 1972.

[233] Ozawa, K. A functional fitting Runge-Kutta method with variable coefficients, *Jpn. J. Ind. Appl. Math.* 18 (2001), 107-130,.

[234] Parlarge, J. Y. Water transport in soils. Ann Rev Fluids Mech, 2 (1980), 77-102.

[235] Paternoster, B. Present state-of-the-art in exponential fitting. A contribution dedicated to Liviu Ixaru on his 70-th anniversary, *Comput. Phys. Comm.* 183 (2012), 2499-2512.

[236] Paternoster, B. Runge-Kutta(-Nyström) methods for ODEs with periodic solutions based on trigonometric polynomials, *Appl. Numer. Math.* 28 (1998), 401-412.

[237] Paternoster, B. Two step Runge-Kutta-Nyström methods for $y'' = f(x, y)$ and P-stability, *Lect. Notes Comput. Sci.* 2331 (2002), 459-466.

[238] Perelson, A. S.; Kirschner, D. E.; Boer, R. D. Dynamics of HIV infection $CD4^+$T cells, *Math. Biosci.* 114 (1993), 81-125.

[239] Perelson, A. S.; Nelson, P. W. Mathematical analysis of HIV-I Dynamics in Vivo. *SIAM Rev.* 41(1) (1999), 3-44.

[240] Petrovic, L.M.; Spasic, D. T.; Atanackovic, T. M. On a mathematical model of a human root dentin. Dental Materials 21 (2005), 125-128.

[241] Peyghami, M. R.; Hadizadeh, M.; Ebrahimzadeh, A. Some explicit class of hybrid methods for optimal control of Volterra Integral Equations, journal of Information and Computing Science, 7(4) (2012), 253-266.

[242] Podhaisky, H.; Weiner, R.; Schmitt, B. Rosenbrock-type 'peer' two-step methods, *Appl. Numer. Math.* 53 (2005), 409-420.

[243] Podlubny, I. Fractional differential equations: an introduction to fractional derivatives, fractional differential equations, to methods of their solution and some of their applications. 198, Academic press, 1998.

[244] Podlubny, I. Fractional Differential Equations, Academic Press, San Diego, 1999.

[245] Povstenko, Y. Z. Signaling problem for time-fractional diffusion-wave equation in a half-space in the case of angular symmetry. *Nonl. Dyn.* 55 (2010), 593-605.

[246] Rahimkhani, P.; Ordokhani, Y.; and Babolian, E. A new operational matrix based on Bernoulli wavelets for solving fractional delay differential equations. *Numer. Algor.* 74 (2017), 223-245. https://doi.org/10.1007/s11075-016-0146-3

[247] Ransome, Y.; Thurber, K.; Swen, M.; Crawford, N.; Germane, D.; Dean, L. Social capital and HIV/AIDS in the United States: Knowledge, gaps, and future directions. SSM-Popul Health 5 (2018), 73-85.

[248] Rashed, M. T. Numerical solution of functional differential, integral and integro differential equations, *Appl. Math. Comput.* 156 (2004), 485-492.

[249] Ray, S. S.; Atangana, A.; Noutchie, S. C.; Kurulay, M.; Bildik N.; Kilicman, A. Fractional calculus and its applications in applied mathematics and other sciences. Mathematical Problems in Engineering, 2014.

[250] Razzaghi, M.; Yousefi, S. Legendre wavelet method for the solution of nonlinear problems in the calculus of variations, *Math. Comput. Model.* 34(1-2) (2001), 45-54.

[251] Riordan, J. An Introduction to Combinatorial Analysis, New York: Wiley, 1980.

[252] Riewe, F. Nonconservative Lagrangian and Hamiltonian mechanics, Phys. Rev. E 53 (2) (1996) 1890-1899.

[253] Riewe, F. Mechanics with fractional derivatives, *Phys. Rev.* E 55 (3) (1997), 3581-3592.

[254] Rossikhin, Y. A.; Shitikova, M. V. Applications of fractional calculus to dynamic problems of linear and nonlinear hereditary mechanics of solids. *Appl. Mech. Rev.* 50 (1997), 15-67.

[255] Ruuth, S. J. Implicit-explicit methods for reaction-diffusion problems in pattern formation, *J. Math. Biol.* 34 (1995) 148-176.

[256] Saadatmandi, A.; Dehghan, M. A new operational matrix for solving fractional-order differential equations, *Comput. Math. Appl.* 59(3) (2010), 1326-1336.

[257] Sadeghi Hafshejani, M.; Karimi Vanani, S.; Sedighi Hafshejani, J. Numerical solution of delay differential equations using Legendre wavelet method, *World. Appl. Sci.* 13 (2011), 27-33.

[258] Saeed, U.; Rehman, M.U. Hermite wavelet method for fractional delay differential equations, *J. Diff. Equa.* (2014), 1-8.

[259] Sahu, P. K.; Ray, S. S. Comparison for accurate solutions of nonlinear Hammerstein fuzzy integral equations, Mathematical Communications, 21(2) (2016), 283-299.

[260] Salmon, J.R.; Ligett, J. A.; Gallager, R. H. Dispersion analysis in homogeneous lakes. *Int. J. Numer. Meth. Eng.* 15 (1980) 1627–42.

[261] Samko, S. G.; Kilbas, A. A.; Marichev, O. I. Fractional Integrals and Derivatives: Theory and Applications. Gordon and Breach, Langhorne, 1993.

[262] Saxena, R. K.; Mathai, A. M.; Haubold H. J. On generalized fractional kinetic equations. Physica A, 344 (2004), 657-664 .

[263] Schiesser, W. E. The Numerical Method of Lines: Integration of Partial Differential Equations, Academic Press, San Diego, 1991.

[264] Schiesser, W. E.; Griffiths, G.W. A Compendium of Partial Differential Equation Models: Method of Lines Analysis with Matlab, Cambridge University Press, 2009.

[265] Schmitt, B. A.; Weiner, R. Parallel start for explicit parallel two-step peer methods, *Numer. Algor.* 53 (2010), 363-381.

[266] Schmitt, B. A.; Weiner, R. Parallel two-step W-methods with peer variables, *SIAM J. Numer. Anal.* 42 (2004), 265-282, .

[267] Schmitt, B. A.; Weiner, R. Efficient A-stable peer two-step methods, *J. Comput. Appl. Math.* 316 (2017), 319-329, .

[268] Schmitt, B. A.; Weiner, R.; Beck, S. Two-step peer methods with continuous output, *BIT* 53 (2013), 717-739.

[269] Schmitt, B. A.; Weiner, R.; Erdmann, K. Implicit parallel peer methods for stiff initial value problems, *Appl. Numer. Math.* 53 (2-4) (2005), 457-470.

[270] Schmitt, B. A.; Weiner, R.; Jebens, S. Parameter optimization for explicit parallel peer two-step methods, *Appl. Numer. Math.* 59 (2009), 769–782.

[271] Schmitt, B. A.; Weiner, R.; Podhaisky, E. Multi-implicit peer two-step W-methods for parallel time integration, *BIT Numerical Mathematics* 45 (2005), 197-217.

[272] Sedaghat, S.; Ordokhani, Y.; and Dehghan, M. Numerical solution of the delay differential equations of pantograph type via Chebyshev polynomials. *Commun. Nonl. Sci. Numer. Simul.* 17 (2012), 4815-4830 .

[273] Shahmorad, S. Numerical solution of the general form linear Fredholm-Volterra integro-differential equations by the Tau method with an error estimation, *Appl. Math. Comput.* 167 (2005) 1418-1429.

[274] Shen, J.; Tang, T. Pectral and high-order methods with applications. Science Press, Beijing, 2006.

[275] Shampine, L. F. Numerical Solution of Ordinary Differential Equations, Chapman Hall, New York, London, 1994.

[276] Shampine, L. F. Computer Solution of Ordinary Differential Equations, W.H. Freeman and Company, San Francisco, 1975.

[277] Simos, T. Error analysis of exponential-fitted methods for the numerical solution of the one-dimensional Schrödinger equation. Physics Letters A 177, 4 (1993), 345-350.

[278] Simos, T. E. Some New Four-Step Exponential-Fitting Methods for the Numerical Solution of the Radical Schrödinger Equation. IMA Journal of Numerical Analysis 11, 3 (1991), 347-356.

[279] Simos, T. E. Exponential fitted methods for the numerical integration of the Schrödinger equation. Computer physics communications 71, 1 (1992), 32-38.

[280] Simos,T. E. A fourth algebraic order exponentially-fitted Runge-Kutta method for the numerical solution of the Schrödinger equation, *IMA Journ. of Numerical Analysis,* 21 (2001), 919-931.

[281] Simos,T. E. An exponentially-fitted Runge-Kutta method for the numerical integration of initial-value problems with periodic or oscillating solutions. *Comput. Phys. Comm.* 115 (1998), 1-8.

[282] Singh, K. M.; Tanaka, M. On exponential variable transformation based boundary element formulation for advection-diffusion problems. *Eng. Anal. Bound. Elem.* 24 (2000) 225-35.

[283] Singh, H. Numerical simulation for fractional delay differential equations. *Int. J. Dyn. Control.* 9 (2021), 463-474 .

[284] Smith, D. A. Human population growth: Stability or explosion? *Math. Mag.* 50 (4) (1977), 186-197.

[285] Smith, G. D. Numerical Solution of Partial Differential Equations-Finite Difference Methods, Clarendon Press, Oxford, 1985.

[286] Soleimani, B.; Weiner, R. A class of implicit peer methods for stiff systems, Journal of Computational and Applied Mathematics, 316 (2017), 358-368,.

[287] Soleimani, B.; Knothb, O.; Weiner, R. IMEX peer methods for fast-wave-slow-wave problems, *App. Num. Math.* 118 (2017) 221-237.

[288] Spencer, S. L.; Berryman, M. J.; Garca, J. A.; Abbott, D. An ordinary differential equation model for the multistep transformation to cancer, *J. Theoret. Biol.* 231 (2004), no. 4, 515-524.

[289] Srivastava, H. M.; Kumar, D.; Singh, H. An efficient analytical technique for fractional model of vibration equation, Applied Mathematical Modelling 45 (2017), 192-204.

[290] Srivastava, H. M.; Daba, M.; Gusu, P.O.; Mohammed, G.W.; Kamsing N.; and Hamed, Y.S. Solutions of General Fractional-Order Differential Equations by Using the Spectral Tau Method. Fractal and Fractional, 6 (2022), 1-7. https://doi.org/10.3390/fractalfract6010007

[291] Srivastava, H.M.; Choi, J. Series Associated with the Zeta and Related Functions, Kluwer, Boston, 2001.

[292] Su, N.; Liu, F.; Anh, V. Tides as a phase modulated waves inducing periodic groundwater flow in coastal aquifers overlaying a sloping impervious base, *Environ. Model. Softw.* 18 (2003) 937-942.

[293] Stein, E. M. Harmonic analysis: real-variable methods, orthogonality, and oscillatory integrals, volume 43 of Princeton Mathematical Series, Princeton University Press, Princeton. NJ, 1993. With the assistance of Timothy S. Murphy. Monographs in Harmonic Analysis, III.

[294] Theys, K.; Libin, P.; Pena, A. C. P.; Nowe, A.; Vandamme, A. M.; Abecasis, A. B. The impact of HIV-1 within host evolution on transmission dynamics, *Curr. Opin. Virol.* 28 (2018), 92-101.

[295] Tohidi, E.; Samadi, O. R. N. Optimal control of nonlinear Volterra integral equations via Legendre polynomials, *IMA J. Math. Control. Inform.* 30 (2013), 67-83.

[296] Tohidi, E.; Bhrawy, A. H.; Erfani, K. A collocation method based on Bernoulli operational matrix for numerical solution of generalized pantograph equation, *Appl. Math. Model.* 37 (2012), 4283-4294.

[297] Van Daele, M.; Vanden Berghe, G.; Vande Vyver, H. Exponentially fitted quadrature rules of Gauss type for oscillatory integrands, *Appl. Numer. Math.* 53 (2005), 509-526.

[298] Vanden Berghe, G.; Van Daele, M. Exponentially-fitted Numerov methods. Journal of Computational and Applied Mathematics 200, 1 (2007), 140-153.

[299] Vanden Berghe, G.; Van Daele, M. Symplectic exponentially- fitted modied Runge-Kutta methods of the Gauss type, revisited. Recent advances in computational and applied mathematics. Springer Netherlands, (2011), 289-306.

[300] Vanden Berghe, G.; Meyer, H. De.; Van Daele, M.; Van Hecke, T. Exponentially fitted explicit Runge-Kutta methods, *Comput. Phys. Commun.* 123 (1999), 7-15.

[301] Vanden Berghe, G.; Ixaru, L. Gr.; Van Daele, M. Optimal implicit exponentially-fitted Runge-Kutta methods, *Comput. Phys. Commun.* 140 (2001), 346-357.

[302] Vanden Berghe, G.; Ixaru, L. Gr.; De Meyer, H. Frequency determination and step-length control for exponentially fitted Runge-Kutta methods, *J. Comput. Appl. Math.* 132 (2001) 95-105.

[303] Vanden Berghe, G.; Van Daele, M.; Van de Vyver, H. Exponential fitted Runge–Kutta methods of collocation type: fixed or variable knot points? *J. Comput. Appl. Math.* 159 (2003) 217-239.

[304] Van de Vyver, H. Frequency evaluation for exponentially fitted Runge-Kutta methods, *J. Comput. Appl. Math.* 184 (2005), 442-463.

[305] Volterra, V. Variations and fluctuations of the number of individuals in animal species living together. Reprinted in R.N. Chapman, Animal Ecology, McGraw Hill, New York, 1931.

[306] Wang, H.; Shu, C. W.; Zhang, Q. Stability and error estimates of local discontinuous galerkin methods with implicit-explicit time-marching for advection-diffusion problems, *SIAM J. Numer. Anal.* 53 (1) (2015) 206-227.

[307] Wang, K. Y.; Wang, Q. S. Lagrange collocation method for solving Volterra-Fredholm integral equations, *Appl. Math. Comput.* 219 (2013), 10434-10440.

[308] Wang, K. Y.; Wang, Q. S. Taylor collocation method and convergence analysis for the Volterra-Fredholm integral equations, *J. Comput. Appl. Math.* 260 (2014), 294-300.

[309] Wang, H.; Xiang. S. Asymptotic expansion and Filon-type methods fora Volterra integral equation with a highly oscillatory kernel, *IMA J. Numer. Anal.* 31 (2011) 469-490.

[310] Wang, W. S.; Li, S. F. On the one-leg θ method for solving nonlinear neutral functional differential equations. *Appl. Math. Comput.* 193 (2007), 285-301 .

[311] Wang, Z. A numerical method for delayed fractional-order differential equations. *J. Appl. Math.* (2013), 1-7.

[312] Wang, L.; Li, M.Y. Mathematical analysis of the global dynamics of a model for HIV infection of CD4+T cells. *Math. Biosci.* 200 (2006), 44-57 .

[313] Weiner, R.; Biermann, K.; Schmitt, B. A.; Podhaisky, H. Explicit two-step peer methods, Computers and Mathematics with Applications, 55 (2008), 609-619.

[314] Weiner, R.; Biermann, K.; Schmitt, B.A.; Podhaisky, H. Explicit two-step peer methods, *Comput. Math. Appl.* 55(4) (2008) 609-619.

[315] Weiner, R.; Schmitt, B.A.; Podhaisky, H.; Jebens, S. Superconvergent explicit two-step peer methods, *J. Comput. Appl. Math.* 223 (2009) 753-764.

[316] Werner, P. W. Some problems in non-artesian ground-water flow, *Trans. Amer. Geophys. Union.* 38 (4) (1958) 511-558.

[317] Wilson, M. W. On the Hahn Polynomials, *SIAM J. Math. Anal.*1(1) (1970), 131-139.

[318] Xiang, S. Efficient Filon-type methods for $\int^b f(x)e^{i\omega g(x)}dx$, *Numer. Math.* 105 (2007) 633-658.

[319] Xiang. S.; Cho, Y. J.; Wang, H.; Brunner, H. Clenshaw-Curtis-Filon-type methods for highly oscillatory Bessel transforms and applications. *IMA J. Nuttier. Anal.* 3l (2011) 1281-1314.

[320] Xiang. S.; H.; Brunner, Efficient methods for Volterra integral equations with highly oscillatory Bessel kernels. *BIT* 53 (2013) 241-263.

[321] Xiu, D.; Karniadakis, G. E. The Wiener-Askey polynomial chaos for stochastic differential equations. SIAM journal on scientific computing, 24(2) (2002), 619-644.

[322] Yang, Y.; Huang, Y. Spectral-collocation methods for fractional pantograph delay-integro differential equations. *Advan. Math. Phys.* (2013), 1-14.

[323] Yddotuzbasi, S., Karacayir, M.: An exponential Galerkin method for solution of HIV infected model of $CD4^+$T-cells. *Comput. Biol. Chem.* 67 (2017), 205-12.

[324] Yu, Z. H. Variational iteration method for solving the multi-pantograph delay equation. *Phys. Lett. A.* 372 (2008), 6475-6479 .

[325] Yüzbas, S. A numerical approach to solve the model for HIV infection of $CD4^+$T-cells. *Appl. Math. Model.* 36 (2012), 5876-5890.

[326] Zaky, M. A. A Legendre spectral quadrature tau method for the multi-term time-fractional diffusion equations, *Comp. Appl. Math.* 2017. https://doi.org/10.1007/s40314-017-0530-1.

[327] Zaky,M. A.; Doha, E. H.; Taha, T. M.; Baleanu, D. New recursive approximations for variable-order fractional operators with applications, Mathematical Modelling and Analysis, 23 (2) (2018), 227-239.

[328] Zaky, M. A.; Machado, J. T. On the formulation and numerical simulation of distributed-order fractional optimal control problems, *Commun. Nonlinear. Sci. Numer. Simul.* 52 (2017), 177-189.

[329] Zhang, H.; Sandu, A.; Blaise, S. Partitioned and implicit–explicit general linear methods for ordinary differential equations, *J. Sci. Comput.* 61 (2014) 119-144.

[330] Zharovsky, E.; Sandu, A.; Zhang, H. A class of implicit-explicit two-step Runge-Kutta methods, *SIAM J. Numer. Anal.* 53 (2015) 321-341.

[331] Zlatev, Z.; Berkowicz, R.; Prahm, L.P. Implementation of a variable stepsize variable formula in the time-integration part of a code for treatment of long-range transport of air pollutants. *J. Comp. Phys.* 55 (1984) 278-301.

[332] Zhao, X. Q. Dynamical Systems in Population Biology, CMS Books in Mathematics, New York, Springer-Verlag, 2003.

[333] Zhao. L.; Huang, C. Exponential fitting collocation methods for a class of Volterra integral equations. *Appl. Math. Comput.* 376 (2020) 121-125.

[334] Zhao. L.; Huang, C. An adaptive Filon-type method for oscillatory integrals without stationary points. *Numer. Algorithms* 75 (2017) 753-775.

[335] Zhao, L.; Fan, Q.; Ming, W. Efficient collocation methods for Volterra integral equations with highly oscillatory kernel. Journal of Computational and Applied Mathematics, 404, 2022.